UNIVERSITAT POLITÈCNICA DE CATALUNYA BARCELONATECH

Multistage scenario trees generation for renewable energy systems optimization

Marlyn Dayana Cuadrado Guevara

Universitat Politècnica de Catalunya

Department of Statistics and Operations Research

Multistage Scenario Trees Generation for Renewable Energy Systems Optimization

By: MsC. Marlyn Dayana Cuadrado Guevara

Advisor: PhD. F.-Javier Heredia Cervera

A thesis submitted for the degree of

Philosophy Doctor (PhD)

In Statistics and Operations Research

Barcelona, Spain 2020

To Jehovah, the Highest.
To my family, my motivation in the life.

In the preparation of the scenarios generation of this thesis, Marlyn Cuadrado was co-advised by Josep Anton Sànchez Espigares.

The work in this thesis was carried out in the Research Group GNOM (Group on Numerical Optimization and Modeling) in the Department of Statistics and Operation Research, UPC, Barcelona, under Coordinated Project Forecasting and Optimization of Wind Generation in Energy Markets (FOWGEM), with reference MTM2013-48462-C2-1-R of the *Ministerio de Economía y Competitividad* (MINECO), Spain.

Marlyn Cuadrado received a Predoctoral Contract BES-2014-070636 for the Formation of Research Personnel from MINECO, Spain, during the period October 2015-September 2019.

Agradecimientos

Personal

Me gustaría expresar mi más sincero agradecimiento a mi director de tesis, F.-Javier Heredia, por todo el conocimiento adquirido de el, por el soporte y disposición en apoyarme en las decisiones que tomé a lo largo de estos años de doctorado. Gracias por la paciencia que me ha tenido, porque creo que sin ella no hubiese sido posible culminar esta tesis doctoral. ¡Has demostrando ser un gran director de tesis!

Gracias también a Josep Sánchez, por ser pieza clave en la culminación de los objetivos estadísticos de esta tesis. Por la disposición en atenderme en consultas académicas, aún cuando llegaba inesperadamente a su despacho. Sin su asesoramiento hubiese sido difícil cumplir con dichos objetivos.

Por otro lado, quiero agradecer a Marcos Rider y Luigi Viola por todo el apoyo recibido en mi estancia doctoral. A Marcos, por el soporte académico, inclusive, por la ayuda recibida al instalarme en una ciudad donde no hablaban mi idioma; e Luigi, por sempre estar presente para aclarar as dúvidas que apareciam no dia a dia durante estes três meses de estadia, que uma vez terminada, sempre esteve disposto a responder todos os meus questionamentos, mesmo que a distância.

Infinitas gracias a mi familia, en especial a mis padres, José e Isol, por todo lo que soy, ellos siempre decían: “a dayanita le gusta estudiar mucho” y mira hasta donde llegué papitos, los amo. A mis hermanos, Johanna, Johan, Jonathan y Lizmar, por su cariño incondicional. Gracias especialmente a mi hermana Johanna y mi cuñado Daniel por el apoyo en la etapa final de la tesis, abriéndome las puertas de su hogar. A mi sobrino Sebastián porque su amor y muestras de cariño me han recargado los ánimos cuando ya casi no tenia fuerzas para terminar la tesis, y mas aún en tiempos de pandemia. Infinitas gracias a ustedes familia.

A mis amigos de la UPC (Carlos, Daniel, Diana, Grace, Jeaneth y Jesús), de la UNICAMP (Erik, Jefferson y Maria Teresa) y de la Iglesia Cristiana Senda de Vida (Pastor Silvio, Pastora Alejandra, Inés Alejandra, Pedro, Marina, Ruth, Verónica, Nélson, Nancy, Anayeli, Johana, Dayana, Karla, Mónica y Rocío), porque en momentos específicos de estos años de doctorado, han sido un apoyo incondicional, gracias por cada tiempo compartido, por la felicidad que me regalaron en los momentos buenos y por cada palabra de ánimo en los momentos malos. Muchas gracias de todo corazón. A los amigos que me regaló Barcelona; Yahiris, Sonia, Gabriela, Carlos, Aníbal y Andy, por todos los tiempos que compartí con ustedes.

Por último, agradecer a los profesores que han marcado mi vida académica hasta el dia de hoy. Al profesor Víctor Griffin (UC-Venezuela), Hugo Lara (UCLA-Venezuela), profesora Elisa Verruschi (UNEXPO-Venezuela) y a los tres profesores que se suman a esta lista, F.- Javier Heredia (UPC-Barcelona), Josep Sánchez (UPC-Barcelona) y Marcos Rider (UNICAMP-Brasil).

Institucional

Extiendo mi agradecimiento al Programa Estatal de Promoción del Talento y su Empleabilidad en I+D+i del Ministerio de Ciencia e Innovación del Gobierno de España por la financiación recibida este tiempo de estudios doctorales.

A la prestigiosa *Universitat Politècnica de Catalunya* por haberme dado la oportunidad de formar parte de esta institución, específicamente como estudiante de doctorado, y a su vez, como personal de investigación en formación. Me llevo de ella su sello "yo soy UPC". Gracias particularmente a la *Unitat d'Assessorament i Suport Laboral a la Recerca* y al *Gabinet de Relacions Internacionals i Empresa-Grie* por el soporte recibido en los trámites relacionado con los contratos de trabajo y permisos de residencia.

A todos los miembros del *Departament d'Estadística i Investigació Operativa*, en especial a Jan Graffelman, Jordi Castro, Sonia Navarro, Carme Macias, Celia Matin, Toni Font y Ana Maria Ortega, por todo el soporte administrativo y técnico que recibí por parte de ustedes durante mi estancia en el departamento, mil gracias.

Al *Group of Numerical Optimization and Modeling (GNOM)* y al proyecto *Forecasting and optimization of wind generation in energy markets (FOWGEM)* por haber formado parte de cada uno de ellos.

A la *Universidade Estadual de Campinas (UNICAMP)* y particularmente a la *Faculdade de Engenharia Elétrica e de Computação (FEEC)* por todo el conocimiento adquirido en los 3 meses de estancia doctoral.

"Y todo lo que hacéis, sea de palabra o de hecho, hacedlo todo en el nombre del Señor Jesús, dando gracias a Dios Padre por medio de él."

Colosenses 3:17.

Gracias mi Dios, por medio de Jesús.

Abstract

The presence of renewables in energy systems optimization have generated a high level of uncertainty in the data, which has led to a need for applying stochastic optimization to modelling problems with this characteristic. The method followed in this thesis is Multistage Stochastic Programming (MSP). Central to MSP is the idea of representing uncertainty (which, in this case, is modelled with a stochastic process) using scenario trees. In this thesis, we developed a methodology that starts with available historical data; generates a set of scenarios for each random variable of the MSP model; defines individual scenarios that are used to build the initial stochastic process (as a fan or an initial scenario tree); and builds the final scenario trees that are the approximation of the stochastic process.

The methodology proposes consists of two phases. In the first phase, we developed a procedure similar to Muñoz et al. (2013), with the difference being that the VAR models are used to predict the next day for each random parameter of the MSP models. In the second phase, we build scenario trees from the Forward Tree Construction Algorithm (FTCA), developed by Heitsch and Römisch (2009a); and an adapted version of Dynamic Tree Generation with a Flexible Bushiness Algorithm (DTGFBA), developed by Pflug and Pichler (2014, 2015). This methodology was used to generate scenario trees for two MSP models. A first model, Multistage Stochastic Wind Battery Virtual Power Plant model (MSWBVPP model) and to a second model, which is the Multistage Stochastic Optimal Operation of Distribution Networks model (MSOODN model). We developed extensive computational experiments for the MSWBVPP model and generated scenario trees with real data, which were based on MIBEL prices and wind power generation of the real wind farm called Espina, located in Spain. For the MSOODN model, we obtained scenario trees by also using real data from the power load provided by FEEC-UNICAMP and photovoltaic generation of a distribution grid located in Brazil. The results show that the scenario tree generation methodology proposed in this thesis can obtain suitable scenario trees for each MSP model.

In addition, results were obtained for the model using the scenario trees as input data. In the case of the MSWBVPP model, we solved three different case studies corresponding to three different hypotheses on the virtual power plant's participation in electricity markets. In the case of the MSOODN model, two test cases were solved, with the results indicating that the EDN satisfied the limits imposed for each test case. Furthermore, the BESS case gave good results when taking into account the uncertainty in the model. Finally, the MSWBVPP model was used to study the relative performance

of the FTCA and DTGFBA scenario trees, specifically by analyzing the value of the stochastic solution for the 366 daily optimal bidding problems. To this end, a variation of the classical VSS (the so-called "Forecasted Value of the Stochastic Solution", FVSS) was defined and used together with the classical VSS.

Resumen

La presencia de energías renovables en la optimización de sistemas energéticos hagenerado un alto nivel de incertidumbre en los datos, lo que ha llevado a la necesidad de aplicar técnicas de optimización estocástica para modelar problemas con estas características. El método empleado en esta tesis es programación estocástica multietapa (MSP, por sus siglas en inglés). La idea central de MSP es representar la incertidumbre (que en este caso es modelada mediante un proceso estocástico), mediante un árbol de escenarios. En esta tesis, desarrollamos una metodología que parte de una data histórica, la cual está disponible; generamos un conjunto de escenarios por cada variable aleatoria del modelo MSP; definimos escenarios individuales, que luego serán usados para construir el proceso estocástico inicial (como un fan o un árbol de escenario inicial); y, por último, construimos el árbol de escenario final, el cual es la aproximación del proceso estocástico.

La metodología propuesta consta de dos fases. En la primera fase, desarrollamos un procedimiento similar a Muñoz et al. (2013), con la diferencia de que para las predicciones del próximo día para cada variable aleatoria del modelo MSP usamos modelos VAR. En la segunda fase construimos árboles de escenarios mediante el "Forward Tree Construction Algorithm (FTCA)", desarrollado por Heitsch and Römisch (2009a); y una versión adaptada del "Dynamic Tree Generation with a Flexible Bushiness Algorithm (DTGFBA)", desarrolado por Pflug and Pichler (2014, 2015). Esta metodología fue usada para generar árboles de escenarios para dos modelos MSP. El primer modelo fue el "Multistage Stochastic Wind Battery Virtual Power Plant model (modelo MSWBVPP)", y el segundo modelo es el "Multistage Stochastic Optimal Operation of Distribution Networks model (MSOODN model)". Para el modelo MSWBVPP desarrollamos extensivos experimentos computacionales y generamos árboles de escenarios a partir de datos reales de precios MIBEL y generación eólica de una granja eólica llamada Espina, ubicada en España. Para el modelo MSOODN obtuvimos árboles de escenarios basados en datos reales de carga, provistos por FEEC-UNICAMP y de generación fotovoltaica de una red de distribución localizada en Brasil. Los resultados muestran que la metodología de generación de árboles de escenarios propuesta en esta tesis, permite obtener árboles de escenarios adecuados para cada modelo MSP.

Adicionalmente, obtuvimos resultados para los modelos MSP usando como datos de entrada los árboles de escenarios. En el caso del modelo MSWBVPP, resolvimos tres casos de estudio correspondiente a tres hipótesis basadas en la participación de una

VPP en los mercados de energía. En el caso del modelo MSOODN, dos casos de prueba fueron resueltos, mostrando que la EDN satisface los límites impuestos para cada caso de prueba, y además, que el caso con BESS da mejores resultados cuando se toma en cuenta el valor la incertidumbre en el modelo. Finalmente, el modelo MSWBVPP fue usado para estudiar el desempeño relativo de los árboles de escenarios FTCA y DTGFBA, específicamente, analizando el valor de la solución estocástica para los 366 problemas de oferta óptima. Para tal fin, una variación del clásico VSS (denominado "Forecasted Value of the Stochastic Solution", FVSS) fue definido y usado junto al clásico VSS.

Contents

List of Figures

List of Tables

List of Abbreviations

A . . . . . Ampere.

ACF . . . . . Auto Correlation Function.

ADF . . . . . Augmented Dickey-Fuller.

AGC . . . . . Automatic Generation Control.

AM . . . . . Adjustment Market.

AMPL . . . . A Mathematical Programming Language.

AR . . . . . Autoregressive.

ARIMA . . . Autoregressive Integrated Moving Average.

ASM . . . . . Ancillary Services Markets.

BESS . . . . . Battery Energy Storage System.

CFI . . . . . Comparative Fit Index.

DER . . . . . Distributed Energy Resource.

DG . . . . . Distributed Generators.

DM . . . . . Day-Ahead Market.

DN . . . . . Distribution Networks.

DSS . . . . . Distribution Substation.

DTGFBA . . Dynamic Tree Generation with Flexible Bushiness Algorithm.

EDN . . . . . Electrical Distribution Networks.

EEV . . . . . Expectation of the Expected Value.

EFV . . . . . Expectation of the Forecasted Value.

EM . . . . . Electricity Markets.

ESD . . . . . Energy Storage Devices.

EV . . . . . Expected Value.

EVPI . . . . . Expected Value of Perfect Information.

EVSS . . . . . Expected Value of the Stochastic Solution.

FEEC . . . . Faculty of Electrical and Computer Engineering.

FSA . . . . . Forward Selection Algorithm.

FTCA . . . . Forward Tree Construction Algorithm.

FV . . . . . Forecasted Value.

FVP . . . . . Forecasted Value Problem.

FVSS . . . . . Forecasted Value of the Stochastic Solution.

GENCO . . . Generation Company.

IB . . . . . Imbalances Settlement.

IEM . . . . . Iberian Electricity Market.

IM . . . . . Intra-day Market.

IMO . . . . . Independent Market Operators.

ISO . . . . . Independent System Operators.

kV . . . . . kilovolt.

kVAr . . . . . Kilo Volt Amperes Reactive or Kilovar.

kW . . . . . kilowatt.

L . . . . . Loads

MAE . . . . . Mean Absolute Error.

MILP . . . . Mixed Integer Linear Programming.

MSLP . . . . Multistage Stochastic Linear Programming.

MSP . . . . . Mulstistage Stochastic Programming.

MSOODN . . Mulstistage Stochastic Optimal Operation of Distribution Networks.

MSWBVPP Mulstistage Stochastic Wind Battery Power Plant.

MTS . . . . . Multivariate Time Series.

MW . . . . . Megawatts.

MWh . . . . . Megawatt hour

NAC . . . . . Non-anticipativity Constraints.

OLTC . . . . On-Load Tap-Charger.

OODN . . . . Optimal Operation of Distribution Networks.

PACF . . . . Partial Auto Correlation Function.

PV . . . . . Photovoltaic.

RM . . . . . Secondary Reserve Market.

RMSE . . . . Root Mean Square Error.

RMSEA . . . Root Mean Square Error of Approximation.

RP . . . . . Recourse Problem.

RS . . . . . Renewable Sources.

RV . . . . . Regulator Voltage.

SAA . . . . . Sample Average Approximation.

SCB . . . . . Switchable Capacitor Bank.

SDDP . . . . Stochastic Dual Dynamic Programming.

SMINP . . . Stochastic Mixed Integer Nonlinear Programming.

SOC . . . . . State of Charge.

SOODN . . . Stochastic Optimal Operation of Distribution Networks.

THCA . . . . Typical Hierarchical Cluster Algorithm.

TSFA . . . . . Time Series Factor Analysis.

UNICAMP . University of Campinas.

VAR . . . . . Vector Autoregression.

VARX . . . . Vector Autoregression with Exogenous Variables.

VDI . . . . . VPP participating in the DM and IM.

VDIR . . . . VPP participating in the DM, IM and RM

VPP . . . . . Virtual Power Plant.

VR . . . . . Voltage Regulator.

VSS . . . . . Value of the Stochastic Solution.

WDI . . . . . a standalone Wind Power Plant bidding to the DM and IM.

WP . . . . . Wind Power.

WPP . . . . . Wind Power Plant.

An advice: study! since the best scientists and philosophers, to learn, they listened to their spirit and their thoughts were put into practice, because the key to success is human thought full of wisdom and understanding.

— *Marlyn Cuadrado (1998)*

1 Introduction

Contents

1.1. Motivation

Given the share of renewables in the energy industry, decision-making involves a high level of uncertainty in the data, which is gradually revealed over time. One way to take into account the uncertainty is through *Multistage Stochastic Programming* (MSP). The term MSP refers to an optimal decision executed for subsequent stages (*multistage*); and different events may occur during these stages (*stochastic*) (Pflug and Pichler, 2014). An MSP can be stated in *nested form* as (Shapiro et al., 2009)

$$\min_{x_0 \in \boldsymbol{\chi}_0} f_0(x_0) + \mathbb{E}\left[\inf_{x_1 \in \boldsymbol{\chi}_1(x_0,\xi_1)} f_1(x_1,\xi_1) + \mathbb{E}\left[\ldots + \mathbb{E}\left[\inf_{x_S \in \boldsymbol{\chi}_S(x_{S-1},\xi_S)} f_S(x_S,\xi_S)\right]\right]\right] \quad (1.1.1)$$

where, $s = 0,\ldots,S$ is the sequence of the data process; $\xi_s \in \mathbb{R}^{m_s}$ is viewed as a *stochastic process*[1]; the decision variables are $x_s \in \mathbb{R}^{n_s}$; and the continuous functions are $f_s : \mathbb{R}^{n_s} \times \mathbb{R}^{m_s} \to \mathbb{R}$. And for $s = 1,\ldots,S$, $\chi_s : \mathbb{R}^{n_{s-1}} \times \mathbb{R}^{m_s} \rightrightarrows \mathbb{R}^{n_s}$ are measurable

[1] A stochastic process is defined as a collection of random variables defined in a common probability space $(\Omega, \mathcal{F}, P)$, where Ω is a sample space, $\mathcal{F}$ is a σ-algebra , and P is a probability measure; and the random variables, indexed by some set $\mathcal{S} = \{0,\ldots,S\}$, all take values in the same mathematical space Ξ , which must be measurable with respect to some σ-algebra Σ (Lamperti, 1977).

closed valued multifunctions[2]. For the first stage, the vector decision ξ_0, the function $f_0 : \mathbb{R}^{n_0} \to \mathbb{R}$, and the set $\chi_0 \subset \mathbb{R}^{n_0}$ are deterministic.

For the formulation (1.1.1), a solution can hardly be found in practice. The usual way to solve this problem is reducing it to a solvable one. This aim can be achieved by, first, approximating the stochastic process (which we will describe as $\{\xi_s\}_{s\in\mathcal{S}}$) through a discrete stochastic process based on *scenario trees*[3] (the main aim is to obtain these scenario trees) and then, second, by defining a formulation related to this approximation.

On the other hand, recent decades have been a notable increase in the use of MSP in renewable energy systems optimization, resulting in applications much more complex and realistic. Also, the progress in numerical methods, software, and computer technologies are offering the possibility to obtain solutions to these applications in short periods of time. As a consequence, the appropriate representation of the stochastic process using scenario trees is crucial for this context. Scenario trees are the basic data structure for the MSP problems, and they serve as a tool for us to develop and represent uncertainty in the applications that we develop here. Accordingly, the present study attempt to answer the following main question:

Is it possible to generate scenario trees which are a good representation of the uncertainty for renewable energy systems optimization?

In order to answer this question, we propose to develop a methodology which allows generating scenario trees, beginning with the available data and using it to obtain the scenario trees. This has two phases: In the first phase, scenarios are generated and are then used to obtain a first approximation of the stochastic process, which may be either a initial tree-structure or a fan of scenarios. To do this, the characterization of the random parameters is first defined. Thereafter, the statistical models are determined. We used Time Series Factor Analysis (TSFA), which was developed by Gilbert et al. (2005) to reduce the high dimensionality of the data. We also use the Vector Autoregressive (VAR) model developed by (Sims, 1980) as a technique to determine the statistical models for each random parameter. Subsequently, we integrate these two techniques to calculate the predictions of the next day for each random parameter. Finally, scenarios are generated based on bootstrapping techniques, and the initial discrete stochastic process is defined by either a initial tree-structure or a fan of scenarios. This procedure is similar to that developed in Muñoz et al. (2013). In the second phase, we build an approximation of the stochastic process by using a scenario tree obtained from algorithms. The first algorithm is the Forward Tree Construction Algorithm (FTCA)

[2] See Appendix A for the basic probability theory.
[3] A scenario tree is an approximated discretized representation of the uncertainty in the data (Kaut, 2003).

developed by Heitsch and Römisch (2009a); and the second algorithm is an adapted version of Dynamic Tree Generation with Flexible Bushiness Algorithm (DTGFBA) developed by Pflug and Pichler (2015).

Additionally, the object of this study is given by two MSP models developing in this thesis: The first model is the Multistage Stochastic Wind Battery Virtual Power Plant model (MSWBVPP model) optimizes participation in the EM (Day-Ahead Market (DM), Intra-day Market (IM) and Secondary Reserve Market (RM)) considering the Imbalance Settlements (IB), of a Virtual Power Plant[4] (VPP), which comprises a Wind Power Plant[5] (WPP) and Battery Energy Storage System (BESS). The second model is the Multistage Stochastic Optimal Operation of Distribution Networks model (MSOODN model), which seeks to optimize the operation of EDN while considering BESS, such that it minimizes the total cost of energy purchased from the Distribution Substation (DSS) and the dispatchable Distributed Generators (DG). Scenario trees need to be built to represent the uncertainty (which, in these cases, will be represented by EM prices, Wind Power (WP) generation, power load and Photovoltaic (PV) generation) for the previous models and for founding optimal solutions. This is the crucial objective of this thesis. We have run extensive computational experiments in order to obtain different configurations of the scenario trees based on real data. These experiments were also used to obtain optimal solutions for each MSP model. Finally, to evaluate the performance of the scenario trees, we define parameters based on the defined bounds for the optimal values of the objective functions in our MSP models, which were inspired by Escudero et al. (2007).

1.2. Objectives

The main objectives of this thesis are as follows:

(i) To develop a literature review of the approaches for generating scenario trees for renewable energy systems optimization. This objective includes the selection of some algorithms for its implementation.

(ii) To develop a scenario tree generation methodology based on forecast models, bootstrapping techniques and the algorithms selected in objective (i) to obtain scenario trees for renewable energy systems optimization.

[4] A VPP is a cluster of dispersed generator units, controllable loads and storage systems, all of which are aggregated in order to operate as a single power plant (Lombardi et al., 2009).

[5] A wind farm is also called a wind park, wind power station or Wind Power Plant (WPP) (Gasch and Twele, 2011).

(iii) To develop appropriated MSP models in renewable energy systems optimization. This objective includes defining the uncertainty and decision process associated with these models.

(iv) To obtain scenario trees by implementing the algorithms developed in objective (ii) for the MSP models developed in objective (iii).

(v) To obtain computational results for the MSP models developed in objective (iii) and to compare the performance of the scenario trees obtained in objective (iv).

1.3. Contributions

There are three main contributions of this thesis.

- In Section 3.3, a methodology for generating scenario trees has been designed. This methodology was developed to generate scenario trees for the MSWBVPP model, but also, its use has been demonstrated in the scenario trees generation for the MSOODN model. This fact prove that the methodology can be used to generate scenario trees for renewable energy systems optimization.
- In Section 3.4, parameters for studying the relative performance of previous scenario trees presented has been developed. These parameters allow a comparison of the scenario trees and determining which tree (or set of trees) provides the best stochastic solution of a model. This comparison is given by the best stochastic solution and the value of the deterministic solution when using the forecasted values of the random variables.
- Two novel MSP models for the renewable energy systems optimization presented in Sections 4.1.3 and 4.2.3 have been formulated: the first model is the MSWBVPP model for the optimal participation of a VPP-BESS, considering all the sessions together with the elements already contemplated DM, RM and IB. And the second model is a formulation for the optimal operation of a radial EDN composed of a DSS, SCB, loads, RS and BESS, called the MSOODN model. Different case studies were solved in order to obtain optimal solutions for each one of these models.

1.4. Structure

This thesis is organized as follows.

- Chapter 2 provides an extensive literature review of the generation of scenario trees. It presents literature reviews first of the general framework, then in regard to the energy industry and, finally, a specific literature review relating to the generation of scenario trees for each model developed in this thesis.
- Chapter 3 introduces the concepts and theoretical foundations needed to contextualize the thesis framework. Firstly, this chapter gives a formal definition for the scenario trees and some associated concepts. Also, it presents MSP formulations in the context of scenario trees. Then it describes the methodology used to generate them, namely by showing the theoretical foundations for the procedure that generates a set of scenarios that are then used for generating scenarios trees, followed by a presentation of the algorithms implemented and the theoretical foundations for generating the trees. Finally, the chapter presents the proposed parameters for evaluating the performance of the trees obtained.
- Chapter 4 presents the scenario tree structure for the models that have been developed in this work. For each model, this chapter introduces the problem addressed. After that, the chapter presents a study of the uncertainty that governs the problem, the decision process defined for this problem, and the scenario tree structure. Finally, the chapter ends by presenting an MSP model for each problem addressed in this thesis.
- Chapter 5 reports the computational results from generating scenario trees based on real data from the Iberian Electricity Market and Naturgy. The trees generated are used as input data for resolving the MSWBVPP model developed in Chapter 4 and which thus obtained the optimal participation of a VPP in an EM. These trees are used as input in the MSWBVPP model. Then, based on these model result, the quality of these scenario trees are evaluated by the parameters developed in this thesis.
- Chapter 6 reports the computational results from generating scenario trees based on real data from an actual photovoltaic power plant and distribution plant in Brazil. The trees generated are used as input data to resolve the MSOODN model developed in Chapter 4. These results are based on the work developed during my pre-doctoral stay in the Faculty of Electrical and Computer Engineering (FEEC) at the University of Campinas (UNICAMP) in the state of Sao Paulo.
- Chapter 7 presents the conclusions and discuses future directions for this work.
- The appendices provides complementary information for a better understanding of this thesis.

Research is to see what everybody else has seen,
and to think what nobody else has thought.

— *Albert Szent-Gyorgyi*

2 Literature Review

Contents

This literature review is divided into four sections. Section 2.1 reviews the approaches to generating scenario trees that are commonly used in the existing literature, specifically in multistage optimization. Section 2.2 takes a general point of view to compile the different approaches to generating scenario trees that the literature proposes for representing uncertainty in Multistage Stochastic Programming (MSP) models used in the field of renewable energy system optimization, specifically in Electricity Markets (EM) and Electrical Distribution Networks (EDN). Sections 2.3 and 2.4, review the most specific literature on generating scenario trees in the study areas addressed by this thesis: EM (Section 2.3) and EDN (Section 2.4).

2.1. Scenario Trees for MSP Models

In the context of MSP models, scenarios have to satisfy certain constraints known as *non-anticipativity conditions*. Such constraints can lead to the tree-structured scenarios that are commonly known as *scenario trees*. In accordance with the definition given by Pflug and Pichler (2014), *scenario trees are circle-free directed graphs with a single root, for which the distance of all leaves are at the same level; to each node, a k-vector of values is assigned and to the leaf nodes probabilities are assigned such that the leaf nodes can be seen as a discrete probability space.* To our knowledge, the term "scenario

tree" in the context of MSP was first used in Kall et al. (1976) to represent a random vector (uncertainty) through a set of realizations and its corresponding probabilities by generating a finite discrete distribution for a Multistage Stochastic Linear Programming (MSLP) model. The use of the scenario trees continues to be developed by different authors, both in theory and in applications. Among the theoretical references, we can find: Dupačová et al. (2000); Heitsch and Römisch (2003); Shapiro et al. (2009); Pflug and Pichler (2014). The most cited references for most cited for developed applications are: Escudero et al. (1993); Pflug (2001); Growe-Kuska et al. (2003); Pallottino et al. (2005); Latorre et al. (2007); Xu et al. (2015). Nowadays, generating scenario trees for MSP problems constitutes a great theoretical and computational challenge in this area of research.

Currently, several approaches are used to generate scenario trees for the representation of uncertainty in MSP models. They are based on different principles: (i) bound-based construction (Frauendorfer, 1996; Kuhn, 2006); (ii) conditional random sampling (Dempster, 2006; Kouwenberg, 2001; Shapiro et al., 2009) and Quasi-Monte Carlo sampling (Pennanen, 2009); (iii) optimization methods based on the moment-matching principle (Høyland and Wallace, 2001; Gülpınar et al., 2004); and (iv) probability metric-based approximations (Heitsch and Römisch, 2011; Pflug and Pichler, 2015). More details of some of the recent works for each principle are shown. Approach (i) attempts to construct two discrete probability measures such that the optimal values of the associated approximate problems represent, respectively, upper and lower bounds for the optimal value of the original stochastic programs. In this context, Frauendorfer (1996) developed a work related to the approximation of convex MSP in which the future uncertainty was modeled as a probability space with a known joint probability distribution; and, from that, sequences of barycentric scenario trees were derived for minorizing and majoring the given problem. Later, Kuhn (2006) investigated this approach in a more general setting for convex MSP. As the name suggests regarding the conditional random sampling approach in (ii), it utilizes conditional sampling schemes and leads to a large number of (pseudo-) random number generators, called conditional distributions. Dempster (2006) took a comprehensive approach to Expected Value of Perfect Information (EVPI) based sequential importance sampling algorithms for dynamic (multistage) stochastic programming problems. Kouwenberg (2001) developed and tested a scenario generation method based on random sampling, an adjusted random sampling approach and the tree-fitting method. Shapiro (2003) presented the Sample Average Approximation (SAA) for MSP problems. This method approximates an MSP model through an explicit function, which is defined as an SAA problem in which estimates of the values are obtained by conditional sampling. Later, Pennanen (2009) developed a general procedure for generating scenario trees by approximating each random variable using Quasi-Monte Carlo sampling. Regarding approach (iii),

this is based on the resolution of programming models that generate a limit number of discrete solutions for satisfying certain statistical properties. The idea is to minimize any measurement that is based on the statistical properties of the results and those specified a priori. Høyland and Wallace (2001) developed an algorithm that produces a consistent and discrete joint distribution with specified values for the first four marginal moments. Their algorithm also produces the correlations for the stochastic programming model. The distribution is constructed by decomposing the multivariate problems into univariate ones using an iterative procedure that combines simulation, Cholesky decomposition, and various transformations. This procedure provides correct correlation without changing the marginal moments. And Gülpınar et al. (2004) developed an optimization method that generates a number of discrete outcomes for satisfying specified statistical properties. The outcomes are obtained by resolving either a sequence of nonlinear optimization models (one at each node of the scenario tree) or one large optimization problem. In this hybrid approach, the optimization problem is reduced in size by the values of the price variables obtained through simulation. Finally, approach (iv) is based on probability distances that are relevant to the stability of MSP. Heitsch and Römisch (2011) broadened the theoretical foundations of generating scenario trees through their study of stability analysis. Numerical experiences were conducted in order to represent the uncertainty of MSP problems by constructing different scenario trees configurations based on demand and price data. And Pflug and Pichler (2015) developed new MPS algorithms for the dynamic generation of scenario trees. The different methods described are based on random vectors, which are drawn from past conditional distributions, and on sample trajectories. The tree structure is not determined beforehand but is instead dynamically adapted in order to meet a distance criterion, which measures the quality of the approximation.

Based on the literature review previously presented, the approach that we are going to select for generating scenario trees in MSP models will be defined by the approach most used in renewable energy systems optimization. The following section shows the literature review into this sense.

2.2. Scenario Trees for Renewable Energy Systems Optimization

Nowadays, there are lots of problems that involve decisions under conditions of uncertainty. In our particular case of a given MSP formulation, our main objective is to represent this uncertainty with scenario trees and use then to obtain optimal results from the MSP models. Table 2.2.1 shows the last two decades' most relevant works about generating scenario trees for MSP in the energy industry. First, the references

are shown (first column). In the second column, the applications for each reference are given. The third column shows the uncertainty, which is equivalent to the random parameter, namely: demand; prices (day-ahead, intra-day, balancing, adjustment, real-time); and renewable supply (wind speed, wind power). The fourth column presents the information with respect to the stages and number of scenarios for the scenario trees of each application. The maximum number of stages and scenarios was 28 and 2500, respectively. Finally, the fifth column shows the approach developed and/or used in each one of the references. The selection of the approach that we are going to use for the generation of scenario trees is defined through the approach most utilized in this literature review. Table 2.2.1 shows that the most used approach is (iv), which we described in Section 2.1. This approach was used in the following works: (a) Plazas et al. (2005) modeled the uncertainty with an asymmetric scenario tree (Gröwe-Kuska et al., 2002) then used a technique for reducing the number of scenarios (Heitsch and Römisch, 2003). (b) Kumbartzky et al. (2017) represented the information structure of MSP models using a scenario tree. They performed a sampling strategy for generating scenarios and developed another strategy for reducing these scenarios similarly to Boomsma et al. (2014). For the reduction of scenarios, they applied the forward selection algorithm developed by Heitsch and Römisch (2009a, 2011). (c) Heredia et al. (2018) presented an MSP model for optimizing the participation of a Virtual Power Plant (VPP) (comprising a Wind Power Plant (WPP) and a Battery Energy Storage System (BESS)) in the EM (Day-Ahead Market (DM), first Intra-day Market session (IM1) and Secondary Reserve Market (RM)) and the imbalance settlement. The uncertainty in this problem was represented by a scenario tree with 28 stages and 83 scenarios consisting of electric energy prices and wind power generation. The Forward Tree Construction Algorithm (FTCA) developed in Heitsch and Römisch (2009a) was used to construct the scenario tree.

Based on this review, one of the algorithms that we are going to use to construct the scenario trees in this thesis is the FTCA developed by Heitsch and Römisch (2009a). This algorithm is based on techniques of recursive scenario reduction and bundling steps, and it was developed chronologically in Dupačová et al. (2003); Heitsch and Römisch (2003); Heitsch and Romisch (2005); Heitsch and Römisch (2009a,b, 2010, 2011). For our purposes, we are going to use the FTCA and Forward Selection Algorithm (FSA) presented in Heitsch and Römisch (2009a). Another recently developed and important algorithm we will use for generating scenario trees is the Dynamic Tree Generation with Flexible Bushiness Algorithm (DTGFBA) for MSP, developed by Pflug and Pichler (2014, 2015). Currently, This algorithm has been used in applications for energy production (Pflug and Pichler, 2014). In this thesis, we are going to develop a version of DTGFBA for generating scenario trees for renewable energy systems optimization.

Reference	Application	Uncertainty	Stages and Scenarios	Approaches
Singh and Mason (2004)	Capacity-expansion planning of electricity distribution networks	Demand	2–6 stages and 2–32 scenarios	Binary scenario tree with prefixed structure
Plazas et al. (2005)	Multimarket optimal bidding for a power producer	Day-ahead spot prices, automatic generation control and balancing market prices	3 stages and 2500 scenarios	A symmetric scenario tree and scenario reduction technique
Triki et al. (2005)	Capacity allocation in multi-auction electricity markets	Day-ahead spot prices, adjustment and balancing clearing prices	3 stages and 32–192 scenarios	Their own scenario tree
Musmanno et al. (2009)	Operation of a producer in a multi-auction electricity market	Clearing prices	4 stages and 300 scenarios	Means of a scenario tree
Morales et al. (2010)	Offering strategy for a wind power producer in an electricity market	Wind speed and day-ahead, adjustment, and balancing market prices	3 stages and 10000 scenarios	A symmetric scenario tree specifically built as a defined procedure
Lorca and Prina (2014)	Medium term power portfolio optimization for a power producer in a competitive electricity market	Market prices and customer demand	6 stages and 128 scenarios	Method based on moment-matching principle
Boomsma et al. (2014)	Bidding in sequential electricity markets	Spot and balancing prices	26 stages and 500 scenarios	Alternately sampling (with stage-wise scenario generation) and reducing (with the k-medoids clustering algorithm) scenarios
Del Granado et al. (2016)	Valuation of distributed electricity storage	Wind power	5 stages and 81 scenarios	Univariate stochastic process
Kumbartzky et al. (2017)	Bidding in a pay-as-bid market	Spot price	3 stages and $5n^{d-1}$, $n = 2{,}1$, $d = 2, ..., 5$ scenarios	Alternately sampling and reducing (with the forward selection algorithm) scenarios
Fatouros et al. (2017)	Optimal operation of Distributed Energy Resource (DER) aggregators	Wind power	6 stages and 1–243 scenarios	Algorithms for reducing scenarios and building scenario trees, developed by Growe-Kuska et al. (2003)
Laur et al. (2018)	The operational issues faced by emerging distribution system operators	Day-ahead, intra-day and real-time prices, demand and generation	3 stages and 81 scenarios	Scenario tree with prefixed structure
Bhattacharya et al. (2018)	Managing energy storage in microgrids	Demand, renewable supply and prices	25 stages and 50–250 scenarios	Sampling procedure for mutually independent random variables
Heredia et al. (2018)	Participation in the EM of WPP with BESS	Markets prices and wind power	28 stages and 83 scenarios	The FTCA
Hafiz et al. (2019)	Energy management and optimal storage sizing for a shared community	Solar generation and electricity demand	1441 stages and 100 scenarios	A similar procedure to that described in Infanger and Morton (1996)
Shang et al. (2020)	Optimizing the maintenance schedules in active Distribution Networks	Wind speed and solar irradiation	3 stages and 6 scenarios	Scenario tree with prefixed structure

Cuadro 2.2.1: Scenario trees for renewable energy systems optimization.

We will present a review of the latest research about scenario tree generation on each study area of this thesis. Two study areas will be the focus of this study. The first area is the EM, specifically, the optimization of EM operation with the presence of renewables. The second area is the EDN, about the optimal operation of EDN with renewables. More details are provided in the following sections.

2.3. Scenario Trees for EM Optimization with Renewables

As mentioned previously, one of the objectives of this thesis is to use scenario trees to represent uncertainty in MSP models that are applied to optimal participation of an EM producer. Based on the literature review, the scenario trees have been used in several works in recent years. Plazas et al. (2005) considered a profit-maximizing thermal producer that participates in three spot markets (day-ahead, Automatic Generation Control (AGC) and balancing markets). In this case, the uncertainty was provided by prices in the day-ahead, AGC, and balancing market. For the characterization of the scenarios, seasonal Autoregressive Integrated Moving Average (ARIMA) models were employed. For the approximation of the stochastic process, a symmetric scenario tree was used. The scenario reduction technique was applied to the stages and then to the resulting tree. For this case, the scenario tree had 3 stages and 2500 scenarios. Musmanno et al. (2009) presented an MSP model of a decision problem for a Generation Company (GENCO) operating in a multi-auction electricity market. The uncertainty was modeled by means of a scenario tree with 4 stages (including the root), while the random variables that were considered are prices in: (a) the day-ahead market, (b) the Adjustment Market (AM), and (c) the Ancillary Services Markets (ASM). The scenario tree had 4 stages and 300 scenarios. Boomsma et al. (2014) focused on bidding in the sequential EM (DM and the hour-ahead balancing market) of a Nordic power producer. In both markets, clearing prices and dispatched volumes were unknown, and the bidding problem was formulated as an MSP. Scenario fans[1] were given for each market and were reduced using a *k-medoids* clustering algorithm. For this case, the scenario tree had 26 stages and 500 scenarios. These works justify the use of the scenario trees in MSP, although the producers considered do not have to deal with additional conditions such as the "non-dispatchability" and uncertainty that govern the availability of wind and/or solar power.

[1] A tree for which every internal node except possibly the root has only one successor is called a fan (Pflug and Pichler, 2016).

An example of a producer that considers these conditions is shown in Morales et al. (2010). They presented the best bid strategy of a Wind Power (WP) producer in an EM. This problem was formulated as an MSP model in which each stage was a market. The uncertainty was governed by the wind availability and the hourly prices of: a DM, the adjustment markets and balancing energy. The characterization of the uncertainty was studied by ARIMA models, and, later a symmetric scenario tree was obtained through a defined procedure. Finally, a fast-forward reduction algorithm (as described in Heitsch and Römisch (2003)) was used to reduce the scenario tree. For that case, the scenario tree had 3 stages and 10^6 scenarios, which were reduced to 10000 scenarios. Related to Imbalance Settlements (IB), (Heredia et al., 2015) developed an MSP model for the optimal participation of a VPP in three different electricity markets: DM, first IM session and RM. The following factors were taken into account: the producer was a VPP composed of WP and BESS; the profitability of private investment in storage units had been analyzed and demonstrated in Akhavan-Hejazi and Mohsenian-Rad (2013); the economic feasibility of investing in BESS could be guaranteed only if the VPP participated in some ancillary services (Heredia et al., 2015); and regulation services were supported by the technical feasibility of a VPP. The uncertainty was base on the historical data of electricity prices, wind power, and imbalance settlement prices. The FTCA was used to obtain a scenario tree with 28 stages and 100 scenarios, which were reduced to 83 scenarios.

The objective of this thesis, in a more general sense, is to formulate an MSP model, to optimize VPP participation in an EM considering all intra-day markets. In order to mitigate the uncertainty in the model, we will generate scenario trees through a procedure based on forecasting and bootstrapping techniques. We will also use set of scenarios and scenario tree construction algorithms. Additionally, we will develop a process for evaluating of the quality of scenario trees.

2.4. Scenario Trees for EDN Optimization with Renewables

The Optimal Operation of Distribution Networks (OODN) problem consists of minimizing the total purchase cost of energy from the Distribution Substation (DSS) and the dispatchable Distributed Generators (DG) over a predetermined period of time, and it is subject to a set of decision variables (Ali, 2013). In this case, the uncertainty occurs in the prices of energy from the dispatchable DG, the prices of energy from the DSS, and in the active/reactive power load. Additionally, when the Renewable Sources (RS) are considered, the energy storage devices (ESD) are increasingly considered to be a means for mitigating challenges introduced by the integration of RS in the

Distribution Network (DN). In this case, new uncertainty enters into the problem and this is associated with the active power generation of non-dispatchable RS. Considering these uncertainties in an optimization model increases the complexity of the problem, which leads to formulating models that are much more difficult to solve and to the need for sophisticated techniques that approximate the stochastic process governing the problem. This thesis is focused on this last point, which is a topic that has taken on more importance in the past decade. To describe these uncertainties and their influence on the OODN, an MSP model can be formulated together with a scenario tree to represent the uncertainty. To date, no study has used an MSP model based on scenario trees for representing uncertainty in the OODN. However, some slightly related works have been published recently. Fatouros et al. (2017) resolved a multi-stage stochastic problem with recourse for the operation of DER aggregators. They propose a novel Stochastic Dual Dynamic Programming (SDDP) approach that captures the temporal dependency of uncertain wind power output, specifically by the integration of an n-order Autoregressive (AR) model. Although the solution strategy does not use scenario trees, this solution was compared with the results obtained from 6 MSP models that represent the uncertainty with different scenario trees that were obtained through a scenario reduction process based on Kantorovich distance Growe-Kuska et al. (2003). The defined scenario trees had 6 stages and from 1 to 243 scenarios. Another work by Bhattacharya et al. (2018) presents an MSP model for managing energy storage in microgrids. This work presents a tree-like network of interconnected buses and power lines emanating from a reference bus (the feeder), which is connected to the main grid. The feeder is often connected to a distribution substation and delivers power procured from the main grid to other microgrid buses. Some or all of those buses have access to distributed storage systems. The operators use both distributed generation (e.g., wind and/or solar), and electricity procured from the main grid to satisfy the net demand and power flow constraints in each stage of the planning horizon. The uncertainty pertains to demand, renewable supply and prices, all of which are modeled as random variables represented in a finite scenario tree. The samples were built from a multivariate truncated normal distribution in which each marginal distribution is also truncated normal. A 25-stage scenario tree was generated for this work. Hafiz et al. (2019) proposed an MSP model for new energy management and storage sizing in the framework of a community composed of multiple houses and distributed solar generation. In this case, the uncertainty represented by the solar Photovoltaic (PV) generation and electricity demand was sampled from probability distributions, which were defined using information based on existent data. It then constructed a sampled scenario tree with different scenarios similar to the procedure described in Infanger and Morton (1996). The test system considered a tree with 1441 stages and 100 scenarios. Finally, Shang et al. (2020) formulated a Stochastic Mixed Integer Nonlinear Programming

model (SMINP) for optimizing the maintenance schedules in active DN. In this case, the uncertainties of DER and the post-outage operation strategies of switching devices are incorporated into the model. In the tree search procedure, an SAA technique is developed for considering uncertainties when estimating the multistage maintenance costs. The scenario tree defined in this work assumed 6 scenarios over 2 stages.

Based on this literature review, we will formulate a novel MSP model that considers energy storage devices for the OODN, where an EDN has Voltage Regulators (VR), Switchable Capacitor Bank (CB), and dispatchable DG. Furthermore, our methodology for resolving the MSP model is innovative because the strategy first defines the scenario trees through construction and reduction techniques, then resolves the optimization model in which the uncertainty serves as input to a scenario tree input. In addition, we are able to obtain scenario trees that better represent the stochastic process governing the problem, due to the possibility of obtaining scenario trees with high dimensionality.

True optimization is the revolutionary contribution of modern research to decision processes.

— *George Dantzig*

3

Scenario Trees for MSP Models

Contents

Multistage Stochastic Programming (MSP) is used to formulate and solve decision problems with uncertain data modeled as a stochastic process. Defining a good representation of the stochastic process is a crucially relevant aspect and the focus of this thesis. The starting point is the fact that historical data is accessible and allows generating scenarios using statistical models, one-step-ahead forecasting and bootstrapping, all of which represent the stochastic process in scenario trees. The final step in this procedure is to evaluate the quality of the obtained scenario trees by defining quality parameters. This chapter is organized as follows. Section 3.1 and Section 3.2, respectively, present a formal definition of scenario trees and the MSP formulations. Section 3.3 presents the scenario tree generation methodology developed in this thesis. Finally, Section 3.4 describes the theoretical development underlying how we evaluate the performance of the obtained scenario trees.

3.1. Formal Definition of Scenario Trees

When the stochastic process has infinite support, the associated MSP model is an infinite-dimensional optimization problem and the solution can hardly be found in practice. Nevertheless, if the stochastic process is approached by a discrete process with

finite support, then the MSP model can be equivalent to a deterministic mathematical model that can be solved with efficient solvers. A discrete stochastic process can be represented by the *scenario tree*, which is a way to model stochastic processes as a discretized probability distribution. Mathematically speaking, a scenario tree is a circle-free directed graph with a single root, for which the distance of all leaves (i.e., nodes with no outgoing edges) are at the same level; a vector of values is assigned to each node; and probabilities are assigned to the leaf nodes such that the leaf nodes can be seen as a discrete probability space (Pflug and Pichler, 2014).

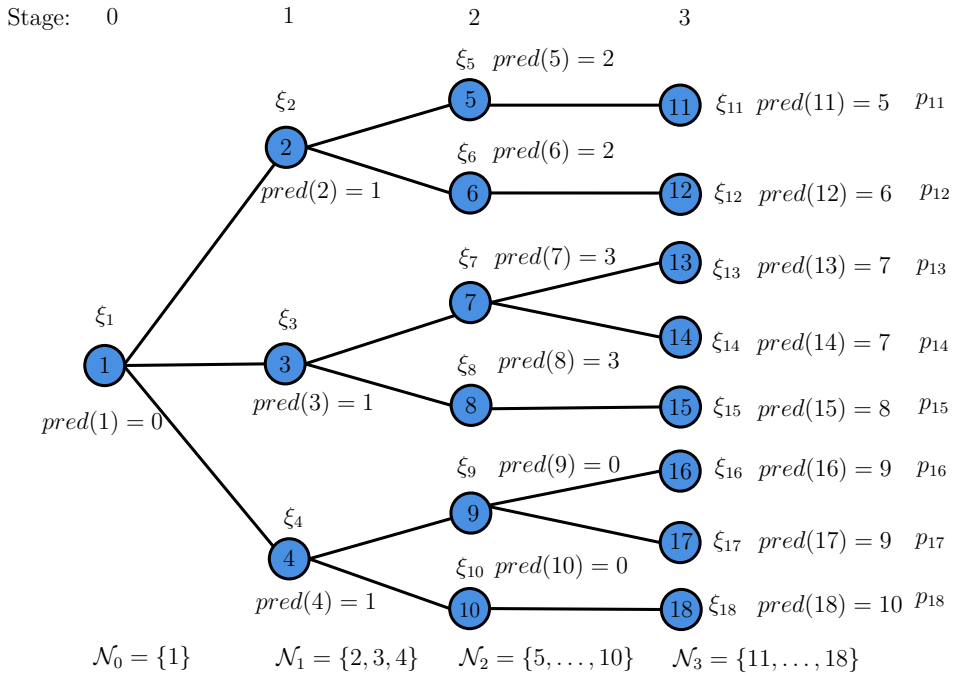

Figura 3.1.1: Illustration of a scenario tree.

However, one may always take a single representative of a class and assign labels or numbers to the nodes. One way consists of defining a node set $\mathcal{N} = \{1, \ldots, N\}$ (where 1 is the root), and then to each node $n \in \mathcal{N}$ (except the root) establish a predecessor $pred(n)$ and a stage s, which is its distance from the root (this is defined as the stage of the node $n \in \mathcal{N}$). Let $\mathcal{S} = \{0, \ldots, S\}$ be the set of stages; then we can dissect the set $\mathcal{N}$ at each stage $\mathcal{N}_s$, such that (cf. Figure 3.1.1):

- $\mathcal{N}_0 = 1$ is the root node,
- $\mathcal{N}_S$ are the leaves, and
- $\mathcal{N}_1, \mathcal{N}_2, \ldots, \mathcal{N}_{S-1}$ are the inner nodes (the complement set of the leaves).

For all nodes $n \in \mathcal{N}_s$, $pred(n) \in \mathcal{N}_{s-1}$ such that $s \in \mathcal{S}$. For example, for $n = 5 \in \mathcal{N}_2$ then $pred(5) = 2 \in \mathcal{N}_1$ (cf. Figure 3.1.1). While $pred(n)$ represents the immediate

predecessor, one may also define the predecessor of a node at each earlier stage. For $n \in \mathcal{N}_s$ and $s' < s$, we have

$$pred_{s'}(n) = m,$$

where $m \in \mathcal{N}_s$, such that $m = pred(pred(\ldots pred(n)\ldots))$, and this predecessor mapping satisfies the relationship $pred_{s'}(pred_s(\cdot)) = pred_s(\cdot)$ for $s^{'} < s$, and $pred_0(\cdot) = 1$ is identical to the root. We can also denote the direct predecessor of a node n by $-n$, and the set of all direct successors by $n+$. If a node n is any successor (direct or not) of node m, we write $m \prec n$ (or $n \prec m$). Thus:

$$m \prec n \text{ is equivalent to: there exist a } s \text{ such that } m = pred_s(n).$$

Alternatively, one may begin with a probability space $(\Omega, \mathcal{F}, P)$ in which mappings are defined in the following way:

$$\begin{aligned} pred &: \Omega \to \Omega_{S-1}, \\ pred &: \Omega_{S-1} \to \Omega_{S-2}, \\ &\vdots \\ pred &: \Omega_1 \to \Omega_0. \end{aligned}$$

It is required that all spaces $\Omega = \Omega_S, \Omega_{S-1}, \ldots, \Omega_0$ are distinct and that the mappings *pred* are all different, since they are defined in different spaces, where Ω_0 is required as a singleton. Let the compositions $pred_s$ be defined as

$$pred_s = pred \circ \ldots \circ pred : \Omega \to \Omega_{S-s}. \tag{3.1.1}$$

Let $\mathcal{F}_s$ be the $\sigma-$algebra generated by $pred_s$. The sequence of $\sigma-$algebra $\mathcal{F}_s$ is a filtration $\mathcal{F} = (\mathcal{F}_0, \ldots, \mathcal{F}_{\mathcal{S}})$, with $\mathcal{F}_0 = \{\emptyset, \Omega\}$ being the trivial $\sigma-$algebra, since Ω_0 is a singleton and $\mathcal{F}_S$ is the power set of Ω. If Ω is finite, it may be identified by the leaf set $\mathcal{N}_s$ of the tree, and the sets Ω_t may be identified with the node sets $\mathcal{N}_s$ at the respective stage s.

Definition 3.1.1 (*Tree Process*)**.** A *tree process* is a stochastic process (v_s), $s \in \mathcal{S}$ with values in some state space $\mathcal{N}_s$, $s \in \mathcal{S}$, where the $\mathcal{N}_s$ are pairwise disjoint and $\mathcal{N}_0$ is a singleton if the generated $\sigma-$algebras $\omega(v_s)$ for all $s \in \mathcal{S}$ satisfy

$$\sigma(v_s) = \sigma(v_0, \ldots, v_s). \tag{3.1.2}$$

The tree process induces a probability distribution P on $\mathcal{N}_s$, and the image space $\mathcal{N}_S$ may be introduced as the basic probability space. Then, we do not lose the generality $\Omega = \mathcal{N}_S$. The generated sigma algebras $\mathcal{F}_s := \sigma(v_s)$ form a filtration $\mathcal{F} = (\mathcal{F}_0, \ldots, \mathcal{F}_\mathcal{S})$, which is evident from Equation (3.1.2).

Another equivalent description that is important to mention is the leaf-path correspondence. This means that the leaves of a tree uniquely determine the paths, which lead from the root to the leaf nodes. As a tree represents a probability space with a filtration structure $\mathcal{F}$, and the elements of Ω are renamed as $1, \ldots, |\Omega|$, then the following correspondence can be used.

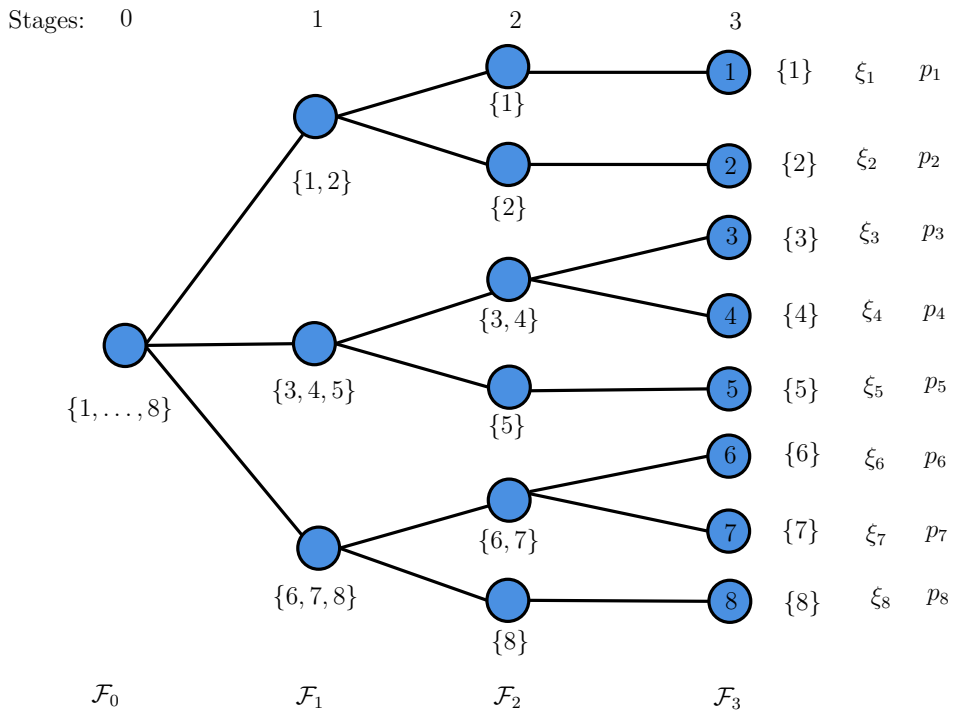

Figura 3.1.2: Illustration of a scenario tree in the leaf-path correspondence form.

In addition, the process $\{\xi_s\}_{s\in\mathcal{S}}$ takes the values ξ_ω for all ω with probability p_ω; thus, they induce a distribution on the filtered probability space $\mathbb{R}^{m_0} \times \mathbb{R}^{m_1} \times \ldots \times \mathbb{R}^{m_S}$ with filtration $(\mathcal{F}_0, \ldots, \mathcal{F}_S)$. This stochastic process is represented by$\{\{\xi_{s\omega}\}_{s\in\mathcal{S}}\}_{\omega\in\Omega}$, where a *scenario* is an outcome of the random process. The induced filtration can be represented in a tree form, the so-called scenario tree. The corresponding scenario values are $(\xi_{0\omega}, \ldots, \xi_{s\omega})$ for $s \in \mathcal{S}$ and $\omega \in \Omega$. Assuming a deterministic first stage (only in root node), then $\xi_\omega = (\xi_0, \xi_{1\omega}, \ldots, \xi_{S\omega})$, $\omega \in \Omega$. A scenario defines the edges in the tree, implying that $(\xi_{0\omega}, \ldots, \xi_{s\omega}, \xi_{s+1\omega})$ is an ancestor of node $(\xi_{0\omega}, \ldots, \xi_{s\omega})$, $s = 1, \ldots, S-1$. The leaf nodes of the scenario tree correspond to the scenarios themselves (having assumed that $\mathcal{F}_S = \mathcal{F}$). An example of a scenario tree is displayed in Figure 3.1.2. It has 18 nodes and 8 leaves, with the nodes being enumerated from 1 to 18. This tree has

4 stages and represents a probability space Ω with a filtration $\mathcal{F}$. The elements of Ω are the leaves ($\Omega = \mathcal{N}_3$), which can be renamed $1, \ldots, 8$, that is, $\Omega = \{1, 2, 3, 4, 5, 6, 7, 8\}$.

The leaves determine the entire root path; therefore, it makes sense to use the following correspondence:

ω	Path
1	corresponds to the path (1,2,5,11)
2	corresponds to the path (1,2,6,12)
3	corresponds to the path (1,3,7,13)
4	corresponds to the path (1,3,7,14)
5	corresponds to the path (1,3,8,15)
6	corresponds to the path (1,4,9,16)
7	corresponds to the path (1,4,9,17)
8	corresponds to the path (1,4,10,18)

The filtration $\mathcal{F} = (\mathcal{F}_0, \ldots, \mathcal{F}_S)$ consists of the $\sigma-$algebra sequence generated by the sets:

$$\begin{aligned}
\mathcal{F}_0 &= \sigma(\{1, \ldots, 8\}) = \{\emptyset, \Omega\}, \\
\mathcal{F}_1 &= \sigma(\{1, 2\}, \{3, 4, 5\}, \{6, 7, 8\}), \\
\mathcal{F}_2 &= \sigma(\{1\}, \{2\}, \{3, 4\}, \{5\}, \{6, 7\}, \{8\}), \\
\mathcal{F}_3 &= \sigma(\{1\}, \{2\}, \{3\}, \{4\}, \{5\}, \{6\}, \{7\}, \{8\}).
\end{aligned}$$

As the stochastic process $\{\xi_\omega\}_{\omega \in \Omega}$ is adapted to the filtration $\mathcal{F}$, the scenarios and probabilities of the tree become:

ω	Scenario	Probability
1	$\xi_1 = (\xi_0, \xi_{11}, \xi_{21}, \xi_{31})$	p_1
2	$\xi_2 = (\xi_0, \xi_{12}, \xi_{22}, \xi_{32})$	p_2
3	$\xi_3 = (\xi_0, \xi_{13}, \xi_{23}, \xi_{33})$	p_3
4	$\xi_4 = (\xi_0, \xi_{14}, \xi_{24}, \xi_{34})$	p_4
5	$\xi_5 = (\xi_0, \xi_{15}, \xi_{25}, \xi_{35})$	p_5
6	$\xi_6 = (\xi_0, \xi_{16}, \xi_{26}, \xi_{36})$	p_6
7	$\xi_7 = (\xi_0, \xi_{17}, \xi_{27}, \xi_{37})$	p_7
8	$\xi_8 = (\xi_0, \xi_{18}, \xi_{28}, \xi_{38})$	p_8

The scenario trees are a distinctive representation of the random process in MSP. The next section presents the MSP formulations and their corresponding relationships with the scenario trees.

3.2. MSP Formulations

The concepts and formulations for the MSP shown in this section are inspired by Shapiro et al. (2009); Defourny et al. (2013); Pflug and Pichler (2014). The process begins by defining the following notation, where the random process starts with a random variable ξ_0 with a single, trivial value.

- s stage index, running from 0 to S.
- $\mathcal{S} = \{0, \ldots, S\}$: the set of stages of uncertainty and any decisions should be adapted to this process.
- $\xi_s \in \mathbb{R}^{m_s}$: the sequence of either the data vector or random variables for stage $s \in \mathcal{S}$.
- $\xi_{[s]} = (\xi_0, \xi_1, \ldots, \xi_s)$: the history of the stochastic process up to stage $s \in \mathcal{S}$.
- $x_s \in \mathbb{R}^{n_s}$: the values of the decision vectors, chosen at stage $s \in \mathcal{S}$, may depend on the information (data) $\xi_{[s]}$ available up to stage $s \in \mathcal{S}$.
- $f_s(\cdot)$: the cost function at stage $s \in \mathcal{S}$, depending on x_s and $\xi_{[s]}$.

As the stochastic process $\{\xi_s\}_{s\in\mathcal{S}}$ has been adapted to the filtration $\mathcal{F}$, the stochastic decision process $\{x_s\}_{s\in\mathcal{S}}$ (with $x_s : \Omega \to \mathbb{R}^{n_s}$) is *nonanticipative* with respect to the stochastic process; that is, decisions x_s can incorporate only information available before or at stage $s \in \mathcal{S}$, but not as a result of future observations. The condition expressed above shows a relationship between decisions and observations. The initial decision x_0 is followed by the observation of the random variable ξ_1; then, immediately afterward, a subsequent decision x_1 is followed by the observation of ξ_2 and so on up to the terminal stage S. This defines the following *decision process*:

$$\xi_0 \to x_0 \to \xi_1 \to x_1 \to \ldots \to x_{S-1} \to \xi_S \to x_S,$$

Let the sequence of the random data process be $\xi_s \in \mathbb{R}^{m_s}$, $s \in \mathcal{S}$, the decision variables $x_s \in \mathbb{R}^{n_s}$, $s \in \mathcal{S}$, the continuous functions $f_s : \mathbb{R}^{n_s} \times \mathbb{R}^{m_s} \to \mathbb{R}$, $s \in \mathcal{S}$ and measurable closed valued multifunctions $\chi_s : \mathbb{R}^{n_{s-1}} \times \mathbb{R}^{m_s} \rightrightarrows \mathbb{R}^{n_s}$, $s \in \mathcal{S}$, such that it fulfills first-stage ξ_0 while the function $f_0 : \mathbb{R}^{n_0} \to \mathbb{R}$ and the set $\chi_0 \subset \mathbb{R}^{n_0}$ are deterministic. Thus, the MSP problem can be written in the *nested formulation*:

$$\min_{x_0 \in \boldsymbol{\chi}_0} f_0(x_0) + \mathbb{E}\left[\inf_{x_1 \in \boldsymbol{\chi}_1(x_0,\xi_1)} f_1(x_1,\xi_1) + \mathbb{E}\left[\ldots + \mathbb{E}\left[\inf_{x_S \in \boldsymbol{\chi}_S(x_{S-1},\xi_S)} f_S(x_S,\xi_S)\right]\right]\right]. \quad (3.2.1)$$

Another approach is to consider decision variables as functions of the data process $\xi_{[s]}$ up to time $s \in \mathcal{S}$, that is: $x_s = \boldsymbol{x}_s(\xi_{[s]})$, $s \in \mathcal{S}$. Such a sequence of (measurable) mapping

$\boldsymbol{x}_s : \mathbb{R}^{m_1} \times \ldots \times \mathbb{R}^{m_s} \to \mathbb{R}^{n_s}, s \in \mathcal{S}$ is called an *implementable policy formulation* (recalling that ξ_0 is deterministic). The MSP model in (3.2.1) can be reformulated considering decision variables as $x_s = \boldsymbol{x}(\xi_{[s]})$, $s \in \mathcal{S}$ in the scenario tree form:

$$\begin{aligned} &\underset{x_0, \boldsymbol{x}_1, \ldots, \boldsymbol{x}_S}{\text{minimize}} \ \mathbb{E}\left[f_0(x_0) + f_1(\boldsymbol{x}_1(\xi_{[1]}), \xi_1) + \ldots + f_S(\boldsymbol{x}_S\left(\xi_{[S]}\right), \xi_S)\right] \\ &\text{subject to } x_1 \in \boldsymbol{\chi}_1,\ \boldsymbol{x}_s(\xi_{[s]}) \in \boldsymbol{\chi}_s(\boldsymbol{x}_{s-1}(\xi_{[s-1]}), \xi_s),\ \forall\, s = 1, \ldots, S, \end{aligned} \tag{3.2.2}$$

where $\boldsymbol{x}_1, \ldots, \boldsymbol{x}_n$ are functions of the data process and, hence, are elements of appropriate functional spaces, while $x_0 \in \mathbb{R}^{n_0}$ is a deterministic vector. If the multistage stochastic process $\{\xi_s\}_{s \in \mathcal{S}}$ is finite, the formulation in Equation (3.2.2) leads to a finite, dimensional optimization problem.

As long as a scenario tree is given, each leaf node ω is determined by its path from the root node. Let $\xi_\omega = (\xi_0, \xi_{1\omega}, \ldots, \xi_{S\omega})$ be the scenario in $\omega \in \Omega$, with an associated probability p_ω, such that $\sum_{\omega \in \Omega} p_\omega = 1$. A mathematical program can be formulated wherein, for each scenario $\omega \in \Omega$, the optimization variables $x_0, x_{1\omega}, \ldots, x_{S\omega}$ are associated for each node on the path from the root to the leaf ω. By aggregating the nonanticipativity condition to the optimization problem, a *deterministic formulation* of the MSP problem is established as:

$$\begin{aligned} &\underset{x_0, x_{1\omega}, x_{2\omega}, \ldots, x_{S\omega}}{\text{minimize}} \ \sum_{\omega \in \Omega} p_\omega \left[f_0(x_0, \xi_0) + f_1(x_{1\omega}, \xi_{1\omega}) + f_2(x_{2\omega}, \xi_{2\omega}) + \ldots + f_S(x_{S\omega}, \xi_{S\omega})\right] \\ &\text{subject to } \ x_0 \in \boldsymbol{\chi}_0, \quad x_{s\omega} \in \boldsymbol{\chi}_s(x_{s\omega}, \xi_{s\omega}), \quad \forall\, s = 1, \ldots, S, \forall\, \omega \in \Omega, \\ &\qquad\qquad x_{s\omega} = x_{sl} \ \text{ such that } \ \xi_{[s]\omega} = \xi_{[s]l},\ \forall s \in \mathcal{S}, \forall\, \omega, l \in \Omega, \end{aligned} \tag{3.2.3}$$

where $\xi_{[s]\omega}$ is the history of random vectors up to stage $s \in \mathcal{S}$ for scenario $\omega \in \Omega$. The final constraints are the nonanticipativity constraints.

The MSP model is then formalized as a mathematical programming problem (3.2.3). The formulation is based on a particular representation of the uncertainty characterized by the stochastic process $\{\{\xi_{s\omega}\}_{s \in \mathcal{S}}\}_{\omega \in \Omega}$ in relation to the decision stages, specifically by means of the scenario trees described in Section 3.3.2. This formulation is used to model the problems presented in this thesis.

3.3. Scenario Tree Generation Methodology

3.3.1. Phase I: Scenario Generation Procedure

In order to generate scenarios $\xi_{s\omega}$, with $s \in \mathcal{S}, \omega \in \Omega$, we have developed a four-step procedure based on Time Series Factor Analysis (TSFA), Vector Autoregressive (VAR)

models and bootstrapping techniques. This is a similar procedure as the one employed in Muñoz et al. (2013), with the difference being that the VAR models are used to predict the next day for each random parameter of the MSP models. The step procedure is as follows. In the first step, the random parameters of the model are characterized as a multivariate time series (Section 3.3.1.1). In the second step, the statistical models for the given time series are determined (Section 3.3.1.2). In the third step, the forecasting models are obtained (Section 3.3.1.3). Finally, in the fourth step, the scenarios are obtained (Section 3.3.1.4). A detailed description of these steps is provided below in each of the following sections.

3.3.1.1. First Step: Time Series Characterization

The stochastic data present in the MSP models of this study are given by the random variables that involve the Electricity Markets (EM) prices, Wind Power (WP) generation, electricity power loads and Photovoltaic (PV) generation. The available historical data from these random variables are time series that are cleared simultaneously that day or one hour before. These time series are commonly involved with multiple interrelated random variables. The time series with these conditions are studied through a multivariate time series analysis. In this part, the basic characteristics of the time series are introduced, and we provide the definition and concepts of Multivariate Time Series (MTS), which are necessary for this study and are based on Peña (2005); Tsay (2013). Finally, we show the characterization of the random variables used in this thesis.

- Stationary or non-stationary time series: when a time series oscillates around a constant level, the series is considered stable or stationary; otherwise, it is nonstationary.
- Trend: when the level of a nonstationary time series increases or decreases with time, it is said that it presents a certain trend.
- Seasonal: if overlapping behavior is presented and it repeats over time, then the time series is seasonal.
- Outliers: these determine the presence of atypical data that may affect the interpretation of the results.
- Variance: this determines whether or not if it is constant over time, or if significant changes exist in the level of variance.

Definition 3.3.1 (*MTS*)**.** A t-dimensional time series $\boldsymbol{\xi}'_d = (\xi_{d1}, \ldots, \xi_{dt}, \ldots, \xi_{dM})$ is a random vector consisting of t random variables. As such, an underlying probability space exists in which the random variables are defined. Let $1 \leq t \leq M$ be the number of

variables (or characteristics) and $1 \leq d \leq N$ be the number of periods. The N number of observations can be collected in a matrix ξ of order $N \times M$:

$$\xi = \begin{pmatrix} \boldsymbol{\xi}'_1 \\ \boldsymbol{\xi}'_2 \\ \vdots \\ \boldsymbol{\xi}'_d \\ \vdots \\ \boldsymbol{\xi}'_N \end{pmatrix} = \begin{pmatrix} \xi_{11} & \xi_{12} & \cdots & \xi_{1t} & \cdots & \xi_{1M} \\ \xi_{21} & \xi_{22} & \cdots & \xi_{2t} & \cdots & \xi_{2M} \\ \vdots & \vdots & \ddots & \vdots & \ddots & \vdots \\ \xi_{d1} & \xi_{d2} & \vdots & \xi_{dt} & \vdots & \xi_{dM} \\ \vdots & \vdots & \ddots & \vdots & \ddots & \vdots \\ \xi_{N1} & \xi_{N2} & \cdots & \xi_{Nt} & \cdots & \xi_{NM} \end{pmatrix}, \tag{3.3.1}$$

where d is the number of observations and t is the number of variables (or characteristics).

Definition 3.3.2 (*Weakly and strictly stationary MTS*)**.** An MTS is said to be *weakly stationary* if:

i) the expectation is a constant vector ($E[\boldsymbol{\xi}_d] = \mu$),

ii) the autocovariance function depends only on τ:

$$Cov[\boldsymbol{\xi}_d, \boldsymbol{\xi}_{d+\tau}] = \gamma(\tau).$$

If $\tau = 0$, this implies that both the variance and the expectation are constant.

In addition, the MTS is *strictly stationary* if the joint distribution of the r vector $(\boldsymbol{\xi}'_{d_1}, \boldsymbol{\xi}'_{d_2}, \ldots, \boldsymbol{\xi}'_{d_r})'$ is the same as that of $(\boldsymbol{\xi}'_{d_1+i}, \boldsymbol{\xi}'_{d_2+i}, \ldots, \boldsymbol{\xi}'_{d_r+i})'$, where r, i are arbitrary positive integers.

In this study, the t index corresponds to the hour of the day for which the multivariate random variables occur, and we focus mainly on the weakly stationary series, because the strictly stationary series are difficult to verify in practice.

Unit Root Test to Verify Stationarity

The Augmented Dickey–Fuller (ADF) test is based on assuming that a time series Y_d can be approximated by a process $AR(p)$ with three variants: zero mean, non-zero mean and linear trend. The null hypothesis of this test is that a unit root is present and that the process is nonstationary. Initially, it is assumed that Y_d follows an $AR(p)$ and the model is transformed as follows.

$$\begin{aligned} Y_d &= \phi_1 Y_{d-1} + \phi_2 Y_{d-2} + \ldots + \phi_{p-1} Y_{d-p+1} + \varepsilon_d \\ Y_d - Y_{d-1} &= (\phi_1 - 1) Y_{d-1} + \phi_2 Y_{d-2} - Y_{d-1} + \ldots + \phi_{p-1} Y_{d-p+1} - Y_{d-1} + \varepsilon_d \\ \Delta Y_d &= \rho Y_{d-1} + \delta_1 \Delta Y_{d-1} + \ldots + \delta_p \Delta Y_{d-p} + \varepsilon_d, \end{aligned}$$

where $\rho = \phi_1 - 1$. The existence of a unit root is equivalent to $\phi_1 = 1$, i.e., $\rho = 0$. The Dickey-Fuller Unit Root test has three cases.

Case 1 (none): assuming that $Y_d \sim AR(p)$ has a mean of zero, then

$$\Delta Y_d = \rho Y_{d-1} + \delta_1 \Delta Y_{d-1} + \ldots + \delta_p \Delta Y_{d-p} + \varepsilon_d,$$

The null hypothesis is $H_0 : \rho = 0$, versus the alternative hypothesis $H_0 : \rho < 0$. The test statistic is denoted by τ, and the rejection criterion can be defined as $\hat{\tau} < \tau_{0,05}$. In R, the ADF test is implemented through the library `urca` by the function `ur.df(y,type="none")`.

Case 2 (drift): assuming that $Y_d \sim AR(p)$ has non–zero mean, then

$$\Delta Y_d = \alpha + \rho Y_{d-1} + \delta_1 \Delta Y_{d-1} + \ldots + \delta_p \Delta Y_{d-p} + \varepsilon_d,$$

with the same hypothesis. In R, it is `ur.df(y,type="drift")`.

Case 3 (trend): assuming that $Y_d \sim AR(p)$ has a linear trend, then

$$\Delta Y_d = \alpha + \beta t + \rho Y_{d-1} + \delta_1 \Delta Y_{d-1} + \ldots + \delta_p \Delta Y_{d-p} + \varepsilon_d,$$

with the same hypothesis. In R, it is `ur.df(y,type="trend")`.

It should be noted that the random variables studied in this thesis are data set sequence that depends on the time interval. Therefore, it is appropriate to define and treat the random variables as MTS and show the descriptive statistics for each of them. These are given below.

- **EM Prices**: These are represented by the prices in the following EM: Day-Ahead Market (DM), Secondary Reserve Market (RM), Intra-day Market (IM) sessions, and Imbalance Settlements (IB). These prices can be considered as MTS that are described as a high-dimensional panel of hourly series (García-Martos et al., 2011; Liebl et al., 2013; Ziel and Weron, 2018). The characteristics that are often considered in this time series are: (a) non-constant mean and variance; (b) daily and weekly seasonality due to the dependence of electricity supply and demand, weather conditions, and social and economic activities that consequently have a calendar effect on weekends and holidays; (c) complex, time-varying volatility structures that are considered typical features of electricity markets; (d) the presence of the mean-reversion effect, meaning there the prices return back to the long-run interpretation of the entire dataset; (e) the presence of jumps and spikes that can be attributed to the difficulty in storing large quantities of electricity; and (f) the presence of outliers (Conejo et al., 2005; Huisman et al., 2007; Koopman

et al., 2007; Panagiotelis and Smith, 2008; Trück, 2011; Liebl et al., 2013). Table 3.3.1 presents the random vectors that define the MTS for the different electricity prices and the dimensionality of this multivariate time series for each hour's prices.

- **WP Generation**: This is represented by the MTS of WP generation (Table 3.3.1). The characteristics of this MTS are: (a) non-constant mean and variance; (b) a strong nonstationary time series due to multiple seasonality and a high percentage of abrupt changes; (c) seasonality due to the seasonal wind speed (the wind is stronger in the spring and autumn than in the winter and summer); (d) the high volatility of the wind; and (e) intermittency, which considered equivalent to high variability (Fan et al., 2009; Giebel et al., 2011; Wu et al., 2013; Ren et al., 2017).

MTS	Time Series
$\boldsymbol{\lambda}^{D} = \left(\boldsymbol{\lambda}_1^{D'}, \ldots, \boldsymbol{\lambda}_d^{D'}, \ldots, \boldsymbol{\lambda}_N^{D'}\right)'$	$\boldsymbol{\lambda}_d^{D'} = \left(\lambda_{d1}^{D}, \ldots \lambda_{dt}^{D}, \ldots, \lambda_{dM}^{D}\right), 1 \leq d \leq N, 1 \leq t \leq M$
$\boldsymbol{\lambda}^{R} = \left(\boldsymbol{\lambda}_1^{R'}, \ldots, \boldsymbol{\lambda}_d^{R'}, \ldots, \boldsymbol{\lambda}_N^{R'}\right)'$	$\boldsymbol{\lambda}_d^{R'} = \left(\lambda_{d1}^{R}, \ldots \lambda_{dt}^{R}, \ldots, \lambda_{dM}^{R}\right), 1 \leq d \leq N, 1 \leq t \leq M$
$\boldsymbol{\lambda}_1^{I} = \left(\boldsymbol{\lambda}_{1,1}^{I'}, \ldots, \boldsymbol{\lambda}_{1,d}^{I'}, \ldots, \boldsymbol{\lambda}_{1,N}^{I'}\right)'$	$\boldsymbol{\lambda}_{1,d}^{I'} = \left(\lambda_{1,d1}^{I}, \ldots, \lambda_{1,dt}^{I}, \ldots, \lambda_{1,dM}^{I}\right), 1 \leq d \leq N, 1 \leq t \leq M$
$\boldsymbol{\lambda}_2^{I} = \left(\boldsymbol{\lambda}_{2,1}^{I'}, \ldots, \boldsymbol{\lambda}_{2,d}^{I'}, \ldots, \boldsymbol{\lambda}_{2,N}^{I'}\right)'$	$\boldsymbol{\lambda}_{2,d}^{I'} = \left(\lambda_{2,d1}^{I}, \ldots, \lambda_{2,dt}^{I}, \ldots, \lambda_{2,dM}^{I}\right), 1 \leq d \leq N, 1 \leq t \leq M$
$\boldsymbol{\lambda}_3^{I} = \left(\boldsymbol{\lambda}_{3,1}^{I'}, \ldots, \boldsymbol{\lambda}_{3,d}^{I'}, \ldots, \boldsymbol{\lambda}_{3,N}^{I'}\right)'$	$\boldsymbol{\lambda}_{3,d}^{I'} = \left(\lambda_{3,d1}^{I}, \ldots, \lambda_{3,dt}^{I}, \ldots, \lambda_{3,dM}^{I}\right), 1 \leq d \leq N, 1 \leq t \leq M$
$\boldsymbol{\lambda}_4^{I} = \left(\boldsymbol{\lambda}_{4,1}^{I'}, \ldots, \boldsymbol{\lambda}_{4,d}^{I'}, \ldots, \boldsymbol{\lambda}_{4,N}^{I'}\right)'$	$\boldsymbol{\lambda}_{4,d}^{I'} = \left(\lambda_{4,d1}^{I}, \ldots, \lambda_{4,dt}^{I}, \ldots, \lambda_{4,dM}^{I}\right), 1 \leq d \leq N, 1 \leq t \leq M$
$\boldsymbol{\lambda}_5^{I} = \left(\boldsymbol{\lambda}_{5,1}^{I'}, \ldots, \boldsymbol{\lambda}_{5,d}^{I'}, \ldots, \boldsymbol{\lambda}_{5,N}^{I'}\right)'$	$\boldsymbol{\lambda}_{5,d}^{I'} = \left(\lambda_{5,d1}^{I}, \ldots, \lambda_{5,dt}^{I}, \ldots, \lambda_{5,dM}^{I}\right), 1 \leq d \leq N, 1 \leq t \leq M$
$\boldsymbol{\lambda}_6^{I} = \left(\boldsymbol{\lambda}_{6,1}^{I'}, \ldots, \boldsymbol{\lambda}_{6,d}^{I'}, \ldots, \boldsymbol{\lambda}_{6,N}^{I'}\right)'$	$\boldsymbol{\lambda}_{6,d}^{I'} = \left(\lambda_{6,d1}^{I}, \ldots, \lambda_{6,dt}^{I}, \ldots, \lambda_{6,dM}^{I}\right), 1 \leq d \leq N, 1 \leq t \leq M$
$\boldsymbol{\lambda}_7^{I} = \left(\boldsymbol{\lambda}_{7,1}^{I'}, \ldots, \boldsymbol{\lambda}_{7,d}^{I'}, \ldots, \boldsymbol{\lambda}_{7,N}^{I'}\right)'$	$\boldsymbol{\lambda}_{7,d}^{I'} = \left(\lambda_{7,d1}^{I}, \ldots, \lambda_{7,dt}^{I}, \ldots, \lambda_{7,dM}^{I}\right), 1 \leq d \leq N, 1 \leq t \leq M$
$\boldsymbol{\lambda}^{IB_+} = \left(\boldsymbol{\lambda}_1^{IB'_+}, \ldots, \boldsymbol{\lambda}_d^{IB'_+}, \ldots, \boldsymbol{\lambda}_N^{IB'_+}\right)'$	$\boldsymbol{\lambda}_d^{IB'_+} = \left(\lambda_{d1}^{IB_+}, \ldots, \lambda_{dt}^{IB_+}, \ldots, \lambda_{dM}^{IB_+}\right), 1 \leq d \leq N, 1 \leq t \leq M$
$\boldsymbol{\lambda}^{IB_-} = \left(\boldsymbol{\lambda}_1^{IB'_-}, \ldots, \boldsymbol{\lambda}_d^{IB'_-}, \ldots, \boldsymbol{\lambda}_N^{IB'_-}\right)'$	$\boldsymbol{\lambda}_d^{IB'_-} = \left(\lambda_{d1}^{IB_-}, \ldots, \lambda_{dt}^{IB_-}, \ldots, \lambda_{dM}^{IB_-}\right), 1 \leq d \leq N, 1 \leq t \leq M$
$\mathbf{p}^{W} = \left(\mathbf{p}_1^{W'}, \ldots, \mathbf{p}_d^{W'}, \ldots, \mathbf{p}_N^{W'}\right)$	$\mathbf{p}_d^{W'} = \left(p_{d1}^{W}, \ldots, p_{dt}^{W}, \ldots, p_{dM}^{W}\right), 1 \leq d \leq N, 1 \leq t \leq M$

Cuadro 3.3.1: MTS for the participation of a VPP in the EM.

- **Electricity Power Load**: One of the parameters of uncertainty for the optimal operation of distribution networks is the active and reactive power load. Table 3.3.2 shows the structure of this MTS. In general, the characteristics of this MTS are: (a) seasonal variation data patterns (daily, weekly and annual) and random noise; (b) nonstationary mean and variance due to weather, socioeconomic factors and randomness; and (c) variations in trend for periods longer than daily periods (these variations are consequences of many external factors such as weather, time, demography, economy, geographical conditions, consumer types and their circumstances) (Nowicka-Zagrajek and Weron, 2002; Hahn et al., 2009; Muñoz et al., 2010; Liu et al., 2014; Dudek, 2016).
- **PV Generation**: This is the MTS considered to be an hourly panel time series (Table 3.3.2). The characteristics are usually: (a) a nonstationary nature; (b) cyclicity due to the nonlinear characteristic of PV power output (total irradiance,

spectral content, and angle of incidence), ambient temperature, wind speed, and prominent variation at different time scales (variation is more frequent in winter due to variable solar irradiation and minor in summer, because of high irradiation); and (c) the influence of load peaking in different seasons. When the power grids generate high solar power, the peak-load will has an impact on the power system (Bacher et al., 2009; Phinikarides et al., 2015; Zhu et al., 2017).

MTS	Time Series
$\mathbf{P}_i^D = \left(\mathbf{P}_{i1}^{D'}, \ldots, \mathbf{P}_{id}^{D'}, \ldots, \mathbf{P}_{iN}^{D'}\right)'$	$\mathbf{P}_{id}^{D'} = \left(P_{id1}^D, \cdots, P_{idt}^D, \ldots, P_{idM}^D\right), 1 \leq d \leq N, 1 \leq t \leq M$
$\mathbf{Q}_i^D = \left(\mathbf{Q}_{i1}^{D'}, \ldots, \mathbf{Q}_{id}^{D'}, \ldots, \mathbf{Q}_{iN}^{D'}\right)'$	$\mathbf{Q}_{id}^{D'} = \left(Q_{id1}^D, \ldots, Q_{idt}^D, \ldots, D_{idM}^D\right), 1 \leq d \leq N, 1 \leq t \leq M$
$\mathbf{p}_i^{pv} = \left(\mathbf{p}_{i1}^{pv'}, \ldots, \mathbf{p}_{id}^{pv'}, \ldots, \mathbf{p}_{iN}^{pv'}\right)'$	$\mathbf{p}_{id}^{pv'} = (p_{id1}^{pv}, \ldots, p_{idt}^{pv}, \ldots, p_{idM}^{pv}), 1 \leq d \leq N, 1 \leq t \leq M$

Cuadro 3.3.2: MTS in the operation of the Electrical Distribution Networks.

3.3.1.2. Second Step: Determining the Statistical Models

In view of high dimensionality of the observed process and the multiple interrelated random variables, it is a top priority to reduce the number of variables (or characteristics) in unobserved variables. For this reason, the technique TSFA proposed by Gilbert et al. (2005, 2006) is applied. After applying the TSFA, we determine the statistical models to obtain forecasting for future use of the following steps in the procedure. The VAR models is used for this purpose (Sims, 1980).

- **Time Series Factor Analysis**

  Factorial analysis is a statistical technique for data reduction. The objective is to explain the correlations between the observed variables in terms of a smaller number of unobserved variables, which are called *factors*. Specifically, the aim is to represent the observed variables as linear combinations of these factors, plus a certain error term.

  When the observed data have a temporal structure (i.e., they are time series), the standard factorial analysis is not adequate because it requires the hypothesis of uncorrelated observations in each variable. To solve these problems, TSFA models were developed in order to summarize most of the information from a large number of time series that are correlated in a smaller number of underlying factors (unobserved variables).

  Definition 3.3.3 (*TSFA model*)**.** Let $\mathbf{F}_d$ be an $k \times 1$ vector of unobserved processes of interest (the factors) for a sample N time periods, which are indicated by $F_{dt}, d = 1, \ldots, N, t = 1, \ldots, k$. Let $\boldsymbol{\xi}_d$ be an $M \times 1$ vector of observed processes

(the indicators) indicated by ξ_{dt}, $d = 1, \ldots, N, t = 1, \ldots, M$. The model that relates the indicators to the factors is thus given by

$$\boldsymbol{\xi}_d = \alpha + \boldsymbol{B}\mathbf{F}_d + \varepsilon_d, \tag{3.3.2}$$

where α is an $M \times 1$ vector of intercept parameters, $\boldsymbol{B}$ is an $M \times k$ matrix parameter of factor loadings (or, simply, loadings), and ε_d is a random $M \times 1$ vector of measurement errors, disturbances, and unique or idiosyncratic factors.

The estimation of the factor loadings can be carried out by the maximum likelihood method, as defined in Equation (3.3.4). In addition to the loadings $\boldsymbol{B}$, this also obtains the covariance matrix $\boldsymbol{\sigma}$ and the covariance matrix for the errors $\boldsymbol{\Omega}$, both of which are $M \times M$ matrix. The factor score on the latent variables $\boldsymbol{F}_d$ is predicted.

Definition 3.3.4 (*Bartlett Predictor for TSFA*)**.** The best linear unbiased predictor of the factor score can be calculated using the Bartlett predictor (Wansbeek and Meijer, 2000) obtained from Equation (3.3.3)

$$\hat{\mathbf{F}}_d = \left(\hat{\boldsymbol{B}}^{'}\boldsymbol{\Omega}^{-1}\hat{\boldsymbol{B}}\right)^{-1}\hat{\boldsymbol{B}}^{'}\boldsymbol{\Omega}^{-1}\boldsymbol{\xi}_d, \tag{3.3.3}$$

where $\hat{\boldsymbol{B}}$ and $\boldsymbol{\Omega}$ are the loading and covariance error matrix, respectively.

The new values $\hat{\varepsilon}_d$ of the error, are obtained from

$$\hat{\boldsymbol{\varepsilon}}_d = \boldsymbol{\xi}_d - \left(\hat{\alpha} - \hat{\boldsymbol{B}}\hat{\boldsymbol{F}}_{\boldsymbol{d}}\right), \tag{3.3.4}$$

where $\hat{\alpha}$ and $\hat{\boldsymbol{B}}$ are the estimate intercept and estimate loadings from the original data, respectively.

An adequate selection of the number of factors is necessary for defining the TSFA model. For this purpose, several criteria are available. We will set down *the Comparative Fit Index (CFI)* and *the Root Mean Square Error of Approximation (RMSEA)*, which are presented in the following.

- The CFI developed by Bentler (1990), which compares the χ-square of two models, is an independent model that has no relationship between the variables model and the model proposed by the researcher. This comparison is corrected by the degrees of freedom of both models. The CFI indicates that values greater than 0.95 are acceptable as an indicator of good fit.

- The RMSEA developed by Steiger (1980) is a potential mechanism for accommodating large sample sizes. RMSEA is a non-negative number, based on the χ-squared statistic that measures the lack of fit per degree of freedom. The RMSEA advises that values less than 0.05 constitute a good fit, values between 0.05 to 0.08 are an acceptable range, values between 0.08 and 0.10 are a marginal range of fit, and values greater than 0.10 are a bad fit.

More details about the TSFA models can be found in the references (Gilbert et al. (2005), Gilbert et al. (2006)).

- **VAR Models**

The vector Autoregressive (VAR) model (Sims, 1980) is a stochastic process model used to capture the linear interdependencies among MTS. This generalizes the Autoregressive models (AR), but for multiple time series. To understand the VAR models of order p (VAR(p)), we developed the VAR(1) models for trivariate time series. However, the results continue to hold for models of order greater than 1 and j-dimensional time series:

Consider the trivariate VAR(1) model:

$$\mathbf{F}_d = \boldsymbol{\phi}_0 + \boldsymbol{\phi}_1 \mathbf{F}_{d-1} + \boldsymbol{\varepsilon}_d. \tag{3.3.5}$$

The explicit form of the model can be written as

$$\begin{bmatrix} F_{d1} \\ F_{d2} \\ F_{d3} \end{bmatrix} = \begin{bmatrix} \phi_{0,1} \\ \phi_{0,2} \\ \phi_{0,3} \end{bmatrix} + \begin{bmatrix} \phi_{1,11} & \phi_{1,12} & \phi_{1,13} \\ \phi_{1,21} & \phi_{1,22} & \phi_{1,23} \\ \phi_{1,33} & \phi_{1,32} & \phi_{1,33} \end{bmatrix} \begin{bmatrix} F_{(d-1)1} \\ F_{(d-1)2} \\ F_{(d-1)3} \end{bmatrix} + \begin{bmatrix} \varepsilon_{d1} \\ \varepsilon_{d2} \\ \varepsilon_{d3} \end{bmatrix}, \tag{3.3.6}$$

or equivalently

$$\begin{aligned} F_{d1} &= \phi_{0,1} + \phi_{11} F_{(d-1)1} + \phi_{1,12} F_{(d-1)2} + \phi_{1,13} F_{(d-1)2} + \varepsilon_{d1} \\ F_{d2} &= \phi_{0,2} + \phi_{21} F_{(d-1)1} + \phi_{1,22} F_{(d-1)2} + \phi_{1,23} F_{(d-1)3} + \varepsilon_{d2} \\ F_{d3} &= \phi_{0,3} + \phi_{31} F_{(d-1)1} + \phi_{1,32} F_{(d-1)2} + \phi_{1,33} F_{(d-1)3} + \varepsilon_{d3}. \end{aligned} \tag{3.3.7}$$

The $\phi_{1,23}$, shows the linear dependence of F_{d2} on $F_{(d-1)2}$ in the presence of $F_{(d-1)1}$ and $F_{(d-1)2}$. All parameters in ϕ_1 can be interpreted in a similar form.

The back-shift operator for VAR(1) can be written as

$$\boldsymbol{\phi}(\boldsymbol{B})\mathbf{F}_d = \boldsymbol{\phi}_0 + \boldsymbol{\varepsilon}_d, \tag{3.3.8}$$

where $\boldsymbol{\phi}(\boldsymbol{B}) = \mathbf{I}_3 - \boldsymbol{\phi}_1 \mathbf{B}^1$ is a matrix polynomial of order 1.

A necessary condition for the VAR(1) series $\mathbf{F}_d$ to be stationarity is that all eigenvalues of $\boldsymbol{\phi}_1$ must be less than 1 in absolute value. If all eigenvalues of $\boldsymbol{\phi}_1$ are less than 1 in absolute value, then the VAR(1) series $\mathbf{F}_d$ is also stationary. The eigenvalues of $\boldsymbol{\phi}_1$ are solutions of the determinant equation:

$$|\lambda \mathbf{I}_j - \boldsymbol{\phi}_1| = 0$$

The necessary and sufficient condition for the stationarity of a VAR(1) model is that the solution of the determinant equation $|\lambda \mathbf{I}_j - \boldsymbol{\phi}_1 \mathbf{B}| = 0$ is greater than 1 in absolute value; that is, the solutions of the determinant equation $|\boldsymbol{\phi}(\boldsymbol{B})| = 0$ are outside the unit circle.

Definition 3.3.5 (*VAR(p) model*)**.** Stationary multivariate processes $(\mathbf{F}_d)$ follow an autoregressive multivariate model, a vectorial of order p, or VAR(p) (Vectorial autoregressive) if and only if

$$\mathbf{F}_d = \boldsymbol{\Phi}_0 + \boldsymbol{\Phi}_1 \mathbf{F}_{d-1} + \boldsymbol{\Phi}_2 \mathbf{F}_{d-2} + \ldots + \boldsymbol{\Phi}_p \mathbf{F}_{d-p} + \boldsymbol{\varepsilon}_d, \tag{3.3.9}$$

for all $d = 1, \ldots, N$, where $(\boldsymbol{\varepsilon}_d) \sim IID(0, \boldsymbol{\Sigma}_\varepsilon)$ and $\boldsymbol{\Phi}_0, \boldsymbol{\Phi}_1, \boldsymbol{\Phi}_2, \ldots, \boldsymbol{\Phi}_p$ are a parameters matrix, such that all the roots of the equation

$$\left| \mathbf{I} - \boldsymbol{\Phi}_1 x - \boldsymbol{\Phi}_2 x^2 - \ldots - \boldsymbol{\Phi}_p x^p \right| = 0$$

are outside the unit circle.

Definition 3.3.6 (*Vector Autoregression with exogenous variables (VARX) model*)**.** Let F_d be a k-dimensional time series and X_d an l-dimensional series of exogenous variables or leading indicators. The general form of a VARX model is

$$\mathbf{F}_d = \boldsymbol{\Phi}_0 + \boldsymbol{\Phi}_1 \mathbf{F}_{d-1} + \boldsymbol{\Phi}_2 \mathbf{F}_{d-2} + \ldots + \boldsymbol{\Phi}_p \mathbf{F}_{d-p} + \boldsymbol{\beta}_1 \mathbf{X}_{d-1} + \boldsymbol{\beta}_2 \mathbf{X}_{d-2} + \ldots + \boldsymbol{\beta}_l \mathbf{X}_{d-l} + \boldsymbol{\varepsilon}_d, \tag{3.3.10}$$

where $\boldsymbol{\varepsilon}_d$ is a sequence of i.i.d. random vectors with mean zero and positive-definite covariance matrix Σ_ε, p and w are non-negative integers, $\boldsymbol{\Phi}_d$ are the usual coefficient matrices, and $\boldsymbol{\beta}_j$ are $k \times m$ coefficient matrices. This model allows for $\mathbf{X}_d$ to affect $\mathbf{F}_d$ instantaneously if $\boldsymbol{\beta}_0 \neq 0$.

The vector autoregressive model with exogenous variables was the first approach in the literature for including exogenous variables in multivariate time series modeling. This type of model is referred to as the VARX(p, l) model, with X signifying exogenous variables. The term exogenous variable is used loosely here, as it may contain independent (or input) variables.

3.3.1.3. Third Step: Calculating Forecasting Models

Prediction is one of the objectives of this study. Our interest is in predicting the following day for the random parameters. As data has been reduced into estimated factors through TSFA, these factors are employed to calculate the one-step-ahead forecasting. VAR(p) models are used for this objective. Lastly, the one-step-ahead forecasting factors for the MTS of this study have been calculated.

- **One-step-ahead Forecasting TSFA Models**

  In order to obtain the one-step-ahead forecasting for the factors, Equation (3.3.11) specifies the forecasting model.

$$\boldsymbol{\xi}_{d+1} = \hat{\boldsymbol{\alpha}} + \hat{\mathbf{B}}\hat{\mathbf{F}}_{d+1} + \boldsymbol{\varepsilon}_{d+1}, \tag{3.3.11}$$

  with $\hat{\mathbf{F}}_{d+1}$ being the vector of predictive factors for $d+1$, $\hat{\alpha}, \hat{\mathbf{B}}$ are the estimation parameters of the model, and $\boldsymbol{\varepsilon}_{d+1}$ is the resulting forecast error for $d+1$.

  Keeping in mind that $1 \leq d \leq N$, then the out-of-sample forecast for $\boldsymbol{\xi}_{N+1}$ is conditional to the information observed until period N. This is demonstrated in Equation (3.3.12).

$$\hat{\boldsymbol{\xi}}_{(N+1)/N} = \hat{\alpha} + \hat{\mathbf{B}}\hat{\mathbf{F}}_{N+1/N}, \tag{3.3.12}$$

  where $\hat{\mathbf{F}}_{N+1/N}$ has been estimated for the VAR models. The forecasting error is calculated with:

$$\hat{\boldsymbol{\varepsilon}}_{N+1} = \boldsymbol{\xi}_{N+1} - \hat{\boldsymbol{\xi}}_{(N+1)/N}. \tag{3.3.13}$$

  where $\boldsymbol{\xi}_{N+1}$ is the original values and $\hat{\boldsymbol{\xi}}_{(N+1)/N}$ is the out-if-sample forecast.

- **One-step-ahead Forecasting VAR(p) Models**

  The vector predicted factor $\hat{\mathbf{F}}_{d+1}$ of Equation (3.3.11) for the forecast of the following day for the random parameters of this study must be obtained.

  Definition 3.3.7 (*One-Step-Ahead prediction VAR*)**.** Therefore, assuming that the VAR model is known, the one-step ahead prediction is:

$$\hat{\mathbf{F}}_{d+1} = \boldsymbol{\Phi}_0 + \boldsymbol{\Phi}_1\hat{\mathbf{F}}_d + \boldsymbol{\Phi}_2\hat{\mathbf{F}}_{d-1} + \ldots + \boldsymbol{\Phi}_p\hat{\mathbf{F}}_{d-p+1} + \boldsymbol{\varepsilon}_{d+1}. \tag{3.3.14}$$

In order to obtain the out-of-sample forecast for $\hat{\mathbf{F}}_{N+1}$, the Equation (3.3.14) will be used. This is:

$$\hat{\mathbf{F}}_{N+1} = \hat{\mathbf{\Phi}}_0 + \hat{\mathbf{\Phi}}_1\hat{\mathbf{F}}_N + \hat{\mathbf{\Phi}}_2\hat{\mathbf{F}}_{N-1} + \hat{\mathbf{\Phi}}_3\hat{\mathbf{F}}_{N-2} + \ldots + \hat{\mathbf{\Phi}}_p\hat{\mathbf{F}}_{N-p+1}. \tag{3.3.15}$$

The forecasting error is calculated with:

$$\tilde{\boldsymbol{\varepsilon}}_{N+1} = \mathbf{F}_{N+1} - \hat{\mathbf{F}}_{N+1}. \tag{3.3.16}$$

where $\mathbf{F}_{N+1}$ is the original values and $\hat{\mathbf{F}}_{N+1}$ is the out-if-sample forecast.

Measurement Error

In this study we use three measurements that are common used as forecast error measures in forecasting (Shcherbakov et al., 2013). These are:

- Mean Absolute Error (MAE) is a measure of error between paired observations expressing the same phenomenon. This is a common measure of forecast error in time series analysis. MAE is given by:

$$MAE = \frac{1}{n}\sum_{i=1}^{n}|\varepsilon_i|$$

- Root Mean Square Error (RMSE) is a frequently measure of the differences between values predicted by a model or an estimator and the values observed.This measure is calculated as:

$$RMSE = \sqrt{\frac{1}{n}\sum_{i=1}^{n}\varepsilon_i^2}$$

3.3.1.4. Fourth Step: Generating Scenarios

The next step in the methodology is to obtain representative scenarios for approximating the multivariate stochastic process of each MSP model in this thesis. For this purpose, we will take care to build an empirical distribution function and its corresponding probabilities in order to approximate the theoretical multivariate stochastic processes. Bootstrap techniques (Efron and Tibshirani, 1994) are applied to obtain representative scenarios that approximate the stochastic process. We use a procedure developed by Muñoz et al. (2013), which is based on TSFA models and bootstrap techniques.

1. The model is estimated, and the estimated parameters are obtained for each random parameter data set, taking into consideration the hourly dependence for these parameters.

2. The estimated residual errors $\hat{\varepsilon}_d$ are obtained with Equation (3.3.4).
3. An i.i.d. resampling of $\tilde{\varepsilon}_d$ from $\mathcal{F}_{\hat{\varepsilon}_d}$, for $d = 1, \ldots, N$ is obtained, wherein $\mathcal{F}_{\hat{\varepsilon}_d}$ is the empirical distribution function of $\hat{\varepsilon}_d$.
4. A bootstrap replica of the data is built, defined by $\tilde{\boldsymbol{\xi}}_d = \hat{\alpha} - \hat{\boldsymbol{B}}\hat{\boldsymbol{F}}_d + \tilde{\varepsilon}_d$.
5. A sample of the future $\tilde{\varepsilon}_{d+1}$ is generated by resampling from $\mathcal{F}_{\hat{\varepsilon}}$ one time.
6. The $\omega \in \Omega \subset \mathbb{N}$ future bootstrap observations $\tilde{\boldsymbol{\xi}}_{N+1,\omega}$ are calculated by using the equation in step 4.

This procedure is applied to each set of random variables described in Section 3.3.1.1. Given that the day $N+1$ is fixed and the decision process of the MSP problem has been established, we proceed to redefine $\tilde{\boldsymbol{\xi}}_{N+1,\omega}$ for $\tilde{\boldsymbol{\xi}}_{\omega}$, where $\tilde{\boldsymbol{\xi}}_{s\omega}$ is a column random vector for stage $s \in \mathcal{S}$ under scenario $\omega \in \Omega$. Therefore, a scenario $\tilde{\boldsymbol{\xi}}_{\omega}$ of the scenario tree $\{\{\tilde{\boldsymbol{\xi}}\}_{s\in\mathcal{S}}\}_{\omega\in\Omega}$ is defined as a vector $\tilde{\boldsymbol{\xi}}_{\omega} = (\tilde{\boldsymbol{\xi}}_0, \tilde{\boldsymbol{\xi}}_{1\omega}, \ldots, \tilde{\boldsymbol{\xi}}_{s\omega}, \ldots, \tilde{\boldsymbol{\xi}}_{S\omega})$ for a certain scenario index $\omega \in \Omega$.

3.3.2. Phase II: Scenario Tree Generation

In this section, we will present two algorithms that allow generating scenario trees for the MSP models presented in this thesis. These algorithms obtain scenario trees that are an approximation of the original multivariate stochastic process. Section 3.3.2.1 shows the Forward Tree Construction Algorithm (FTCA), and Section 3.3.2.2 presents a slightly modified version of the Dynamic Tree Generation with Flexible Bushiness Algorithm (DTGFBA). The theoretical foundation is presented for both algorithms.

3.3.2.1. Forward Tree Construction Algorithm (FTCA)

The FTCA is based on recursive deletion and the bundling of scenarios from some given scenario set originating from historical or simulated data. The strategy consists of modifying a given fan of individual scenarios by bundling scenarios according to the scenario reduction technique. The scenario reduction approach was first developed in Dupačová et al. (2003) and enhanced in Heitsch and Römisch (2003). Let us recall its main ideas. We consider a discrete distribution P with scenarios ξ_i and probabilities $p_i, i = 1, \ldots, N$, and another discrete distribution Q supported by a subset of scenarios $\xi_j, j \in \{1, \ldots, N\}J$, of P and probabilities $q_j, j \in J$, i.e, the index set J describes the set of deleted scenarios. The procedure uses a certain Monge-Kantorovich transportation distance for multivariate probability distributions. The theoretical foundation and the FTCA are shown below.

- **Theoretical Foundation**

  The theoretical foundation is a summary of the theory developed in Heitsch et al. (2006); Heitsch and Römisch (2009a,b). Details are provided regarding the concepts of probability metrics for measuring the distance distance between probability distributions, specifically in terms of distances and metrics for the Monge-Kantorovich mass transportation problem.

  The Monge-Kantorovich mass transportation problems take the form:

$$\inf\left\{\int_{\Xi\times\Xi} c(\omega,\tilde{\omega})\eta d(\omega,\tilde{\omega}) : \eta\in\mathcal{P}(\Xi\times\Xi), \pi_1\eta = P \text{ and } \pi_2\eta = Q\right\}, \tag{3.3.17}$$

  where Ξ is a closed subset of $\mathbb{R}^m$ (for some $m\in\mathbb{N}$); η_1 and η_2 denote the projections onto the first and second component, respectively; c is a non-negative, symmetric and continuous cost function; and P and Q are probability measures in $\mathcal{P}(\Xi)$.

  A type of cost function is

$$c(\xi,\tilde{\xi}) = \mathbf{d}(\xi,\tilde{\xi})^r = |\xi-\tilde{\xi}|^r \quad (\xi,\tilde{\xi}\in\Xi), \tag{3.3.18}$$

  for some $r\geq 1$, and $|\cdot|$ is a norm or semi-norm in $\mathbb{R}^m$.

  The cost in Equation (3.3.18) leads to the *L_r-minimal metric* ℓ_r, which is defined by

$$\ell_r^r(P,Q) = \inf\left\{\int_{\Xi\times\Xi} |\xi-\tilde{\xi}|^r \eta(d\xi,d\tilde{\xi}) : \eta\in\mathcal{P}(\Xi\times\Xi), \pi_1\eta = P \text{ and } \pi_2\eta = Q\right\}. \tag{3.3.19}$$

  For stochastic programs that containing information constraints, distance between probability distributions may fail. An alternative study of multistage models consists of optimization problems in functional spaces (Heitsch and Römisch, 2009a), and it explains the norm (which is called *filtration distance*)

$$\|\xi\|_r = \left(\sum_{\omega\in\Omega}\mathbb{E}[|\xi_\omega|^r]\right)^{\frac{1}{r}}, \tag{3.3.20}$$

  in the Banach space $L_r(\Omega,\mathcal{F},\mathbb{P},\mathbb{R}^m)$ with $m = \sum_{s=1}^{s} m_s$ for the Ξ-value random inputs.

  Furthermore, the L_r-seminorm $\|\cdot\|_{r,s}$ with $m = \sum_{s=1}^{S} m_s$, is defined as:

$$\|\xi\|_{rs} = (\mathbb{E}[|\xi|_s^r])^{\frac{1}{r}} = \left(\sum_{i=1}^{N} p_i|\xi_i|_s^r\right)^{\frac{1}{r}}, \tag{3.3.21}$$

where $|\cdot|_s$ is the semi-norm in $\mathbb{R}^m$, which is defined by $|\xi|_s = |(\xi_1, \ldots, \xi_s, 0, \ldots, 0)|$ for each $\xi = (\xi_1, \ldots, \xi_S) \in \mathbb{R}^m$.

Let ξ and $\tilde{\xi}$ be random vectors in any given probability space $(\Omega, \mathcal{F}, \mathbb{P})$ with probability distributions P and Q. Since the probability distribution $\bar{\eta}$ of the pair $(\xi, \tilde{\xi})$ of two random vectors is feasible for the minimization problem (3.3.19), the following is obtained:

$$\ell_r(P, Q) \leq \|\xi - \tilde{\xi}\|_r, \tag{3.3.22}$$

where ξ and $\tilde{\xi}$ are discrete random vectors with, respectively, scenarios ξ^i and probabilities $p_i, i = 1, \ldots, N$ and scenarios ξ^j with probabilities $q_j, j = 1, \ldots, M$ respectively are the result. Consequently,

$$\ell_r^r(P, Q) = \min \left\{ \sum \eta_{ij} |\xi^i - \tilde{\xi}^j|^r : \eta_{ij} \geq 0, \sum_i \eta_{ij} = q_j, \sum_j \eta_{ij} = p_i \right\}, \tag{3.3.23}$$

is the optimal value of a linear transportation problem.

Taking into account the inequality in Equation (3.3.22) and the optimal $\ell_r^r(P, Q)$ in Equation (3.3.23), a scenario tree ξ_{tr} can be constructed from $\tilde{\xi}$ such that the L_r-distance

$$\|\tilde{\xi} - \xi_{tr}\|_r,$$

is bounded by a prescribed tolerance $\varepsilon > 0$.

- **Algorithm**

The study and implementation of FTCA is described in Heitsch and Römisch (2009a). A summary of this algorithm is given below.

Let $\tilde{\xi}$ be a stochastic process on any probability space $(\Omega, \mathcal{F}, \mathbb{P})$, with scenarios $\tilde{\xi}_i = (\xi_{0i}, \ldots, \xi_{Si}) \in \mathbb{R}^m$, probabilities $p_i > 0, i = 1, \ldots, N$, and fixed initial node $\tilde{\xi}_0^* = \tilde{\xi}_{01} = \ldots = \tilde{\xi}_{0N}$. The stochastic process $\tilde{\xi}$ can be structured by a fan of scenarios. The FTCA is implemented for constructing a tree process ξ_{tr} can be constructed from $\tilde{\xi}$, such that the L_r-distance is $\|\tilde{\xi} - \xi_{tr}\|_r \leq \varepsilon$ with $\varepsilon > 0$.

The idea behind FTCA consists of using recursive scenario reduction to form clusters of scenarios on the time horizon $0, \ldots, S$ in order to increase stage s. The L_r-seminorm $\|\cdot\|_{r,s}$ is used in stage s.

The procedure recursively determines the stochastic processes $\tilde{\xi}_s$ that have scenarios $\tilde{\xi}_{si}$ with probabilities p_i, $i \in I = \{1, \ldots, N\}$ and $\mathcal{C}_s = \{C_s^1, \ldots, C_s^k, \ldots, C_s^{K_s}\}$ of I, such that

$$C_s^k \cap C_s^{k'} = \emptyset,\ k \neq k' \text{ and } \bigcup_{k=1}^{K_s} C_s^k = I,$$

where $\mathcal{C}_s$ is called the *scenario cluster index set.*

FTCA is described below:

- *Initialization:* fixed $\tilde{\xi}_0 = \tilde{\xi}$, i.e., $\tilde{\xi}_{0\omega} = \tilde{\xi}_\omega, \omega \in I$, and $\mathcal{C}_0 = \{I\}$.
- *Stage s:* every cluster C_{s-1}^k (i.e., every scenario subset $\left\{\tilde{\xi}_{s-1\omega}\right\}_{\omega \in C_{s-1}^k}$) is considered separately and subjected to scenario reduction with respect to the semi-norm $|\cdot|_s$ that leads to index sets I_s^k and J_s^k of remaining and deleted scenarios being created, where:

$$I_s^k \cup J_s^k = C_{s-1}^k$$

and

$$J_s^k = \bigcup_{s \in I_s^k} J_{si}^k = \{j \in J_s^k : s = i_s^k(j)\} \text{ and } i_s^k(j) \in \arg\min_{\omega \in I_s^k} |\tilde{\xi}_{s-1\omega} - \tilde{\xi}_{s-1j}|$$

A mapping shall be defined as $\alpha_s : I \longrightarrow I$, such that

$$\alpha_s(j) = \begin{cases} i_s^k(j), & j \in J_s^k, k = 1, ..., K_{s-1} \\ j, & \text{otherwise.} \end{cases} \tag{3.3.24}$$

Thereunto the scenario of the stochastic process $\tilde{\xi}_s = \{\tilde{\xi}_{sl}\}_{l=1}^{\Omega}$ is defined by

$$\tilde{\xi}_\tau^{si} = \begin{cases} \tilde{\xi}_\tau^{\alpha_\tau(i)}, & \tau \leq s \\ \tilde{\xi}_\tau^i, & \text{otherwise,} \end{cases} \tag{3.3.25}$$

with probabilities p_ω for each $\omega \in I$. The partition $\mathcal{C}_s$ at stage s is defined by

$$\mathcal{C}_s = \left\{\alpha_s^{-1}(i) : i \in I_s^k, k = 1, \ldots, K_{s-1}\right\}.$$

Each element of the index set I_s^k defines a new cluster; thus, the partition $\mathcal{C}_s$ is a refinement of the partition $\mathcal{C}_{s-1}$. The scenario set I_s is defined with scenario cluster $\bar{I}_{si}$, and the cluster probabilities π_s^i take the following form:

$$I_s = \bigcup_{k=1}^{K_{s-1}} I_s^k$$

$$\bar{I}_{si} = \{i, j : j \in J_{si}^k\} = \mathcal{C}_s^k \text{ and } \pi_{si} = \sum_{j \in \mathcal{C}_s^k} p_j \text{ if } i \in I_s^k \text{ for some } k = 1, \ldots, K_{s-1}.$$

The branching degree of scenario ω at s coincides with the cardinality of $\bar{I}_{si}$.

- *State $S+1$:* the scenario and the probabilities of the scenario tree $\xi_{tr} = \tilde{\xi}^S$ are given by the structure of the final partition $\mathcal{C}_S$, which takes the form (for each $k = 1, \ldots, K_S$.)

$$\xi_{tr}^k = \left(\xi_0^*, \xi_1^{\alpha_1(i)}, \ldots, \xi_T^{\alpha_T(i)}\right) \text{ and } \pi_S^\omega \text{ if } i \in C_S^k.$$

Therefore, the summarized FTCA generates a variety of scenario trees that satisfy a given approximation tolerance with respect to the L_r-distance, which is shown in Algorithm 1. The Forward Selection Algorithm (FSA) is used to calculate the disjoint index sets J_s^k and I_s^k. It is shown in Algorithm 2.

Algorithm 1: FTCA

Input: $\tilde{\xi}^1$,p_ω,ε_s
Output: ξ_{tr},p_ω,$\mathcal{C}_S$
Initialization: $\tilde{\xi}_{1\omega} = \tilde{\xi}$, and $\mathcal{C}_0 = \{\{1, \ldots, N\}\}$
Step s: Let $\mathcal{C}_{s-1} = \{C_{s-1}^1, \ldots, C_{s-1}^{K_{s-1}}\}$.
Determine:
- Disjoint index sets I_s^k and J_s^k such that $I_s^k \cup J_s^k = C_{s-1}^k$.
- The mapping $\alpha_s(\cdot)$ according to Equation (3.3.24).
- A stochastic process $\tilde{\xi}_s$ having N scenarios $\tilde{\xi}_{s\omega}$ with probabilities p_ω according to Equation (3.3.25) such that $\|\tilde{\xi}_s - \tilde{\xi}_{s-1}\|_{r,s} \leq \varepsilon_s$.
- Set $\mathcal{C}_s = \{\alpha_s^{-1}(\omega) : \omega \in I_s^k, k = 1, \ldots, K_{s-1}\}$
Step $S+1$: Let $\mathcal{C}_S = \{C_S^1, \ldots, C_S^{K_S}\}$.
Construct:
- A stochastic process ξ_{tr} having K_S scenarios $\xi_{tr,s}^k = \alpha_s(\omega)$ if $\omega \in C_S^k$, k=1, ..., K_S $s = 1, \ldots, S$.

Algorithm 2: FSA

Input: $\hat{\xi}^s, p_\omega, J_{s1}^k, I_{s1}^k$
Output: J_s^k, I_s^k
Initialization: $J_{s1}^k = C_{s-1}^k, I_{s1}^k = \emptyset$
Step i: for certain stop criterion for i,
Let $u_i \in \arg \min_{u \in J_{s,i-1}^l} \sum_{l \in J_{s,i-1}^l \setminus \{u\}} p_l \min_{j \notin J_{s,i-1}^l \setminus \{u\}} |\tilde{\xi}_l - \tilde{\xi}_j|^r$.
$J_{si}^k = J_{si-1}^k \setminus \{u_i\}$
$I_{si}^k = I_{si-1}^k \cup \{u_i\}$
Final Step:Stop criterion for i satisfied, then:
$J_s^k = J_{si}^k$
$I_s^k = I_{si}^k$.

At stage s, the FTCA stops clustering scenarios as soon as the L_r-seminorm between the tree at s and $s-1$ is reduced as follows for ε_s:

$$\|\tilde{\xi}_s - \tilde{\xi}_{s-1}\|_{r,s} \leq \varepsilon_s. \tag{3.3.26}$$

The individual tolerances ε_s at branching points are chosen, such that:

$$\varepsilon_s = \varepsilon_{rel,s} \cdot \varepsilon_{max,s}. \tag{3.3.27}$$

At this point, the maximum tolerance for each stage $\varepsilon_{max,s}$ is the best possible distance between the following values: the probability distribution in stage s of the initial scenario tree and the distribution of one of its scenarios having gained unit mass for stage s, thus:

$$\varepsilon_{emax,s} = \min \|\tilde{\xi}_{sl} - \tilde{\xi}_s\|_{r,s} \quad \forall s \in \mathcal{S}, \tag{3.3.28}$$

where $l = arg \min_{l \in \mathcal{C}_0} \|\tilde{\xi}_l - \tilde{\xi}\|_r$.

In addition, the relative tolerance for each stage $\varepsilon_{rel,s}$ for stage $s \in \mathcal{S}$, is defined by the recursive equation

$$\varepsilon_{erel,s} = \varepsilon_{erel,s-1} + \delta_{s-1}, \tag{3.3.29}$$

with $\delta_s = \delta_{s-1} + \Delta$.

3.3.2.2. Dynamic Tree Generation with Flexible Business Algorithm (DTGFBA)

An algorithm is presented in this section for the dynamic generation of scenario trees. It approximates probability measures using a concept that is appropriated for providing a distance for the stochastic process, which is the *Nested Distance*. The theoretical foundation and the DTGFBA are shown below.

- **Theoretical Foundation**

  The theoretical foundation is a summary of the theory developed in Pflug and Pichler (2015) and Pflug and Pichler (2014), as presented below.

  Let P be a probability model and $\tilde{P}$ another probability model. The focus is on exactly how close $\tilde{P}$ is to P. For this purpose, we lay out the concept of closeness for probability measures based on distances and norm.

  Definition 3.3.8 (Distance and Semi-Distance)**.** Let $\mathcal{P}$ be a set of probability measures on $\mathbb{R}^m$. A distance $\mathbf{d}$ on $\mathcal{P} \times \mathcal{P}$ satisfies the following three conditions:

  i) *Non-negativity*: for all $P_1, P_2 \in \mathcal{P}$,

  $$\mathbf{d}(P_1, P_2) \geq 0.$$

  ii) *Symmetry*: for all $P_1, P_2 \in \mathcal{P}$,

  $$\mathbf{d}(P_1, P_2) = \mathbf{d}(P_1, P_2).$$

iii) *Triangle Inequality*: for all $P_1, P_2, P_3 \in \mathcal{P}$,

$$\mathbf{d}(P_1, P_2) \leq \mathbf{d}(P_1, P_3) + \mathbf{d}(P_3, P_2).$$

A semi-distance $\mathbf{d}(\cdot, \cdot)$ is called a *distance* if it satisfies the strictness property:

iv) *Strictness*: if $\mathbf{d}(P_1, P_2) = 0$, then $P_1 = P_2$

A principle for defining distances and semi-distances consists of choosing a family of integrable functions $\mathcal{H}$, which are defined by

$$\mathbf{d}_{\mathcal{H}} = \sup_{h \in \mathcal{H}} \left| \int h dP_1 - \int h dP_2 \right|.$$

If $\mathcal{H}$ is *separating*, i.e., if for every pair P_1, P_2 there is a function $h \in \mathcal{H}$ such that $\int h \mathbf{d} P_1 \neq \int h \mathbf{d} P_2$, then $\mathbf{d}_{\mathcal{H}}$ is strict and is thus a distance.

The function c is often associated with the interpretation that moving a particle $\omega \in \Omega$ to $\tilde{\omega} \in \Omega$ costs $c(\omega, \tilde{\omega})$; therefore, it is often called a *cost function*, which is

$$c : \Omega \times \Omega \to \mathbb{R}, \tag{3.3.30}$$

thus linking two sample spaces Ω and $\tilde{\Omega}$.

A common definition considers the cost function as:

$$c(\cdot, \cdot) = \mathbf{d}(\cdot, \cdot)^r : \Omega \times \Omega \to \mathbb{R},$$

where $\mathbf{d}$ is a distance on Ω and $r \geq 1$.

Typically, the probability space $(\Omega, \mathcal{F}, P)$ does not carry. However, it has been assumed that Ω inherits a distance or semi-distance from a random variable $\xi : \Omega \to \mathbb{R}^{m_s}$ (for $s \in \mathbb{N}$) by

$$\mathbf{d}(\omega, \omega') = \|\xi_\omega - \xi_{\omega'}\|,$$

where $\|\cdot\|$ is a certain norm in $\mathbb{R}^{m_s}$.

Definition 3.3.9 (*Inherited Distance*)**.** If ξ is an $\mathbb{R}^{m_s}$-valued random variable on Ω and $\tilde{\xi}$ is an $\mathbb{R}^{m_s}$-valued random variable on $\tilde{\Omega}$, then the *inherited distance* between elements Ω and $\tilde{\Omega}$ can be defined by the transportation cost function $c(\omega, \tilde{\omega})$

$$\mathbf{d}(\omega, \tilde{\omega}) = c(\omega, \tilde{\omega}) = \mathbf{d}(\xi_\omega, \tilde{\xi}_{\tilde{\omega}}),$$

for a given distance $\mathbf{d} \in \mathbb{R}^{m_s}$, which is often $\mathbf{d}(w, v) = \|w - v\|$ for a certain norm $\|\cdot\|$ in $\mathbb{R}^{m_s}$.

Multiple and subsequent stages are considered in multistage stochastic problems. To this end, let $(\Omega, \mathcal{F}, P)$ and $(\tilde{\Omega}, \tilde{\mathcal{F}}, \tilde{P})$ be two probability spaces, and let $\xi : \Omega \longrightarrow \Xi$ and $\tilde{\xi} : \tilde{\Omega} \longrightarrow \Xi$ be two random variables with a common image space $\Xi \subseteq \mathbb{R}^{ms}$, which is endowed with a metric $\mathbf{d}$. It is assumed that $(\Xi, \mathbf{d})$ is a Polish space and the Wasserstein distance $\mathbf{d}_r$ in $\mathcal{P}_r(\Xi)$ is well-defined. At this point, this distance is extended for the stochastic process $\{\xi\}_{s=0}^{S}$, which is defined on a filtered probability space $(\Omega, \mathcal{F}, P)$, and for another process $\{\tilde{\xi}\}_{s=0}^{S}$, which is defined on $(\tilde{\Omega}, \tilde{\mathcal{F}}, \tilde{P})$.

If a stochastic process $\xi_s : \Omega \longrightarrow (\Xi_s, \mathbf{d}_s)$, $s = 0, \ldots, S$ is considered, then these random variable $\{\xi_s\}_{s=0}^{S}$ can be compounded to a single random variable ξ via

$$\begin{aligned} \xi_s : \Omega &\longrightarrow \Xi_0 \times \Xi_1 \times, \ldots, \times \Xi_S \\ \omega &\longmapsto (\xi_{0\omega}, \ldots, \xi_{S\omega}), \end{aligned} \tag{3.3.31}$$

where each ω is mapped to its path (the trajectory) in the space $\Xi = \Xi_0 \times \Xi_1, \ldots, \Xi_S$. This setting generalizes the usual definition of a stochastic process as the state of the partial observations:

$$\xi_s = proj_s \circ \xi : \Omega \to \Xi_s, \quad s = 0, \ldots, S,$$

which may vary at different times ($proj_s \circ \xi : \Xi \to \Xi_s$ is the natural projection).

From this point forward, any one of the spaces Ξ_s is equipped with a distance function $\mathbf{d}_s$, there being many metrics $\mathbf{d}$ such that $(\Xi, \mathbf{d})$ is a metric space. Given two processes $\{\xi\}_{s=0}^{S}$ and $\{\tilde{\xi}\}_{s=0}^{S}$ (in the same space Ξ_s) in, respectively, $\Omega(\tilde{\Omega})$ a semi-distance becomes inherent to $\Omega \times \tilde{\Omega}$ in an analogous way, as in Definition 3.3.9. Let us look, for example, at the ℓ^2-distance:

$$\mathbf{d}(\omega, \tilde{\omega}) = \left(\sum_{s=0}^{S} w_s \cdot \mathbf{d}_s \left(\xi_{s\omega}, \tilde{\xi}_{s\tilde{\omega}} \right)^2 \right)^{\frac{1}{2}} \quad \left(\xi, \tilde{\xi} \in \Xi \right), \tag{3.3.32}$$

The Wasserstein distance must be extended to stochastic processes that take into account all sigma algebras contained in the filtration of the filtered probability spaces. The nested distance is this generalization.

Definition 3.3.10 (*The nested distance*)**.** assuming that the two probability models $\mathbb{P} = (\Omega, (\mathcal{F}_s), P, \xi)$ and $\tilde{\mathbb{P}} = (\tilde{\Omega}, (\tilde{\mathcal{F}}_s), \tilde{P}, \tilde{\xi})$ are given, then the nested distance of order $r \geq 1$, for which a distance $\mathbf{d} : \Omega \times \tilde{\Omega} \to \mathbb{R}$ is defined, is the optimal value of the optimization problem:

$$\begin{aligned}
&\underset{(\text{in } \pi)}{\text{minimize}} \left(\int \int \mathbf{d}(u,v)^r \pi(du,dv) \right) \\
&\text{subject to } \pi\left(A \times \tilde{\Omega} | \mathcal{F}_s \oplus \tilde{\mathcal{F}}_s\right) = P(A|\mathcal{F}_s) \quad (A \in \mathcal{F}_s, s = 0,\ldots,S) \text{ and} \\
&\qquad \pi\left(\Omega \times B | \mathcal{F}_s \oplus \tilde{\mathcal{F}}_s\right) = \tilde{P}(B|\tilde{\mathcal{F}}_s) \quad (B \in \tilde{\mathcal{F}}_s, s = 0,\ldots,S), \qquad (3.3.33)
\end{aligned}$$

where the infimum in Problem (3.3.33) is among all bivariate probability measures $\pi \in \mathcal{P}(\Omega \times \tilde{\Omega})$, which are measures for $\mathcal{F} \oplus \tilde{\mathcal{F}}$. Its optimal value (the nested, or multistage distance) is denoted by

$$\mathbb{d}_r\left(\mathbb{P}, \tilde{\mathbb{P}}\right),$$

In order to establish the corresponding linear program for the nested distance, trees that model the whole space and filtration are used. It is essential that $j \prec i$ is denoted as that node j, which is a predecessor of node i, although it is not necessarily the immediate predecessor. Problem (3.3.33) is redefined as:

$$\begin{aligned}
&\underset{(\text{in } \pi)}{\text{minimize}} \sum_{i,j} \pi_{i,j} \cdot d_{i,j}^r \\
&\text{subject to } P(i) \cdot \sum_{i' \succ k, j' \succ l} \pi_{i',j'} = P(k) \cdot \sum_{j' \succ n} \pi_{i,j'} \quad (k \prec i), \qquad (3.3.34) \\
&\qquad \tilde{P}(j) \cdot \sum_{i' \succ k, j' \succ l} \pi_{i',j'} = \tilde{P}(l) \cdot \sum_{i' \succ k} \pi_{i',j} \quad (l \prec j), \\
&\qquad \pi_{i,j} \geq 0, \sum_{i,j} \pi_{i,j} = 1,
\end{aligned}$$

where P and $\tilde{P}$ are given. Problem (3.3.34) is a linear program.

- **Algorithm**

The goal of DTGFBA algorithm (Algorithm 3) is to construct a valuated process that best represents the process $\{\xi\}_{s=1}^S$. The basic stochastic process $\{\xi\}_{s=1}^S$ is defined in a probability space $(\Omega, \mathcal{F}, P)$, which has been estimated, i.e., its distribution $\mathbb{P}$ has been identified. The construction of a discretization stochastic process becomes the next priority $\{\tilde{\xi}\}_{s=1}^S$, which is defined in $\tilde{\Omega}$ where its valuated probability tree $\tilde{\mathbb{P}}$ (the scenario tree) will be identified with a distance between elements of $u \in \Omega$ and $v \in \tilde{\Omega}$, which are defined by

$$\mathbf{d}(u,v) = \sum_{s=1}^{S} \mathbf{d}_s\left(\xi_{su}, \tilde{\xi}_{sv}\right).$$

For this purpose, the nested distance has been calculated for Problem (3.3.33). In order to study and implement the DTGFBA, the algorithm developed in Pflug

and Pichler (2015) was used as the basis. This allows for a predetermined error ε_t, which must not be exceeded, and it also requires that the bushiness at each node be predetermined. Algorithm 3 presents the DTGFBA that we will use. In addition, Algorithm 4 is a Typical Hierarchical Cluster Algorithm (THCA), which is used for partitioning a larger set of points into k clusters in item (ii) of Algorithm 3. This is an acceptable configuration for the subsequent optimization algorithm.

Algorithm 3: DTGFBA

1 **Parameters**: let S be the desired height of the tree, $(b_1, \ldots, b_S)$, be the minimal bushiness values and $(\varepsilon_1, \ldots \varepsilon_S)$ the maximal stagewise transportation distances. These two vectors are fixed in advance.

2 **Determining the Root**: the value of the process at the root is $\tilde{\xi}_0$ and its stage is 0. The root is set as the current open node.

3 **While** there are open nodes, **Do**
(i) Let l be the next open node and let $s < S$ be its stage. Let $\tilde{\xi}_0, \ldots, \tilde{\xi}_{s-1}, \tilde{\xi}_s$ be the already fixed values at node l and its predecessors. The initial number of successors of l is set to $k = b_{s+1}$.
(ii) Call a typical hierarchical cluster algorithm (Algorithm 4) to find the k cluster. Let $\left(z^{(1)}, \ldots, z^{(k)}\right)$ be the cluster's medians of k observed samples taken from the distribution by $F_{s+1}(\cdot|\tilde{\xi}_s, \tilde{\xi}_{s-1}, \ldots, \tilde{\xi}_0)$. Next, compute the distance d by means of the linear program in Problem (3.3.34).
(iii) If d is larger than d_{s+1}, then b is increased by one and return to (ii) then returned to. Otherwise step (iv) is implemented.
(iv) The b successor nodes of node l are stored using the values $z^{(l)}$ and their optimal conditional probabilities p_l. The new successors are then marked as open.

4 **Stopping criterion**: if all nodes at stage $S-1$ have been considered as parent nodes, the generation of the tree is finished.

Algorithm 4: THCA

1 **Sampling**: Suppose that n points $\{z^{(1)}, \ldots, z^{(n)}\} \in \mathbb{R}^m$ are given, endowed with metric $\mathbf{d}$. The set $Z = \{z^{(i)} : i = 1, \ldots, n\}$ is iteratively partitioned into disjoint clusters, such that their number decreases from step to step. At the beginning, each point is a cluster of itself.

2 **Iteration**: Supposing that the current partition of the set is $\mathbb{R}^m = \biguplus_j C_j$, the pair of clusters (C_j, C_l) must be found for which

$$\sup\{\mathbf{d}(z, z') : z \in C_j, z' \in C_l\},$$

is minimal. A new cluster is then created by merging C_j and C_l.

3 **Stopping criterion**: if the number of clusters has decreased to the desired number k, then the end has been reached. Otherwise it continues by going to 2.

3.4. Performance Evaluation of Scenario Trees

To evaluate the performance of the generated scenario trees, we establish parameters that have been inspired by the ideas developed in Escudero et al. (2007). These parameters are based on the definitions of the *Value of the Stochastic Solution*(VSS),

which were established for two-stage models. These definitions are applied to the new parameters for the MSP models presented in this study.

The deterministic equivalent model is expanded:

$$\begin{aligned} \underset{x_0, x_{1\omega}, x_{2\omega}, \ldots, x_{S\omega}}{\text{minimize}} \; & \sum_{\omega \in \Omega} p_\omega \left[f_0(x_0, \xi_0) + f_1(x_{1\omega}, \xi_{1\omega}) \ldots + f_S(x_{S\omega}, \xi_{S\omega}) \right] \\ \text{subject to} \; & x_0 \in \boldsymbol{\chi}_0, \quad x_{s\omega} \in \boldsymbol{\chi}_s(x_{s\omega}, \xi_{s\omega}), \quad \forall\, s = 1, \ldots, S, \, \forall\, \omega \in \Omega, \\ & x_{s\omega} = x_{sl} \;\; \text{such that} \;\; \xi_{[s]\omega} = \xi_{[s]l}, \, \forall s \in \mathcal{S}, \, \forall\, \omega, \, l \in \Omega, \end{aligned} \tag{3.4.1}$$

where $x_{s\omega}$ denotes the decision variables related of stage $s \in \mathcal{S}$ under scenario $\omega \in \Omega$, $\xi_{s\omega}$, which is the realization of stage $s \in \mathcal{S}$ under scenario $\omega \in \Omega$ in the scenario tree; p_ω is the probability of scenario $\omega \in \Omega$. The decision variables $x_{s\omega}$ are participated to stage s. The *recourse variables* denoted by $y_{s\omega}$ correspond to recourse actions that are taken at stage s in order to correct the strategic decision elevated to stage s. The *state decision variable* denoted by $z_{s\omega}$, (the first stage is deterministic and called z_0, as it is the *first state decision variable*). Thus, $x_{s\omega} = (y_{s\omega}, z_{s\omega})$.

Let the *Recourse Problem* (RP) be the optimal value of the objective function of the model given in Equation (3.4.1), that is:

$$\text{RP} = \underset{x_0, x_{1\omega}, x_{2\omega}, \ldots, x_{S\omega}}{\text{minimize}} \sum_{\omega \in \Omega} p_\omega \left[f_0(x_0^*, \xi_0) + f_1(x_{1\omega}^*, \xi_{1\omega}) + \ldots + f_S(x_{S\omega}^*, \xi_{S\omega}) \right], \tag{3.4.2}$$

where $x_{s\omega}^*$, is the optimal decision variable in stage $s \in \mathcal{S}$ and scenario $\omega \in \Omega$.

Let the vector $\xi_{s\omega} = \xi_s^E$ be defined as the average scenario for stage $s \in \mathcal{S}$ and a certain scenario $\omega \in \Omega$. The Expected Value (EV) problem is defined as the following deterministic model:

$$\begin{aligned} EV = \underset{(y_s, z_s),\, s \in \mathcal{S}}{\text{minimize}} \; & \left[f_0((y_0, z_0), \xi_0^E) + f_1((y_1, z_1), \xi_1^E) + \ldots + f_S((y_S, z_S), \xi_S^E) \right] \\ \text{subject to} \; & (y_s, z_s) \in \boldsymbol{\chi}_s, \, \forall\, s \in \mathcal{S}, \end{aligned} \tag{3.4.3}$$

where $x_s^E = (y_s^E, z_s^E)$ is the optimal solution for the model in Equation 3.4.3, and the optimal value of the objective function is called the *Expected Value* (EV).

If $z_{s\omega} = z_s^E$ and $z_0 = z_0^E$ in Equation 3.4.3, we obtain the problem:

$$\begin{aligned} EEV = \underset{(y_s, z_s^E),\, s \in \mathcal{S}}{\text{minimize}} \; & \sum_{\omega \in \Omega} p_\omega \left[f_0((y_{0\omega}, z_0^E), \xi_0) + f_1((y_{1\omega}, z_1^E), \xi_1) + \ldots + f_S((y_{S\omega}, z_S^E), \xi_S) \right] \\ \text{subject to} \; & x_0^E \in \boldsymbol{\chi}_0, \quad (y_{s\omega}, z_s^E) \in \boldsymbol{\chi}_s((y_{s\omega}, z_s^E), \xi_{s\omega}), \quad \forall\, s = 1, \ldots, S, \, \forall\, \omega \in \Omega, \\ & y_{s\omega} = y_{sl} \;\; \text{such that} \;\; \xi_{[s]\omega} = \xi_{[s]l}, \, \forall s \in \mathcal{S}, \, \forall\, \omega, \, l \in \Omega. \end{aligned} \tag{3.4.4}$$

The value of the objective function of model 3.4.4 at the optimal solution is known as the *Expectation of the Expected Value* (EEV), and can be used to define the solution called *Expected Value of the Stochastic Solution* (EVSS).

$$\text{EVSS} = RP - EEV. \tag{3.4.5}$$

A value that relates the $EVSS$ to the RP is detailed, that is:

$$\text{EVSSr} = 100 \times \frac{EVSS}{RP}. \tag{3.4.6}$$

This represents how much the RP solution $x^* = (x_0, x_{1\omega}, \ldots, x_{S\omega})$, $\forall \omega \in \Omega$ improves the EV solution x^E in terms of the expectation of the total profits, according to the representation of the future expressed through $\xi = (\xi_0, \xi_{1\omega}, \ldots, \xi_{S\omega})$, $\forall \omega \in \Omega$.

On the other hand, consider the *Forecasted Value Problem* (FVP):

$$\begin{aligned} FVP = \underset{(y_s, z_s),\, s \in \mathcal{S}}{\text{minimize}} \; & \left[f_0((y_0, z_0), \xi_0^F) + f_1((y_1, z_1), \xi_1^F) + \ldots + f_S((y_S, z_S), \xi_S^F) \right] \\ \text{subject to } & (y_s, z_s) \in \boldsymbol{\chi}_s, \; \forall\, s \in \mathcal{S}, \end{aligned} \tag{3.4.7}$$

where $x_s^F = (y_s^F, z_s^F)$ is the optimal solution (called the *Forecast Value* (FV)) and ξ_s^F is a scenario forecast in stage $s \in \mathcal{S}$.

The *Expectation of the Forecasted Value* (EFV) is the expected value associated to the optimal objective function of 3.4.8, as illustrated in the following model:

$$\begin{aligned} EFV = \underset{(y_s, z_s^F),\, s \in \mathcal{S}}{\text{minimize}} \; & \sum_{\omega \in \Omega} p_\omega \left[f_0((y_{0\omega}, z_0^F), \xi_0) + f_1((y_1, z_1^F), \xi_1) + \ldots + f_S((y_S, z_S^F), \xi_S) \right] \\ \text{subject to } & x_0^F \in \boldsymbol{\chi}_0, \quad (y_{s\omega}, z_s^F) \in \boldsymbol{\chi}_s((y_{s\omega}, z_s^F), \xi_{s\omega}), \quad \forall\, s = 1, \ldots, S, \; \forall\, \omega \in \Omega, \\ & y_{s\omega} = y_{sl} \;\text{ such that }\; \xi_{[s]\omega} = \xi_{[s]l}, \; \forall s \in \mathcal{S}, \; \forall\, \omega, \, l \in \Omega. \end{aligned} \tag{3.4.8}$$

Then, the *Forecasted Value of the Stochastic Solution* (FVSS) is defined as:

$$FVSS = RP - EFV. \tag{3.4.9}$$

This parameter represents how much the RP solution x^* improves the FV solution x_s^F, $s \in \mathcal{S}$ in terms of the expectation of the total profits, according to the representation of the future expressed through ξ.

The same relationship shown in Equation 3.4.6 is defined for $FVSS$ and RP. This is:

$$\text{FVSSr} = 100 \times \frac{FVSS}{EFV}. \tag{3.4.10}$$

The definition of a good mathematical problem
is the mathematics it generates rather
than the problem itself.

— *Andrew Wiles*

4

Scenario Trees for MSP Models in Renewable Energy Systems

Contents

As has been introduced, the scenario trees are a way to represent the uncertainty that results from a sequence of decisions in the stages of Multistage Stochastic Programming (MSP) problems. In this chapter, two MSP models are presented. The first of these models is an Electricity Markets (EM) application for optimizing Virtual Power Plant (VPP) (which comprises a Wind Power Plant (WPP) and Battery Energy Storage System (BESS)) participation in the MIBEL (Day-Ahead Market (DM), Intra-day Market (IM) and Secondary Reserve Market (RM)) considering Imbalance Settlements (IB) (Section 4.1). The second model is an Electrical Distribution Networks (EDN) application for the optimal operation of EDN while considering BESS (Section 4.2), such that it minimizes the total cost of energy purchased from the Distribution Substation (DSS), Distributed Generators (DG) and RSs. For each model, several important aspects are presented in the following. Firstly, the real problems being treated are introduced (Sections 4.1.1 and 4.2.1). Secondly, we study the uncertainty and decision process of

each problem, which have resulted in the scenario tree structures we apply to the MSP models (Sections 4.1.2 and 4.2.2). Finally, the Multistage Stochastic Wind Battery Virtual Power Plant model (MSWBVPP model) and the Multistage Stochastic Optimal Operation of Distribution Networks model (MSOODN model) are presented in Sections 4.1.3 and 4.2.3, respectively. The scenario tree structures and MSP models are the main results of this chapter.

4.1. Scenario Tree for the MSWBVPP Model

In this section, we provide all the details about the general structure of the scenario tree for the MSWBVPP model. Firstly, Section 4.1.1 provides a brief introduction to EM and renewables. In this case, we explain how a WPP-BESS (our VPP) can participate in EM. Then, Section 4.1.2 gives details about the uncertainty and decision process that govern the problem and thus result in the definition of the scenario tree. Finally, Section 4.1.3 presents the modeled MSWBVPP.

4.1.1. EM and Renewables

An EM is a system that allow producers and consumers to buy and sell energy, thereby fixing an electricity clearing price by means of the price mechanism. On the Iberian peninsula, the EM is known as the Iberian electricity market (MIBEL[1] being its Spanish acronym), and it integrates both the Portuguese and Spanish electrical systems. In general, EM involve two different entities: 1) the *market agents*, which are companies authorized to participate in the EM as sellers or buyers; and, 2) the *market operators*, who are public companies committed to the organization and management of the markets. Regarding the market operators, there are two types: 1) the Independent Market Operators (IMO), which are responsible for the economic management; and 2) the Independent System Operators (ISO), who are in charge of the operations management of the system. In the MIBEL, the IMO is called OMIE[2]; and the ISO is called REE[3]. OMIE manages the DM where agents (producers, consumers, retailers, etc.) sell and buy electricity, as well as the IM where agents may once again buy and sell electricity, if necessary, to fill the gap between scheduled and current production. REE guarantees optimal operation of the electricity system through technical restrictions, ancillary services markets (primary, secondary and tertiary markets), and IB. Figure

[1] Mercado Ibérico de la Electricidad – MIBEL. http://mibel.com/es/home_es/
[2] Operador del Mercado Ibérico de Electricidad – OMIE. http://www.omie.es/inicio
[3] Red Eléctrica de España – REE. https://www.ree.es/es

4.1.1 shows a graphic description of the MIBEL, where the squares with red borders indicate the services will be taken into account this study.

The MIBEL works in the following way. Tomorrow is day N and today is day $N-1$. At 12:00 on day $N-1$, the first auction takes place: the DM. In this market, the energy price (clearing price) for the next 24 hours is negotiated *before* the DM closes. The REE checks the program (technical restriction) resulting from the DM. In the event this is not technically feasible, modifications are generally sent to the OMIE. After the DM closes, the REE manages the ancillary services markets that aim to ensure that the supply is carried out under conditions of safety and profitability at all times. There are three ancillary services: primary, secondary and tertiary. Primary corresponds to small imbalances, which are obligatory for all generators. Secondary (or RM) maintains the generation-demand balance by correcting deviations. Tertiary restores the reserve in the case that it is being used, which would be carried out at the last hour of day N. After the RM, we have the first IM session, which allows the agents participating in the DM to manage their previous positions. This is an effective mechanism for resolving incidents and changes in the forecasted supply and demand.

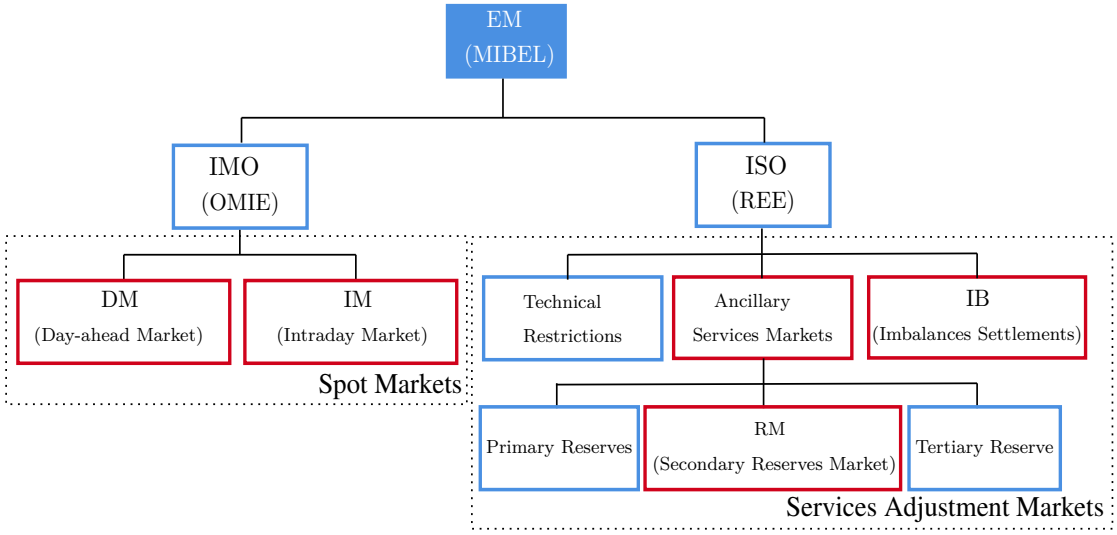

Figura 4.1.1: The MIBEL structure.

The sequence of processes in each session of the IM are as follows: throughout the six sessions that are distributed throughout each day, supply and demand can be adjusted at all hours. The opening hours are 17:00, 21:00, 01:00, 04:00, 09:00 and 14:00, from the first to the final session, respectively. In each IM trading session, the deviation can be identified a few hours before dispatch and is treated by the IB[4]. In Figure 4.1.2, we

[4] More details in: https://www.boe.es/eli/es/res/2015/12/23/(3) for the day-ahead and intraday markets, and https://www.boe.es/diario_boe/txt.php?id=BOE-A-2015-13875 for the ancillary services markets and imbalance settlement.

summarize the MIBEL operation. Regarding the IM, the arrows show the opening hours for each IM session and the bars under the blue arrow, their respective programming horizon. The arrows of each IM session has the same colour as their bar.

On the other hand, the market participants are companies authorized to buy and sell energy. Among these, two must be highlighted: 1) the *price maker*, which is a firm whose products have a single demand and is able to set its cum price; and 2) the *price taker*, who mandatorily accepts the common price of the market, which is usually imposed by the price maker. As the objects of this study, we deal with a special type of price takers known as *renewable energy producers*. These producers are renowned for their irrefutable significance in recent decades, due to environmental concerns, the intense growth of emerging countries, the ensuing inflationary effect on primary energy sources, and liberalization of Europe's energy sector. In particular, the renewable energy producers that we study are producers that use wind to provide power through turbines. These are known as wind energy producers (referred to here as WPP[5]).

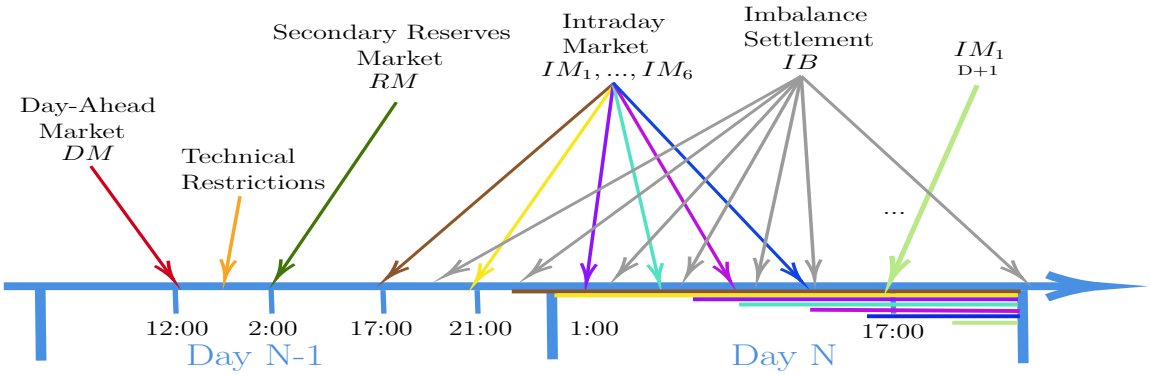

Figura 4.1.2: The MIBEL operation.

In the MIBEL, WPP started participating in the spot market before 1 January 2008 and received a clearing price plus a fixed subsidy in accordance with an incentive system. The rules of this participation were defined in RD 436/2004[6]. Later, the initial regulation was modified to establish an efficient incentive system for stimulating investment. This modification is mandated in RD 661/2007[7]. During 2010, a strong debate began on the regulation of new installations, with diverging opinions on the role of developing wind energy in the Spanish market. On the one hand, the government underlined the necessity to reduce the subsidy deficit; while on the other hand, wind energy companies rejected any possibility of performing like other technologies in the market, since investment costs in the sector were still very high. In recent years, the maturity and volume achieved

[5] A WPP is a collection of wind turbines that act together as a single power station (Breeze, 2016).
[6] RD 436/2004, from March 12: https://www.boe.es/eli/es/rd/2004/03/12/436
[7] RD 661/2007, from May 25: https://www.boe.es/eli/es/rd/2007/05/25/661/con

by renewable energy sources (mainly wind) have driven important regulatory changes in Spain. These took effect in 2014 when RD 413/2014[8] authorized participation in the services adjustment market of WPP, who in 2016 began to participate in at least two of the Services Adjustment Markets, specifically the IB and tertiary market. All these reasons justify the need to develop competitive strategies for a WPP participation in the EM, and this has been the goal of researchers in the last few years.

Currently, Wind Power (WP) is the renewable energy source that, together with photovoltaic solar energy, represents the first of the modern renewable technologies. Nevertheless, due to its intermittency, this source acts without any control, which may lead to inefficiency in both a technical and economical sense. In recent years, studies have focused on smoothing out WP fluctuation in order to dispatch it correctly to the power grid, thus avoiding system faults. On the other hand, in a competitive, deregulated electricity market, the financial issues relevant to economic revenue are of the most significance for these types of energy sources, because the amortization of investment and operability cost is a priority for these producers. Nowadays, one solution for addressing these challenges can be found in the use of a storage system with proper control mechanisms; thus, these drawbacks can be resolved by means of a VPP comprising a WPP and storage system.

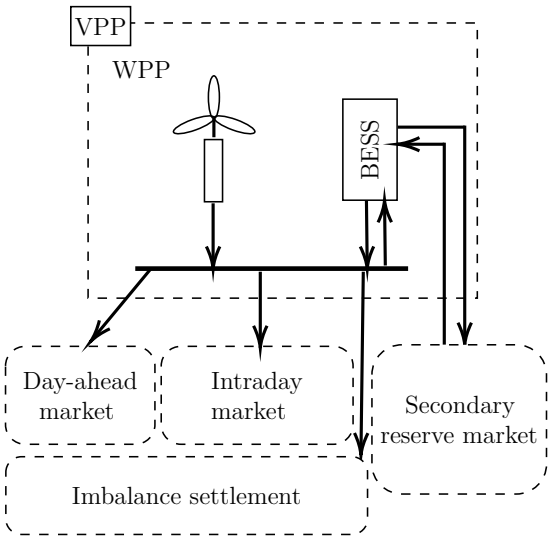

Figura 4.1.3: Operation of a VPP in the EM.

A VPP is a cluster of generator units, controllable loads and storage systems aggregated together to operate as a single power plant (Lombardi et al., 2009). In our case, the VPP consists of a WPP and BESS. We are interested in this producer sending bids to the MIBEL, especially in the spot markets (DM and IM) and in two of the

[8] RD 413/2014, from June 6: https://www.boe.es/eli/es/rd/2014/06/06/413.

services adjustment markets (RM and IB). Figure 4.1.3 displays the representation of the VPP operating in the MIBEL. This figure illustrates the VPP comprising of a WP and a BESS that can offer energy to the DM and it can offer or sell to all IM sessions; henceforth, the deviations of this operation can be controlled by participation in the IBs. In particular, the energy stored in the BESS can be offered and sold directly in the RM.

In Spain, two experimental projects where conducted using a VPP comprising WPP and BESS: 1) by Acciona in Barasoain (2013)[9], and 2) by Gamesa in La Muela (2016)[10]. The first is a wind storage solution connected to the network and which provides advanced technology services for analyzing and improving the quality of the energy that is injected into the system. The second is an 'off-grid' system that supplies energy to areas with no access to the electricity network. Neither of these exceeds the MW of storage and they are connected to a single wind turbine. Nowadays, Iberdrola has the first non-experimental wind farm with a storage system, generating 21 MW of power with 12 MW of storage[11]. These latest developments confirm that a VPP can be an efficient tool for supporting intermittence, and it can attenuate the fluctuations of WP to the point that even VPP can participate in the MIBEL just like as any other producers.

In general, the operation of the VPP is justified through some research by Ding et al. (2016); Heredia et al. (2018); Wang et al. (2019); González-Garrido et al. (2019); Banshwar et al. (2019); Wozabal and Rameseder (2020). In each of these studies, a VPP strategy is proposed for optimal participation in the EM. In particular, we propose a generalization of the study shown in Heredia et al. (2018), although here we consider the entire spot market.

4.1.2. Uncertainty and the Decision Process

As part of the study, the uncertainty presents in the MSWBVPP model is analyzed. Thus, we propose using scenario trees to obtain an appropriate representation of this uncertainty. In order to achieve this goal, we need to define the relationship between the model's parameters and variables as well as the elements of these scenario trees, which is the objective of this section. Firstly, the random parameters are defined in Table 4.1.1. Note that each random variable is a vector, which in most cases is high

[9] Available at: https://www.acciona-energia.com/areas-of-activity/wind-power/major-projects/experimental-wind-power-area-barasoain/

[10] Available at: http://www.ite.es/en/gamesa-completa-desarrollo-sistema-offgrid-la-puesta-marcha-una-bateria-almacenamiento-prototipo/

[11] Available in Spanish at: https://elperiodicodelaenergia.com/iberdrola-promueve-el-primer-parque-eolico-con-sistema-de-almacenamiento-de-espana-en-canarias/

dimensionality. Secondly, the uncertainty is represented by the decision variables that are defined by the VPP operations, which are subject to market bidding and the hourly operations of the BESS (charges and discharges), as well as the hourly IB. In Table 4.1.2, the decision variables associated with this problem are laid out. These also have the characteristic of high dimensionality.

$\boldsymbol{\lambda}^D \in \mathbb{R}^{24}$	Clearing prices of the DM.
$\boldsymbol{\lambda}^R \in \mathbb{R}^{24}$	Clearing prices of the RM.
$\boldsymbol{\lambda}^I_1 \in \mathbb{R}^{24}$	Clearing prices of the first IM session (IM1).
$\boldsymbol{\lambda}^I_2 \in \mathbb{R}^{24}$	Clearing prices of the second IM session (IM2).
$\boldsymbol{\lambda}^I_3 \in \mathbb{R}^{20}$	Clearing prices of the third IM session (IM3).
$\boldsymbol{\lambda}^I_4 \in \mathbb{R}^{17}$	Clearing prices of the fourth IM session (IM4).
$\boldsymbol{\lambda}^I_5 \in \mathbb{R}^{13}$	Clearing prices of the fifth IM session (IM5).
$\boldsymbol{\lambda}^I_6 \in \mathbb{R}^{9}$	Clearing prices of the sixth IM session (IM6).
$\boldsymbol{\lambda}^I_7 \in \mathbb{R}^{3}$	Clearing prices of the seventh IM session (IM7), (This is the first session the of present day).
$\boldsymbol{\lambda}^{IB_+} \in \mathbb{R}^{24}$	Prices for positive IB.
$\boldsymbol{\lambda}^{IB_-} \in \mathbb{R}^{24}$	Prices for negative IB.
$\mathbf{p}^W \in \mathbb{R}^{24}$	Hourly WP production.

Cuadro 4.1.1: Random parameters of VPP participation in the EM.

$\mathbf{p}^D \in \mathbb{R}^{24}$	Energy of the price-accepting bid for the 24 DM auctions.
$\mathbf{r}^U, \mathbf{r}^D \in \mathbb{R}^{24}$	upward/downward secondary reserve bid for the 24 RM auctions.
$\mathbf{p}^I_1 \in \mathbb{R}^{24}$	Energy of the price-accepting bid for the 24 IM1 auctions.
$\mathbf{p}^I_2 \in \mathbb{R}^{24}$	Energy of the price-accepting bid for the 24 IM2 auctions.
$\mathbf{p}^I_3 \in \mathbb{R}^{20}$	Energy of the price accepting bid for the 20 IM3 auctions.
$\mathbf{p}^I_4 \in \mathbb{R}^{17}$	Energy of the price-accepting bid for the 17 IM4 auctions.
$\mathbf{p}^I_5 \in \mathbb{R}^{12}$	Energy of the price-accepting bid for the 13 IM5 auctions.
$\mathbf{p}^I_6 \in \mathbb{R}^{6}$	Energy of the price-accepting bid for the 6 IM6 auctions.
$\mathbf{p}^I_7 \in \mathbb{R}^{3}$	Energy of the price-accepting bid for the 3 IM7 auctions, (this is the IM1 of the present day).
$\mathbf{c}, \mathbf{d} \in \mathbb{R}^{24}$	Hourly charges/discharges of the BESS.
$\mathbf{p}^{IB_+}, \mathbf{p}^{IB_-} \in \mathbb{R}^{24}$	Imbalances (positive and negative) of the 24 VPP auctions.

Cuadro 4.1.2: Operational decision variables of VPP participation in the EM.

Regarding IB, these are deviations between the true real-time generation of the VPP and the energy cleared in the DM and IM. These IB satisfy the following conditions: If the real generation exceed the cleared energy, some collection rights will be paid to the VPP owner ($\boldsymbol{\lambda}^{IB'_+}$). Otherwise, if the real generation is less than the cleared energy, the

VPP owner must face some payment obligations ($\boldsymbol{\lambda}^{IB'_-}$). To simplify the notation, we will apply $\boldsymbol{\lambda}^{IB} = \left(\boldsymbol{\lambda}^{IB'_+}, \boldsymbol{\lambda}^{IB'_-}\right)'$ for the prices and $\mathbf{p}^{IB} = \left(\mathbf{p}^{IB'_+}, \mathbf{p}^{IB'_-}\right)'$ for energy to refer to the complete set of positive and negative imbalances.

On the other hand, to relate the random variables with decision variables is appropriate to define the decision process that explain the situation. In this case, for optimal VPP participation in the EM, the initial day is today (day $N-1$). For this day, it is necessary to define the VPP's operational plan for the next day (day N). We take into consideration that various market elements have been negotiated and cleared on day $N-1$ and that other elements have been settled on day $N+1$. The decision process with the temporal distribution is defined as follows:

- *Stage 0* is associated with the DM. At this stage, the DM bid (the first-state variables p^D) is submitted to OMIE no later than 12:00.
- *Stage 1* is where OMIE makes the DM clearing prices (λ^D) public by 13:00, and the state variable of the bid to the RM (r^U, r^D) is submitted to OMIE no later than 14:00. There are no recourse variables for this stage.
- *Stage 2* is associated with the RM and the IM1. OMIE makes the RM clearing prices λ^R public by 14:00, and the bid to IM1 (state variable p_1^I) can be submitted to OMIE until 16:00. Again, there are not any recourse variables for this stage.
- *Stage 3* is associated with the IM1 and the IM2. The clearing prices to the IM1 (λ_1^I) are published at 19:00 and the bid to IM2 (state variable p_2^I) can be submitted to OMIE until 22:00. Again, there are no recourse variables for this stage.
- *Stage 4 to 33* have two forms for the decision sequence.

  i) *Stages 4 , 7 , 11 , 16 , 21 , 28*: the clearing prices for the remaining IM sessions ($\lambda_2^I, \ldots, \lambda_7^I$) are publicly communicated some time after each stage. The operation of the BESS for these stages is decided (whether energy is charged or drained from the batteries, indicated, respectively, by state variables c_t and d_t for $t \in \{1, 3, 6, 10, 14, 20\}$). There are no recourse variables for these stages.

  ii) *Stages 5–6 , 8–10 , 12–15 , 17–20 , 22–27 , 29–33*: the VPP and BESS operations. During these stages, there will be some wind production (the state variables p_t^W, $t = 1, \ldots, 24$), each possible outcome of which sets a different value for the imbalances (the recourse variables p_t^{IB}, $t = 1, \ldots, 24$). Following this, the BESS operation is decided (c_t, d_t, $t = 2, 4, 5, 7, 8, 9, 11, 12, 13, 15, \ldots, 19, 21, \ldots, 24$).

- *Stage 34*: the final imbalance value is known.

Table 4.1.3 describes the decision process along with the different stages of the problem. Each row corresponds to a decision stage.

Let $\mathcal{S} = \{s \in \mathbb{N} : s = 1, ..., 34\}$ be the set of stages for this problem. The stochastic process that governs this problem is defined as follows

$$\left\{\tilde{\boldsymbol{\xi}}_s\right\}_{s\in\mathcal{S}} \tag{4.1.1}$$

and $\mathbf{x}_s = (\mathbf{y}_s, \mathbf{z}_s)'$ is the decision variable for stage $s \in \mathcal{S}$. For instance:

- Index of stage s (first column)
- Random variable $\tilde{\boldsymbol{\xi}}_s$ of stage $s \in \mathcal{S}$ (second column)
- *Recourse variables* $\mathbf{z}_s$ *of stage* $s \in \mathcal{S}$ (third column): recourse actions to be taken after the random variables at the given stage $s \in \mathcal{S}$ are disclosed
- *State variables* $\mathbf{y}_s$ *of stage* $s \in \mathcal{S}$ (fourth column): these are the decisions to be taken at stage $s \in \mathcal{S}$, before the random variable at state $s + 1$ is known.

Therefore, the decision sequences for this stage (as defined by the decision process) are:

$$\textit{decided}\ \mathbf{x}_0 \xrightarrow{\textit{observed}} \tilde{\boldsymbol{\xi}}_1 \xrightarrow{\textit{decided}} \mathbf{x}_1 \xrightarrow{\textit{observed}}, \ldots, \xrightarrow{\textit{decided}} \mathbf{x}_{34} \xrightarrow{\textit{observed}} \tilde{\boldsymbol{\xi}}_{34}$$

where $\mathbf{x}_0 = \mathbf{y}_0, \mathbf{x}_1 = \mathbf{y}_1, \mathbf{x}_2 = \mathbf{y}_2, \mathbf{x}_3 = \mathbf{y}_3, \mathbf{x}_4 = \mathbf{y}_4$, coincide with state variables, respectively, of the energy of the price-accepting bid for the 24 DM auctions, upward/-downward secondary reserve bid for the 24 RM auctions, energy of the price-accepting bid for the 24 IM1 auctions, energy of the price-accepting bid for the 24 IM2 auctions and the charges/discharges of the BESS in hour 1. On the other hand, the decision process ends with the observation of IB parameter $\boldsymbol{\lambda}^{IB}$ in stage 34.

As an example:

- For $s = 5$, the random variable is given by $\tilde{\boldsymbol{\xi}}_5 = \tilde{p}_1^W$, where $\tilde{p}_1^W$ is the first component of the scenario vector $\tilde{p}^W$; the decision variable is given by $\mathbf{x}_5 = (\boldsymbol{p}_1^{IB}, c_2, d_2)'$.
- For $s = 17$, the random variable is given by $\tilde{\boldsymbol{\xi}}_{\mathbf{17}} = \tilde{\boldsymbol{\lambda}}_5^I = (\tilde{\lambda}_{5,1}^I, \ldots, \tilde{\lambda}_{5,24}^I)'$, and the decision variable is given by $\mathbf{x}_{16} = (c_{10}, d_{10})'$.

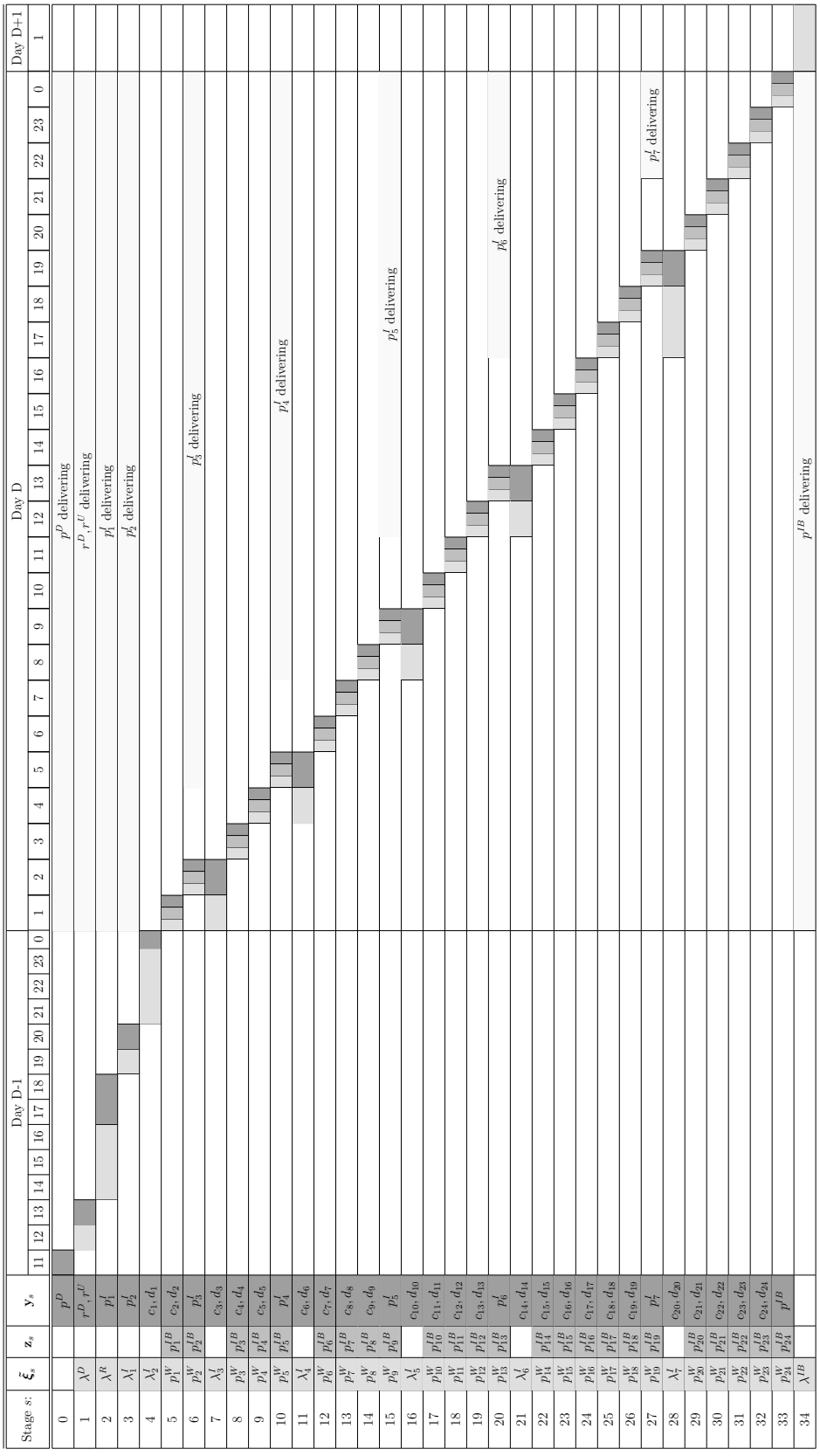

Cuadro 4.1.3: Decision stages of the MSWBVPP model.

Figure 4.1.4 illustrates the structure of the scenario tree for the case study. For the sake of clarity, a binary tree (2 realizations per node) is represented, but there can be more branches. The branches correspond to the disclosure of some random variable of stage $s \in \mathcal{S}$; the nodes are associated with different sets of the decision variables. The scenario tree in Figure 4.1.4 has 34 stages. The nodes are associated with the decision variables $\mathbf{x}_s$, $s \in \mathcal{S}$. The edges are the realizations of a multistage stochastic process $\{\tilde{\boldsymbol{\xi}}_s\}_{s\in\mathcal{S}}$. The red path is a scenario of the tree. By establishing as a basis that $\Omega = \{\omega : \omega = 1, ..., N\}$ is the scenario index, the scenario associated with index $\omega \in \Omega$ therefore has the related probabilities $P_\omega > 0,\ \omega \in \Omega$, such that $\sum_{\omega\in\Omega} P_\omega = 1$, which is defined as:

$$\tilde{\boldsymbol{\xi}}_\omega = \Big(\tilde{\boldsymbol{\lambda}}_\omega^{D'}, \tilde{\boldsymbol{\lambda}}_\omega^{R'}, \tilde{\boldsymbol{\lambda}}_{1\omega}^{I'}, \tilde{\boldsymbol{\lambda}}_{2\omega}^{I'}, \tilde{p}_{1\omega}^{W}, \tilde{p}_{2\omega}^{W}, \tilde{\boldsymbol{\lambda}}_{3\omega}^{I'}, \tilde{p}_{3\omega}^{W}, \ldots, \tilde{p}_{5\omega}^{W}, \tilde{\boldsymbol{\lambda}}_{4\omega}^{I'}, \tilde{p}_{6\omega}^{W}, \ldots, \tilde{p}_{9\omega}^{W}, \tilde{\boldsymbol{\lambda}}_{5\omega}^{I'}, \tilde{p}_{10\omega}^{W}, \ldots, \tilde{p}_{13\omega}^{W}, \tilde{\boldsymbol{\lambda}}_{6\omega}^{I'}, \tilde{p}_{14\omega}^{W}, \ldots, \tilde{p}_{19\omega}^{W}, \tilde{\boldsymbol{\lambda}}_{7\omega}^{I'}, \tilde{p}_{20\omega}^{W}, \ldots, \tilde{p}_{24\omega}^{W}, \tilde{\boldsymbol{\lambda}}_{\omega}^{IB'}\Big)' \tag{4.1.2}$$

Figure 4.1.4, shows the representation of scenarios $\tilde{\boldsymbol{\xi}}_\omega$ in the tree (red line) with its probability P_ω.

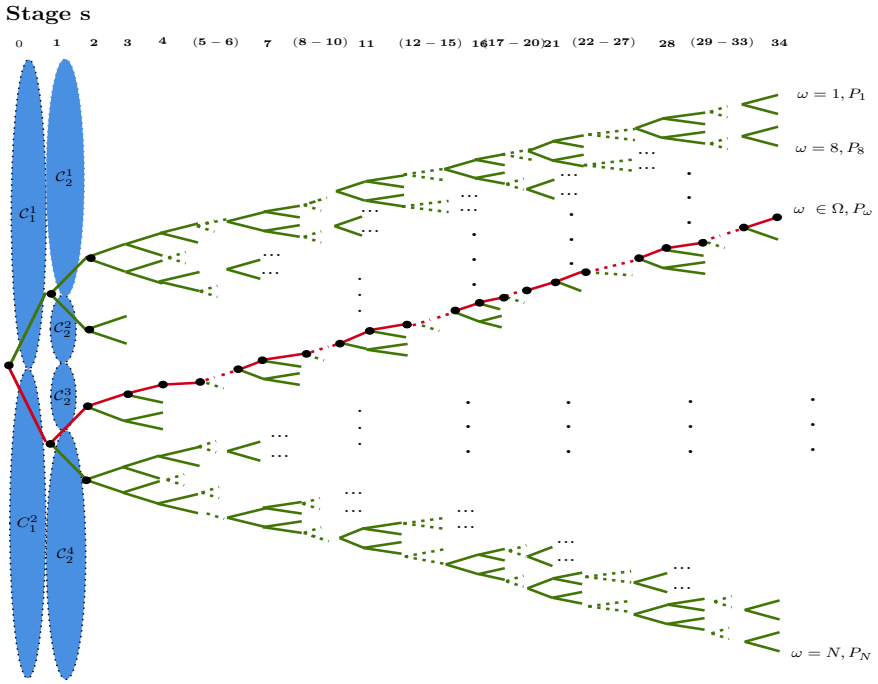

Figura 4.1.4: Scenario tree structure for the MSWBVPP model.

If two scenarios belong to the same group in a given stage and have the same realization of the uncertain parameter up to that stage, then they belong to the same set. This set is defined as a scenario cluster. There are as many clusters as there are different possible values for the associated random variable that is defined at every

stage. Let $\mathcal{C}$ be the set of scenario clusters and $\mathcal{C}_s$ the subset of scenario clusters that belong to state $s \in \mathcal{S}$, such that $\mathcal{C} = \bigcup_{s\in\mathcal{S}} \mathcal{C}_s$; and $\mathcal{C}_s^k$ is the scenario cluster k for stage $s \in \mathcal{S}$. For instance, Figure 4.1.4 shows two clusters associated with the first stage (DM), where each one has a different value for the DM clearing prices. Consequently, the set of clusters for stage 1 is:
$\mathcal{C}_1 = \{C_1^1, C_1^2\}, |\mathcal{C}_1| = 2$
with the following two clusters:
$\mathcal{C}_1^1 = \{C_{11}^1, C_{12}^1 \ldots, C_{1|\mathcal{C}_1^1|}^1\}$, $\mathcal{C}_1^2 = \{C_1^2, C_1^2 \ldots, C_{1|\mathcal{C}_1^2|}^1\}$.

The DM clearing price for each scenario $\tilde{\boldsymbol{\lambda}}_1^D, \tilde{\boldsymbol{\lambda}}_2^D$ is assigned to clusters $\mathcal{C}_1^1, \mathcal{C}_1^2$, respectively. If the DM has 4 time periods, then $\tilde{\boldsymbol{\lambda}}_1^D = (\tilde{\lambda}_{11}^D, \tilde{\lambda}_{21}^D, \tilde{\lambda}_{31}^D), \tilde{\boldsymbol{\lambda}}_2^D = (\tilde{\lambda}_{12}^D, \tilde{\lambda}_{22}^D, \tilde{\lambda}_{32}^D)$, where the second index indicates the hour where the DM clearing price is known. Also, as the scenario clusters are related in accordance with non-anticipativity principle for the MSP model, we have the following assertions; $\tilde{\lambda}_{t\omega}^D = \tilde{\lambda}_{t1}^D$ for every $\omega \in \mathcal{C}_1^1, t \in \{1, 2, 3\}$ and $\tilde{\lambda}_{1\omega}^D = \tilde{\lambda}_{12}^D$ for every $\omega \in \mathcal{C}_1^2, t \in \{1, 2\}$. In general, this is $\tilde{\boldsymbol{\lambda}}_{1\omega}^D = \tilde{\boldsymbol{\lambda}}_{1k}^D$ for every $\omega \in \mathcal{C}_1^k$. This establishes that the values in the decision variables at every stage $s \in \mathcal{S}$ must coincide with those scenarios belonging to the same cluster $\mathcal{C}_s^k$, that is:

$$r_{t\omega}^U = r_{tl}^U \text{ and } r_{t\omega}^D = r_{tl}^D, \forall t \in \mathcal{T}, \omega, l \in \mathcal{C}_s^k, \omega \neq l, \mathcal{C}_s^k \in \mathcal{C}_s^k, k = 1, \ldots, |\mathcal{C}_s|, s \in \mathcal{S}.$$

For stage 2, the scenario clusters have a size of four: $\mathcal{C}_2 = \{C_2^1, C_2^2, C_2^3, C_2^4\}, |\mathcal{C}_2| = 4$, with the four clusters being $\mathcal{C}_2^1 = \{C_{21}^1, C_{22}^1, \ldots, C_{2|\mathcal{C}_2^1|}^1\}$, $\mathcal{C}_2^2 = \{C_{21}^2, C_{22}^2, \ldots, C_{2|\mathcal{C}_2^2|}^2\}$, $\mathcal{C}_2^3 = \{C_{21}^3, C_{22}^3, \ldots, C_{2|\mathcal{C}_2^3|}^3\}$, and $\mathcal{C}_2^4 = \{C_{21}^4, C_{22}^4, \ldots, C_{2|\mathcal{C}_2^4|}^4\}$. These are associated with the RM clearing prices $\tilde{\boldsymbol{\lambda}}_\omega^R, \omega = 1, \ldots, 4$. The first two scenarios belong, respectively, to the first two clusters $\mathcal{C}_2^1, \mathcal{C}_2^2$ and the final two scenarios are associated to the final two clusters $\mathcal{C}_2^3, \mathcal{C}_2^4$. Figure 4.1.4 demonstrates the scenario clusters pertaining to the two first stages. The same definitions and relationships can be sequentially applied to the next stages.

4.1.3. The MSWBVPP Model

Heredia et al. (2018) introduced a MSP model of a VPP comprising a WPP and BESS that operated in the DM, RM, IM1, and IB. Here, we proposed expanding on that work by generalizing the VPP's participation in all IM sessions are considered. The MSP model to be developed has many periods for each decision stage of the VPP's participation in the EM. Regarding the operability of the VPP, each hourly time period represents a stage. The decision variables for the optimal participation of a VPP will correspond to the quantity bids of all markets in each stage of the BESS together with the associated imbalances. The sets, subsets, parameters, random parameters, and

decision variables of the model are listed. Then, the objective function and constraints are presented. The mathematical formulation is as follows:

Sets

$\mathcal{S}$:	Index set of stage s.
Ω:	Index set of scenarios ω.
$\mathcal{T}$:	Index set of time period t.
$\mathcal{I}$:	Index set of IM session i.
$\mathcal{C}$:	Set of scenario clusters.
$\mathcal{T}_i \subseteq \mathcal{T}$:	Set of hours where the IM session i acts.
$\mathcal{I}_t \subseteq \mathcal{I}$:	Subsets of IM session $i \in \mathcal{I}$ that act in time period $t \in \mathcal{T}$.
$\mathcal{C}_s \subseteq \mathcal{C}$:	Subset of scenario clusters that belong to stage $s \in \mathcal{S}$
$\mathcal{C}_s^k \subseteq \mathcal{C}_s$:	Subset of scenario clusters k for stage $s \in \mathcal{S}$.

Random Parameters

$\tilde{\lambda}_{t\omega}^{D}$:	DM clearing price in time period $t \in \mathcal{T}$ and scenario $\omega \in \Omega$ (€/MWh).
$\tilde{\lambda}_{t\omega}^{R}$:	RM clearing price in time period $t \in \mathcal{T}$ and scenario $\omega \in \Omega$ (€/MWh).
$\tilde{\lambda}_{it\omega}^{I}$:	Clearing price of IM session $i \in \mathcal{I}$ in time period $t \in \mathcal{T}_i$ and scenario $\omega \in \Omega$ (€/MWh).
$\tilde{\lambda}_{it\omega}^{I}$:	Clearing price of IM session $i \in \mathcal{I}$ in time period $t \in \mathcal{T}_i$ and scenario $\omega \in \Omega$ (€/MWh).
$\tilde{\lambda}_{t\omega}^{IB_+}, \tilde{\lambda}_{t\omega}^{IB_-}$:	Positive and negative IB price at time period $t \in \mathcal{T}$ and scenario $\omega \in \Omega$ (€/MWh).
$\tilde{p}_{t\omega}^{W}$:	WP Production at time period $t \in \mathcal{T}$ and scenario $\omega \in \Omega$ (MWh).
P_ω:	Probability of scenario $\omega \in \Omega$.

Parameters

d^{max}:	BESS's maximum charging/discharging rate (MW).
γ^{RTE}:	Round trip efficiency.
e^{max}:	Battery capacity (MWh).
$soc^0, soc^{\lvert\mathcal{T}\rvert}$:	Minimum/maximum State Of Charge (SOC).
cyc^{max}:	Maximum number of charge/discharge cycles before end of life.
EOL:	End of life of BESS (years).
$\underline{p}_t^W, \overline{p}_t^W$:	Lower/upper bound of forecasted wind production for a given time period $t \in \mathcal{T}$ (MWh)
Δt^{SR}:	Time response of the RM (hours).

$\underline{p}^I_{it\omega}, \overline{p}^I_{it\omega}$: Lower/upper bound of the IM session $i \in \mathcal{I}$ energy bid for time period $t \in \mathcal{T}_i$ and scenario $\omega \in \Omega$ (MWh).

$\overline{p}^{IB_+}_{t\omega}, \overline{p}^{IB_-}_{t\omega}$: Upper bound to the positive and negative IB price at time period $t \in \mathcal{T}$ and scenario $\omega \in \Omega$ (€/MWh).

$\underline{p}^D_t = 0{,}1 \cdot min_{s\in\mathcal{S}}\, \tilde{p}^W_{t\omega})$: Lower bound of the energy bid in DM at time period $t \in \mathcal{T}$ (MWh).

$\overline{p}^D_t = (d_{max} + max_{s\in\mathcal{S}}\, \tilde{p}^W_{t\omega})$: Upper bound of the energy bid in DM at time period $t \in \mathcal{T}$ (MWh).

Variables

p^D_t: Energy of the price-accepting bid for time period $t \in \mathcal{T}$ of the DM (MWh).

$r^U_{t\omega}, r^D_{t\omega}$: Upward/downward RM bid of the VPP at time period $t \in \mathcal{T}$ and scenario $\omega \in \Omega$ (MW).

$p^I_{it\omega}$: Energy of the price-accepting bid of IM session $i \in \mathcal{I}$ at time period $t \in \mathcal{T}_i$ and scenario $\omega \in \Omega$ (MWh).

$p^{IT}_{t\omega}$: Total energy of the price-accepting bid of IM at time period $t \in \mathcal{T}$ and scenario $\omega \in \Omega$ (MWh).

$c_{t\omega}, d_{t\omega}$: Charges/discharges of the BESS at time period $t \in \mathcal{T}$ and scenario $\omega \in \Omega$.

$p^{IB_+}_{t\omega}, p^{IB_-}_{t\omega}$: IB (positive and negative) of the VPP at time period $t \in \mathcal{T}$ and scenario $\omega \in \Omega$ (MWh).

$soc_{t\omega}$: SOC at time period $t \in \{0\} \cup \mathcal{T}$ finalization and scenario $\omega \in \Omega$.

$$ip^D_t = \begin{cases} 1 \text{ if the VPP is bidding to the DM at time period } t \in \mathcal{T}, \\ 0 \text{ otherwise.} \end{cases}$$

$$id_t = \begin{cases} 1 \text{ if BESS is discharging at time period } t \in \mathcal{T} \text{ and scenario } \omega \in \Omega, \\ 0 \text{ otherwise.} \end{cases}$$

The formulation of the MWBVPP is as follows:

$$\text{Max} \quad \sum_{t\in\mathcal{T}} \overline{\lambda}^D_t \cdot p^D_t + \sum_{t\in\mathcal{T},\omega\in\Omega} P_\omega \cdot \tilde{\lambda}^R_{t\omega} \cdot \left(r^U_{t\omega} + r^D_{t\omega}\right) + \sum_{i\in\mathcal{I}, t\in\mathcal{T}_i, \omega\in\Omega} P_\omega \cdot \tilde{\lambda}^I_{it\omega} \cdot p^I_{it\omega} + \sum_{t\in\mathcal{T},\omega\in\Omega} P_\omega \cdot \tilde{\lambda}^{IB_+}_{t\omega} \cdot p^{IB_+}_{t\omega} + \sum_{t\in\mathcal{T},\omega\in\Omega} P_\omega \cdot \tilde{\lambda}^{IB_-}_{t\omega} \cdot p^{IB_-}_{t\omega} \quad (4.1.3)$$

s.t.

$$\underline{p}^D_t \cdot ip^D_t \le p^D_t \le \overline{p}^D_t \cdot ip^D_t \qquad \forall t \in \mathcal{T} \quad (4.1.4)$$

$$\overline{p}^I_{it\omega} ip^D_t \le p^I_{it\omega} \le \underline{p}^I_{it\omega} ip^D_t \qquad \forall i \in \mathcal{I}, \forall t \in \mathcal{T}_i, \forall \omega \in \Omega \quad (4.1.5)$$

$$p^{IT}_{t\omega} = \sum_{i\in\mathcal{I}_t} p^I_{it\omega} \qquad \forall t \in \mathcal{T}, \forall \omega \in \Omega \quad (4.1.6)$$

$$0 \le d_{t\omega} \le d^{max} \cdot id_{t\omega} \qquad \forall t \in \mathcal{T}, \forall \omega \in \Omega \quad (4.1.7)$$

$$0 \le c_{t\omega} \le d^{max} \cdot (1 - id_{t\omega}) \qquad \forall t \in \mathcal{T}, \forall \omega \in \Omega \quad (4.1.8)$$

$$soc_{t\omega} = soc_{t-1\omega} + \frac{\Delta t(c_{t\omega} - \frac{d_{t\omega}}{\gamma^{RTE}})}{e^{max}} \qquad \forall t \in \mathcal{T}, \forall \omega \in \Omega \qquad (4.1.9)$$

$$soc^{min} \leq soc_{t\omega} \leq soc^{max} \qquad \forall t \in \mathcal{T}, \forall \omega \in \Omega \qquad (4.1.10)$$

$$soc_{0\omega} = soc^0, soc_{t\omega} = soc^T \qquad \forall \omega \in \Omega \qquad (4.1.11)$$

$$\frac{\sum_{t\in\mathcal{T},\omega\in\Omega} P_\omega \left(d_{t\omega} + c_{t\omega}\right)}{2 \cdot e_{max}} \leq \frac{cyc^{max}}{(365 \cdot EOL)} \qquad \forall t \in \mathcal{T}, \forall \omega \in \Omega \qquad (4.1.12)$$

$$r^U_{t\omega} + r^D_{t\omega} \leq 2 \cdot d^{max} \cdot ip^D_t \qquad \forall t \in \mathcal{T}, \forall \omega \in \Omega \qquad (4.1.13)$$

$$0 \leq r^U_{t\omega} \leq d^{max} - (d_{t\omega} - c_{t\omega}) \qquad \forall t \in \mathcal{T}, \forall \omega \in \Omega \qquad (4.1.14)$$

$$0 \leq r^D_{t\omega} \leq d^{max} - (c_{t\omega} - d_{t\omega}) \qquad \forall t \in \mathcal{T}, \forall \Omega \in \Omega \qquad (4.1.15)$$

$$soc^{min} + \frac{\Delta t^{SR} \frac{r^U_{t\omega}}{\gamma^{RTE}}}{e^{max}} \leq soc_{t\omega} \leq soc^{max} + \frac{\Delta t^{SR} \cdot r^D_{t\omega} \cdot \gamma^{RTE}}{e^{max}} \forall t \in \mathcal{T}, \forall \omega \in \Omega \qquad (4.1.16)$$

$$(4.1.17)$$

$$p^{IB+}_{t\omega} - p^{IB-}_{t\omega} = \left(\tilde{p}^W_{t\omega} + d_{t\omega}\right) - \left(p^D_t + p^{IT}_{t\omega} + c_{t\omega}\right) \qquad \forall t \in \mathcal{T}, \forall \omega \in \Omega \qquad (4.1.18)$$

$$0 \leq p^{IB+}_{t\omega} \leq \overline{p}^{IB+}_{t\omega}, 0 \leq p^{IB-}_{t\omega} \leq \overline{p}^{IB-}_{t\omega} \qquad \forall t \in \mathcal{T}, \forall \omega \in \Omega \qquad (4.1.19)$$

$$r^U_{t\omega} = r^U_{tl} \qquad s = 1, \forall t \in \mathcal{T}, \forall \omega, l \in \mathcal{C}^k_s, \omega \neq l, \mathcal{C}^k_s \in \mathcal{C}_s, k = 1, ..., |\mathcal{C}_s| \qquad (4.1.20)$$

$$r^D_{t\omega} = r^D_{tl} \qquad s = 1, \forall t \in \mathcal{T}, \forall \omega, l \in \mathcal{C}^k_s, \omega \neq l, \mathcal{C}^k_s \in \mathcal{C}_s, k = 1, ..., |\mathcal{C}_s| \qquad (4.1.21)$$

$$p^I_{it\omega} = p^I_{itl} \qquad i = 1, s = 2, \forall t \in \mathcal{T}, \forall \omega, l \in \mathcal{C}^k_s, \omega \neq l, \mathcal{C}^k_s \in \mathcal{C}_s, k = 1, ..., |\mathcal{C}_s| \qquad (4.1.22)$$

$$p^I_{it\omega} = p^I_{itl} \qquad i = 2, s = 3, \forall t \in \mathcal{T}_i, \forall \omega, l \in \mathcal{C}^k_s, \omega \neq l, \mathcal{C}^k_s \in \mathcal{C}_s, k = 1, ..., |\mathcal{C}_s| \qquad (4.1.23)$$

$$c_{t\omega} = c_{tl} \qquad s = 4, 5, \forall t \in \mathcal{T}, \forall \omega, l \in \mathcal{C}^k_s, \omega \neq l, \mathcal{C}^k_s \in \mathcal{C}_s, k = 1, ..., |\mathcal{C}_s| \qquad (4.1.24)$$

$$p^I_{it\omega} = p^I_{itl} \qquad i = 3, s = 6, \forall t \in \mathcal{T}_i, \forall \omega, l \in \mathcal{C}^k_s, \omega \neq l, \mathcal{C}^k_s \in \mathcal{C}_s, k = 1, ..., |\mathcal{C}_s| \qquad (4.1.25)$$

$$c_{t\omega} = c_{tl} \qquad s = 7, ..., 9, \forall t \in \mathcal{T}, \forall \omega, l \in \mathcal{C}^k_s, \omega \neq l, \mathcal{C}^k_s \in \mathcal{C}_s, k = 1, ..., |\mathcal{C}_s| \qquad (4.1.26)$$

$$p^I_{it\omega} = p^I_{itl} \qquad i = 4, s = 10, \forall t \in \mathcal{T}_i, \forall \omega, l \in \mathcal{C}^k_s, \omega \neq l, \mathcal{C}^k_s \in \mathcal{C}_s, k = 1, ..., |\mathcal{C}_s| \qquad (4.1.27)$$

$$c_{t\omega} = c_{tl} \qquad s = 11, ..., 14, \forall t \in \mathcal{T}, \forall \omega, l \in \mathcal{C}^k_{s-1}, \omega \neq l, \mathcal{C}^k_s \in \mathcal{C}_s, k = 1, ..., |\mathcal{C}_s| \qquad (4.1.28)$$

$$p^I_{it\omega} = p^I_{itl} \qquad i = 5, s = 15, \forall t \in \mathcal{T}_i, \forall \omega, l \in \mathcal{C}^k_s, \omega \neq l, \mathcal{C}^k_s \in \mathcal{C}_s, k = 1, ..., |\mathcal{C}_s| \qquad (4.1.29)$$

$$c_{t\omega} = c_{tl} \qquad s = 16, ..., 19, \forall t \in \mathcal{T}, \forall \omega, l \in \mathcal{C}^k_{s-1}, \omega \neq l, \mathcal{C}^k_s \in \mathcal{C}_s, k = 1, ..., |\mathcal{C}_s| \qquad (4.1.30)$$

$$p^I_{it\omega} = p^I_{itl} \qquad i = 6, s = 20, \forall t \in \mathcal{T}_i, \forall \omega, l \in \mathcal{C}^k_s, \omega \neq l, \mathcal{C}^k_s \in \mathcal{C}_s, k = 1, ..., |\mathcal{C}_s| \qquad (4.1.31)$$

$$c_{t\omega} = c_{tl} \qquad s = 21, ..., 26, \forall t \in \mathcal{T}, \forall \omega, l \in \mathcal{C}^k_s, \omega \neq l, \mathcal{C}^k_s \in \mathcal{C}_s, k = 1, ..., |\mathcal{C}_s| \qquad (4.1.32)$$

$$p^I_{it\omega} = p^I_{itl} \qquad i = 7, s = 27, \forall t \in \mathcal{T}, \forall \omega, l \in \mathcal{C}^k_s, \omega \neq l, \mathcal{C}^k_s \in \mathcal{C}_s, k = 1, ..., |\mathcal{C}_s| \qquad (4.1.33)$$

$$c_{t\omega} = c_{tl} \qquad s = 28, ..., 32, \forall t \in \mathcal{T}\backslash\{0\}, \forall \omega, l \in \mathcal{C}^k_s, \omega \neq l, \mathcal{C}^k_s \in \mathcal{C}_s, k = 1, ..., |\mathcal{C}_s| \qquad (4.1.34)$$

$$p^{IB+}_{t\omega} = p^{IB+}_{tl} \qquad s = 33, \forall t \in \mathcal{T}\backslash\{0\}, \forall \omega, l \in \mathcal{C}^k_s, \omega \neq l, \mathcal{C}^k_s \in \mathcal{C}_s, k = 1, ..., |\mathcal{C}_s| \qquad (4.1.35)$$

$$p^{IB-}_{t\omega} = p^{IB-}_{tl} \qquad s = 33, \forall t \in \mathcal{T}\backslash\{0\}, \forall \omega, l \in \mathcal{C}^k_s, \omega \neq l, \mathcal{C}^k_s \in \mathcal{C}_s, k = 1, ..., |\mathcal{C}_s| \qquad (4.1.36)$$

The objective function (4.1.3) maximizes the expected value of the total profit of the VPP. The constraints (4.1.4) and (4.1.5) are associated with the conditions for spot markets (DM and IM), which define the relationships of energy bids in the DM and IM as well as the binary variables in accordance with the DM offer. The constraints

(4.1.6)–(4.1.12) are conditions for the BESS operation. Specifically, the constraints (4.1.6) defines the total energy bid of IM as being equal to the sum of energy bid in each IM session. The constraints (4.1.7) and (4.1.8) describe the charging/discharging state and limits and defines the binary variable $id_{t\omega}$. The constraint (4.1.9) expresses the value of the SOC at the end of time period $t \in \mathcal{T}$ in terms of the charge/discharge. The constraint (4.1.10) imposes the safety and technical limits on the SOC. The constraint (4.1.11) defines the value of the SOC at the beginning and end of the optimization horizon. The constraint (4.1.12) limits the total number of cycles. The constraints (4.1.13)–(4.1.18) are conditions for the RM. Thus, The constraint (4.1.13) defines the VPP period $t \in \mathcal{T}$ in which it is allowed to bid on the RM, as this is specifically where the DM bid has been accepted. The constraints (4.1.14) and (4.1.15) determine the limits of the BESS's reserve availability. The constraint (4.1.16) modifies the operational range of the SOC according to the value of the downward and upward reserve bid. Finally, constraints (4.1.18) and (4.1.19) impose some limits to the value of the imbalances. In order to represent the decision-making process in the MSP model, the nonanticipativity constraints in (4.1.20)–(4.1.36) are established. These constraints maintain that, at every stage of the scenario tree, the variables associated with those scenarios in the same scenario cluster must have the same value.

4.2. Scenario Tree for the MSOODN Model

The focus of this section is on the problems of optimizing the operation of EDN while taking into account the presence of renewables in the network. First, Section 4.2.1 defines the problem under consideration. Section 4.2.2 elaborates on the uncertainty and on the decision process, which are represented in a scenario tree. Finally, Section 4.2.3 presents the novel MSOODN model.

4.2.1. EDN and Renewables

EDN is a system of interconnected elements such as, storage facilities and transportation systems that receive inventories to be delivered to the customers. Deciding on an EDN involve evaluating minimum losses, voltage deviations at the consumer end, and maximum reliability. All together, these are referred to as: the Optimal Operation of the EDN problem (OODN).

The specific components of an EDN are as follows. The Loads (L) are network components that consume active electric power. An On-Load Tap-Charger (OLTC) and a Voltage Regulator (VR) aim to improve voltage levels in EDN. A Distribution Substation (DSS) is a synchronous machine source of both active and reactive power; it transforms voltage from high to low, or vice versa; and it performs a number of

several other vital functions. A Switchable Capacitor Bank (SCB), is a group of several capacitors with the same rating that are connected in series or parallel to each other in order to store electrical energy, and it is thus used to counteract or correct a power factor lag or phase shift in an alternating power current supply. The Impedance (R) is the effective resistance of an electrical circuit or component of alternating currents, which arise from the combined effects of ohmic resistance and reactance. Finally, we have the Ground, which is a direct electrical connection to the earth. The objective of OODN is to minimize the total cost of energy purchased from the DSS and DG while taking into account the following control variables: active and reactive DG of dispatchable power; the number of SCB units in operation; and the tap position of OLTC. Figure 4.2.1 illustrates an EDN with seven nodes and several transmission lines.

Traditionally, dispatchable generated power consists of conventional energy sources, which are primarily coal, natural gas, and oil. However, recent sources of renewable energy have more and more been receiving considerable attention. The most common Renewable Sources (RS) are; Solar, Wind, Water (Hydropower), Biomass and Geothermal. RS is propitious to reducing carbon emissions. A drawback is they cannot usually be scheduled, due to their intermittent character, thus resulting in power-supply issues in the EDN. Therefore, a BESS is normally used to mitigate the adverse effects that the RS may have on a consumer's renewable energy, specifically by reducing the active power loss, alleviating the voltage fluctuations, and minimizing the electricity cost. Figure 4.2.2 shows an EDN with solar and wind RS.

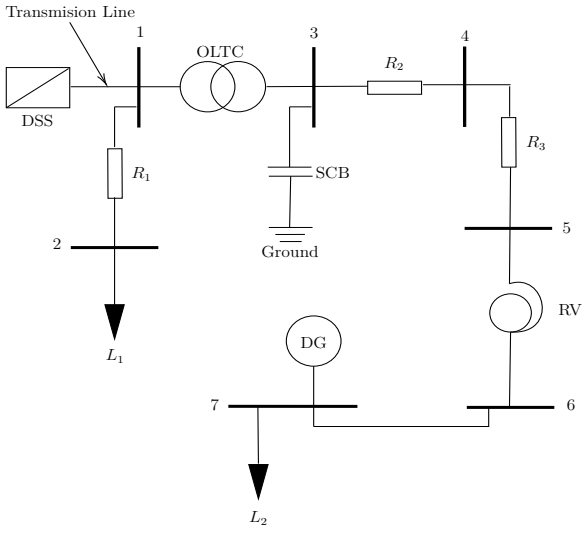

Figura 4.2.1: Illustration of a EDN.

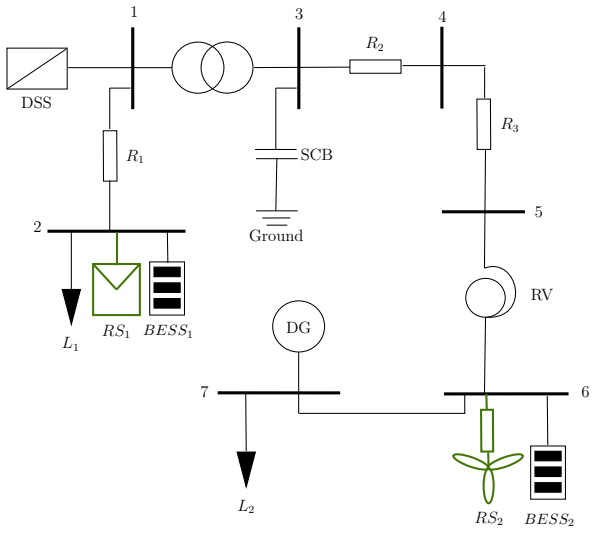

Figura 4.2.2: Illustration of a EDN with RS.

The presence of RS in EDN injects uncertainty into the process of optimization, because the decisions that must be made depend on power generation produced by RS. Other sources of uncertainty in the OODN are related to DG energy loads and purchase prices. This study scrutinizes the uncertainty in loads and RS power generation having that the OODN can be view as a Stochastic Optimal Operation of Distribution Network (denoted by SOODN). Also, when we optimize the SOODN in a given future horizon, the use of multistage (or multiperiod) is recommended. This is called MSOODN. Here, we develop a new MSOODN model that considers a radial EDN with DSS, RS, BESS, Loads, Impedances and SCB, together with uncertainty in the loads and RS power generation.

4.2.2. Uncertainty and the Decision Process

The uncertainty for the MSOODN problem is reflected in the loads and power generation of the RS, and it is represented by the random parameters of the MSP model. In Table 4.2.1, the vectors of random parameters for MSOODN are shown.

$\mathbf{P}_i^D \in \mathbb{R}^{24}$	Active power load in node i of EDN.
$\mathbf{Q}_i^D \in \mathbb{R}^{24}$	Reactive power load in node i of EDN.
$\mathbf{P}_i^{pv} \in \mathbb{R}^{24}$	Active power generation of solar photovoltaic RS in node i of EDN.

Cuadro 4.2.1: Random parameters of the MSOODN problem.

The decision variables correspond to the BESS operation and the EDN steady-state operation. Decision variables are presented in Table 4.2.2.

$\mathbf{V}_i$:	Voltage magnitude for 24 hours at node i (kV).
$\mathbf{I}_{ij}$:	Current magnitude for 24 hours of branch ij (A).
$\mathbf{P}_i^S$:	Active power supplied for 24 hours by substation at node i (kV).
$\mathbf{Q}_i^S$:	Reactive power supplied for 24 hours by substation at node i $(kvar)$.
$\mathbf{P}_{ij}$:	Active power flow of branch ij for 24 hours (kV).
$\mathbf{Q}_{ij}$:	Reactive power flow of branch ij at time period t and scenario w $(kvar)$.
$\mathbf{P}_i^{ch}, \mathbf{P}_i^{dis}$:	Active power of charge and discharge of the BESS at node i for 24 hours of EDN operation (kW).
$\mathbf{SOC}_i$:	State of charge of the BESS at node i for 24 hours of EDN operation. (%).
$\mathbf{L}_i^{shed}$:	Load shedding at node i for 24 hours of EDN operation.
$\mathbf{b}_i^{ch}, \mathbf{b}_i^{dis}$:	Operation state of the BESS at node i, for 24 hours of EDN operation (%).

Cuadro 4.2.2: Decision variables of the MSOODN problem.

On the other hand, the decision process for MSOODN is programmed during different time periods. Today is day $N-1$, and a plan for each time period in day N needs to be defined. This is:

- *Hour 0:* decisions are made after hour 1 for the BESS operation in the EDN (the first-state variable).
- *Hour 1-23:* loads and PV generation corresponding to each hour are known (random variables). During these hours, there will be some voltage and current magnitude and active/reactive power supplied by DSS, and active/reactive power flow in the transmission lines (recourse variables). Prior to these hours, decisions are made regarding the charges and discharges of the BESS in the EDN (state variables).
- *Hour 24:* the loads and PV generation after hour 24 are known; the recourse variables are decided on for this hour.

Table 4.2.3 shows the decision process that lays out the sequences of the decision stage and the events in an hourly time period per day.

The stages (time periods) are defined as $\Omega_t = \{t : t = 0, ..., 24\}$, and they correspond to the hourly time period per day. The stochastic process is defined by:

$$\tilde{\boldsymbol{\xi}} = \left\{\tilde{\boldsymbol{\xi}}_t\right\}_{t=1}^{24}, \tag{4.2.1}$$

where $\tilde{\boldsymbol{\xi}}_t = \left(\tilde{P}_{it}^D, \tilde{Q}_{it}^D, \tilde{P}_{it}^{uv}\right)$, is the realization of the random variable for $t \in \Omega_t$.

Let $\mathbf{x}_t = (\mathbf{y}_t, \mathbf{z}_t)$ be the sets of the decision variables in the MSOODN model. The $\mathbf{y}_t, \mathbf{z}_t$ that correspond to the recourse variables and state variables are defined by Equations (4.2.2) and (4.2.3):

$$\mathbf{y}_t = \left(V_{it}, I_{ijt}, P^S_{it}, Q^S_{it}, P_{ijt}, Q_{ijt}, P^{ch}_{it}, SOC_{it}, L^{shed_{it}}, b^{ch}_{it}, b^{dis}_{it}\right), \tag{4.2.2}$$

and

$$\mathbf{z}_t = \left(b^{ch}_{it}, b^{dis}_{it}, \alpha^+_{it}, \alpha^-_{it}, \beta^+_{it}, \beta^+_{it}\right), \tag{4.2.3}$$

where $\mathbf{y}_t$ defines decisions for the voltage and current magnitude, active/reactive power supplied by the DSS, and active/reactive power flow at the transmission lines; and $\mathbf{z}_t$ decides the charges and discharges of the BESS in the EDN.

Therefore, the decision sequences for this stage (as defined by the decision process) are:

$$\textit{decided}\ \mathbf{x}_0 \xrightarrow{observed} \tilde{\boldsymbol{\xi}}_1 \xrightarrow{decided} \mathbf{x}_1 \xrightarrow{observed}, \ldots, \xrightarrow{observed} \tilde{\boldsymbol{\xi}}_{24} \xrightarrow{decided} \mathbf{x}_{24}$$

where $\mathbf{x}_0 = \mathbf{z}_0$ defines the operation of the BESS at the beginning of hour 1, and $\mathbf{x}_{24} = \mathbf{y}_{24}$ is the possible outcomes solution, which is composed of different values for the network's electrical magnitudes, BESS load, and load shedding at the end of hour 24.

The sequential decision process is modeled appropriately as an MSP problem. The multivariate stochastic process (Equation (4.2.1)) is approximated by a multivariate stochastic process $\boldsymbol{\xi}_{tr}$ with scenarios $\omega \in \Omega_\omega$, and it presumed to be as follows:

$$\boldsymbol{\xi} \approx \boldsymbol{\xi}_{tr} = \{\{\boldsymbol{\xi}_t\}_{t\in\Omega_t} : \omega \in \Omega_\omega\},$$

By establishing as a basis that $\Omega = \{\omega : \omega = 1, ..., N\}$ is the scenario index, the scenario associated with index $\omega \in \Omega$ therefore has the related probabilities $P_\omega > 0,\ \omega \in \Omega$, such that $\sum_{\omega\in\Omega} P_\omega = 1$, which is defined as:

$$\tilde{\boldsymbol{\xi}}_\omega = \left(\tilde{P}^D_{1\omega}, \tilde{Q}^D_{1\omega}, \tilde{P}^{uv}_{1\omega}, \ldots, \tilde{P}^D_{24\omega}, \tilde{Q}^D_{24\omega}, \tilde{P}^{uv}_{24\omega}\right)'$$

A scenario tree approximates the multistage stochastic process $\boldsymbol{\xi}_{tr}$. Figure 4.2.3, represents a binary scenario tree structure; moreover, without losing generality, the scenario tree can have more scenarios for this problem. The scenario tree has 32 scenarios ($|\Omega_\omega| = 32$) with their associated probabilities, which are denoted by $\pi_\omega, \omega \in \Omega_\omega$, and 24 time periods (running time $t = 0$).

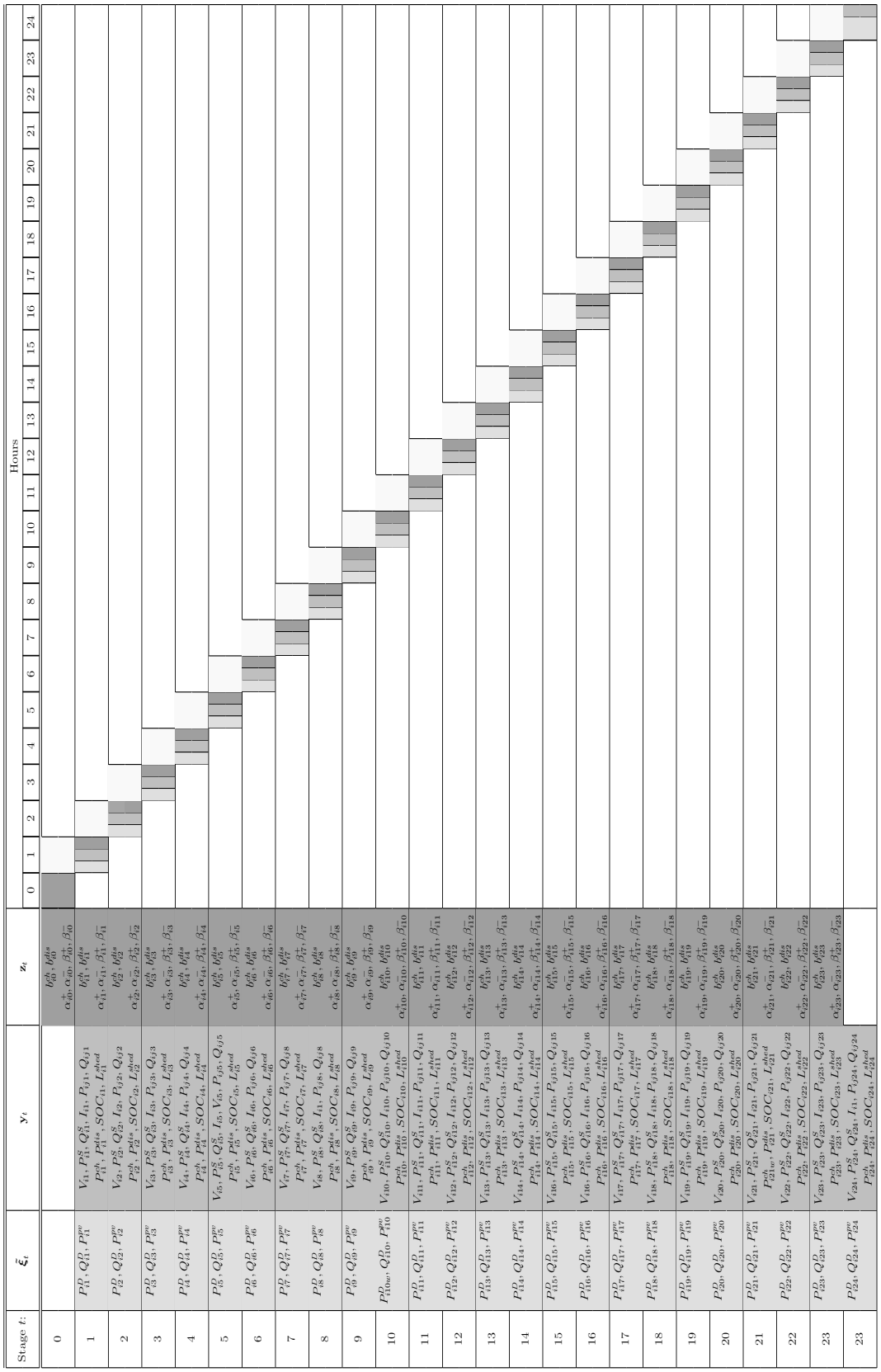

Cuadro 4.2.3: Sequence of random disclosures and decision stage.

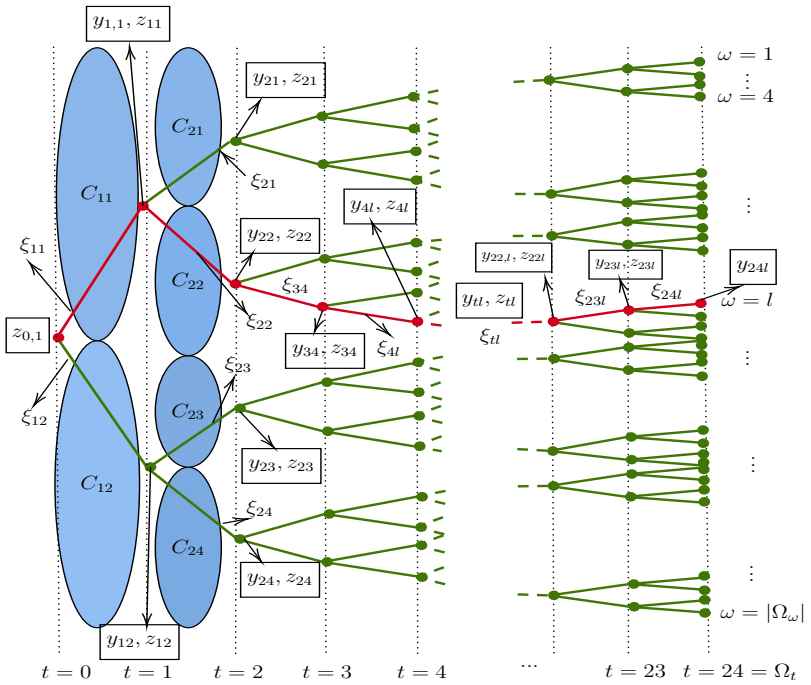

Figura 4.2.3: Scenario tree structure for the MSOODN model.

Due to the tree structure of the process $\boldsymbol{\xi}_{tr}$, the value of the random parameter for all the scenarios shares a node at time period t. For instance, scenarios 1 to 4 share the same node 1 at time period 1; consequently, the value $\tilde{\xi}_{1,\omega} = \tilde{\xi}_{11}$ for $\omega = 1, ..., 4$, is as stated:

$$\tilde{\xi}_{1\omega} = \tilde{\xi}_{11},\ \omega = \mathcal{C}_1^1 = \{1, 2, 3, 4\}.$$

The same relationships are found for every edge k and stage t, as follows:

$$\tilde{\xi}_{t\omega} = \tilde{\xi}_{tk},\ \omega = \mathcal{C}_t^k,\ \forall k \in \mathcal{C}_t,\ \forall t \in \Omega_t/\{0\},$$

where the set $\mathcal{C}_t$ is defined as the scenario cluster set of stage t, and $\mathcal{C}_t^k$ is the scenario cluster k at stage t.

Figure 4.2.3 demonstrates the scenario cluster for stages 1 and 2 (or time periods). Time period 1 has the scenario clusters $\mathcal{C}_1^1, \mathcal{C}_1^2$; and time period 2 has $\mathcal{C}_2^1, \mathcal{C}_2^2, \mathcal{C}_2^3, \mathcal{C}_2^4$.

For $t = 1, \ldots, 23$, the recourse variable $\mathbf{y}_t$ and the optimal value of time period $\mathbf{z}_t$ depend on the realization of the random variables $\tilde{\boldsymbol{\xi}}_{[t]}$. This condition is called the *non-anticipativity principle* for MSP. Optimal decisions are made at every stage t; i.e., variables $\mathbf{y}_t, \mathbf{z}_t$, cannot depend on the realizations of the random parameter in future stages. In other words, the value of $\mathbf{y}_{t\omega}^*$ and $\mathbf{z}_{t\omega}^*$ must be the same for every scenario ω sharing the same value of $\tilde{\boldsymbol{\xi}}_{[t]}$ (i.e., sets $\mathcal{C}_t^k$). What guarantees this principle is denoted as *Non-anticipativity Constraints* (NAC), being:

$$\mathbf{y}_{t\omega} = \mathbf{y}_{t\omega'},\ \ \forall \omega, \omega' = \mathcal{C}_t^k,\ \forall k \in \mathcal{C}_t,\ \forall t \in \Omega_t \setminus \{0\}$$

$$\mathbf{z}_{t\omega} = \mathbf{z}_{t\omega'}, \ \ \forall \omega, \omega^{'} = \mathcal{C}_{kt}, \ \ \forall k \in \mathcal{C}_t, \ \ \forall t \in \Omega_t \setminus \{|\Omega_t|\}$$

The NAC applied for $t = 0$ implies that there will be a single value of the variable $\mathbf{x}_0$, which is the only set of variables that does not depend on the scenario. This is recorded before the first time period corresponding to what is known as the *here and now*, which includes the optimal operation of the BESS for the next stage (time period) with respect to any possible outcome of the stochastic process $\tilde{\boldsymbol{\xi}}$.

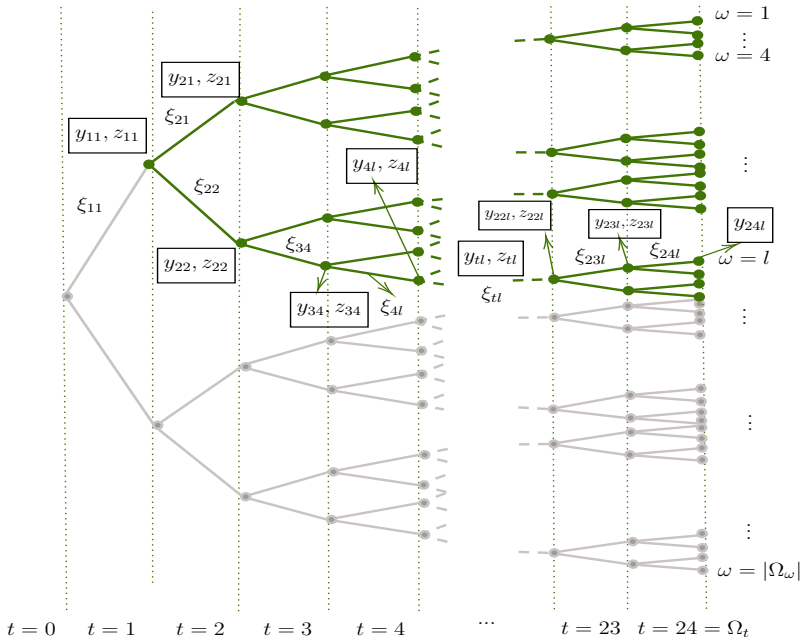

Figura 4.2.4: Scenario tree for stage 2, to known $\boldsymbol{\xi}_1$.

Before stage 0, the value of $\tilde{\boldsymbol{\xi}}_1$ is known, which allows for a new analogous problem to be solved one step ahead with a scenario tree being the subtree of $\boldsymbol{\xi}_{tr}$ associated with $\tilde{\boldsymbol{\xi}}_1$. For instance, should $\tilde{\boldsymbol{\xi}}_1 = \tilde{\boldsymbol{\xi}}_{11}$, then the scenario tree would be the one shown in Figure 4.2.4.

In the scenario tree of Figure 4.2.4, the value of the decision for stage 1 has been set at its optimal values $\mathbf{y}_1^*$ and $\mathbf{z}_1^*$. At this point, the value of $\tilde{\boldsymbol{\xi}}_2$ is known. The new problem's decision variables $\mathbf{y}$ and $\mathbf{z}$ are those associated with scenarios $\omega = 1, ..., 8$ and time periods $t = 2, ..., |\Omega_t|$. The variables $\mathbf{z}_{21}$ becomes the new "here and now". This procedure can be applied to the successive stages in order to obtain the BESS's optimal operation for all time periods of interest.

4.2.3. The MSOODN model

Here, a new MSOODN model for the optimal operation of distribution networks with BESS is set out. This model contemplates the following assumptions:

- A radial EDN composed of a DSS, SCB, L, photovoltaic RS and BESS.
- The loads are represented as random active and reactive power.
- The power generation of photovoltaic RS are represented as a random active power.

For any time period $t \in \Omega_t$, we apply the structure of the multistage stochastic process in the form of a scenario tree, the different elements, sets, parameters and decision variables. The mathematical formulation for this as follows:

Sets

Ω_n:	Index set of nodes.
Ω_b:	Index set of branches.
Ω_t:	Index set of time periods/decision stages.
Ω_w:	Index set of scenarios.
$\Omega_{\mathcal{S}}$:	index set of distribution substation nodes.
Ω_{cb}:	Index set of fixed capacitor banks.
Ω_{vr}:	Index set of voltage regulators.
Ω_{dg}:	Index set of dispatchable distributed generators.
Ω_{pv}:	Index set of solar photovoltaic RS.
Ω_{bt}:	Index set of battery storage systems.
$\mathcal{C}_t$:	Cluster set of time period $t \in \Omega_t$.
$\mathcal{C}_t^k \subseteq \mathcal{C}_t$:	Cluster k of cluster set $\mathcal{C}_t$ for time period $t \in \Omega_t$ $(k = 1, \ldots, \lvert\mathcal{C}_t\rvert)$.

Parameters

γ_i:	Load curtailment penalty $i \in \Omega_n$ (US$/KWh).
$c_t^{\mathcal{S}}$:	Energy procurement price by the utility in time period $t \in \Omega_t$ (US$/KWh).
Δ_t:	Duration time of each load level in time period $t \in \Omega_t$ (hours).
R_{ij}:	Resistance of branch $ij \in \Omega_b$ (Ω).
X_{ij}:	Reactance of branch $ij \in \Omega_b$ Ω_b (Ω).
Z_{ij}:	Impedance of branch $ij \in \Omega_b$ (Ω).
$\overline{I}ij$:	Maximum current magnitude of branch $ij \in \Omega_b$ (A).
$\underline{V}, \overline{V}$:	Minimum/maximum voltage magnitude (kV).
V:	Nominal voltage magnitude (kV).
$\overline{S}_i^S$:	Maximum apparent power limit of substation at node $i \in \Omega_n$ (kVA).
$\underline{P}_i^{ch}, \overline{P}_i^{ch}$:	Minimum/maximum charging power of BESS at node $i \in \Omega_n$ (kW).

$\underline{SOC}_i, \overline{SOC}_i$: Minimum/maximum stage of of BESS charge at node $i \in \Omega_n$ (%).

$\eta_i^{ch}, \eta_i^{dis}$: Charging/discharging efficiency of the BESS at node $i \in \Omega_n$.

$\overline{\Delta}_{ij}^{cb}$: Maximum variation of capacitor bank units at node $i \in \Omega_{cb}$ operating in the considered time period.

$\overline{\Delta}_{ij}^{vr}$: Maximum variation of steps of the tap of the voltage regulator in branch $ij \in \Omega_{vr}$ in the considered time period.

$\overline{\Delta}_i^{bt,ch}, \overline{\Delta}_i^{bt,dis}$: Maximum number of BESS charging/discharging cycles at node $i \in \Omega_n$.

Q_i^{cb}: Reactive power injection of the fixed capacitor bank at node $i \in \Omega_n$ (kVAr).

$\underline{pf}_i^{dg}, \overline{pf}_i^{dg}$: Lower/upper limit of the capacity power factor for the distributed generator at node $i \in \Omega_n$.

$\overline{\mathcal{S}}_i^{dg}$: Maximum apparent power limit of the distributed generator at node $i \in \Omega_n$ (kVA).

q_i^{cb}: Reactive power capacity of each module of the capacitor bank at node $i \in \Omega_{cb}$ (kVAr).

$\overline{n}_i^{cb}$: Maximum integer number of capacitor bank units at node $i \in \Omega_{cb}$.

r_{ij}^{vr}: Regulation percentage of the voltage regulator connected to branch $ij \in \Omega_{vr}$.

$\overline{l}_{ij}^{vr}$: Maximum number of steps of the voltage regulator in branch $ij \in \Omega_{vr}$.

Random Parameters

π^{ω}: Probability of scenario $\omega \in \Omega_{\omega}$.

$\tilde{P}_{it\omega}^{\mathcal{D}}$: Active power load at node $i \in \Omega_n$ at time period $t \in \Omega_t$ and scenario $\omega \in \Omega_{\omega}$ (kW).

$\tilde{Q}_{it\omega}^{\mathcal{D}}$: Reactive power load at node $i \in \Omega_n$ at time period $t \in \Omega_t$ and scenario $\omega \in \Omega_{\omega}$ (kvar).

$\tilde{P}_{it\omega}^{pv}$: Active power generation of solar photovoltaic plant at node $i \in \Omega_n$ at time period $t \in \Omega_t$ and scenario $\omega \in \Omega_{\omega}$ (kW).

Decision Variables

$V_{it\omega}$: Voltage magnitude at node $i \in \Omega_n$ at time period t and scenario $\omega \in \Omega_{\omega}$ (kV).

$V_{ijtk\omega}^{c}$: Correction variable used in the linearization of the voltage regulator model $ij \in \Omega_{vr}$ at time period t and scenario $\omega \in \Omega_{\omega}$ (kV).

$I_{ijt\omega}$: Current magnitude of branch $ij \in \Omega_b$ at time period $t \in \Omega_t$ and scenario $\omega \in \Omega_{\omega}$ (A).

$V_{it\omega}^{sqr}, I_{ijt\omega}^{sqr}$: Squares of V_{itw} and $I_{ijt\omega}$ $(kV^2)/A^2$).

$P^{\mathcal{S}}_{it\omega}$: Active power supplied by substation at node $i \in \Omega_n$, at time period $t \in \Omega_t$ and scenario $\omega \in \Omega_\omega$ (kW).

$P^{dg}_{it\omega} \geq 0$: Active power generation of the distributed generator at node $i \in \Omega_n$, at time period $t \in \Omega_t$ and scenario $\omega \in \Omega_\omega$ (kW).

$Q^{\mathcal{S}}_{it\omega}$: Reactive power supplied by substation at node $i \in \Omega_n$, at time period $t \in \Omega_t$ and scenario $\omega \in \Omega_\omega$ (kVAr).

$Q^{dg}_{it\omega}$: Reactive power generation of the distributed generator at node $i \in \Omega_n$, at time period $t \in \Omega_t$ and scenario $\omega \in \Omega_\omega$ (kVAr).

Q^{cb}_{it}: Reactive power injection of the capacitor bank $i \in \Omega_{cb}$, at time period $t \in \Omega_t$ and scenario $\omega \in \Omega_\omega$ (kVAr).

$P_{ijt\omega}$: Active power flow of branch $ij \in \Omega_b$, at time period $t \in \Omega_t$ and scenario $\omega \in \Omega_\omega$ (kW).

$Q_{ijt\omega}$: Reactive power flow of branch $ij \in \Omega_b$, at time period $t \in \Omega_t$ and scenario $\omega \in \Omega_\omega$ (kvar).

$SOC_{it\omega}$: State of charge of BESS at node $i \in \Omega_n$ at time period $t \in \Omega_t$, and scenario $\omega \in \Omega_\omega$ (%).

$n^+_{it\omega} \geq 0, n^-_{it\omega} \geq 0$: Auxiliary variables used to linearize the term $|n^{cb}_{it\omega} - n^{cb}_{it-1\omega}|$.

$l^+_{ijt\omega} \geq 0, l^-_{ijt\omega} \geq 0$: Auxiliary variables used to linearize the term $|l^{vr}_{ijt\omega} - l^{vr}_{ijt-1\omega}|$.

$\alpha^+_{it\omega} \geq 0, \alpha^-_{it\omega} \geq 0$: Auxiliary variables used to linearize the term $|b^{ch}_{it\omega} - b^{ch}_{it-1\omega}|$.

$\beta^+_{it\omega} \geq 0, \beta^-_{it\omega} \geq 0$: Auxiliary variables used to linearize the term $|b^{dis}_{it\omega} - b^{dis}_{it-1\omega}|$.

$L^{shed}_{it\omega}$: Load shedding at node $i \in \Omega_n$, at time period $t \in \Omega_t$ and scenario $\omega \in \Omega_\omega$.

$b^{ch}_{it\omega}, b^{dis}_{it\omega}$: BESS operation state at node $i \in \Omega_n$, time period $t \in \Omega_t$, and scenario $\omega \in \Omega_\omega$.

Binary Variables

$P^{ch}_{it\omega}, P^{dis}_{it\omega}$: Active power of BESS charge and discharge at node $i \in \Omega_i$ at time period $t \in \Omega_t$, and scenario $\omega \in \Omega_\omega$ (kW).

$b^{vr}_{ijtk\omega}$: Binary variable that defines the operation region for the tap of the voltage regulator in branch $ij \in \Omega_{vr}$, time period $t \in \Omega_t$ and scenario $\omega \in \Omega_\omega$.

Integer Variables

$n^{cb}_{it\omega}$: Number of capacitor bank units in operation at node $i \in \Omega_{cb}$, time period $t \in \Omega_t$ and scenario $\omega \in \Omega_\omega$.

$l^{vr}_{ijt\omega}$: Number of tap steps of the voltage regulator connected to branch $ij \in \Omega_{vr}$, time period $t \in \Omega_t$ and scenario $\omega \in \Omega_\omega$.

The MSOODN formulation is the following:

$$\text{Min} \sum_{\omega\in\Omega_\omega} \pi^{\omega} \sum_{t\in\Omega_t} \Delta_t \left(\sum_{i\in\Omega_{\mathcal{S}}} c_t^{\mathcal{S}} P_{it\omega}^{\mathcal{S}} + \sum_{i\in\Omega_n} \gamma_i \tilde{P}_{it\omega}^{\mathcal{D}} L_{it\omega}^{shed} \right) \tag{4.2.4}$$

s.t.

$$\sum_{ki\in\Omega_b} P_{kit\omega} - \sum_{ij\in\Omega_b} \left(P_{ijt\omega} + Rij I_{ijt\omega}^{sqr} \right) + P_{it\omega}^{\mathcal{S}} + \sum_{i\in\Omega_{pv}} \tilde{P}_{it\omega}^{pv}$$
$$+ \sum_{i\in\Omega_{bt}} \left(P_{it\omega}^{dis} + P_{it\omega}^{ch} \right) = \tilde{P}_{it\omega}^{\mathcal{D}} \left(1 - L_{it\omega}^{shed} \right) \qquad \forall i \in \Omega_n, \forall t \in \Omega_t, \forall \omega \in \Omega_\omega \tag{4.2.5}$$

$$\sum_{ki\in\Omega_b} Q_{kit\omega} - \sum_{ij\in\Omega_b} \left(Q_{ijt\omega} + X_{ij} I_{ijt\omega}^{sqr} \right) + Q_{it\omega}^{\mathcal{S}} + Q_{it}^{cb}$$
$$= \tilde{Q}_{it\omega}^{\mathcal{D}} \left(1 - L_{it\omega}^{shed} \right) \qquad \forall i \in \Omega_n, \forall t \in \Omega_t, \forall \omega \in \Omega_\omega \tag{4.2.6}$$

$$0 \le L_{it\omega}^{shed} \le 1 \qquad \forall i \in \Omega_n, \forall i \Omega_t \in \forall \omega \in \Omega_\omega \tag{4.2.7}$$

$$I_{ijt\omega}^{sqr} \cdot V_{ijt\omega}^{sqr} \ge P_{ijt\omega}^2 + Q_{ijt\omega}^2 \qquad \forall ij \in \Omega_b, \forall t \in \Omega_t, \forall \omega \in \Omega_\omega \tag{4.2.8}$$

$$0 \le \overline{I}_{ijt\omega}^{sqr} \le \overline{I}_{ij}^2 \qquad \forall ij \in \Omega_b, \forall t \in \Omega_t, \forall \omega \in \Omega_\omega \tag{4.2.9}$$

$$\underline{V}^2 \le V_{it\omega}^{sqr} \le \overline{V}^2 \qquad \forall i \in \Omega_n, \forall t \in \Omega_t, \forall \omega \in \Omega_\omega \tag{4.2.10}$$

$$V_{it\omega}^{sqr} - V_{jt\omega}^{sqr} = 2 \left(R_{ij} P_{ijt\omega} + X_{ij} Q_{ijt\omega} \right) + Z_{ij}^{sqr} I_{ijt\omega}^{sqr} \qquad \forall ij \in \Omega_b, \forall t \in \Omega_t, \forall \omega \in \Omega_\omega \tag{4.2.11}$$

$$\left(P_{it\omega}^{dg} \right)^2 + \left(Q_{it\omega}^{dg} \right)^2 \le \left(\overline{S}^{dg} \right)^2 \qquad \forall ij \in \Omega_{dg}, \forall t \in \Omega_t, \forall \omega \in \Omega_\omega \tag{4.2.12}$$

$$- P_{it\omega}^{dg} \cdot tan \left(cos^{-1} \left(\overline{pf}_i^{dg} \right) \right) \le Q_{it\omega}^{dg} \qquad \forall i \in \Omega_{dg}, \forall t \in \Omega_t, \forall \omega \in \Omega_\omega \tag{4.2.13}$$

$$Q_{it\omega}^{dg} \le P_{itw}^{dg} \cdot tan \left(cos^{-1} \left(\underline{pf}_i^{dg} \right) \right) \qquad \forall i \in \Omega_{dg}, \forall t \in \Omega_t, \forall \omega \in \Omega_\omega \tag{4.2.14}$$

$$Q_{itw}^{cb} = n_{it\omega}^{cb} \cdot q_i^{cb} \qquad \forall i \in \Omega_{cb}, \forall t \in \Omega_t, \forall \omega \in \Omega_\omega \tag{4.2.15}$$

$$0 \le n_{it\omega}^{cb} \le \overline{n}_i^{cb} \qquad \forall i \in \Omega_{cb}, \forall t \in \Omega_t, \forall \omega \in \Omega_\omega \tag{4.2.16}$$

$$\sum_{tin\omega_t} \left(n_{it\omega}^{+} + n_{it\omega}^{-} \right) \le \overline{\Delta}_i^{cb} \qquad \forall i \in \Omega_{cb}, \omega \in \Omega_\omega \tag{4.2.17}$$

$$n_{it\omega}^{cb} - n_{it-1\omega}^{cb} \le n_{it\omega}^{+} + n_{it\omega}^{-} \qquad \forall i \in \Omega_{cb}, \forall t \in \Omega_t, \omega \in \Omega_\omega \tag{4.2.18}$$

$$V_{jt\omega}^{sqr} = \sum_{k=0}^{2\overline{l}_{ij}^{vr}} \left[\left(1 + r_{ij}^{vr} \frac{(k - \overline{l}_{ij}^{vr})}{\overline{l}_{ij}^{vr}} \right)^2 \cdot V_{ijt\omega k}^{c} \right] \qquad \forall ij \in \Omega_{vr}, \forall t \in \Omega_t, \forall \omega \in \Omega_\omega \tag{4.2.19}$$

$$\underline{V}^{sqr} \cdot b_{ijtk\omega}^{vr} \le V_{ijtk\omega}^{c} \le \overline{V}^{sqr} \cdot b_{ijtk\omega}^{vr} \qquad \forall ij \in \Omega_{vr}, \forall t \in \Omega_t, \forall \omega \in \Omega_\omega$$
$$\forall k = 0, \ldots, 2\overline{l}_{ij}^{vr} \tag{4.2.20}$$

$$\underline{V}^{sqr} (1 - b_{ijtk\omega}^{vr}) \le V_{id}^{sqr} - V_{ijtk\omega}^{c} \le \overline{V}^{sqr} (1 - b_{ijtk\omega}^{vr}) \qquad \forall ij \in \Omega_{vr}, \forall t \in \Omega_t, \forall \omega \in \Omega_\omega$$
$$\forall k = 0, \ldots, 2\overline{l}_{ij}^{vr} \tag{4.2.21}$$

$$\sum_{tin\omega_t} \left(l_{it\omega}^{+} + l_{it\omega}^{-} \right) \le \overline{\Delta}_i^{vr} \qquad \forall i \in \Omega_{cb}, \omega \in \Omega_\omega \tag{4.2.22}$$

$$\sum_{k=0}^{2\overline{l}_{ij}^{vr}} \left[(k - \overline{l}_{ij}^{vr}) b_{ijtk\omega} \right] - \sum_{k=0}^{2\overline{l}_{ij}^{vr}} \left[(k - \overline{l}_{ij}^{vr}) b_{ijt-1k\omega} \right] \qquad \forall ij \in \Omega_{vr}, \forall t \in \Omega_t, \omega \in \Omega_\omega$$
$$= l_{ijt\omega}^{+} - l_{ijt\omega}^{-} \qquad \forall k = 0, \ldots, 2\overline{l}_{ij}^{vr} \tag{4.2.23}$$

$$\left(P_{itw}^{\mathcal{S}} \right)^2 + \left(Q_{itw}^{\mathcal{S}} \right)^2 \le \left(\overline{S}^{\mathcal{S}} \right)^2 \qquad \forall ij \in \Omega_{\mathcal{S}}, \forall t \in \Omega_t, \forall \omega \in \Omega_\omega \tag{4.2.24}$$

$$SOC_{it\omega} = SOC_{it-1\omega} + \Delta_t \left(P^{ch}_{it\omega}\eta^{ch}_i - \frac{P^{dis}_{it\omega}}{\eta^{dis}_i} \right) \forall i \in \Omega_{bt}, \forall t \in \Omega_t, \forall \omega \in \Omega_\omega \quad (4.2.25)$$

$$\underline{SOC}_i \leq SOC_{it\omega} \leq \overline{SOC}_i \quad \forall i \in \Omega_{bt}, \forall t \in \Omega_t, \forall \omega \in \Omega_\omega \quad (4.2.26)$$

$$\underline{P}^{ch}_i \cdot b^{ch}_{it\omega} \leq P^{ch}_{it\omega} \leq \overline{P}^{ch}_i \cdot b^{ch}_{it\omega} \quad \forall i \in \Omega_{bt}, \forall t \in \Omega_t, \forall \omega \in \Omega_\omega \quad (4.2.27)$$

$$\underline{P}^{dis}_i \cdot b^{dis}_{it\omega} \leq P^{dis}_{it\omega} \leq \overline{P}^{dis}_i \cdot b^{dis}_{it\omega} \quad \forall i \in \Omega_{bt}, \forall t \in \Omega_t, \forall \omega \in \Omega_\omega \quad (4.2.28)$$

$$b^{ch}_{it\omega} + b^{dis}_{it\omega} \leq 1 \quad \forall i \in \Omega_{bt}, \forall t \in \Omega_t, \forall \omega \in \Omega_\omega \quad (4.2.29)$$

$$b^{ch}_{it\omega} + b^{ch}_{it-1\omega} = \alpha^{+}_{it\omega} + \alpha^{-}_{it\omega} \quad \forall i \in \Omega_{bt}, \forall t \in \Omega_t, \forall \omega \in \Omega_\omega \quad (4.2.30)$$

$$\sum_{t \in \Omega_t} (\alpha^{+}_{it\omega} + \alpha^{-}_{it\omega}) \leq \overline{\Delta}^{ch}_{ij} \quad \forall i \in \Omega_{bt}, \forall \omega \in \Omega_\omega \quad (4.2.31)$$

$$\alpha^{+}_{it\omega} \leq 1 \quad \forall i \in \Omega_{bt}, \forall \omega \in \Omega_\omega \quad (4.2.32)$$

$$\alpha^{-}_{it\omega} \leq 1 \quad \forall i \in \Omega_{bt}, \forall \omega \in \Omega_\omega \quad (4.2.33)$$

$$b^{ch}_{it\omega} + b^{ch}_{it-1\omega} = \beta^{+}_{it\omega} + \beta^{-}_{it\omega} \quad \forall i \in \Omega_{bt}, \forall t \in \Omega_t, \forall \omega \in \Omega_\omega \quad (4.2.34)$$

$$\sum_{t \in \Omega_t} (\beta^{+}_{it\omega} + \beta^{-}_{it\omega}) \leq \overline{\Delta}^{dis}_{ij} \quad \forall i \in \Omega_{bt}, \forall \omega \in \Omega_\omega \quad (4.2.35)$$

$$\beta^{+}_{it\omega} \leq 1 \quad \forall i \in \Omega_{bt}, \forall \omega \in \Omega_\omega \quad (4.2.36)$$

$$\beta^{-}_{it\omega} \leq 1 \quad \forall i \in \Omega_{bt}, \forall \omega \in \Omega_\omega \quad (4.2.37)$$

$$V^{sqr}_{it\omega} = V^{sqr}_{it\omega'} \quad \forall i \in \Omega_{bt}, \forall t \in \Omega_t \setminus \{0\}, \forall \omega, \omega' \in \mathcal{C}^k_t, \omega \neq \omega', \mathcal{C}^k_t \in \mathcal{C}_t, k = 1, ..., |\mathcal{C}_t| \quad (4.2.38)$$

$$P^{\mathcal{S}}_{it\omega} = P^{\mathcal{S}}_{it\omega'} \quad \forall i \in \Omega_{bt}, \forall t \in \Omega_t \setminus \{0\}, \forall \omega, \omega' \in \mathcal{C}^k_t, \omega \neq \omega', \mathcal{C}^k_t \in \mathcal{C}_t, k = 1, ..., |\mathcal{C}_t| \quad (4.2.39)$$

$$Q^{\mathcal{S}}_{it\omega} = Q^{\mathcal{S}}_{it\omega'} \quad \forall i \in \Omega_{bt}, \forall t \in \Omega_t \setminus \{0\}, \forall \omega, \omega' \in \mathcal{C}^k_t, \omega \neq \omega', \mathcal{C}^k_t \in \mathcal{C}_t, k = 1, ..., |\mathcal{C}_t| \quad (4.2.40)$$

$$P^{dg}_{it\omega} = P^{dg}_{it\omega'} \quad \forall i \in \Omega_{dg}, \forall t \in \Omega_t \setminus \{0\}, \forall \omega, \omega' \in \mathcal{C}^k_t, \omega \neq \omega', \mathcal{C}^k_t \in \mathcal{C}_t, k = 1, ..., |\mathcal{C}_t| \quad (4.2.41)$$

$$Q^{dg}_{it\omega} = Q^{dg}_{it\omega'} \quad \forall i \in \Omega_{dg}, \forall t \in \Omega_t \setminus \{0\}, \forall \omega, \omega' \in \mathcal{C}^k_t, \omega \neq \omega', \mathcal{C}^k_t \in \mathcal{C}_t, k = 1, ..., |\mathcal{C}_t| \quad (4.2.42)$$

$$n^{cb}_{it\omega} = n^{cb}_{it\omega'} \quad \forall i \in \Omega_{cb}, \forall t \in \Omega_t \setminus \{0\}, \forall \omega, \omega' \in \mathcal{C}^k_t, \omega \neq \omega', \mathcal{C}^k_t \in \mathcal{C}_t, k = 1, ..., |\mathcal{C}_t| \quad (4.2.43)$$

$$Q^{cb}_{it\omega} = Q^{cb}_{it\omega'} \quad \forall i \in \Omega_{cb}, \forall t \in \Omega_t \setminus \{0\}, \forall \omega, \omega' \in \mathcal{C}^k_t, \omega \neq \omega', \mathcal{C}^k_t \in \mathcal{C}_t, k = 1, ..., |\mathcal{C}_t| \quad (4.2.44)$$

$$V^{c}_{ijtk\omega} = V^{c}_{ijtk\omega'} \quad \forall i, j \in \Omega_{vr}, \forall t \in \Omega_t \setminus \{0\}, \forall \omega, \omega' \in \mathcal{C}^k_t, \omega \neq \omega', \mathcal{C}^k_t \in \mathcal{C}_t, k = 1, ..., |\mathcal{C}_t| \quad (4.2.45)$$

$$b^{vr}_{ijtk\omega} = b^{vr}_{ijtk\omega'} \quad \forall i, j \in \Omega_{vr}, \forall t \in \Omega_t \setminus \{0\}, \forall \omega, \omega' \in \mathcal{C}^k_t, \omega \neq \omega', \mathcal{C}^k_t \in \mathcal{C}_t, k = 1, ..., |\mathcal{C}_t| \quad (4.2.46)$$

$$I^2_{it\omega} = I^2_{it\omega'} \quad \forall i \in \Omega_{bt}, \forall t \in \Omega_t \setminus \{0\}, \forall \omega, \omega' \in \mathcal{C}^k_t, \omega \neq \omega', \mathcal{C}^k_t \in \mathcal{C}_t, k = 1, ..., |\mathcal{C}_t| \quad (4.2.47)$$

$$P_{ijt\omega} = P_{ijtw'} \quad \forall ij \in \Omega_b, \forall t \in \Omega_t \setminus \{0\}, \forall \omega, \omega' \in \mathcal{C}^k_t, \omega \neq \omega', \mathcal{C}^k_t \in \mathcal{C}_{t-1}, k = 1, ..., |\mathcal{C}_t| \quad (4.2.48)$$

$$Q_{ijt\omega} = Q_{ijt\omega'} \quad \forall ij \in \Omega_b, \forall t \in \Omega_t \setminus \{0\}, \forall \omega, \omega' \in \mathcal{C}^k_t, \omega \neq \omega', \mathcal{C}^k_t \in \mathcal{C}_{t-1}, k = 1, ..., |\mathcal{C}_t| \quad (4.2.49)$$

$$L^{shed}_{it\omega} = L^{shed}_{it\omega'} \quad \forall i \in \Omega_{bt}, \forall t \in \Omega_t \setminus \{0\}, \forall \omega, \omega' \in \mathcal{C}^k_t, \omega \neq \omega', \mathcal{C}^k_t \in \mathcal{C}_t, k = 1, ..., |\mathcal{C}_t| \quad (4.2.50)$$

$$Q^{scb}_{it\omega} = Q^{scb}_{it\omega'} \quad \forall i \in \Omega_{bt}, \forall t \in \Omega_t \setminus \{0\}, \forall \omega, \omega' \in \mathcal{C}^k_t, \omega \neq w', \mathcal{C}^k_t \in \mathcal{C}_t, k = 1, ..., |\mathcal{C}_t| \quad (4.2.51)$$

$$P^{ch}_{it\omega} = P^{ch}_{it\omega'} \quad \forall i \in \Omega_{bt}, \forall t \in \Omega_t \setminus \{0\}, \forall \omega, \omega' \in \mathcal{C}^k_t, \omega \neq \omega', \mathcal{C}^k_t \in \mathcal{C}_t, k = 1, ..., |\mathcal{C}_t| \quad (4.2.52)$$

$$P^{dis}_{it\omega} = P^{dis}_{it\omega'} \quad \forall i \in \Omega_{bt}, \forall t \in \Omega_t \setminus \{0\}, \forall \omega, \omega' \in \mathcal{C}^k_t, \omega \neq \omega', \mathcal{C}^k_t \in \mathcal{C}_t, k = 1, ..., |\mathcal{C}_t| \quad (4.2.53)$$

$$SOC_{it\omega} = SOC_{it\omega'} \quad \forall i \in \Omega_{bt}, \forall t \in \Omega_t \setminus \{0\}, \forall \omega, \omega' \in \mathcal{C}^k_t, \omega \neq \omega', \mathcal{C}^k_t \in \mathcal{C}_t, k = 1, ..., |\mathcal{C}_t| \quad (4.2.54)$$

$$b^{ch}_{it\omega} = b^{ch}_{it\omega'} \quad \forall i \in \Omega_{bt}, \forall t \in \Omega_t \setminus \{|\Omega_t|\}, \forall \omega, \omega' \in \mathcal{C}^k_t, \omega \neq \omega', \mathcal{C}^k_t \in \mathcal{C}_t, k = 1, ..., |\mathcal{C}_t| \quad (4.2.55)$$

$$b^{dis}_{it\omega} = b^{dis}_{it\omega'} \quad \forall i \in \Omega_{bt}, \forall t \in \Omega_t \setminus \{|\Omega_t|\}, \forall \omega, \omega' \in \mathcal{C}^k_{t-1}, \omega \neq \omega', \mathcal{C}^k_t \in \mathcal{C}_t, k = 1, ..., |\mathcal{C}_t| \quad (4.2.56)$$

$$n^{+}_{it\omega} = n^{+}_{it\omega'} \quad \forall i \in \Omega_{cb}, \forall t \in \Omega_t \setminus \{|\Omega_t|\}, \forall \omega, \omega' \in \mathcal{C}^k_t, \omega \neq \omega', \mathcal{C}^k_t \in \mathcal{C}_t, k = 1, ..., |\mathcal{C}_t| \quad (4.2.57)$$

$$n^{-}_{it\omega} = n^{-}_{it\omega'} \quad \forall i \in \Omega_{cb}, \forall t \in \Omega_t \setminus \{|\Omega_t|\}, \forall \omega, \omega' \in \mathcal{C}^k_t, \omega \neq \omega', \mathcal{C}^k_t \in \mathcal{C}_t, k = 1, ..., |\mathcal{C}_t| \quad (4.2.58)$$

$$l^{+}_{it\omega} = l^{+}_{it\omega'} \quad \forall i,j \in \Omega_{vr}, \forall t \in \Omega_t \setminus \{|\Omega_t|\}, \forall \omega, \omega' \in \mathcal{C}^k_t, \omega \neq \omega', \mathcal{C}^k_t \in \mathcal{C}_t, k = 1, ..., |\mathcal{C}_t| \quad (4.2.59)$$

$$l^{-}_{it\omega} = l^{-}_{it\omega'} \quad \forall i,j \in \Omega_{vr}, \forall t \in \Omega_t \setminus \{|\Omega_t|\}, \forall \omega, \omega' \in \mathcal{C}^k_t, \omega \neq \omega', \mathcal{C}^k_t \in \mathcal{C}_t, k = 1, ..., |\mathcal{C}_t| \quad (4.2.60)$$

$$\alpha^{+}_{it\omega} = \alpha^{+}_{it\omega'} \quad \forall i \in \Omega_{bt}, \forall t \in \Omega_t \setminus \{|\Omega_t|\}, \forall \omega, \omega' \in \mathcal{C}^k_t, \omega \neq \omega', \mathcal{C}^k_t \in \mathcal{C}_t, k = 1, ..., |\mathcal{C}_t| \quad (4.2.61)$$

$$\alpha^{-}_{it\omega} = \alpha^{-}_{it\omega'} \quad \forall i \in \Omega_{bt}, \forall t \in \Omega_t \setminus \{|\Omega_t|\}, \forall \omega, \omega' \in \mathcal{C}^k_t, \omega \neq \omega', \mathcal{C}^k_t \in \mathcal{C}_t, k = 1, ..., |\mathcal{C}_t| \quad (4.2.62)$$

$$\beta^{+}_{it\omega} = \beta^{+}_{it\omega'} \quad \forall i \in \Omega_{bt}, \forall t \in \Omega_t \setminus \{|\Omega_t|\}, \forall \omega, \omega' \in \mathcal{C}^k_t, \omega \neq \omega', \mathcal{C}^k_t \in \mathcal{C}_t, k = 1, ..., |\mathcal{C}_t| \quad (4.2.63)$$

$$\beta^{-}_{it\omega} = \beta^{-}_{it\omega'} \quad \forall i \in \Omega_{bt}, \forall t \in \Omega_t \setminus \{|\Omega_t|\}, \forall \omega, \omega' \in \mathcal{C}^k_t, \omega \neq \omega', \mathcal{C}^k_t \in \mathcal{C}_t, k = 1, ..., |\mathcal{C}_t| \quad (4.2.64)$$

From the main grid, the objective function (4.2.4) minimizes the expected value for the energy procurement cost, and the expected cost is not served. The constraints (4.2.5)–(4.2.11) represent the conditions of the EDN's steady-state operations. Specifically, the constraint (4.2.5) represents the steady-state operation of a balanced radial EDN, which includes the active power losses of branch ij, the active power injected by the photovoltaic-RS plants, the active power injected or consumed by the BESS, and the active power consumed by loads. The constraint (4.2.6) represents the reactive power balance, which considers the reactive power losses of the branch ij, the reactive power injection of a capacitor bank for voltage support, and the reactive power consumed by loads. The constraint (4.2.7) provides the conditions to enable load shedding. In order to cope with the non-linearities of the steady-state operation model of the EDN, certain constraints for the MSOODN model are redefined with other constraints resulting from the linearization of some variables. The constraint (4.2.8) calculates the branch current magnitudes. The constraints (4.2.9) and (4.2.10) express in linear form, respectively, the voltage limits of the nodes and the conductor currents at their maximum supported current. The constraint (4.2.11) is the sum of contributions from all devices to the active and reactive power balance equations. The constraints (4.2.12)–(4.2.14) model the operation of dispatchable DG. The constraints (4.2.15)–(4.2.18) model the SCB operations. The constraints (4.2.19)–(4.2.23) model the VR operations. The constraints (4.2.24) models the generation capacity of DSS. The constraints (4.2.25)–(4.2.37), in general, provide the BESS conditions. More specifically, Constraints (4.2.25) and (4.2.26) are the conditions and limits for the SOC value; the set of constraints (4.2.27)–(4.2.29) define the BESS operation based on a binary variable for the charging mode and the discharging mode, both of which are restricted by their minimum and maximum limits; and the constraints (4.2.30)–(4.2.37) provide the linearization of conditions related to the maximum number of charging cycles. First, the different binary variables for two auxiliary continuous variables are replaced. Then, the BESS charging mode is identified by the sum of the auxiliary variables. Lastly, limits are imposed on these auxiliary variables. The constraints (4.2.38)–(4.2.64) show the NAC associated with to the optimal operation of a distribution network while considering BESS. These

constraints result of in the information that represents the problem's uncertainty that is gathered the scenario tree.

4.3. Analysis of the Decision Processes Developed

In this section, a brief analysis of the differences between the decision processes presented in Sections 4.1.2 and 4.2.2 of the MSWBVPP and MSOODN models is developed. Table 4.3.1 shows the main characteristics of the decision processes. Firstly, the uncertainty is defined by different sets of the random variables for each decision process. For the MSWBVPP model, the uncertainty is defined by the EM prices and WP generation. By contrast, for the MSOODN model, it is defined by the power load and PV generation. Secondly, the stages are defined by different facts. For the MSWBVPP model, the stages refer to the steps and time periods in the decision process. In this case, a stage is defined by the EM bid (step) or charge/discharge of the BESS or IB bid in hour(s) defined. On the other hand, the stages of the MSOODN model are referred to time periods where the decision variable is known (decisions are made after hour t for the BESS operation in the EDN or loads and PV generation after hour t are decided). Lastly, the lengths between subsequent stages are different. For the MSWBVPP model, these lengths are unequal, because they depend on the time periods in occur a step. For example, the horizon for the IM1 session is 24 hours, and the horizon for IM6 is 9 hours. Conversely, for the MSOODN model, the length between subsequent stages is equal for each stage. This length is defined by random variables that occur in each hour t, i.e., in each hour the values of the loads and PV generation are known.

	MSWBVPP model	MSOODN model
Uncertainty	EM prices and PW generation	Power Loads and PV generation
Stages	Steps and time periods	Time periods
Lengths between stages	Unequal lengths	Equal lengths

Cuadro 4.3.1: Main characteristics of the decision processes.

Figure 4.3.1 presents the two final characteristics represented in a time line. The first time line (Figure (a)) represents the stages and the lengths between them, the early stages of the decision process for the MSWBVPP model. The stages are characterized by a combination of decision step and time periods and the length between stages are unequal. On the other hand, for the MSOODN model, the second time line (Figure (b)) shows that the stages are time periods with equal lengths between these stages. The scenario tree generation methodology was developed taking into account these

differences. The scenario trees structure resulting for the MSWBVPP and MSOODN models are shown in Figures 4.1.4 and 4.2.3, respectively.

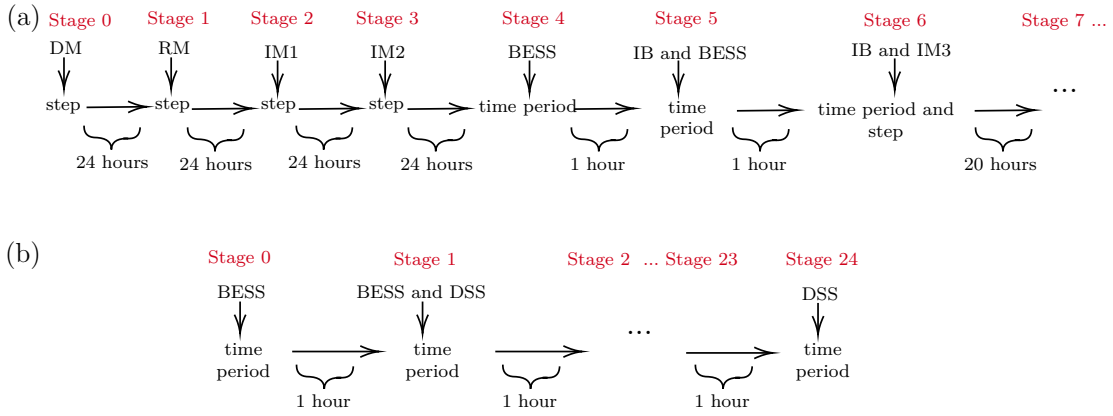

Figura 4.3.1: Some characteristics of the decision processes for the MSP models.

4.4. Optimizer Selection to Solve the MSP Models Developed

Since the MSP models of this research have been modelled in its deterministic representation (see Section 3.2), and that the main objective of this thesis is the representation of the uncertainty using scenario trees, we have limited to use available general-purpose solvers to solve the models. In this regard, we show the type of programming model which represents each MSP model in order to use appropriate algorithms to solve these models. The MSWBVPP model is a Mixed-Integer Linear Program (MILP) model for which exists solvers that lead to good solutions in a relatively short amount of time (Frangioni and Gentile, 2006). On the other hand, the MSOODN model is a Mixed-Integer Second-Order Cone Programming (MISOCP) model which is a generalization of Mixed-Integer Linear Optimization. In this case, convergence to the optimum is guaranteed using classical optimization techniques (Macedo et al., 2015).

Based on this information, we propose to use CPLEX - an executable program developed by IBM ILOG - to solve both models. CPLEX is a software that can read a problem interactively or from files in standard formats, solve the problem, and deliver the solution collectively or into text files (Cplex, 2009). This program includes an optimization suite of state-of-the-art solvers to resolve several types of programming models (Linear Programming (LP), Mixed-Integer Programming (MIP), Quadratic Programming (QP) and Quadratically-Constrained Programming problems (QCP), among others). For MILP models, CPLEX has the branch-and-cut algorithm which comprises a full set of presolving techniques, cutting planes, search strategies, and

heuristic techniques for finding feasible solutions. Also, it has the dynamic search algorithm which is a type of special search algorithm that can solve MILP. For MISOCP models, CPLEX has two basic algorithms: (a) Second Order Cones Programming-Branch and Bound (SOCP-B&B); (b) Outer Approximation-Branch and Bound (OA-B&B). In our case, we have used the branch-and-cut algorithm to solve the MSWBVPP model, with the following parameters definitions: presolve_eps=1.0e-07; and mipgap=0.005. And for the MSOODN model, we have used the SOCP-B&B algorithm to obtain optimal solutions, with a mipgap=0.01.

Everything should be made as simple
as possible, but not simpler.

— *Albert Einstein*

5

Numerical Experience with Scenario Trees for the MSWBVPP Model

Contents

In this chapter, we present and discuss the numerical results obtained from using the scenario tree generation methodology (presented in Chapter 3) on the Multistage Stochastic Wind Battery Virtual Power Plant model (MSWBVPP model) given in

Chapter 4. Firstly, Section 5.3 presents the numerical results obtained after implementing of the procedure described in Section 3.1. After that, Section 5.4 presents the numerical results of scenario trees obtained through implementing the algorithms given in Section 3.3.2. Finally, Section 5.7 shows the numerical results for the quality evaluation of the trees developed in Section 3.4.

5.1. VPP in EM Test

Our test considers the daily operations over the 24-h time periods $T = \{1, \ldots, 24\}$ of a Virtual Power Plant (VPP) operating in Day-Ahead Market (DM), Secondary Reserve Market (RM), Intra-day Markets (IM) and Imbalance Settlement (IB). Figure 5.1.1 shows the VPP in the Electricity Markets (EM) test that contains a Wind Power (WP) with power peaks of 18 MW and a Battery Energy Storage System (BESS) with a maximum capacity of 30 MWh. The objective was to maximize the expected value of the total profit of the VPP. The total profit was given by the incomes generated by sales of energy in the EM.

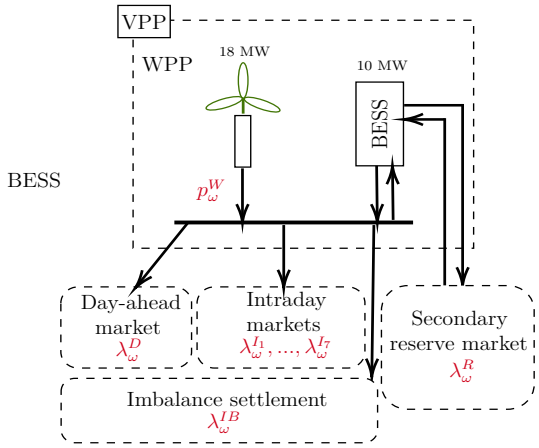

Figura 5.1.1: Operation of the VPP in the EM test.

As already stated, our aim is to find the optimal operation of the VPP with respect to any possible outcome of the random variables. The random variables are associated with the EM prices $(\boldsymbol{\lambda}^D, \boldsymbol{\lambda}^R, \boldsymbol{\lambda}^I_1, \ldots, \boldsymbol{\lambda}^I_7, \boldsymbol{\lambda}^{IB})$ and WP generation $(\mathbf{p}^W)$. These are given in Figure 5.1.1. The purpose of the following is to represent these random parameters through a scenario tree built by the scenario tree procedure developed in this thesis.

5.2. Initial Considerations

All implementations of this chapter were carried out on a DELL PowerEdge R630 Server with 2 x Xeon E5-2697 v4 (2,3 GHz, 18Cores/36Threads, 45 MB cache) and RAM 256 GB (8 x 32 GB RDIMM, 2400 MT/s). The first phase of the methodology

generated scenarios by implementing the statistical and forecasting models together with the bootstrapping technique, all of which were done using the software R-studio (Team et al., 2015). For the second phase of the methodology, the algorithms were implemented in AMPL (A Mathematical Programming Language) (Fourer et al. (1993)). Finally, all runs of the MSWBVPP model were performed using AMPL to call the optimizer CPLEX 12.8.0.0[1]

5.3. Phase I: Scenario Generation

Similarly to Muñoz et al. (2013), we use factors when applying the Time Series Factor Analysis (TSFA) technique for the data reduction. However, in contrast with that study, we decided to use Vector Autoregressive (VAR) models for the one-step-ahead forecast of the factors. Subsequently, we undid the TSFA transformation used for obtaining the prediction of the next day for each hour's random variables. Lastly, we generated scenarios through bootstrap techniques. Section 5.3.1 shows the time series characterization, and Sections 5.3.2–5.3.3 present the numerical experience resulting from the adjusted statistical models and developed forecasts. Finally, we present the numerical experience which yields the sets of scenarios that we use to generate the scenario trees (Section 5.3.4).

5.3.1. MTS Characterization

As is well known for the optimal participation of a VPP in the EM, the uncertainty is based on clearing prices and WP generation. This uncertainty is unknown and needs to be forecasted. If the forecast is more accurate, the VPP can control its expected benefits and bidding strategies, for which our objective in this case is to define good accuracy. We previously focused on developing an easy procedure based on the TSFA models used in electricity prices, but we are now going to use it in WP generation too. The procedure is inspired by the work developed in Muñoz et al. (2013), with the difference being that we use VAR models for one-step-ahead forecasting. Remembering the Multivariate Time Series (MTS) concept, an MTS can be collected in a matrix as shown in (5.3.1).

Our procedure is based on the interpretation of the EM prices and WP generation as an MTS of an M-hour panel. The data used are the MIBEL prices and the WP generation of one wind farm called *Espina*, located in Leon, Spain. The period covered

[1] CPLEX, 2016. [Online]. Available: http://www-01.ibm.com/software/commerce/optimization/cplex-optimizer/.

is 1 January 2015 to 31 December 2016 (in this case, $N = 731$). We used this data for the model's adjustment and the verification of generated forecasts.

$$\boldsymbol{\xi} = \begin{pmatrix} \boldsymbol{\xi}_1' \\ \boldsymbol{\xi}_2' \\ \vdots \\ \boldsymbol{\xi}_d' \\ \vdots \\ \boldsymbol{\xi}_N' \end{pmatrix} = \begin{pmatrix} \xi_{11} & \xi_{12} & \cdots & \xi_{1t} & \cdots & \xi_{1M} \\ \xi_{21} & \xi_{22} & \cdots & \xi_{2t} & \cdots & \xi_{2M} \\ \vdots & \vdots & \ddots & \vdots & \ddots & \vdots \\ \xi_{d1} & \xi_{d2} & \vdots & \xi_{dt} & \vdots & \xi_{dM} \\ \vdots & \vdots & \ddots & \vdots & \ddots & \vdots \\ \xi_{N1} & \xi_{N2} & \cdots & \xi_{Nt} & \cdots & \xi_{NM} \end{pmatrix} \tag{5.3.1}$$

For the MIBEL prices, data come from the website of System Operator Information System (e·sios: https://www.esios.ree.es/es), and they consist of the twenty-four hourly prices for each day (in €/Mwh) of the MIBEL. Figure 5.3.1 represents the plots of each MTS for the EM in the MIBEL (in this case DM, IM, RM, and IB). We showed the MTS plots in such a way that the concept of MTS can be understood. Figure 5.3.1 exhibits the MTS of the DM, RM and IM hourly prices. Figures 5.3.1a and 5.3.1b show the MTS of the DM hourly prices $\left(\boldsymbol{\lambda}^D\right)$ and the RM hourly prices $\left(\boldsymbol{\lambda}^R\right)$, respectively. As seen in these figures, they have M= 24 random variables. Figures 5.3.1c–5.3.1i refer to the MTS of the IM hourly prices $\left(\boldsymbol{\lambda}_1^I, \boldsymbol{\lambda}_2^I, \boldsymbol{\lambda}_3^I, \boldsymbol{\lambda}_4^I, \boldsymbol{\lambda}_5^I, \boldsymbol{\lambda}_6^I, \boldsymbol{\lambda}_7^I\right)$. In this case, the number of random variables varies, depending on the IM referenced, that is $M = \{24, 24, 20, 17, 13, 9, 3\}$, respectively.

In the context of the MSP methodology applied to EM problems, the issue of generating scenarios for imbalancing prices arises. The special relationship linking the imbalancing prices and the day-ahead market makes generating scenarios for the imbalancing prices quite different from generating scenarios for the rest of the random variables involved in these kinds of problems. For this reason, instead of working directly with $\boldsymbol{\lambda}^{IB^+}, \boldsymbol{\lambda}^{IB^-}$, we are going to use a transformation of parameter λ^{IB}, which is defined by the terms $\boldsymbol{\lambda}^{IB^+}$, $\boldsymbol{\lambda}^{IB^-}$ and $\boldsymbol{\lambda}^D$. This is given by the following function (with $d = 1, \cdots, N, t = 1, \cdots, M$.)

$$\lambda_{dt}^{IB}(\lambda_{dt}^{IB^+}, \lambda_{dt}^{IB^-}, \lambda_{dt}^{D}) = \begin{cases} \frac{\lambda_{dt}^{IB^+}}{\lambda_{dt}^{D}} \leq 1 & \text{if} \quad \lambda_{dt}^{IB^-} = \lambda_{dt}^{D} \\ \frac{\lambda_{dt}^{IB^-}}{\lambda_{dt}^{D}} \geq 1 & \text{if} \quad \lambda_{dt}^{IB^+} = \lambda_{dt}^{D} \\ 1 & \text{if} \quad \lambda_{dt}^{IB^+} = \lambda_{dt}^{IB^-} \\ E\left[\frac{\lambda_{dt}^{IB^-}}{\lambda_{dt}^{D}} \mid \mathbf{r}_t > 1\right] & \text{if} \quad \lambda_{dt}^{IB^+} = \lambda_{dt}^{D} = 0, \\ & \qquad \lambda_{dt}^{IB^-} = \lambda_{dt}^{D} > 0 \end{cases} \tag{5.3.2}$$

Table 5.3.2 defines the MTS for the IB transformation parameter, where λ_{dt}^{IB} is defined by Equation (5.3.2)).

MTS	Time Series
$\lambda^{IB} = \left(\lambda_1^{IB'}, \ldots, \lambda_d^{IB'}, \ldots, \lambda_N^{IB'}\right)', 1 \leq d \leq N$	$\lambda_d^{IB'} = \left(\lambda_{d1}^{IB}, \ldots, \lambda_{dt}^{IB}, \ldots, \lambda_{dM}^{IB}\right), 1 \leq t \leq M$

Cuadro 5.3.1: MTS of the IB transformation parameter.

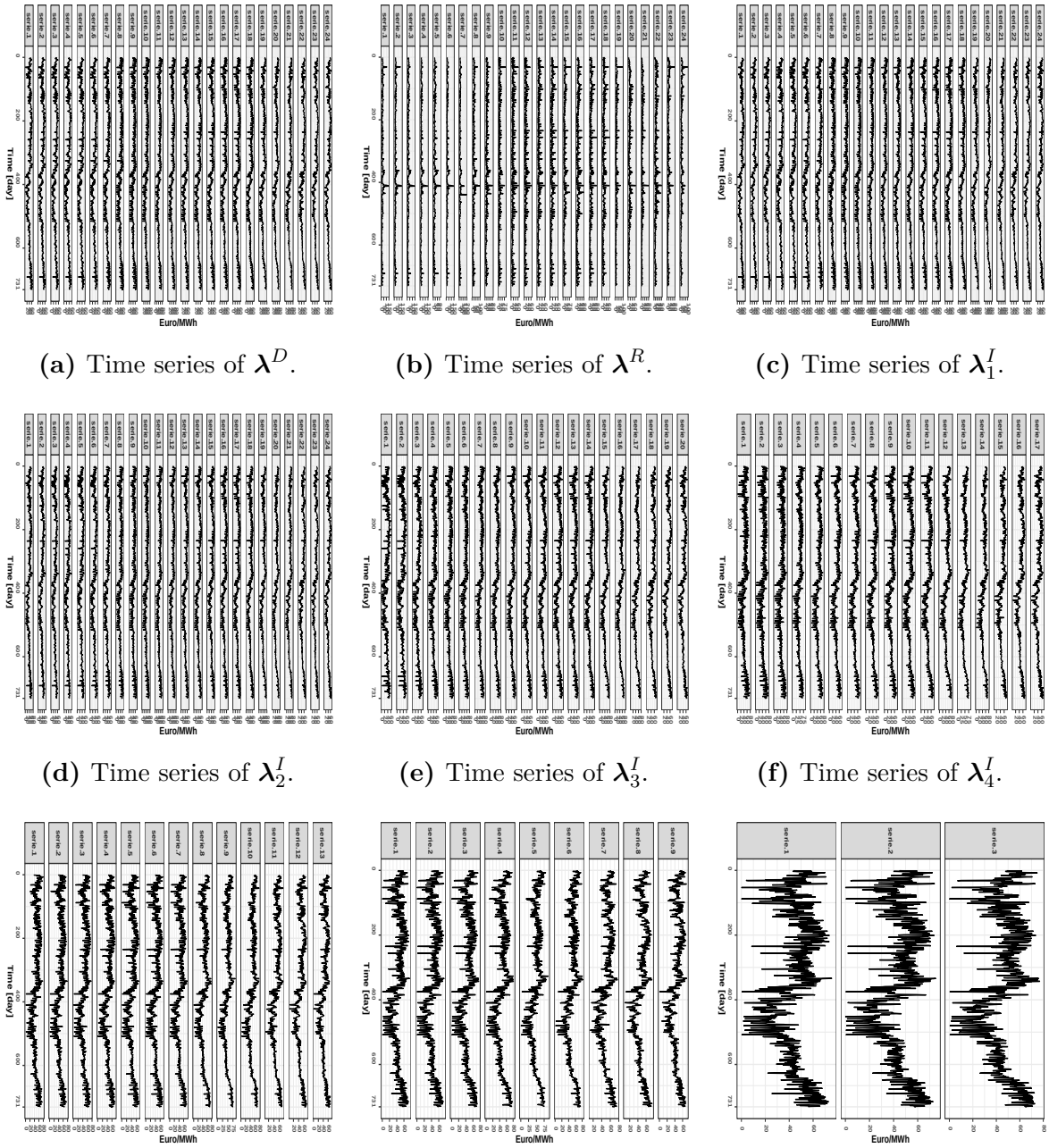

(a) Time series of $\boldsymbol{\lambda}^D$. **(b)** Time series of $\boldsymbol{\lambda}^R$. **(c)** Time series of $\boldsymbol{\lambda}_1^I$.

(d) Time series of $\boldsymbol{\lambda}_2^I$. **(e)** Time series of $\boldsymbol{\lambda}_3^I$. **(f)** Time series of $\boldsymbol{\lambda}_4^I$.

(g) Time series of $\boldsymbol{\lambda}_5^I$. **(h)** Time series of $\boldsymbol{\lambda}_6^I$. **(i)** Time series of $\boldsymbol{\lambda}_7^I$.

Figura 5.3.1: MTS of DM,RM and IM prices.

Figure 5.3.2 exhibits the MTS of IB hourly prices and its transformation parameter, where they have $M = 24$ random variables. Figures 5.3.2a–5.3.2b, show the MTS of positive and negative IB hourly prices, respectively $\left(\boldsymbol{\lambda}^{IB^+}, \boldsymbol{\lambda}^{IB^-}\right)$. Figure 5.3.2c shows the plots of λ^{IB}.

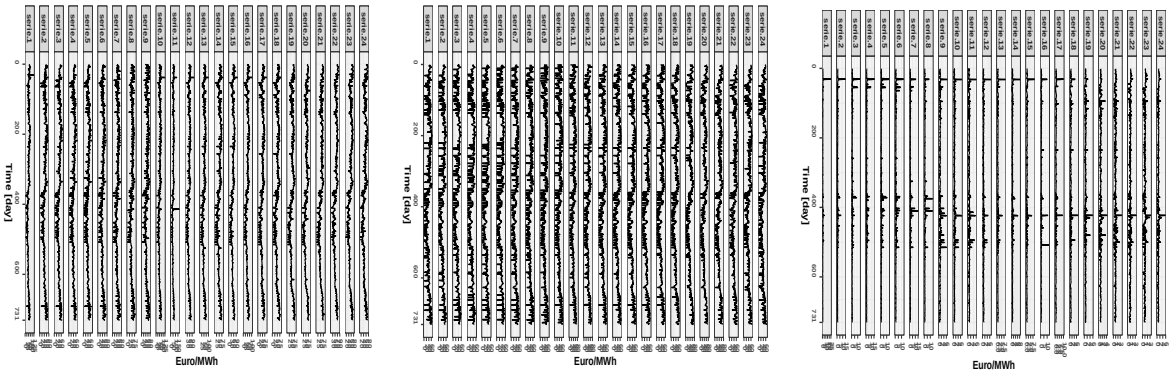

(a) Time Series of $\boldsymbol{\lambda}^{IB^+}$. **(b)** Time Series of $\boldsymbol{\lambda}^{IB^-}$. **(c)** Time Series of λ^{IB}.

Figura 5.3.2: MTS of IB prices and its IB parameter.

Looking at all the plots (Figures 5.3.1 and 5.3.2), the general characteristics of the MTS of the EM hourly prices and the IB transformation parameter show that the series has no constant mean and variance, suggesting that the series are nonstationary. Also, other characteristics can be observed, such as multiple seasonality (corresponding to a daily and weekly periodicity); high frequency and volatility; and the presence of picks, outliers and calendar effects (such as weekends and holidays).

Furthermore, the WP generation relied on data provided by *Naturgy* (https://www.naturgy.es/) for the wind farm called *Espina*, located in Leon, Spain. Table 5.3.2 shows the general features of this wind farm.

Wind farm name:	Espina
Wind farm type:	Onshore wind farm
Country/zone/city:	Leon/Castilla/La Espina
Turbine numbers:	9 turbines (power 2000 kW, diameter 87 m)
Total nominal power:	18,000 kW

Cuadro 5.3.2: Description of the wind farm Espina[2].

[2] Information available online at: https://www.thewindpower.net/windfarm_en_10569_espina.php.

Figure 5.3.3 refers to the MTS of WP generation ($\mathbf{p}^W$), which has $M = 24$ random variables (hours a day). The characteristics that we observed are strong non-stationary processes, high volatility and variability, and the presence of outliers.

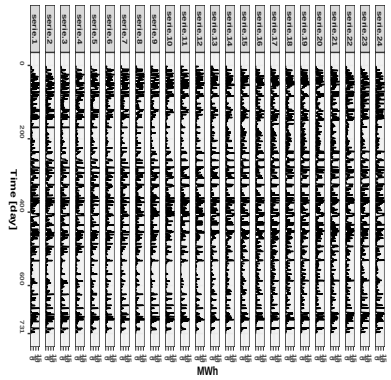

Figura 5.3.3: Time series of $\mathbf{p}^W$.

5.3.2. Statistical Models

This section shows the numerical experience of the adjusted statistical models for a particular set of data. In Section 5.3.2.1, we defined the data that we use as a sample for model adjustment and the data that we use for model validation. Then, Section 5.3.2.2 presents the results obtained from the computational experiences that were performed in order to achieve a reduction in the number of MTS variables that the TSFA technique produced in this part of the study. Finally, Section 5.3.2.3 shows the results obtained from adjusting the VAR models for either the common factors and some MTS of this study. The validation of each adjusted model is also presented in this section.

5.3.2.1. Initial Data

The MIBEL prices and WP generation are the random variables that we are going to treat in this part of the study. The goal is to determine statistical models in order to obtain short-term forecasts. Concerning this, we use the data over the period 1 January 2015 to 30 December 2016 as a sample for the estimation and model selection. The first year (1 January to 31 December 2015) is used for initial calibration, and then we update this data by adding a new day, e.g., 1 January 2016. This process is repeated until 30 December 2016. This is the rolling calibration window. In Summary, we will have 365 data calibrations and will adjust 366 models, by which the data calibration of the final model has as between 1 January 2015 to 30 December 2016. Furthermore, we define models for each MTS, where the number of variables is $t = 1, \ldots, M$, with $M \in \{24, 20, 17, 13, 9, 3\}$.

5.3.2.2. TSFA Models

Given that the MTS are highly dimensional, we wish to reduce these using TSFA. This technique allows identifying common unobserved factors, which represent the relationship between the hours of the day. The TSFA model is given by

$$\boldsymbol{\xi}_d = \hat{\alpha} + \hat{\boldsymbol{B}}\hat{\mathbf{F}}_d + \hat{\varepsilon}_d \tag{5.3.3}$$

where for all $d = 1, \ldots, N$, $\boldsymbol{\xi}_d$ is an $M \times 1$ vector of random variables, α is an M-row vector of intercept parameters, $\hat{B}$ is an $M \times k$ matrix parameter of factor loadings, $\hat{\mathbf{F}}_d$ is an $k \times 1$ vector of the Bartlett predictor (or common factors) values obtained through the estimation, and $\hat{\varepsilon}_d$ is a random $M \times 1$ vector of estimated measurement errors.

We fix a number of the model's factors given by Equation 5.3.3, which is based on the the Comparative Fit Index (CFI) and the Root Mean Square Error of Approximation (RMSEA) criteria described in Section 3.3.1.2. Table 5.3.3 presents the CFI and RMSEA values that were defined in order to obtain the number of factors in each case. The third column gives the CFI, showing that the values are greater than 0.95. The fourth-column presents the RMSEA values. For $\boldsymbol{\lambda}^D, \boldsymbol{\lambda}^R, \boldsymbol{\lambda}^I_1, \boldsymbol{\lambda}^I_2, \boldsymbol{\lambda}^I_3, \boldsymbol{\lambda}^R, \mathbf{P}^W$, the values are between 0.05 and 0.08, thus constituting an acceptable range of fit. Then, for the cases $\boldsymbol{\lambda}^I_4, \boldsymbol{\lambda}^I_5$, the values are lower than 0.05, establishing a good fit. Lastly, for $\boldsymbol{\lambda}^I_6$, the criterion presents a bad fit in certain cases and an acceptable range of fit in the other cases. Table 5.3.3 shows the relationship between the MTS and the common factors. The first and fourth columns show the names of the original MTS and the common factors, respectively. The second and sixth columns present the original numbers of variables (M) and numbers of factors (k) obtained, respectively. The reduction in the data is clear, as we were able to reduce 203 variables to 97 factors. Finally, it is important to stress that, due to the low dimensionality of $\boldsymbol{\lambda}^I_7$, the use of TSFA was not necessary.

MTS	Number of Variables (M)	CFI	RMSEA	MTS Common Factor ($\hat{\mathbf{F}}$)	Number of Factors (k)
$\boldsymbol{\lambda}^D$	24	[0.993,0.995]	[0.0658,0.0785]	$\hat{\mathbf{F}}^D$	11
$\boldsymbol{\lambda}^R$	24	[0.986,0.986]	[0.0756,0.0770]	$\hat{\mathbf{F}}^R$	10
$\boldsymbol{\lambda}^I_1$	24	[0.994,0.997]	[0.0685,0.0678]	$\hat{\mathbf{F}}^I_1$	11
$\boldsymbol{\lambda}^I_2$	24	[0.996,0.995]	[0.0623,0.0575]	$\hat{\mathbf{F}}^I_2$	11
$\boldsymbol{\lambda}^I_3$	20	[0.996,0.996]	[0.0557,0.0588]	$\hat{\mathbf{F}}^I_3$	9
$\boldsymbol{\lambda}^I_4$	17	[0.998,0.991]	[0.0389,0.0445]	$\hat{\mathbf{F}}^I_4$	8
$\boldsymbol{\lambda}^I_5$	13	[0.998,0.999]	[0.0226,0.0499]	$\hat{\mathbf{F}}^I_5$	6
$\boldsymbol{\lambda}^I_6$	9	[0.993,0.999]	[0.0564,0.124]	$\hat{\mathbf{F}}^I_6$	4
$\boldsymbol{\lambda}^{IB}$	24	[0.987,0.982]	[0.0783,0.0798]	$\hat{\mathbf{F}}^{IB}$	12
$\mathbf{p}^W$	24	[0.996,0.998]	[0.0562,0.0796]	$\hat{\mathbf{F}}^W$	15
Total	203				97

Cuadro 5.3.3: Number of TSFA factors defined for each MTS.

To show the results of the models selected, we present the numerical experience for one day. For the rest of the days, the results are very similar. For the sample, the data chosen corresponds to 1 January 2015 to 30 December 2016, and we adjust the TSFA model for this case. Figure 5.3.4 shows the common factor plots resulting from the adjustment.

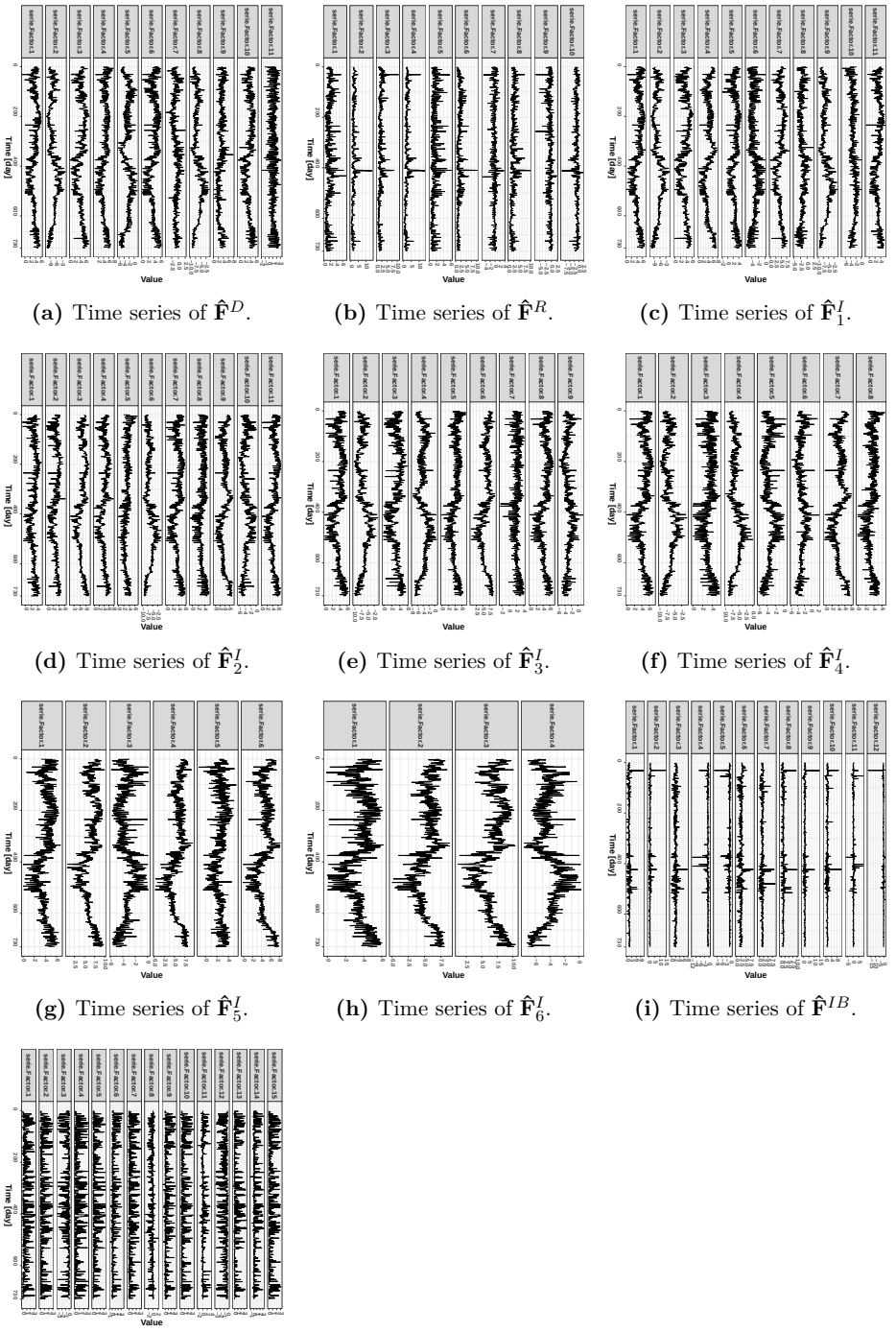

(a) Time series of $\hat{\mathbf{F}}^D$. **(b)** Time series of $\hat{\mathbf{F}}^R$. **(c)** Time series of $\hat{\mathbf{F}}^I_1$.

(d) Time series of $\hat{\mathbf{F}}^I_2$. **(e)** Time series of $\hat{\mathbf{F}}^I_3$. **(f)** Time series of $\hat{\mathbf{F}}^I_4$.

(g) Time series of $\hat{\mathbf{F}}^I_5$. **(h)** Time series of $\hat{\mathbf{F}}^I_6$. **(i)** Time series of $\hat{\mathbf{F}}^{IB}$.

(j) Time series of $\hat{\mathbf{F}}^W$.

Figura 5.3.4: MTS Common factors ($\hat{\mathbf{F}}$).

As an estimation result, we use the *communality*, which represents the proportion of common variance present in a variable. A variable that has no unique variance would have a communality of 1; by contrast, a variable that shares none of its variance with any other variable would have a communality of 0 (Field, 2013).

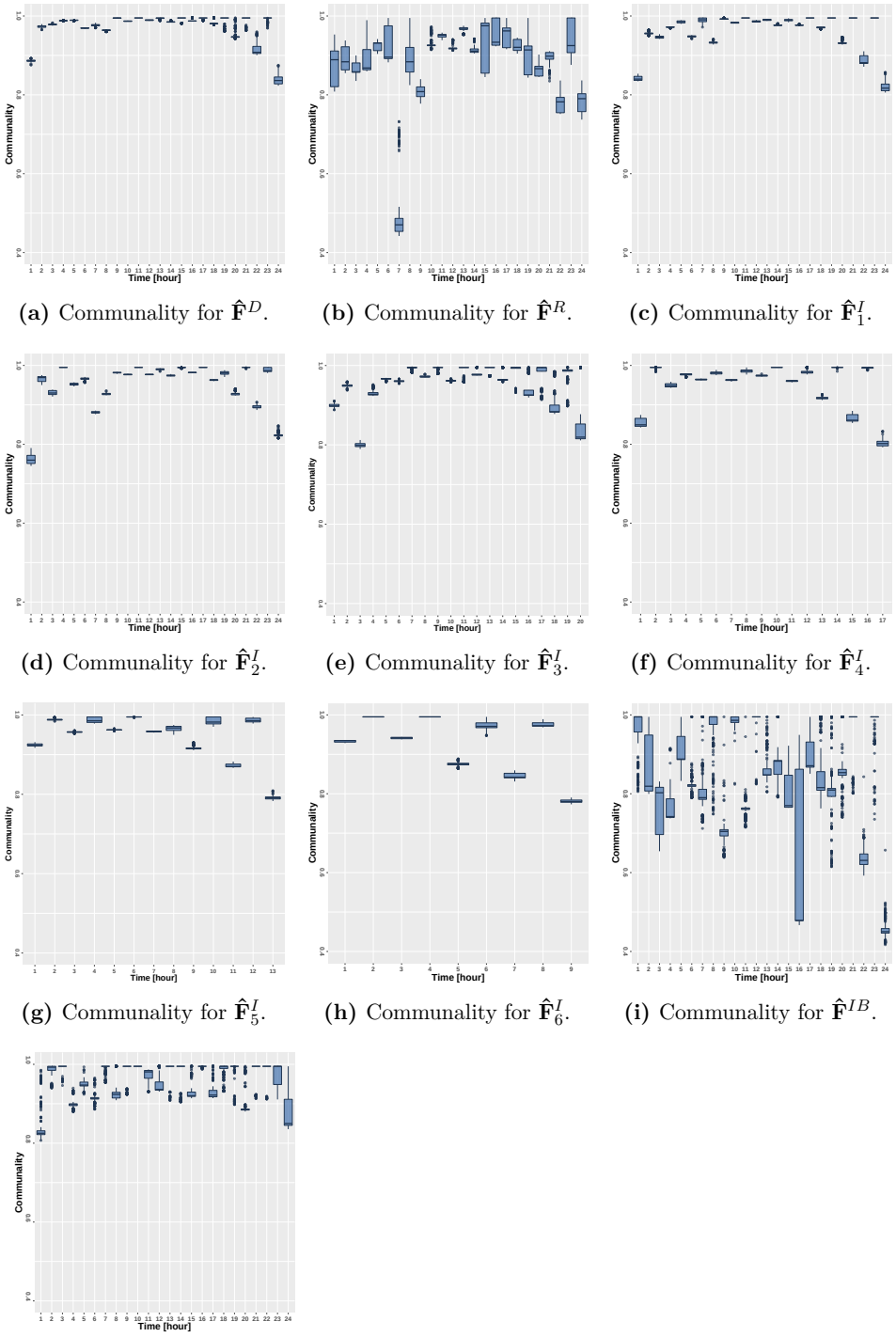

(a) Communality for $\hat{\mathbf{F}}^D$. **(b)** Communality for $\hat{\mathbf{F}}^R$. **(c)** Communality for $\hat{\mathbf{F}}^I_1$.

(d) Communality for $\hat{\mathbf{F}}^I_2$. **(e)** Communality for $\hat{\mathbf{F}}^I_3$. **(f)** Communality for $\hat{\mathbf{F}}^I_4$.

(g) Communality for $\hat{\mathbf{F}}^I_5$. **(h)** Communality for $\hat{\mathbf{F}}^I_6$. **(i)** Communality for $\hat{\mathbf{F}}^{IB}$.

(j) Communality for $\hat{\mathbf{F}}^W$.

Figura 5.3.5: Communality boxplots for $\hat{\mathbf{F}}$.

Figure 5.3.5 shows the communalities. In almost all cases, the communalities have values near 1 (except for hour 7 of $\hat{\mathbf{F}}^D$ and hours 16, 24 of $\hat{\mathbf{F}}^R$), showing that the proportion of the variance of the original variables are adequately explained by the common factors.

5.3.2.3. VAR Models

The following step is to estimate models for the common factors and $\boldsymbol{\lambda}_7^I$. We will use VAR models for this purpose. As is well known, the VAR models are used to model stationary MTS where there are dynamic dependencies between the different series. Therefore, before we estimate a model through VAR models, one of the important points is to always check if the time series we analyzed are stationary. This is important because, if the MTS are non-stationary, we could get improper estimate tests, which might lead to choosing the wrong model. Based on this information, we check if the common factors and $\boldsymbol{\lambda}_7^I$ are stationary. There are statistical tests to check whether a series is stationary. Among these tests are the Dickey–Fuller, KPSS, and the Phillips–Perron test. For our purpose,we used the Augmented Dickey–Fuller (ADF) test (see Section 3.3.1.1 for more details), which is a version of the Dickey–Fuller test. We check the stationarity using case 2 of the ADF, because the common factors and the IM7 prices are governed by weak stationarity in mean.

Figure 5.3.6 gives the boxplots of the values of the test statistics at the 95 % significance level. We compared the ADF test statistics (In R, these are the boxplots of tau2) to the critical values (red line). We reject the null hypothesis of a unit root with drift if the value of the test statistics is lower than the critical value. Also, Figure 5.3.6 shows that the boxplots are below the red line, which indicates that the null-hypothesis is rejected for all the cases. Therefore, the MTS are stationary.

After verification of the stationarity, we proceed to estimate models for the common factors and $\boldsymbol{\lambda}_7^I$. For all cases, the adjustment is significantly affected by the weekend data, such that we defined exogenous variables based on the penalization imposed by this. Furthermore, the order of the VARX model was fixed at $p = 8$, in such a way that it was greater than the weekly seasonal component of the original MTS. Based upon the above considerations, the VARX model is given by:

$$\hat{\mathbf{F}}_d = \boldsymbol{\Phi}_0 + \boldsymbol{\Phi}_1\hat{\mathbf{F}}_{d-1} + \boldsymbol{\Phi}_2\hat{\mathbf{F}}_{d-2} + \boldsymbol{\Phi}_3\hat{\mathbf{F}}_{d-3} + \boldsymbol{\Phi}_4\hat{\mathbf{F}}_{d-4} + \boldsymbol{\Phi}_5\hat{\mathbf{F}}_{d-5} + \ldots + \boldsymbol{\Phi}_8\hat{\mathbf{F}}_{d-8} + \boldsymbol{\beta}_0\mathbf{X}_d + \boldsymbol{\varepsilon}_d \quad (5.3.4)$$

for all $d = 1, \ldots, N$, where $(\boldsymbol{\varepsilon}_d) \sim IID(0, \boldsymbol{\Sigma}_\varepsilon)$, $\boldsymbol{\Phi}_0, \boldsymbol{\Phi}_1, \boldsymbol{\Phi}_2, \ldots, \boldsymbol{\Phi}_8$ are parameter matrices, $\boldsymbol{\beta}_0$ is the coefficient matrix for the exogenous variable, $\mathbf{X}_d$ is the exogenous variable and $\hat{\mathbf{F}}$ is the time series of the common factors $\hat{\mathbf{F}}^D, \hat{\mathbf{F}}^R, \hat{\mathbf{F}}_1^I, \ldots, \hat{\mathbf{F}}_6^I, \hat{\mathbf{F}}^{IB}, \hat{\mathbf{F}}^W$ or $\boldsymbol{\lambda}_7^I$.

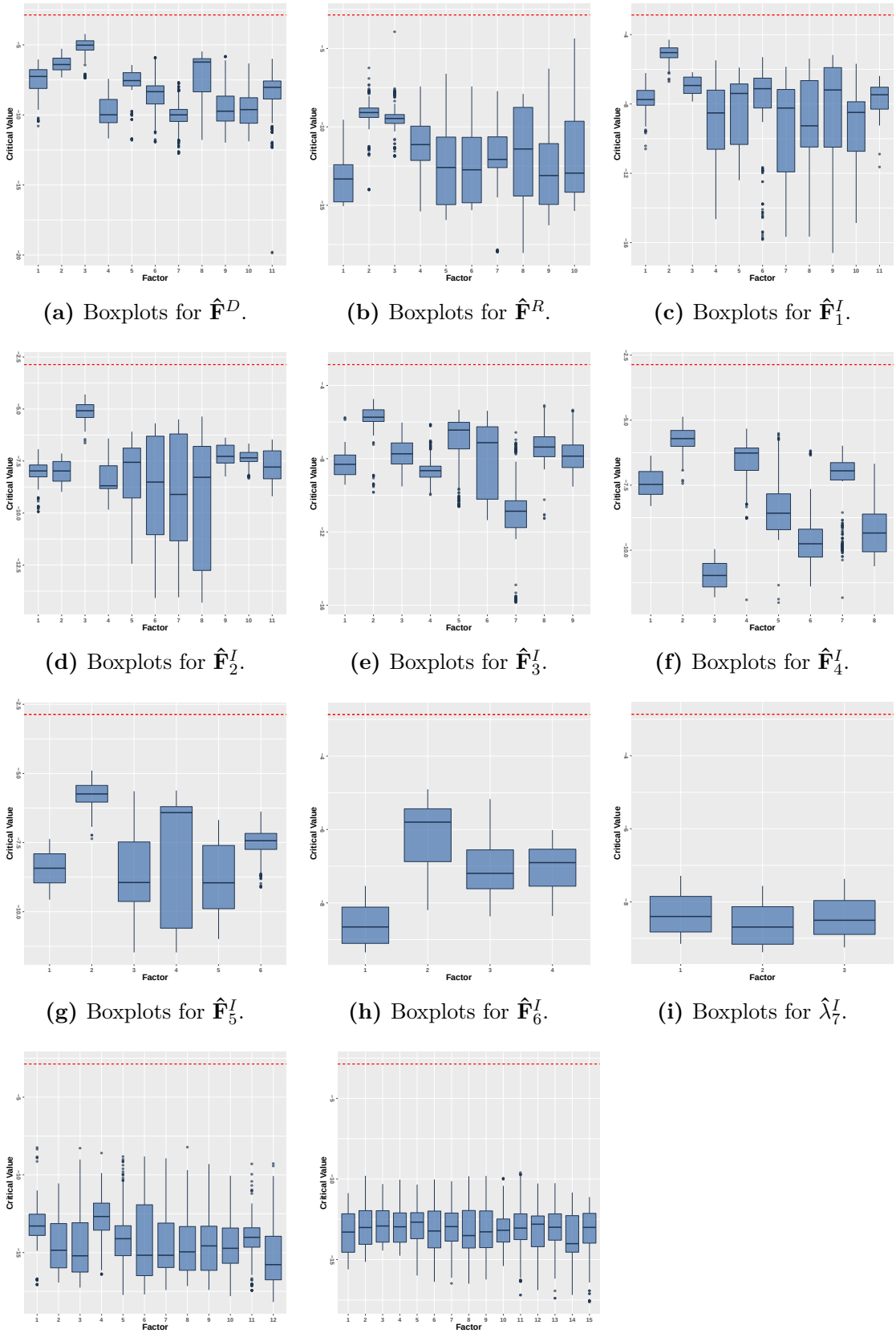

(a) Boxplots for $\hat{\mathbf{F}}^D$. **(b)** Boxplots for $\hat{\mathbf{F}}^R$. **(c)** Boxplots for $\hat{\mathbf{F}}^I_1$.

(d) Boxplots for $\hat{\mathbf{F}}^I_2$. **(e)** Boxplots for $\hat{\mathbf{F}}^I_3$. **(f)** Boxplots for $\hat{\mathbf{F}}^I_4$.

(g) Boxplots for $\hat{\mathbf{F}}^I_5$. **(h)** Boxplots for $\hat{\mathbf{F}}^I_6$. **(i)** Boxplots for $\hat{\lambda}^I_7$.

(j) Boxplots for $\hat{\mathbf{F}}^{IB}$. **(k)** Boxplots for $\hat{\mathbf{F}}^W$.

Figura 5.3.6: Boxplots of unit root test for $\hat{\mathbf{F}}$.

On the other hand, the adjusted models are validated by some plots that study the effects of noncompliance with fundamental assumptions. Appendix B.1 shows a brief overview of these plots. Assumptions such as homoscedasticity, normality, and independence are established. We present the validation for only one day at a time, while the rest were validated in the same way and the results are similar. Appendix B.1 presents four plots for this fact: (a) Residual Plots; (b) QQ-plot; and (c–d) the ACF and PACF of the residuals. All these are obtained for each common factor $(\hat{\mathbf{F}}^D, \hat{\mathbf{F}}^R, \hat{\mathbf{F}}^I_1, \ldots, \hat{\mathbf{F}}^I_6, \hat{\mathbf{F}}^{IB}, \hat{\mathbf{F}}^W)$ and $\boldsymbol{\lambda}^I_7$ (Figures B.1.1–B.1.11, respectively). Each of the plots show that the assumptions of the models are verified and, thereby, we can be sure that the adjusted models are suitable for forecasting.

5.3.3. Forecasting Models

The use of MSP models in the electric power industry is supported by a good representation of the stochastic process that governs the situations to be modeled. Therefore, the objective is to obtain forecasts fairly accurately with appropriate statistical methods. In the above section, the statistical models based on TSFA and Vector Autoregression with exogenous variables (VARX) techniques were defined and, now, our interest is in using them to define the forecasting models in order to, first, predict future values of the real problem's random variables and, second, define an approximation of the stochastic process for modeling the problem's stochasticity in the future. On the basis of these considerations, Section 5.3.3.1 gives the one-step-ahead forecast models for the common factors and the MTS of $\boldsymbol{\lambda}^I_7$; while Section 5.3.3.2 defines the one-step-ahead forecast model for these original random variables and presents their respective results (with the exception of $\boldsymbol{\lambda}^I_7$, because it has already been predicted by VARX models).

5.3.3.1. Forecasting with VAR Models

In order to be able to predict future values for the random variables, we need to forecast the common factors and the respective residuals $\hat{\varepsilon}'_d$. As shown in Section 5.3.2.3, we use VARX models in this case. The sample covers the period 1 January 2015 to 30 December 2016 (in a sense of the rolling calibration window), and we conduct the out-of-sample tests through the one-step-ahead forecast (typically 24 hours ahead) for all days of the year 2016 (in total, 366 forecasts). On the other hand, we will use the same technique to obtain forecasts for the seventh intraday prices. The forecast VARX(8) model is defined as

$$\hat{\mathbf{F}}_{N+1} = \hat{\boldsymbol{\Phi}}_0 + \hat{\boldsymbol{\Phi}}_1\hat{\mathbf{F}}_{N-1} + \hat{\boldsymbol{\Phi}}_2\hat{\mathbf{F}}_{N-2} + \hat{\boldsymbol{\Phi}}_3\hat{\mathbf{F}}_{N-3} + \hat{\boldsymbol{\Phi}}_4\hat{\mathbf{F}}_{N-4} + \ldots + \hat{\boldsymbol{\Phi}}_8\hat{\mathbf{F}}_{N-8} + \hat{\boldsymbol{\beta}}_0\hat{\mathbf{X}}_N \quad (5.3.5)$$

where $N{+}1$ indicates the one-step-ahead, $\hat{\mathbf{F}}_{N+1}$ is the common factor and $\hat{\boldsymbol{\beta}}_0, \hat{\boldsymbol{\Phi}}_0, \hat{\boldsymbol{\Phi}}_1, \ldots, \hat{\boldsymbol{\Phi}}_8$ are the estimated parameters of the model.

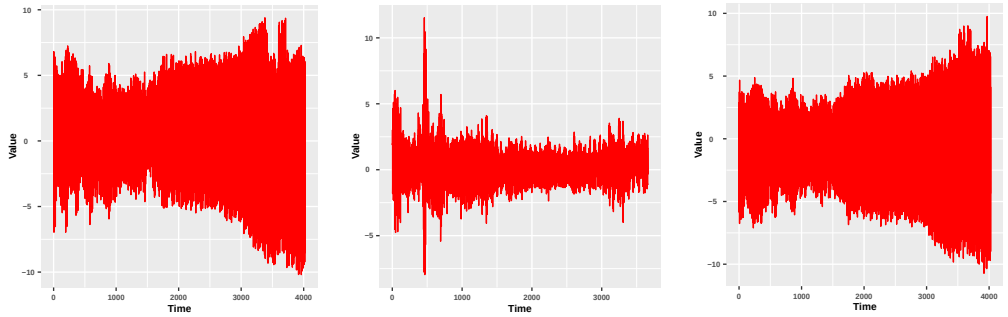

(a) $\hat{\mathbf{F}}^{D}_{N+1}$ forecast.

(b) $\hat{\mathbf{F}}^{R}_{N+1}$ forecast.

(c) $\hat{\mathbf{F}}^{I}_{1,N+1}$ forecast.

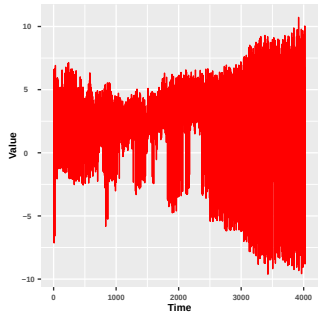

(d) $\hat{\mathbf{F}}^{I}_{2,N+1}$ forecast.

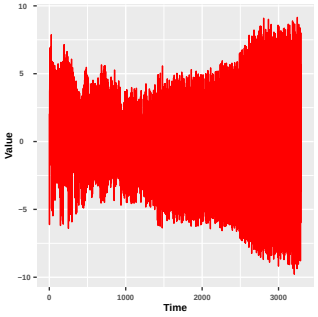

(e) $\hat{\mathbf{F}}^{I}_{3,N+1}$ forecast.

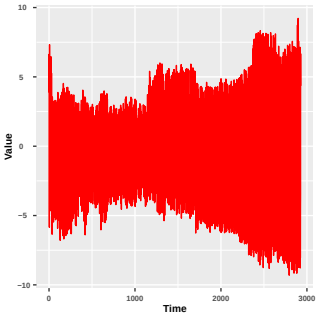

(f) $\hat{\mathbf{F}}^{I}_{4,N+1}$ forecast.

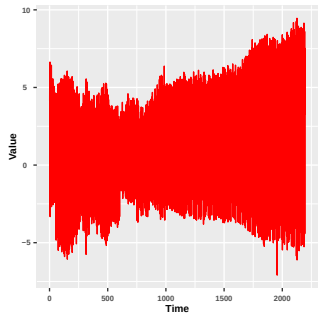

(g) $\hat{\mathbf{F}}^{I}_{5,N+1}$ forecast.

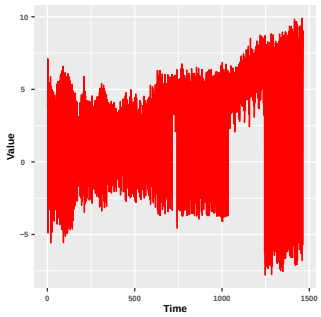

(h) $\hat{\mathbf{F}}^{I}_{6,N+1}$ forecast.

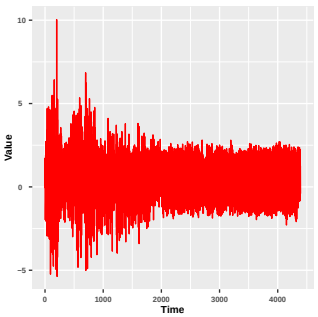

(i) $\hat{\mathbf{F}}^{IB}_{N+1}$ forecast.

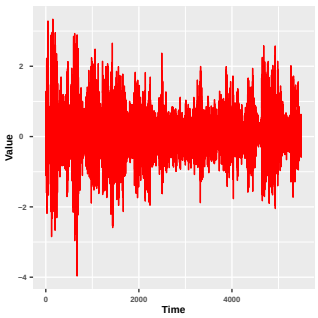

(j) $\hat{\mathbf{F}}^{W}_{N+1}$ forecast.

Figura 5.3.7: $\hat{\mathbf{F}}'_{N+1}$ forecast with the VARX models.

Figure 5.3.7 shows the one-step-ahead forecasts for the common factors over the period 1 January 2016 to 31 December 2016.

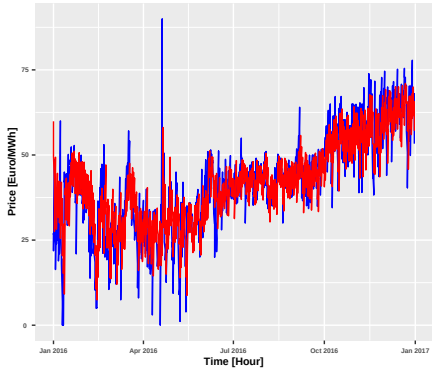

Figura 5.3.8: $\hat{\lambda}^{I}_{7N+1}$ forecast with VARX model.

Furthermore, the forecast for $\boldsymbol{\lambda}^{I}_{7}$ is shown in Figure 5.3.8. The real values are the blue line and the forecast values are the red line.

5.3.3.2. Forecasting with TSFA Models

To obtain the forecasts for the remaining MTS, we used the forecasting TSFA model. This is given by:

$$\hat{\boldsymbol{\xi}}_{N+1} = \hat{\alpha} + \hat{\boldsymbol{B}}\hat{\mathbf{F}}_{N+1}, \tag{5.3.6}$$

where $N+1$ indicates the one-step-ahead, $\hat{\mathbf{F}}_{N+1}$ are the forecasts of the common factor and $\hat{\alpha}, \hat{\boldsymbol{B}}$ are the estimate parameters of the model.

A simple substitution of these elements in Equation (5.3.6) gives the one-step-ahead forecasting models for the original MTS. Figure 5.3.9 shows the one-step-ahead forecasts for the year 2016 (1 January to 31 December). The real values (blue line) are compared with the estimates (red line) provided by the model. Therefore, Table 5.3.4 shows the out-of-sample errors for each forecast model.

	$\hat{\lambda}^{D}_{N+1}$	$\hat{\lambda}^{R}_{N+1}$	$\hat{\lambda}^{I}_{1N+1}$	$\hat{\lambda}^{I}_{2N+1}$	$\hat{\lambda}^{I}_{3N+1}$	$\hat{\lambda}^{I}_{4N+1}$	$\hat{\lambda}^{I}_{5N+1}$	$\hat{\lambda}^{I}_{6N+1}$	$\hat{\lambda}^{I}_{7N+1}$	$\hat{\lambda}^{IB}_{N+1}$	$\hat{\mathbf{p}}^{W}_{N+1}$
MAE	4.6732	5.5526	4.6732	4.9538	5.1361	5.1739	5.0711	5.4028	5.7401	0.5139	2.9905
RMSE	6.1364	8.7220	6.1364	6.5145	6.8348	6.8909	6.7893	7.0709	7.8263	0.9297	4.2799

Cuadro 5.3.4: Average errors for each forecasting model.

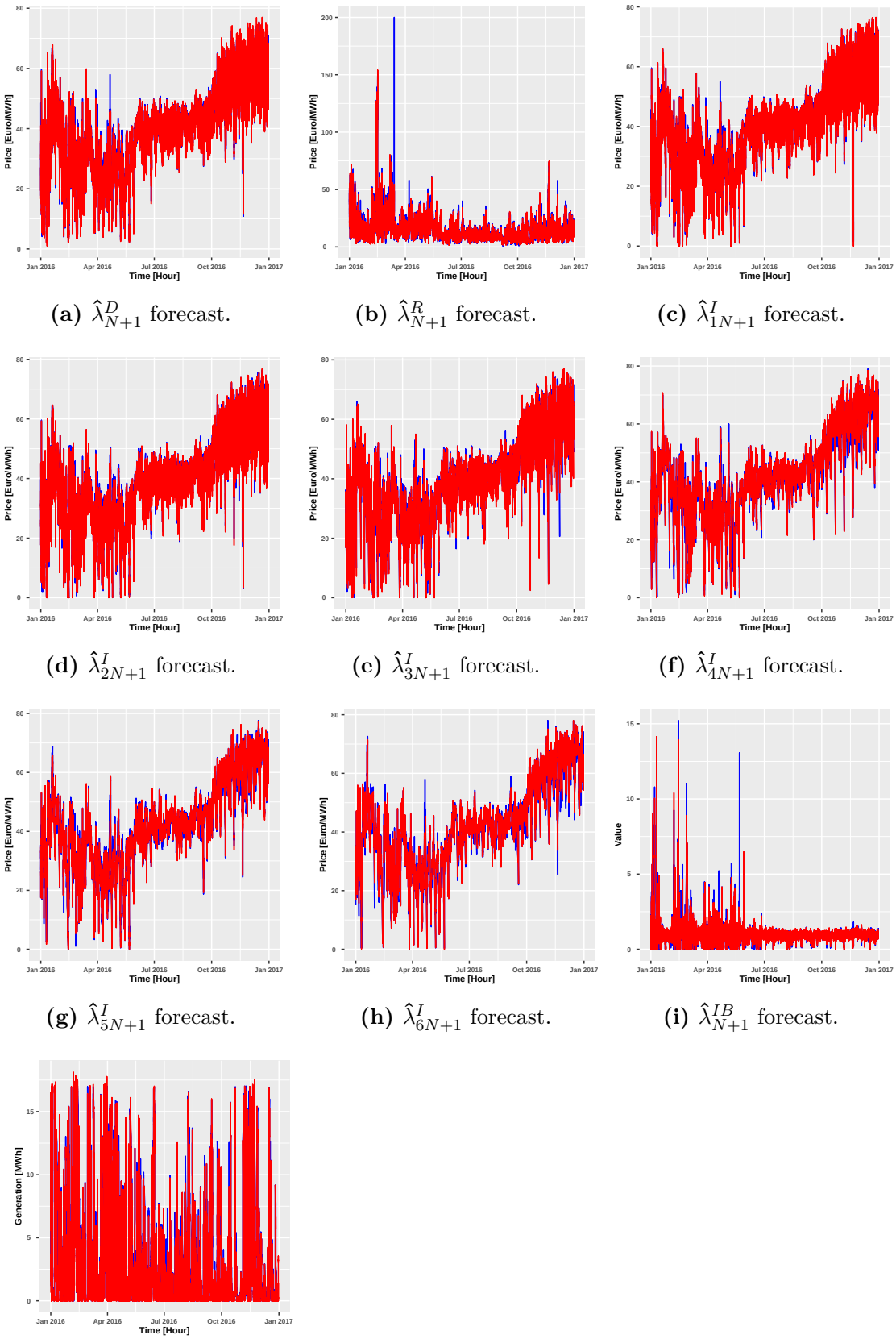

(a) $\hat{\lambda}^{D}_{N+1}$ forecast. **(b)** $\hat{\lambda}^{R}_{N+1}$ forecast. **(c)** $\hat{\lambda}^{I}_{1N+1}$ forecast.

(d) $\hat{\lambda}^{I}_{2N+1}$ forecast. **(e)** $\hat{\lambda}^{I}_{3N+1}$ forecast. **(f)** $\hat{\lambda}^{I}_{4N+1}$ forecast.

(g) $\hat{\lambda}^{I}_{5N+1}$ forecast. **(h)** $\hat{\lambda}^{I}_{6N+1}$ forecast. **(i)** $\hat{\lambda}^{IB}_{N+1}$ forecast.

(j) $\hat{\mathbf{p}}^{W}_{N+1}$ forecast.

Figura 5.3.9: MTS forecasts with TSFA models.

To conclude this part of the study, we can say that the development of the forecasting models does not require profound knowledge for identifying the models, being this, which is an advantage that facilitates the automatic implementation and regular use by the electricity companies.

5.3.4. Scenario Generation

For the scenario generation, we used the procedure based on forecasting results and bootstrapping techniques, which was given in Section 3.3.1.4. The results of this procedure are the scenario sets of the random variables, which will be used to define a configuration of the initial scenarios that is adequate enough to build scenario trees. The bootstrap procedure was tested with the same year used for testing the forecasting models (1 January to 31 December 2016). As a result, we obtained 366 sets of scenarios. Figures B.3.1–B.3.22 show scenario sets for four specific days: (a) Friday, 15 January 2016; (b) Monday, 06 June 2016; (c) Sunday, 16 October 2016; and (d) Thursday, 17 November 2016. In each of the figures, the real value is the red line, the forecasted value is the blue line and the bootstrap replicas are the black lines. In Appendix B, Figures B.3.1–B.3.11 present the scenario sets composed of 1000 scenarios, which will be used to build scenario trees by means of the Forward Tree Construction Algorithm (FTCA). Figures B.3.12–B.3.22 show the scenario sets with 10000 scenarios that will be used for generating scenario trees by means of the Dynamic Tree Generation with Flexible Bushiness Algorithm (DTGFBA).

Overall, the results show that, in general, scenario sets cover the red and blue lines, a condition which is positive for obtaining scenario trees in the future. Nevertheless, in cases when the forecasted value (red line) is really far from the real value (blue line), the bootstrap replicas do not cover the real value. This fact can be inconvenient for obtaining good results for the MSWBVPP model. Figures B.3.3d, B.3.10d, B.3.11d, B.3.13d, B.3.21d and B.3.22d of Appendix B show this fact.

5.4. Phase II: Scenario Tree Generation

The uncertainty analysis and definition of the decision process developed in Section 4.1.2 of Chapter 4 has allowed us to define the structure of the scenario tree for the MSP Models in EM and Electrical Distribution Netwoks (EDN). In the following sections, we will present the development of Phase II, which concerns scenario tree generation for the MSP models developed in this thesis. Section 5.4.1 draws on the initial considerations of the numerical experience by generating scenario trees; and Sections 5.4.2 and 5.4.3, respectively, present the computational results of the scenario trees obtained with the

FTCA and DTGFBA. Finally, Section 5.5 shows an analysis for the total instances executed by each scenario trees algorithm.

5.4.1. Initial Considerations for the Algorithms

The scenario tree algorithms used in this thesis are based on the assumption that an initial set of individual scenarios are available and that these are used for defining a fan or an initial scenario tree. For this reason, it is necessary to define the individual scenarios to be used for this purpose. Section 4.1.2 shows the definition of the individual scenario in Equation (4.1.2). We remind the reader of this definition below:

$$\tilde{\boldsymbol{\xi}}_{\omega} = \Big(\tilde{\boldsymbol{\lambda}}_{\omega}^{D'}, \tilde{\boldsymbol{\lambda}}_{\omega}^{R'}, \tilde{\boldsymbol{\lambda}}_{1\omega}^{I'}, \tilde{\boldsymbol{\lambda}}_{2\omega}^{I'}, \tilde{p}_{1\omega}^{W}, \tilde{p}_{2\omega}^{W}, \tilde{\boldsymbol{\lambda}}_{3\omega}^{I'}, \tilde{p}_{3\omega}^{W}, \ldots, \tilde{p}_{5\omega}^{W}, \tilde{\boldsymbol{\lambda}}_{4\omega}^{I'}, \tilde{p}_{6\omega}^{W}, \ldots, \tilde{p}_{9\omega}^{W}, \tilde{\boldsymbol{\lambda}}_{5\omega}^{I'}, \tilde{p}_{10\omega}^{W}, \ldots, \tilde{p}_{13\omega}^{W}, \tilde{\boldsymbol{\lambda}}_{6\omega}^{I'}, \tilde{p}_{14\omega}^{W}, \ldots, \tilde{p}_{19\omega}^{W}, \tilde{\boldsymbol{\lambda}}_{7\omega}^{I'}, \tilde{p}_{20\omega}^{W}, \ldots, \tilde{p}_{24\omega}^{W}, \tilde{\boldsymbol{\lambda}}_{\omega}^{IB'}\Big)' \tag{5.4.1}$$

where each component of the vector is called a *realization* of the individual scenario.

The initial data consist of a finite number of these scenarios (Section 5.3.4). The components of the vector are the EM prices and WP generation that are organized in accordance with the decision process. Equal probabilities are assigned to each scenario. Table D.1.1 of Appendix D shows the dimensionality of these individual scenarios. Note that the total length of the individual scenarios is 206, a considerably large length that will produce a scenario tree of great size. Furthermore, these scenarios have 34 stages, and each of these has a time horizon going from 1 to 24 time steps per day, a further indication that the resulting scenario trees will be very large.

5.4.2. Scenario Trees Obtained by FTCA

The main objective of the FTCA strategy consists of modifying a given fan of individual scenarios by bundling scenarios according to the scenario reduction technique. Therefore, we are interested in defining fans in order to apply the FTCA and obtain scenario trees for each test of the MSWBVPP model. In this numerical experience, we defined fans with the first node (root node) that corresponds to a fixed value at stage $s = 0$. Furthermore, the scenarios have equal probabilities. Table 5.4.1 provides the general characteristics of the initial fan structure.

Components	Scenarios	Stages	Initial Nodes
206	1000	34	34000

Cuadro 5.4.1: Dimensions of the initial fan provided by the MSWBVPP model.

Figure 5.4.1 shows the plot of the initial fan for the MSWBVPP model. The idea is to reduce the fan in such a way that we get a scenario tree with at least half of the scenarios. The initial values of the input parameters of the FTCA were fixed while taking this purpose into account.

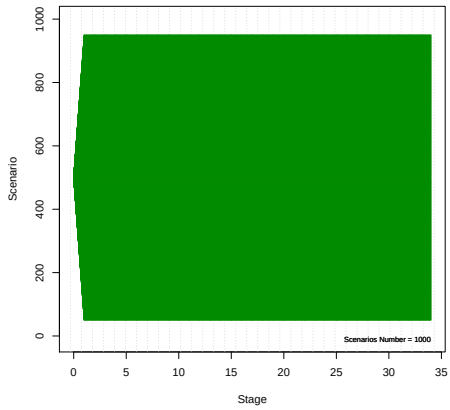

Figura 5.4.1: Initial fan structure for the FTCA.

After having defined the fan, we proceed to obtain scenario trees using the FTCA. To this end, we used Algorithm 1, which iteratively applies Algorithm 2, to every stage of $\tilde{\boldsymbol{\xi}}$. The implementations of these algorithms are given in Appendix C. The tests were performed to generate scenario trees for the year 2016 (in total, 366 scenario trees). Regarding the algorithm, the FTCA stops clustering scenarios at stage s as soon as the norm between the tree t at $t-1$ is reduced below ε_s:

$$\|\tilde{\boldsymbol{\xi}}_s - \tilde{\boldsymbol{\xi}}_{s-1}\|_{r,s} \leq \varepsilon_s \tag{5.4.2}$$

The relative tolerances ε_s were calculated by Equation (3.3.26) in all test runs, where $\varepsilon_{rel,s}$ and $\varepsilon_{max,s}$ were calculated by Equations (3.3.28) and (3.3.29), respectively. The initial values of the parameters associated with these calculations are $\varepsilon_{rel,0} = 0$, $\delta_0 = 0{,}85$ and $\Delta = 0{,}005$. Tables D.1.1 and D.1.2 show the values of $\varepsilon_{rel,s}$, ε_s and $\varepsilon_{max,s}$ for one test. The $\varepsilon_{rel,s}$ values are equal for the all tests, in contrast to $\varepsilon_s, \varepsilon_{max,s}$, where the values are different for each test. We defined the norm $\|\cdot\|_{r,s}$ by Equation (3.3.21), where r is fixed at 2.

Table 5.4.2 displays the results of some numerical tests for the year 2016 (1 January to 31 December). The second and third column enables us to compare the sizes of the

initial scenario fan given in Table 5.4.1 with the scenario trees in terms of the number of, respectively, scenarios and nodes. On the other hand, Figure 5.4.2 illustrates the structure of some scenario trees generated by the FTCA. This figure shows the plots of four scenario trees with the branching structure and epsilon tolerances specified in, Tables D.1.1 and D.1.2. The numerical results illustrate that the FTCA can get scenario trees to represent the uncertainty in the MSWBVPP model. Also, one characteristic of the results obtained is that, for tolerance fixes, the numbers of scenarios and nodes vary for each day of the test. This is because these depend on the distances between probability distributions.

Scenario Tree	Number of Scenarios	Final Nodes
Scenario Tree for Friday 15-January-2016	553	13522
Scenario Tree for Monday 06-June-2016	621	12505
Scenario Tree for Sunday 16-October-2016	620	12833
Scenario Tree for Thursday 17-November-2016	587	11932

Cuadro 5.4.2: Results of the FTCA for some days of the year in 2016.

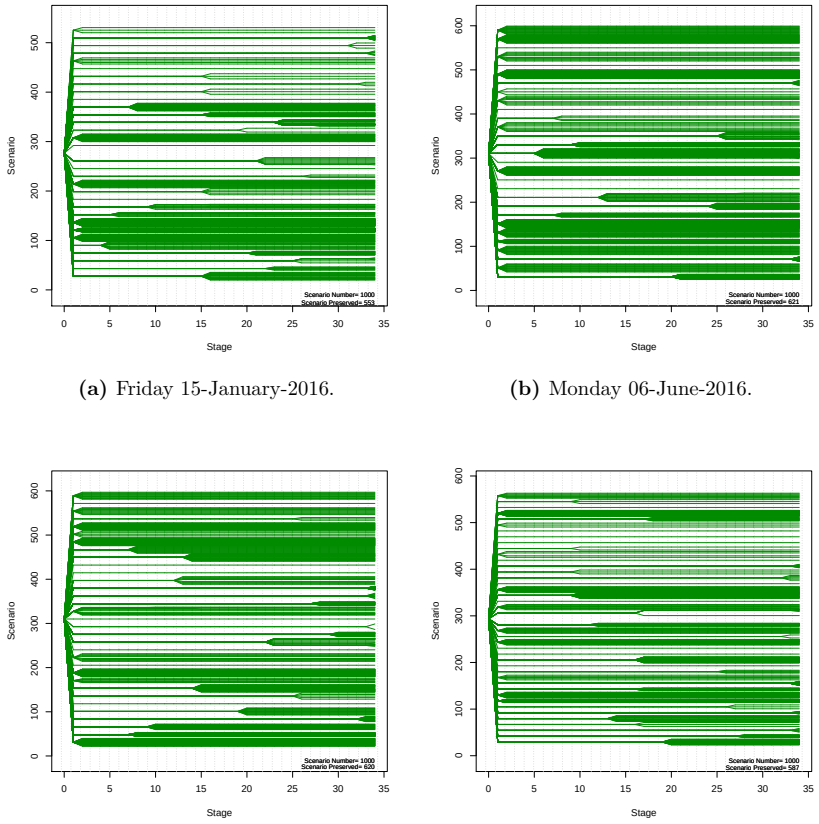

(a) Friday 15-January-2016. **(b)** Monday 06-June-2016.

(c) Sunday 16-October-2016. **(d)** Thursday 17-November-2016.

Figura 5.4.2: Some scenario trees obtained by the FTCA for the MSWBVPP model.

5.4.3. Scenario Trees Obtained by DTGFBA

Another algorithm used to identify the random input data for the MSWBVPP model was the DTGFBA (Algorithm 3 together with Algorithm 4 of Section 3.3.2.2). Remember that the DTGFBA is an algorithm for constructing an approximating tree from observed paths in terms of the nested distance up to a prescribed precision. In this case, the observed paths are vectors, as in Equation (5.4.1), and they are individual scenarios obtained by the procedure for generating scenario trees. These paths are assumed to be a sequence of random variables that are independent and identically distributed (i.i.d.) with an arbitrary length of known distribution. the DTGFBA was implemented in AMPL and the details are given in Serra Castilla et al. (2019). The tests started out with a matrix that containing a total of 10,000 paths, where the length of each path is 206 (the order of the matrix is 10,000 rows and 206 columns). The paths have associated equal probabilities and the number of stages is 34. The initial values of the algorithm for one test are shown in Table D.1.3 of Appendix D and the values of b_s are the same for all tests. Conversely, the values of ε_s are different for each test because it depends on the input values of each test day. The ε_s (the maximal stagewise transportation distances) was calculated in the following form:

$$\varepsilon_s = \Delta_j \max_{s \in \mathcal{S}} \sum_{s' \in \mathcal{S}} \frac{d_{s,s'}}{|\mathcal{S}|} \tag{5.4.3}$$

where $d_{s,s'}$ is the Euclidean distance, and Δ_j is a penalization that causes the difference between the Δ_j values for the EM prices ($j = 1$) and WP generation ($j = 2$).

In addition, for the case of WP generation, Δ_1 was fixed at 0.99; and, for the EM prices, Δ_2 is equal to 1. On the other hand, the implemented DTGFBA allows choosing of deciding the minimum number of scenarios for each stage. This parameter was defined as $n_s = b_s + 4$. Table D.1.3 of Appendix D shows the values defined in this case. Another feature to take into account when building scenario trees with this algorithm is the selection of scenario values. For the EM prices, the selection was defined randomly by a uniform distribution between 1 and 10,000, with the values of the matrix being selected according to the positions of this distribution. For WP generation, the selection was made considering the values of previous stages that have the same nature.

In the same way as with the FTCA, the tests were performed to generate scenario trees for the year 2016 (1 January to 31 December). Thus, scenario trees can be built by the DTGFBA. Table 5.4.3 presents the results obtained for the DTGFBA over four days. This table shows the number of scenarios and final nodes for the same days as those of the FTCA. Figure 5.4.3 displays the scenario trees. Analysing the results, we can observe that the scenario trees for each day varies notably according to the number

of scenarios and nodes. As a final remark, we can say that DTGFBA is able to get scenario trees to represent the uncertainty in the MSWBVPP model.

Scenario Tree	Number of Scenarios	Final Nodes
Scenario Tree for Friday 15-January-2016	829	3629
Scenario Tree for Monday 06-June-2016	182	4278
Scenario Tree for Sunday 16-October-2016	594	5845
Scenario Tree for Thursday 17-November-2016	502	5316

Cuadro 5.4.3: Results of the DTGFBA for some days of the year 2016.

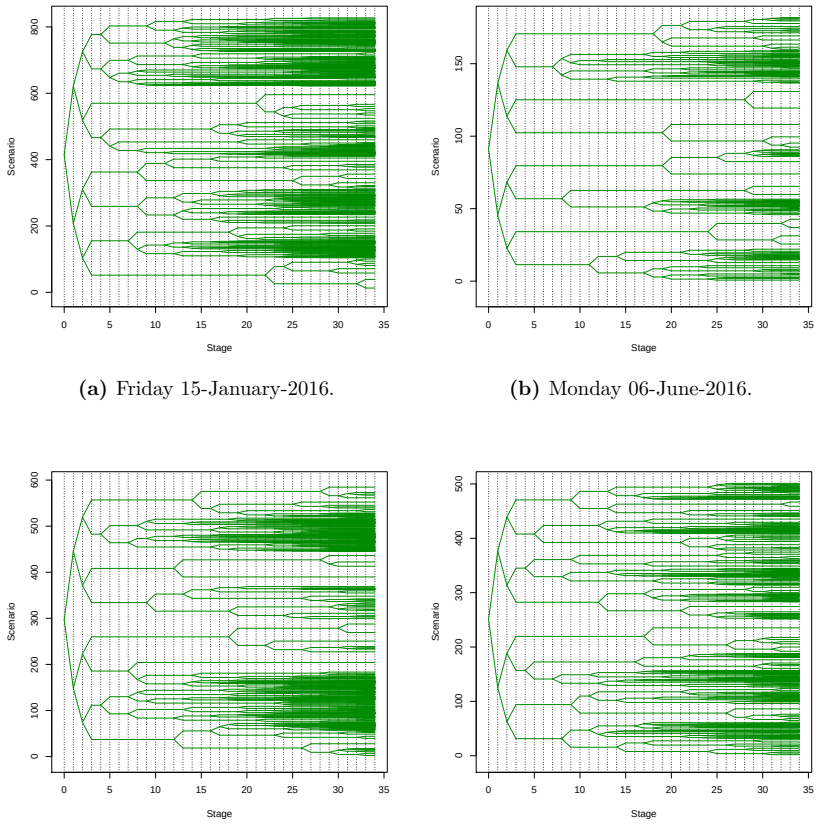

(a) Friday 15-January-2016.

(b) Monday 06-June-2016.

(c) Sunday 16-October-2016.

(d) Thursday 17-November-2016.

Figura 5.4.3: Some scenario trees obtained by the DTGFBA for the MSWBVPP model.

5.5. Comparative Analysis of the Sets of Scenario Trees Obtained

Figure 5.5.1 displays the boxplots of the elapsed time, number of scenarios and number of nodes for the 366 scenario trees obtained by the FTCA and DTGFBA. The elapsed time was obtained in ampl with built-in timing parameter *_ampl_elapsed_time*.

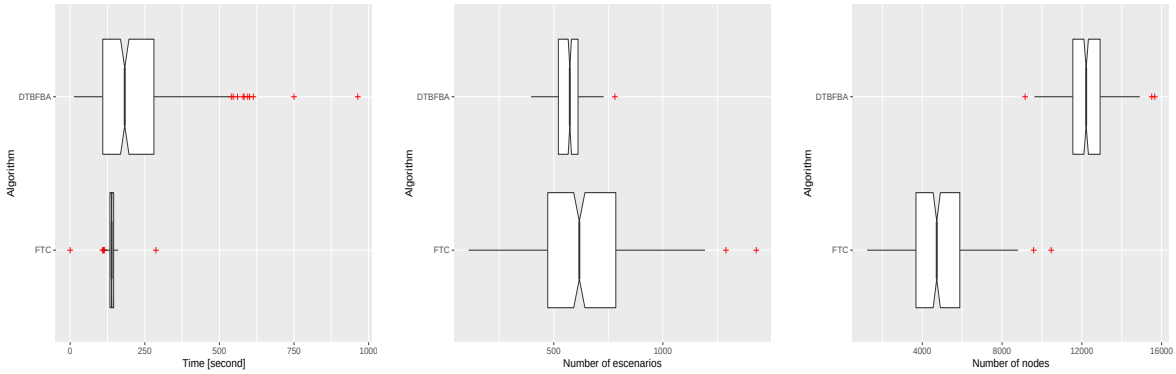

(a) Elapsed time. **(b)** Number of scenarios. **(c)** Number of nodes.

Figura 5.5.1: Execution time and number of scenarios and nodes of the total scenario trees.

Figure 5.5.1a shows that the execution time is not an issue for concern when generating scenario trees, because it is very low for both algortihms. The elapsed time not exceeding 250 seconds for both algorithms, only with some outliers data that, in the worst case, reached a little more than 250 seconds for the FTC and, at the utmost, 1000 seconds for the DTGFBA. Regarding the number of scenarios, Figure 5.5.1b displays boxplots of the number of scenarios of the trees obtained in all instances. In both algorithms, the number of scenarios was on average approximately equal (at around 500 to 650 scenarios). The initial parameters of both algorithms were fixed in a way that the average number of scenarios were about the same. However, the variability of the number of scenarios was most obvious in the DTGFBA. Finally, Figure 5.5.1c shows the comparison of the number of nodes of the set of scenario trees generated by each algorithm. In this case, the variability observed in the number of nodes for both set of trees is very clear. The number of nodes of the scenario trees generated by the FTCA is, on average, a little more than 12000 nodes. By contrast, the number of nodes of the trees obtained by the DTGFBA is less than the number of nodes of the trees obtained by the FTCA. In average, it is a little more than 4000 nodes.

5.6. Computational Results for the MSWBVPP Model with Scenario Trees

In this section, a set of computational tests have been performed in order to validate the MSWBVPP model developed in Section 4.1.3. The model was used to analyze the optimal operation of a VPP in the Iberian Electricity Market, and it consists of:

- An on-shore wind plant called *Espina*, located in the north of Spain with 9 wind turbines and a total nominal output of 18MW.

- A Li-ion-based BESS with the characteristics shown in Table 5.6.1. These characteristics are based on the systems described in Díaz-González et al. (2012); we energize the world 2019 (2019)

$d_{max} = 10$ MW	$EOL = 20 years$	$soc^0 = soc^t = 0{,}6$	$soc^{min} = 0{,}3$
$e_{max} = 30$ MW	$cyc^{max} = 6000$	$soc^{max} = 0{,}9$	$\gamma^{RTE} = 0{,}8$

Cuadro 5.6.1: BESS parameters.

5.6.1. Case Studies

Three different case studies were solved in order to analyze the impact of the BESS and the participation in the RM:

- **Case study 1 (WDI)**: a standalone Wind Power Plant (WPP) bidding to the DM and IM.
- **Case study 2 (VDI)**: a VPP (that is, a WPP plus a BESS) participating in the DM and IM but not allowed to participate in the RM.
- **Case study 3 (VDIR)**: a VPP participating in the DM, IM and RM.

The optimal solution of the three case studies can be visualized with the help of several graphical representations:

(a) The mean WPP generation scenarios, the optimal value of the DM, IM and RM quantity bid: $p_{t\omega}^{D^*}, p_{it\omega}^{IT^*}, r_{t\omega}^{U^*}, r_{t\omega}^{D^*}$

(b) The optimal value of imbalances: $p_{t\omega}^{IB^{+*}}, p_{t\omega}^{IB^{-*}}$

(c) The optimal value of the battery charge and discharge: $c_{t\omega}^*, d_{t\omega}^*$

(d) The optimal value of the state of charge (SOC): $soc_{t\omega}^*$.

The complete set of graphs (a)–(d) for the scenarios shown in Tables 5.4.2 and 5.4.3 were included in Section D.2 of Appendix D. Although a detailed analysis of the optimal solution of the MSWBVPP model is beyond the objectives of this thesis, it is worth commenting on the graphs in order to have a general understanding of the results. As an example, let us briefly analyze the results for the three test cases corresponding to Thursday, 17 November 2016, specifically regarding both the FTCA and DTGFBA scenario trees. Algorithmic options for CPLEX were a relative MILP gap of 0.5 % (mipgap=0.005) and 9 threads (threads=9). Regarding the formulation options for AMPL, a value of presolve_eps=1.0e-07 was set to avoid some numerical infeasibilities.

5.6.1.1. Case Study 1 (WDI): WPP Bidding to the DM and IM.

In this first test case, the WPP operates alone without BESS backup. Of course, graphs (c) and (d) are void due to the absence of the BESS. The results for Thursday, 17 November 2016 are depicted in Figures 5.6.1 and 5.6.2.

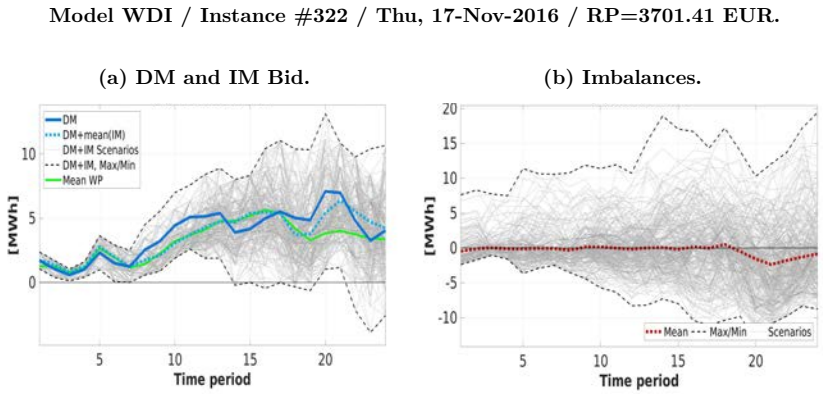

Figura 5.6.1: Results for the WDI case with scenario tree obtained by the FTCA.

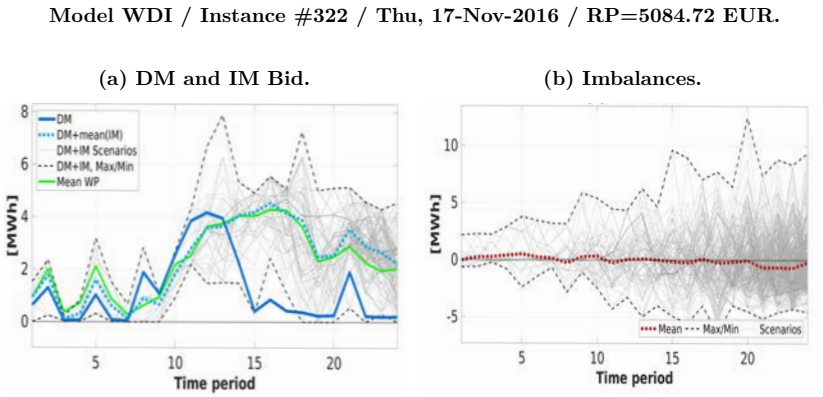

Figura 5.6.2: Results for the WDI case with scenario tree obtained by the DTGFBA.

Figures 5.6.1 and 5.6.2 show the value of the recourse variables corresponding to each scenario (thin continuous lines), their mean value (thick coloured dashed lines) and the maximum and minimum values at each time period (thin dashed lines). Figures 5.6.1a and 5.6.2a show the optimal bid to the DM and IM for every scenario, $p_t^{D^*} + p_{it\omega}^{IT^*}$. In these same graphs, the continuous dark blue thick line is the bid to the DM alone ($p_t^{D^*}$, the first-stage variable) while the pale blue thick dashed line is the bid to the DM plus the average bid to the IM (that is, $p_t^{D^*} + \overline{p}_{it}^{IT^*}$). We can observe some big differences between the two lines representing $p_t^{D^*}$ and $p_t^{D^*} + \overline{p}_{it}^{IT^*}$, specifically for the DTGFBA tree. It also merits mentioning the big discrepancies among the optimal bids

and expected profits (value of Recourse Problem (RP)) when comparing the two FTCA and DTGFBA scenario trees.

5.6.1.2. Case Study 2 (VDI): VPP Bidding to DM and IM.

In this second test case, the BESS is allowed to operate in coordination with the WPP, but the resulting VPP can only submit bids to the DM and IM; that is, bids to the RM are forbidden. Figures 5.6.3 and 5.6.4 show the optimal solution for this test case. The most important difference with respect to the previous case study is, of course, the BESS activity and how it affects the optimal bid to the DM and IM (see Figures 5.6.3c and 5.6.4c):

- In the FTCA solution, the operation of the BESS consists of a deep charging period at around $t = 5$ and two other charging periods: a very shallow first one at around $t = 10$ and a very deep second one at $t = 20$.
- In the DTGFBA solution, charges and discharges are always shallower than in the FTCA case, with two charging periods at around $t = 5$ and $t = 17$ and two discharging periods at around $t = 10$ and $t = 20$.

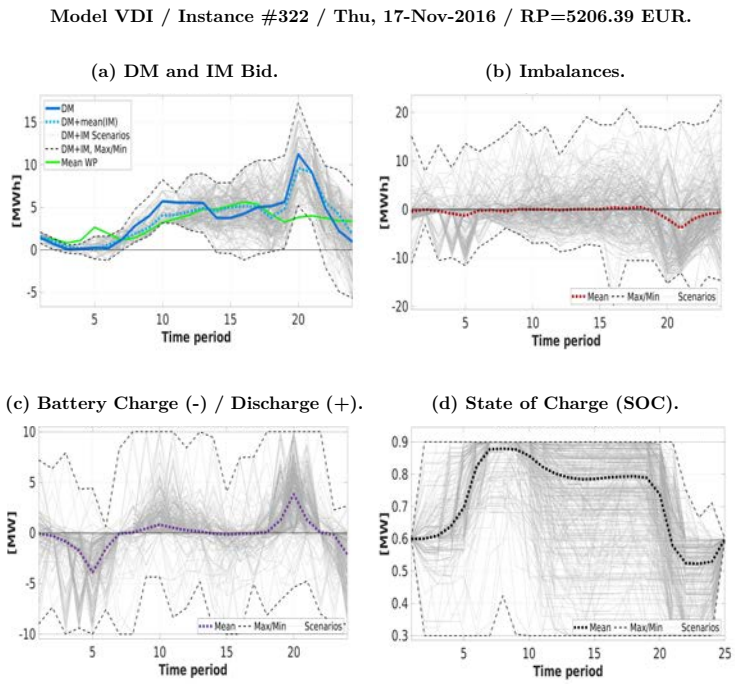

Figura 5.6.3: Results for the VDI case with scenario tree obtained by the FTCA.

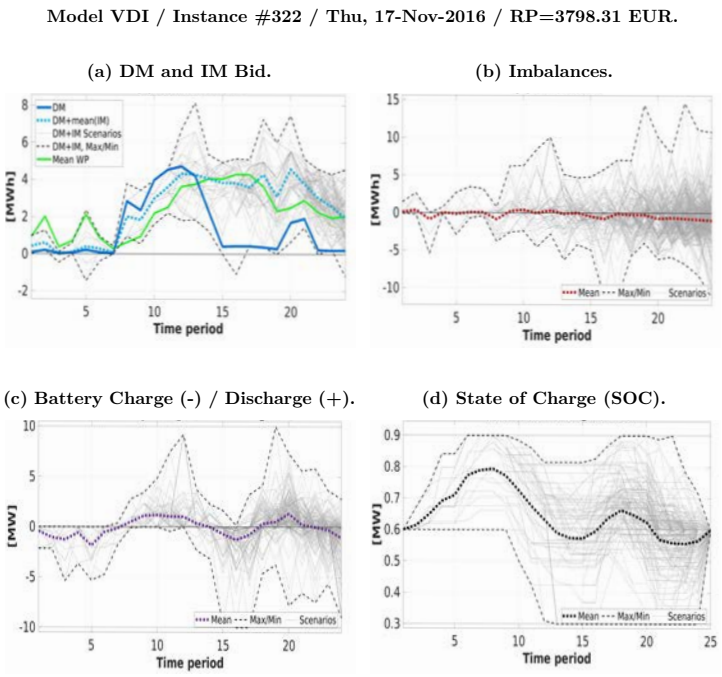

Figura 5.6.4: Results for the VDI case with scenario tree obtained by the DTGFBA.

The SOC of the BESS (Figures 5.6.3d and 5.6.4d) varies according to the charges/discharges. Again, we can observe the great difference between the solution of the FTCA and DTGFBA, not only in terms of both the optimal bids and BESS operation, but also with respect to the expected net profits RP, which are 37 % greater with the FTCA than with DTGFBA. It should be pointed out that this result does not mean the actual profits using the FTCA are 37 % higher than when using DTGFBA (as we will see later on), because those net benefits depend on the tree itself, which is therefore an unfair value to compare. In contrast to what is usually assumed in the literature, the availability of a BESS does not necessary imply a drastic reduction in the imbalances (see Figure 5.6.3d for the FTCA and Figure 5.6.4b for the DTGFBA). In fact, that result is not surprising at all, for two reasons. First, IM is a highly efficient balancing tool for reducing the mismatch between forecasted and actual WP generation. Second, the proposed model does not try to explicitly reduce imbalances, as these imbalances are evaluated only in terms of the its economic value/penalization. In other words, the imbalance prices are only relatively important when compared to both DM/IM prices and the value of the stored energy; therefore, from a merely economic point of view, it would sometimes be worth incurring some imbalances.

5.6.1.3. Case Study 3 (VDIR): A VPP Participating in DM, IM and RM.

In this last case study, we analyze the results when the VPP is allowed to participate in the RM. One of the most interesting consequences of incorporating the RM into the

model is that the different decision variables are distributed more narrowly than in the WDI and VDI test cases. This is a general trend, but it can be very clearly observed in that VPP–RM example when looking at the BESS operation obtained through the DTGFBA tree, as well as through in Figures 5.6.4c, 5.6.4d, 5.6.6c and 5.6.6d. In particular, the graphed charges/discharges in Figure 5.6.6c for the DTGFBA tree are the same for every scenario from $t = 1$ to $t = 12$. Consequently, so are the SOC (graph in Figure 5.6.6d). The reduction in the dispersion of the value of the decision variables is a result of the RM having paramount importance relative to the spot markets, DM and IM. This is explained bellow.

Again, the purpose of attaching a BESS to a WPP is not so that the DM+IM bid can better track the actual WP generation but, rather, to maximize the net profit of the VPP operation (see, for instance, the graph in Figure 5.6.6d). There is a great discrepancy between the expected total DM+IM bid at 10:00 (dotted pale blue thick line) and the expected WP generation (solid thick green line) at $t = 10$. This is because of the BESS's deep discharge during that period, which allows the maximum possible profits from the RM prices throughout the whole day.

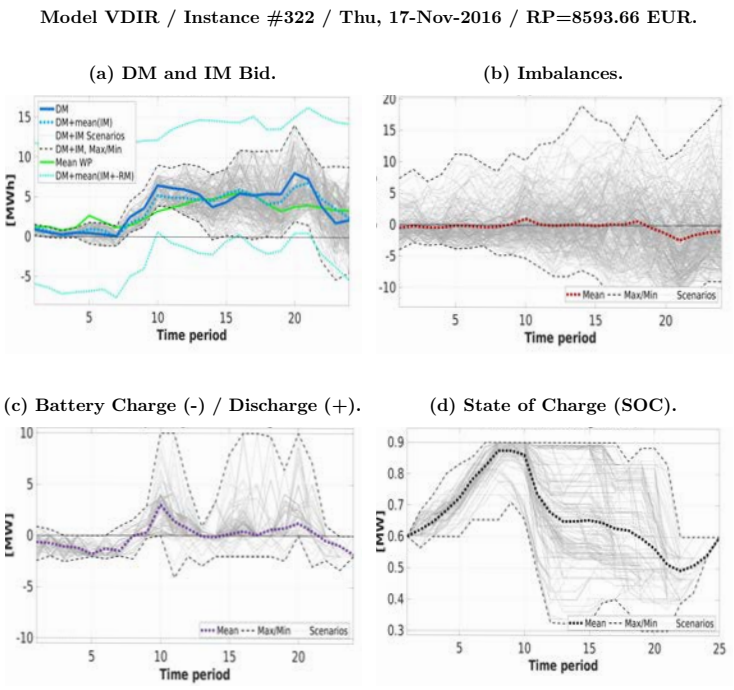

Figura 5.6.5: Results for the VDI case with scenario tree obtained by the FTCA.

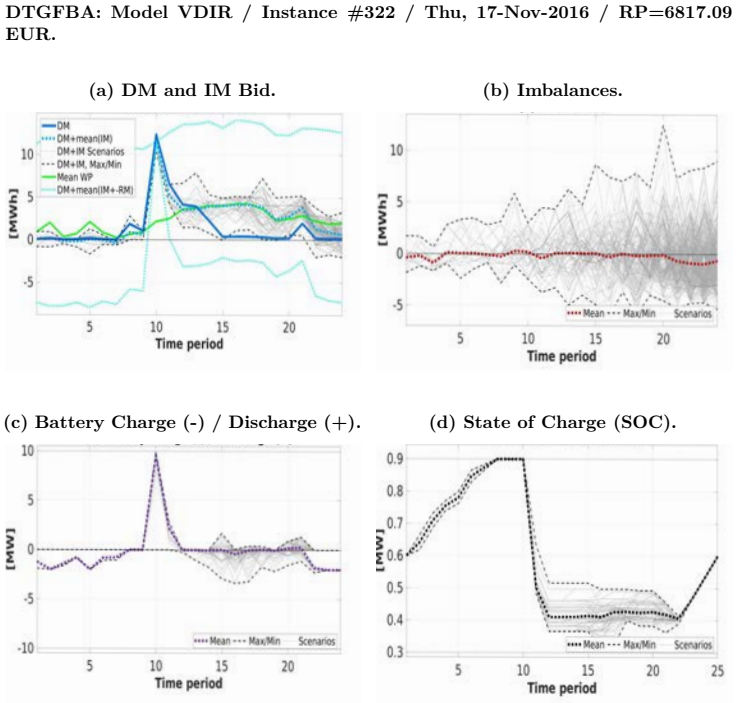

Figura 5.6.6: Results for the VDI case with scenario tree obtained by the DTGFBA.

The last great difference between the VDIR test case and the previous ones: the huge increase in the expected net profit RP. While the increase in the RP between the WDI and VDI test cases is less than 3 %, the RP for the VDIR is greater than in the VDI test case by 65 % (FTCA) and 79 % (DTGFBA). This is a well known result that has been reported in several previous studies (see, for instance, Heredia et al. (2015, 2018)). Regarding the reason for this increase in the value of RP when the VPP is allowed to bid to the RM, a detailed analysis can be found in Heredia et al. (2018). However, to state it plainly: while the DM remunerates the VPP proportionally for real-time WPP generation, the RM proportionally pays for the VPP's reserve band, $r^{U^*}_{t\omega} + r^{D^*}_{t\omega}$, which is much greater than the average WPP generation. Despite the fact that the mean prices of the DM are usually greater than the mean RM price, the final result is that the incomes from the RM are much higher than those from the DM.

5.7. Study of the Performance of Scenario Trees

The analysis conducted in the previous sections revealed two problems in regard to assessing the comparative performance of the two sets of scenario trees obtained through the scenario tree generation methodology:

- First, the results (optimal bids, net profit RP, and others) depend strongly on the calendar date of the instance being optimized. As an example, when we look at

the RP for the FTCA trees of the four dates considered in the VDIR test case (see the following section), it ranges from €8,329.49 to €16,034.59 (92 % variation), and the Value of the Stochastic Solution (VSS) goes from 0.89 % to 3.45 % of the RP value. Thus, we cannot justifiably arrive at any significant conclusions from analyzing just one or a reduced number of instances of the MSWBVPP model.

- Second, the previous section has shown that, in order to compare the relative performance of the two FTCA and DTGFBA methodologies implemented in this thesis, we must be very careful to select a set of key indicators that does not depend on the tree itself. The classical key indicators for assessing the value of the stochastic solution is usually the RP (that is, the optimal value of the objective function of the MSWBVPP model); the Expected Value of Perfect Information (EVPI); and VSS. The issue here is that all these three indicators depend on the tree, and they therefore do not allow for a proper comparison between the FTCA and DTGFBA.

In order to overcome these two concerns, we propose performing an ex ante analysis based on the solution of 366 models (one model for each day of 2016) of the day D with information about the day $D-1$, through the following methodology:

i. To cope with the issue of the results depending strongly on the specific calendar date, we propose performing a statistical analysis of the results for a full one-year period using the same VPP as in the previous section. To this end, the MSWBVPP model was solved for the three case studies (WDI, VDI and VDIR) and for the two scenario trees (FTCA and DTGFBA), covering the complete one-year period from 1 January to 31 December 2016, thus making a total of 2196 instances. We have called this dataset 2016_MSWBVPP.

ii. To analyze the quality of the solution independently of the tree distribution, we proposed using – in addition to the usual variables RP and VSS – a modification of the classical VSS (which we denote hereafter as EVVS in order make the notation uniform), called Forecasted Value of the Stochastic Solution (FVSS). This indicator is calculated using the forecasted values of the random variables that were used to generate the two kinds of scenario trees. The FVSS are identical for the two trees under comparison. This is an alternative to using the same expected random variables calculated with the probability distribution of the tree, which, needless to say, depends on the tree itself.

iii. Finally, to determine if the value of variables of the RP, Expected Value of the Stochastic Solution (EVSS) and FVSS have significant statistical differences between the different test cases (WDI, VDI and VDIR) and tree scenarios (FTCA

and DTGFBA), we are going to compare the distributions of these variables in the 2016_MSWBVPP dataset, both informally and formally:

- Informally, we compare the notched boxes in the boxplot representation, assuming that, if the notches of two boxes do not overlap, there is 'strong evidence' (95 % confidence) that their medians differ (Chambers et al., 1983).
- Formally, we calculate the $p-$value of the null hypothesis of equal median values, specifically by using the Wilcoxon signed-rank test (p_{WSR}) (Gibbons and Chakraborti, 2014)

5.7.1. 2016_MSWBVPP Data Set

Figure 5.7.1 shows the distribution (boxplots, minimum, average and maximum values) of the size and RP (or expected net profits) for the 2196 instances of the 2016_MSWBVPP. The first row is for the FTCA and the second row is for the DTGFBA. The data displayed in this figure are:

- nS: number of scenarios.
- nv: total number of variables (continuous and binary), after the presolve phase of AMPL.
- nb: number of binary variables, after the presolve phase of AMPL.
- nc: total number of constraints, after the presolve phase of AMPL.
- $etime$: elapsed time, in seconds (command solve_elapsed_time of AMPL). All the runs were performed keeping the workload of the workstations low enough to avoid conflict between the different processes so the elapsed time is a fair approximation of the actual execution time.
- RP: value of RP (in euros).

Figure 5.7.1 shows that the larger number of DTGFBA scenario trees of course leads to larger greater problems (larger nv, nb and nc) and execution times ($etime$). Nevertheless, execution time is not a concern in these kinds of problems, as it is always below ten minutes even for the largest instance ($nv = 492,970$, $nb = 34,320$, $nc = 1,035,982$), which is completely reasonable for a day-ahead optimization problem. Figure 5.7.1 also shows that the optimal value of the objective function (which is the RP) is consistently greater for the FTCA trees than for the DTGFBA trees. We analyse that relationship in detail later in this section. However, as pointed out before, RP does not give a fair comparison between the FTCA and DTGFBA, because the RP value is a calculated expectation with respect to the two different trees, and it would

only be comparable if the two trees were absolutely identical, which is not the case even though they were generated from the same forecasting model. In fact, in order to fairly compare the performance of the two families of trees, we are going to introduce in the next section the idea of FVSS, which is based on the exogenous forecasting of the random variables of the MSWBVPP model. This is a variation of the classical EVSS, based on endogenous expectations.

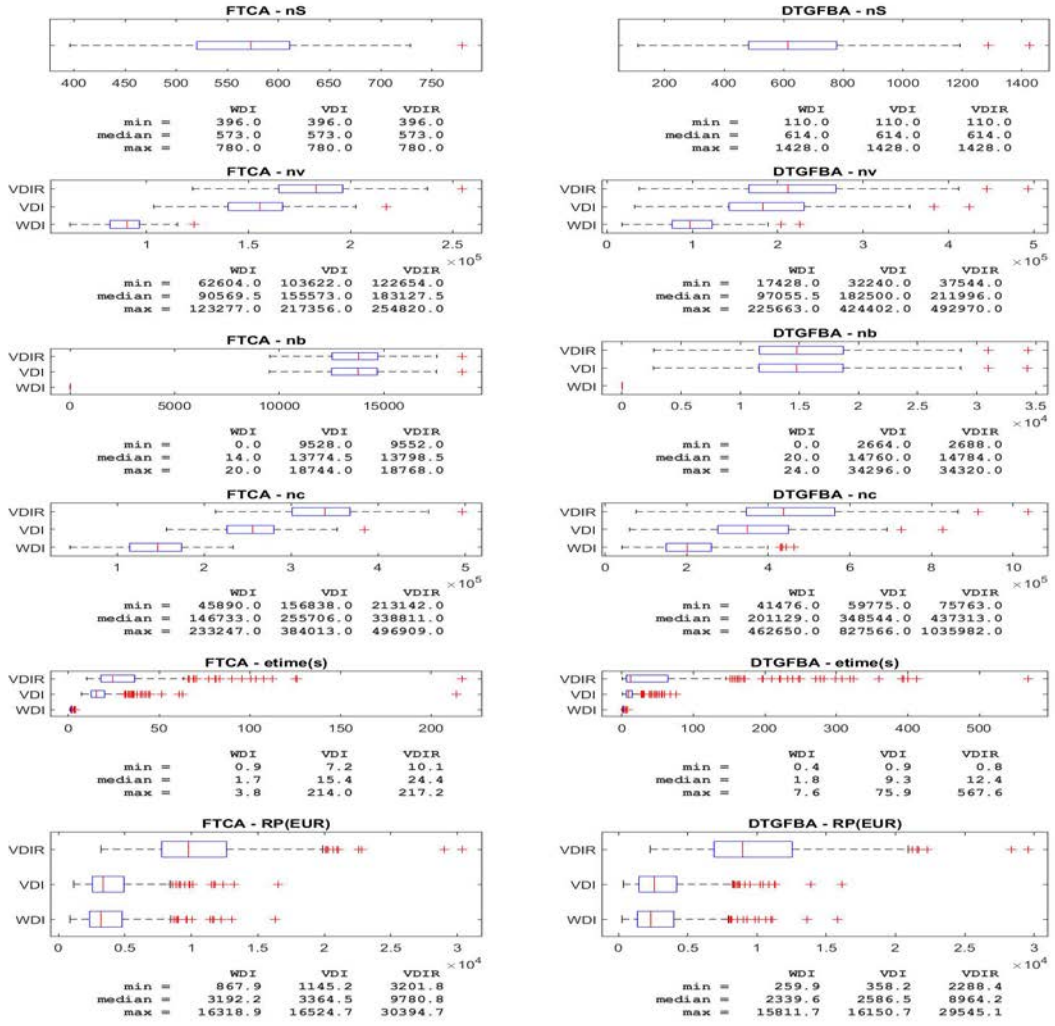

Figura 5.7.1: Size, execution time and optimal value of the objective function (RP).

5.7.2. Forecasted Value of the Stochastic Solution (FVSS)

To assess the quality of the stochastic solution for the 2016_MSWBVPP dataset, we use the procedure to find the VSS for multistage problems proposed in Escudero et al. (2007). The key idea in this approach is to split all the decision variables into two sets. The first one is the so-called state variables, which play the role of the first-stage variables in two-stage SP problems. The second is so-called recourse variables,

which are analogous to the second-stage variables in two-stage stochastic programming problems. Actually, this variable's separation was already introduced in Section 5.7.1, where the vector of decision variables was split into two parts: $x' = (y', z')$, with $y' = (p^{D'}, r^{D'}, r^{U'}, p_i^{I'}, c', d')$ being the vector of state variables; and $z' = p^{IB'}$, which is the vector of the recourse variables (see Table 4.1.3). The procedure for calculating the FVSS is:

1. The solution $\hat{x} = (\hat{y}, \hat{z})'$ is found for the deterministic MSWBVPP model associated with to the forecasted value of the random parameters $\hat{\xi}_{N+1}$ (see Equation (5.3.6)). That is, we solve an instance of the MSWBVPP model with a scenario tree consisting of a single scenario $\hat{\xi}_1 = \hat{\xi}_{N+1}, \Omega = \{1\}$. Let the value of the optimal solution (called FV) of the MSWBVPP model for the solution $\hat{x}$.

2. Let Expectation of the Forecasted Value (EFV) be the optimal value of the objective function of the MSWBVPP model, with $y := \hat{y}$, and solving for the recourse variables $\hat{z}$ (Equation (4.1.19)) to enforce feasibility.

3. Finally, the forecasted value of the stochastic solution is defined as (Equation (3.4.9))

$$FVSS = RP - EFV. \tag{5.7.1}$$

The meaning of the FVSS is analogous to the meaning of the EVSS: it is the improvement of the objective function (expected net profit) that is achieved by MSWBVPP model in comparison to the deterministic solution with $\hat{\xi}_{N+1}$. To facilitate the analysis, we are going to forego using the value of the FVSS and instead use the relative FVSS referred to as VFSSr, which is defined as (Equation (3.4.10)):

$$\text{FVSSr} = 100 \times \frac{FVSS}{EFV}. \tag{5.7.2}$$

5.7.3. The Value of the Stochastic Solution's Dependency on the Test Cases WDI, VDI and VDIR

Figure 5.7.2 shows the distribution of the values of RP, EVSSr and FVSSr for the 2016_MSWBVPP dataset. Observing the boxplots, it is quite clear that the distributions of the indicators RP, $EVSSr$ and $FVSSr$ do not follow a normal distribution, as they are strongly skewed to the right. Every graph is accompanied with a table displaying some descriptive statistics (minimum and maximum value, mean and median) and the p-value for the Wilcoxon signed-rank test p_{WSR} for every set of paired data: WDI–VDI,

WDI–VDIR, VDI–VDIR. Due to the existence of extreme outliers, which are especially strong for the FVSSr value, outliers to the right of the vertical dashed lines were compressed for the sake of clarity. We observe in Figure 5.7.2 that the value of p_{WSR} is virtually zero for every set of paired data, showing that the null hypothesis of equal median values can be rejected in all instances, even for the value of RP in the test cases WDI and VDI, where notches overlap. Therefore, the graphical comparison is not conclusive.

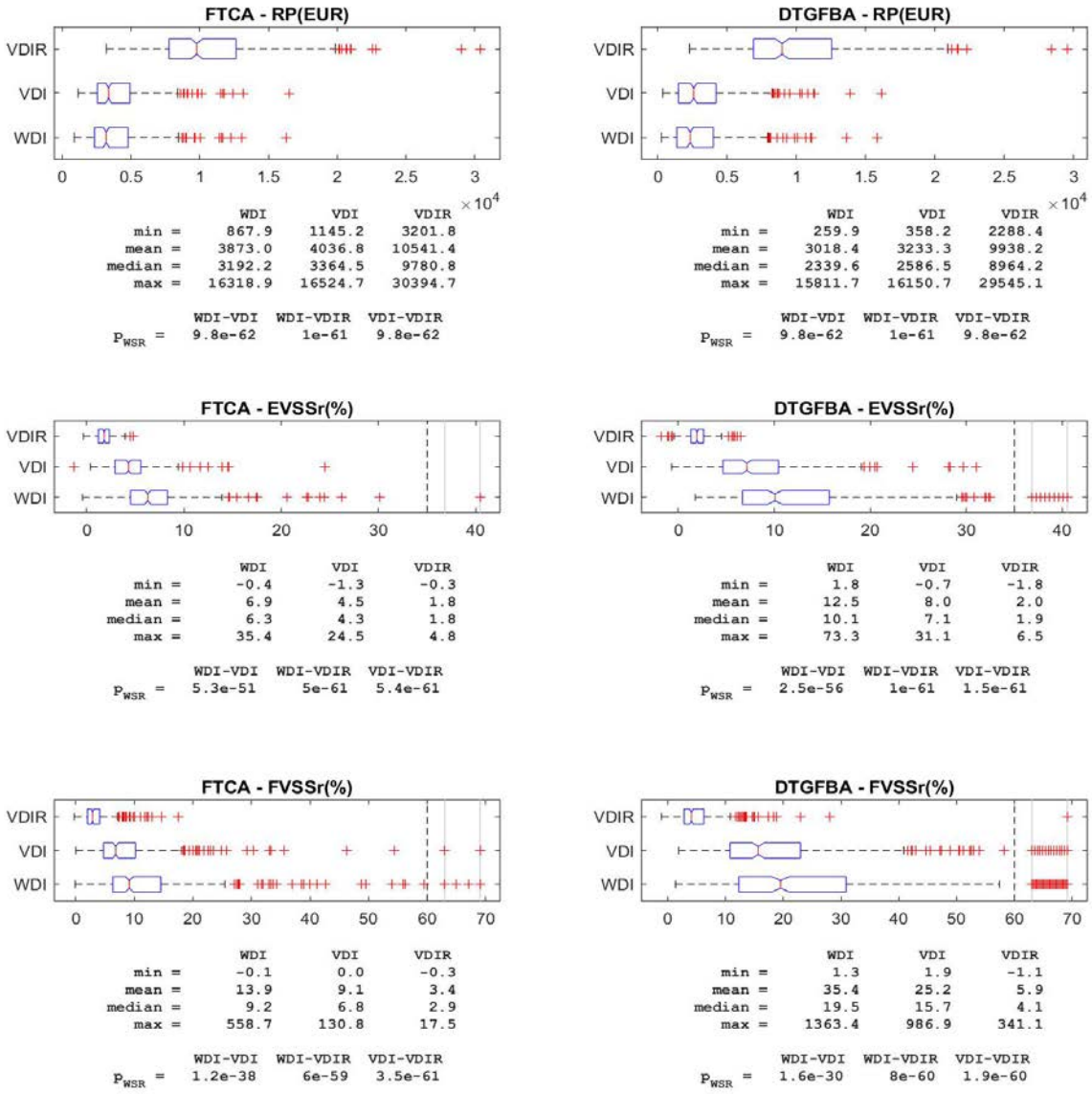

Figura 5.7.2: Dependency of the RP, EVSSr and FVSSr on the WDI, VDI and VDIR test cases.

Figure 5.7.2 allows us to state some conclusions about the numerical study, which are valid for both the FTCA and DTGFBA instances:

- *Although statistically different, the value of RP is quite similar for the WDI and VDI instances.* It is much greater for the VDIR instances than for the WDI and VDI instances. The reason for that was explained in the previous section.
- *The value of the stochastic solution (both $EVSSr$ and $FVSSr$) consistently decreases for the WDI, VDI and VDIR cases.* The explanation for that trend is that, on the one hand, incorporating the BESS into the VDI test case allows mitigating the intrinsic randomness of wind generation in the WDI test case. This consequently reduces the importance of stochasticity. On the other hand, the incomes from the RM are of paramount importance in comparison with the DM, IM and IB, and this induces an optimal solution for both the stochastic and deterministic problems that are close to the BESS operation, which in turn maximizes the RM returns.
- *The value of $FVSSr$ is consistently greater that the value of $EVSSr$* (this is supported again by the Wilcoxon SR test). Likewise, *outliers are far more severe in FVSSr than in EVSSr.* Outliers in $FVSSr$ can be as high as 1363.4 % (the WDI case, Wednesday, 6 April 2016), at more than 70 times the interquartile distance from the 3rd quartile. It is worth mentioning that this extreme value of $FVSSr$ does not reveal any flaw in the calculation of this quantity: the value of the EFV for this outlier is very small (actually negative) at EFV=€-46.10, meaning that the deterministic solution based on the forecasted values is very bad (actually, incurring losses). Furthermore, the value of the expected profits for the stochastic program is RP=€582.9, and therefore the relative Forecasted Value of the Stochastic Solution (FVSS) is:

$$FVSSr = 100 \times \frac{RP - EFV}{|EFV|} = 100 \times \frac{629}{46{,}1} = 1363{,}4\,\% \tag{5.7.3}$$

5.7.4. Comparative Performance of the FTCA and DTGFBA Scenarios Trees

In this section, we would like to compare the performance of the two FTCA and DTGFBA families of trees in terms of the values they provide for RP, namely $EVSSr$ and $FVSSr$. We would also like to pay special attention to key indicator $FVSSr$, thus following the same methodology as in the previous section.

Figure 5.7.3 shows the comparison of the results from the FTCA and DTGFBA trees with respect to the value of RP, specifically for the three test cases of WDI, VDI and VDIR. We see that, in all cases, the median is greater for the FTCA trees than for the DTGFBA trees (36 %, 30 % and 9 %, respectively, for WDI, VDI and VDIR). Indeed, not only is RP better, so is every indicator: min, max, quartiles and mean.

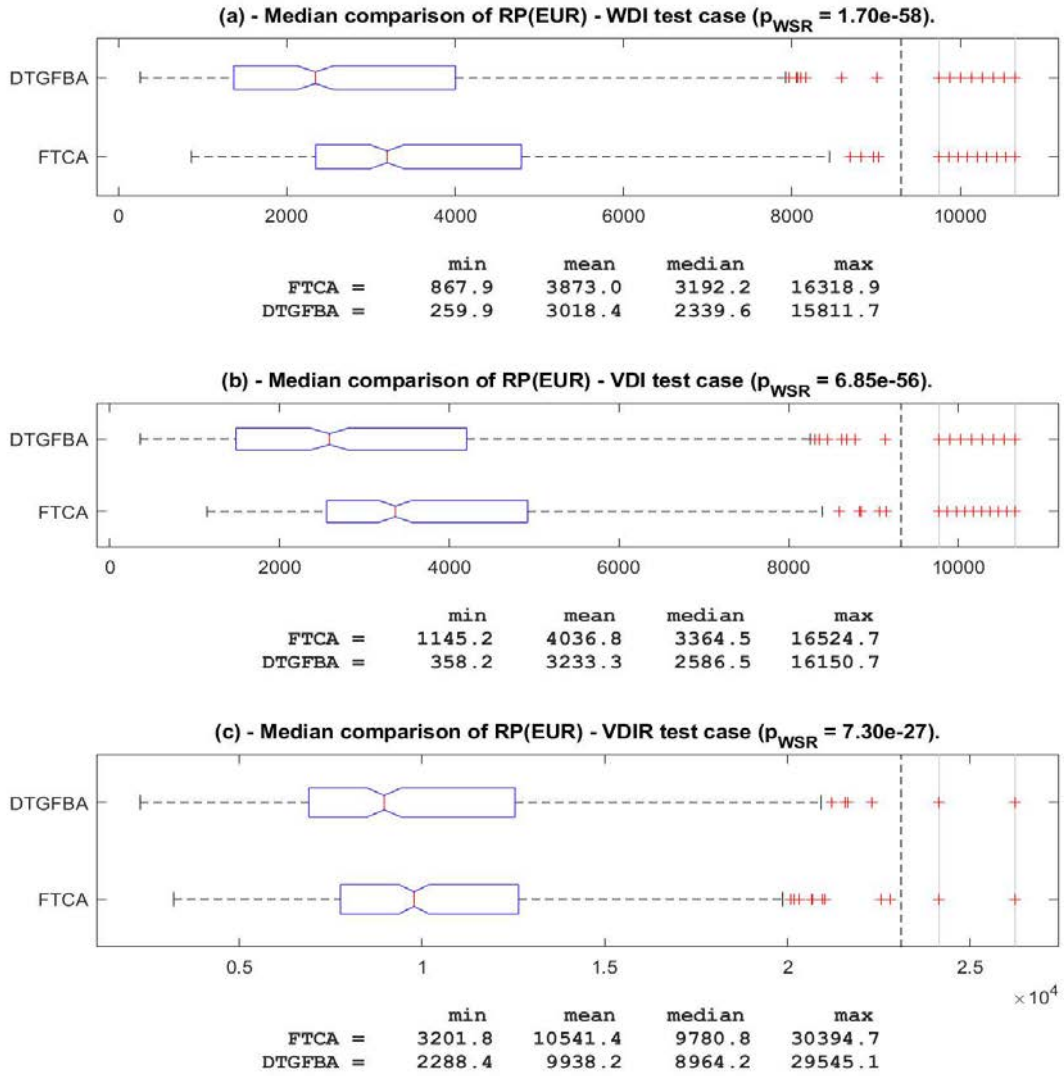

Figura 5.7.3: Comparison of the RP medians in the FTCA and DTGFBA trees.

Figure 5.7.4 displays the same results for the variable $EVSSr$, that is, the value of the stochastic solution compared to the deterministic solution. This variable is associated with the mean $\tilde{\xi}^{FTCA}$ and $\tilde{\xi}^{DTGFBA}$ of the FTCA and DTGFBA scenario trees, respectively, and with $\tilde{\xi}^{FTCA} \neq \tilde{\xi}^{DTGFBA}$ A in general. Therefore, the value of $EVSSr$ completely depends on the structure of every scenario, which compromises its suitability for a fair comparison. Contrary to what happened with the variable RP, in this case, it is the DTGFBA tree family that outperforms almost every indicator (min, max, mean, median and quartiles). Regarding the median comparison, it is 60 %, 65 % and 5 % greater for, respectively, the WDI, VDI and VDIR test cases. It is worth mentioning that the graphical test does not allow rejecting the null hypothesis of equal median for the VDIR test case, as the notches overlaps; however, it does the value of $p_{WSR} = 0{,}000123$.

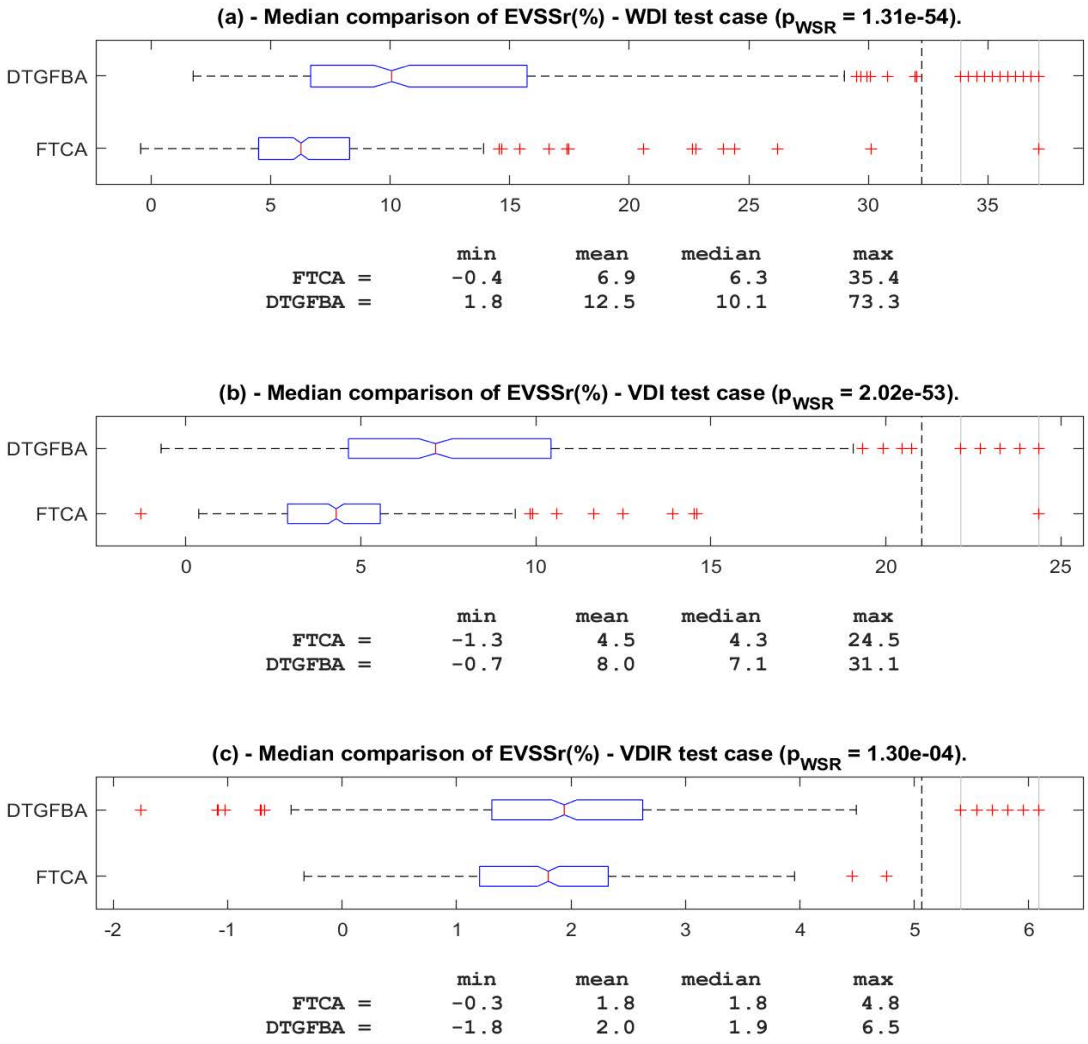

Figura 5.7.4: Comparison of the EVSSr medians in the FTCA and DTGFBA trees.

Finally, Figure 5.7.5 displays the results from comparing the variables $FVSSr$ in the FTCA and DTGFBA tree families. Remember that this variable is the one that provides the most reliable results, as it uses the deterministic solution associated with the forecasted values of the random variables $\hat{\xi}$, which is the same for the two FTCA and DTGFBA families. Therefore, although the calculation of $FVSSr$ still depends partially on the tree itself, it allows for a fairer comparison than the variable $EVSSr$. The results in Figure 5.7.5 confirm and strengthen the conclusions of the $EVSSr$ analysis: the value of the stochastic solution provided by the DTGFBA scenario trees unambiguously outperforms the one provided by the FTCA scenario trees. Every single indicator (except the minimum value for the VDIR test case) is better, and the medians for the DTGFBA scenario trees are 120 %, 130 % and 41 % higher for, respectively, the WDI, VDI and VDIR test cases.

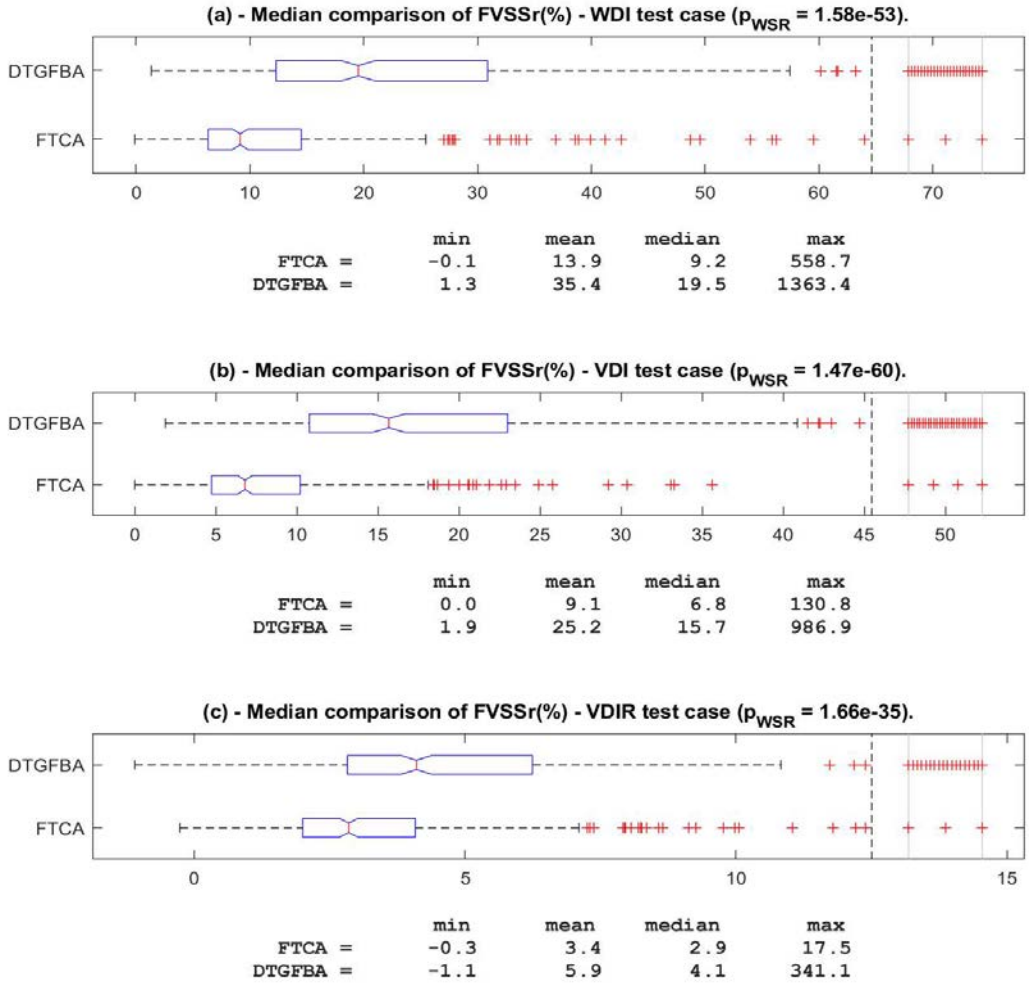

Figura 5.7.5: Comparison of the FVSSr medians in the FTCA and DTGFBA trees.

Table 5.7.1 summarizes the results of our study on the relative performance of the FTCA and DTGFBA scenario trees. Based on these results, we can conclude that the DTGFBA scenario trees provide the best stochastic solutions, as they generally improve the value of the deterministic solution obtained with the forecasted values of the random variables (the mean value of $FVSSr$, see Figure 5.7.5) by 35.4 % in the WDI instances, by 25.2 % for VDI and by 5.9 % in the VDIR instances.

$\frac{DTGFBA-FTCA}{FTCA}$	WDI	VDI	VDIR
RP	36 %	30 %	9 %
EVSSr	60 %	65 %	5 %
FVSSr	120 %	130 %	40 %

Cuadro 5.7.1: Relative performance between the FTCA and DTGFBA trees.

It is not the result of scientific research that ennobles humans and enriches their nature, but the struggle to understand while performing creative and open-minded intellectual work.

— Albert Einstein

6

Numerical Experience with Scenario Trees for the MSOODN Model

Contents

The main purpose of this chapter is to apply the scenario tree generation methodology developed in this thesis to another real-world problem in the energy environment. In this case, we apply it to a problem in Electrical Distribution Systems (EDN) suggested by the Faculty of Electrical and Computer Engineering (FEEC) at the University of Campinas (UNICAMP), which was part of a pre-doctoral stay developed in this university. The proposed problem is linked to the Optimal Operation of Distribution Networks (OODN) and using the MSP to consider the uncertainty that governs this problem. The aim is to establish scenario trees and obtain the final results that explain and optimize the situation that is being modeled. This chapter is organized as follows. First, Section 6.1 describes the test system used for obtaining scenario trees for the Multistage Stochastic Optimal Operation of Distribution Networks (MSOODN) model.

Second, Section 6.2 presents the development of the first phase of the methodology that obtains the scenario sets used to generate the scenario trees. Third, Section 6.3 shows the scenario trees obtained with the algorithms and, finally, Section 6.4 gives the results for the MSOODN model with the scenario trees obtained.

6.1. 11-node Test System

In order to validate the proposed MSP model, an 11-node test system by Levron and Shmilovitz (2012) was used to generate scenario trees. Figure 6.1.1 shows the test system with 11 nodes containing two photovoltaic RS with power peaks of 1 MW and 0.5 MW at nodes 8 and 5, respectively; two BESS at nodes 4 and 11 with capacities for 0.4 MWh each and a self-discharge rate of $\beta_i^{sd} = 0{,}021$; a CB of 0.3 MVAr at node 2; and five loads. Additionally, for each load, level the duration is $\Delta_t = 0{,}5$ h, and the minimum/maximum voltage magnitude is $\underline{V} = 0{,}95$ pu and $\overline{V} = 1{,}05$ pu, respectively. The objective was to minimize the cost of energy purchase from node 1, where the costs are deterministic parameters. Impedances are in percentages of the basis (power and voltage magnitude) and equal to the transformer's nominal ratings. It was also assumed that both ESDs had the same value of efficiency: $\eta_i^{ch} = \eta_i^{dis} = 0{,}95$. The maximum daily change in the operation of the ESDs was equal to 2.

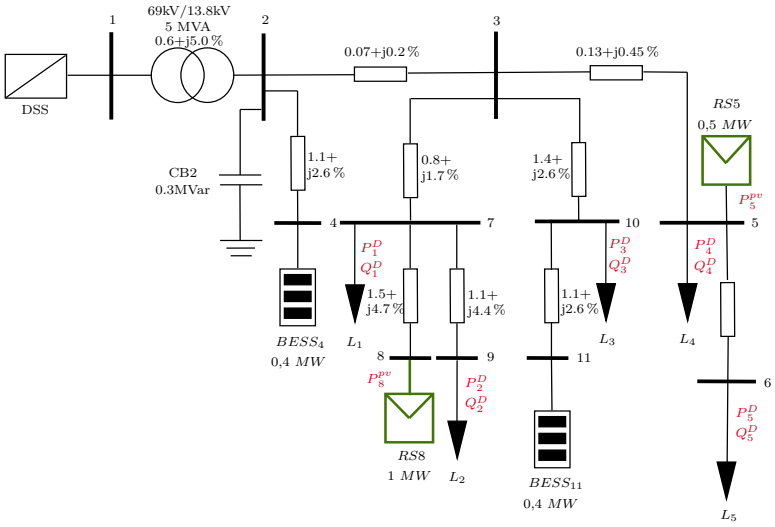

Figura 6.1.1: 11-node test system of Levron et al.

Uncertainty is represented by the active/reactive power loads $P_1^D, Q_1^D, \ldots, P_5^D, Q_5^D$ and active power of the photovoltaics p_5^{pv}, p_8^{pv} (red parameters in Figure 6.1.1). The goal is to represent this uncertainty correctly. In this case, we applied the two phases of the scenario tree procedure developed in this thesis to obtain scenario trees in order to approximate the stochastic process associated with the MSOODN model.

6.2. Phase I: Scenario Generation

As discussed above, the uncertainty in the optimal operation problem of radial EDN is present in: the active and reactive power loads; and the active power of the PV source. On the other hand, one of the aims of this study is to obtain the scenario sets from real data using the developed techniques. Based on these considerations, this section shows the development of the first phase of the methodology of this thesis, which results in obtaining the scenario sets needed to build scenario trees for the MSOODN model. This section is organized as follows. Section 6.2.1 presents the characterization of the MTS for this problem. Sections 6.2.2 and 6.2.3 show, respectively, the defined statistical and forecasting models for obtaining the final forecasts, and Section 6.2.4 gives the scenario sets, which are the final results of this section.

6.2.1. MTS Characterization

The data for the active power load (in MWh) was provided by FEEC–UNICAMP and is based on 110 distribution transformers located in São Paulo. Each MTS for an active power load has $M = 24$ random variables (corresponding to 24 hours a day) covering 8 April to 16 August 2016. In view of the discontinuity of the data in the time period mentioned above, we had to find a period of time where measurements are available for 5 transformers. This period was from 21 April to 26 May 2016. Regarding the reactive power loads, historical data was not available; therefore, this data was calculated based on the active power load. On the other hand, these loads do not have acceptable values to use in the node test system of Levron. For this reason, we had to standardize this data to obtain comparable values. This consideration was calculated as follows:

$$\mathbf{P}^D_{it\omega} = \frac{P^D_{levron,it}}{E[\mathbf{P}^D_{orig,it\omega}]} \cdot \mathbf{P}^D_{orig,it\omega}, \text{ and } \mathbf{Q}^D_{it\omega} = \frac{\mathbf{Q}^D_{levron,it}}{E[\mathbf{Q}^D_{levron,it\omega}]} \cdot \mathbf{Q}^D_{calc,it\omega}$$

where $P^D_{levron,it}, Q^D_{levron,it}$ are the active and reactive power load values of Levron, respectively; $\mathbf{P}^D_{orig,it\omega}$ is the original MTS of the active power load; and $\mathbf{Q}^D_{calc,it\omega}$ is the reactive power load, which is calculated as follows:

$$\mathbf{Q}^D_{orig,it\omega} = \mathbf{P}^D_{orig,it\omega} \cdot \sqrt{\frac{1}{fp^2} - 1}, \quad fp = cos\left(tan^{-1}\left(\frac{Q^D_{levron,it}}{P^D_{levron,it}}\right)\right).$$

Figures 6.2.1 and 6.2.2 display the MTS of, respectively, the $\mathbf{P}^D_i, \mathbf{Q}^D_i, i = 1, \ldots, 5$. The MTS of $\mathbf{P}^D_i$ and $\mathbf{Q}^D_i$ have $N = 36$ number of observations.

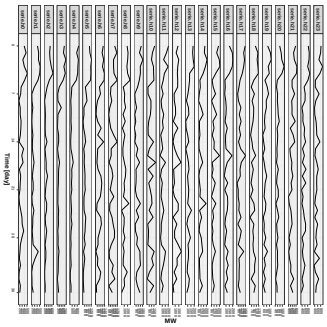

(a) Time series of $\mathbf{P}_1^D$.

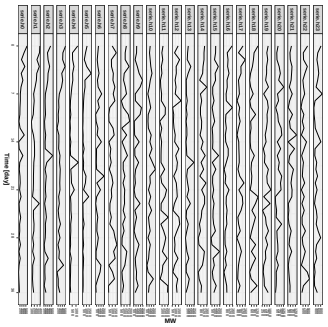

(b) Time series of $\mathbf{P}_2^D$.

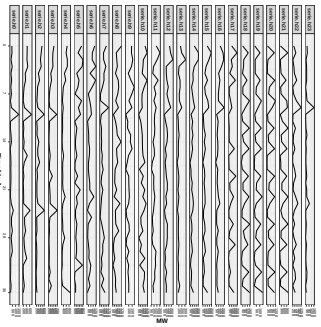

(c) Time series of $\mathbf{P}_3^D$.

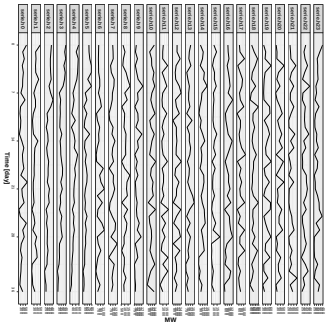

(d) Time series of $\mathbf{P}_4^D$.

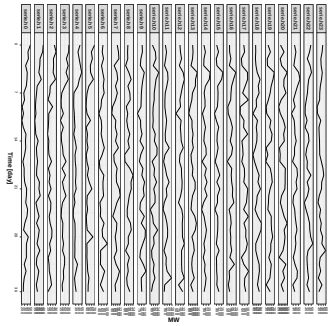

(e) Time series of $\mathbf{P}_5^D$.

Figura 6.2.1: MTS of Active Power Load.

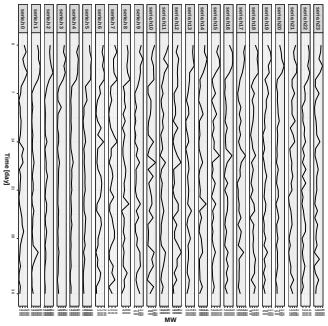

(a) Time series of $\mathbf{Q}_1^D$.

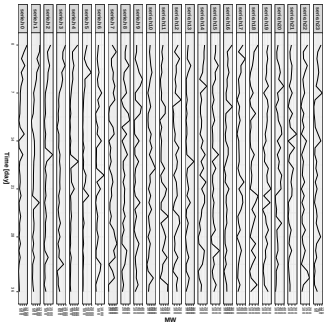

(b) Time series of $\mathbf{Q}_2^D$.

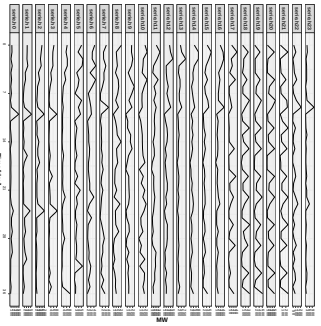

(c) Time series of $\mathbf{Q}_3^D$.

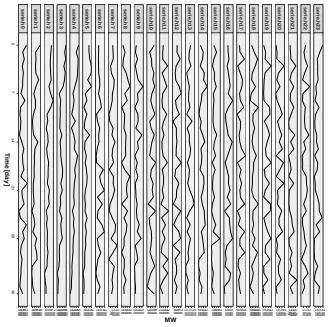

(d) Time series of $\mathbf{Q}_4^D$.

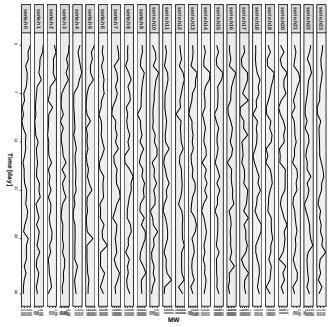

(e) Time series of $\mathbf{Q}_5^D$.

Figura 6.2.2: MTS of Reactive Power Load.

According to Figure 6.2.2, the statistical characteristics of these MTS are: a certain seasonal variation for weekly and non-stationary behaviour. These conditions may result from external factors like weather, geographical conditions and other types of circumstances.

About the active power generation of the non-dispatchable renewable source, the data was provided by CPFL energy (https://www.cpfl.com.br/Paginas/default.aspx), who own the *Usina Solar Fotovoltaica Tanquinho* plant, one of the largest in Brazil and the first in the state of São Paulo. The installed capacity is of 1.1 MWp (megawatt-peak). The data available is from the period 1 April 2017 to 27 March 2018 (in this case, $N = 315$). The historical data is used to represent the Photovoltaic (PV) generation for $RS8$. Regarding the PV generation of $RS5$ the data was fixed as the data of RS8 divided by two. Figure 6.2.3 shows the MTS of PV generation (in kWh) for $RS5$ ($\mathbf{p}_5^{pv}$) and $RS8$ ($\mathbf{p}_8^{pv}$).

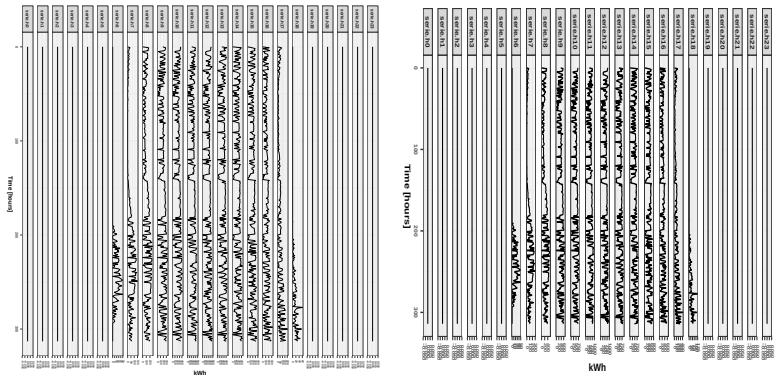

(a) Time series of $\mathbf{p}_5^{pv}$. **(b)** Time series of $\mathbf{p}_8^{pv}$.

Figura 6.2.3: MTS of Active Power Load of the PV.

Looking at the plots in Figure 6.2.3, the PV generation is an hourly panel of time series ($M = 24$). Also, the statistical characteristics that we observe in the plots are high variability and the presence of peaks. On the other hand, the MTS of PV generation has positive values during the hours of sunlight (between 6:00 am to 7:00 pm), while the remaining hours equal zero.

6.2.2. Statistical Models

In this section, we proceed to adjust statistical models for each of the MTS associated with the MSOODN model. Firstly, Section 6.2.2.1 presents the characteristics of the initial data for the test system, and Sections 6.2.2.2 and 6.2.2.3 show the adjusted statistical models.

6.2.2.1. Initial Data

Concerning the adjusted models, we defined the time period used for the calibration. In the case of active and reactive power load, the calibration data were fixed for the period from 21 April to 25 May 2016 and, in the case of PV generation, the period was defined from 1 April 2017 to 7 February 2018. For these cases, we obtained the day-ahead forecasts for the final day (26 May 2016 for the power load and 8 February 2018 for PV generation) of each time period. Unfortunately, the availability of data that coincided with the forecast day was impossible to obtain. However, according to our main purpose, which is to build scenario trees for the test system of Levron, we focused our efforts on getting acceptable statistical forecasts for the days mentioned previously.

6.2.2.2. Statistical Models for Power Load

In the case of the MTS, $\mathbf{P}_i^D$ and $\mathbf{Q}_i^D$, $i = 1, \ldots, 5$, the Time Series Factor Analysis (TSFA) techniques could not be applied for reducing their dimensionality. That is because the statistical proofs, the Root Mean Square Error of Approximation (RMSEA) and the Comparative Fit Index (CFI), did not yield results that could define a number of factors. In this case, the next option was to check if Vector Autoregressive (VAR) models could be used to adjust each MTS. For this, the first step was to verify if the MTS are stationary. Figures 6.2.4 and 6.2.5 display the plots of the Augmented Dickey–Fuller (ADF) test values for MTS. This test was evaluated at a 95 % significance level and defined in the drift case. Neither case satisfied the test in its entirety, since not all points were below the red line, proving that the VAR models cannot be used.

In view of the non-stationarity condition of some time series of $\mathbf{P}_i^D, \mathbf{Q}_i^D, i = 1, \ldots, 5$, we chose to adjust the Autoregressive Integrated Moving Average (ARIMA) models for each time series individually. In general, the ARIMA model in its *backshift notation* is given by:

$$(1 - \phi_1 B - \ldots - \phi_p B^p)\,(1 - B)^l\, y_d = c + (1 + \theta_1 B + \ldots + \theta_p B^p)\,\varepsilon_d \tag{6.2.1}$$

where p is the order of the autoregressive part, l is the degree of the first differentiation involved, q is the order of the moving average part, B is the backward shift operator, y_d is the time series of each MTS ($\mathbf{P}_i^D, \mathbf{Q}_i^D, i = 1, \ldots, 5$), ε_d is white noise, c is the average of the changes between consecutive observations, and $\phi_1, \ldots, \phi_p, \theta_1, \ldots, \theta_p$, are the parameters for the AR and MA part, respectively.

To implement the statistical models, we used a function of R studio called *auto.arima*[1], which returns the best ARIMA model according to AIC, AICc or BIC values.

[1] Information available on: https://cran.r-project.org/web/packages/forecast/forecast.pdf

This function conducts a search over a possible model within the order constraints provided. The models that we obtained through this approach for each series of $\mathbf{P}_i^D$ and $\mathbf{Q}_i^D$ with $i = 1 \ldots, 5$, are given in Tables B.2.1-B.2.5 of Appendix B.

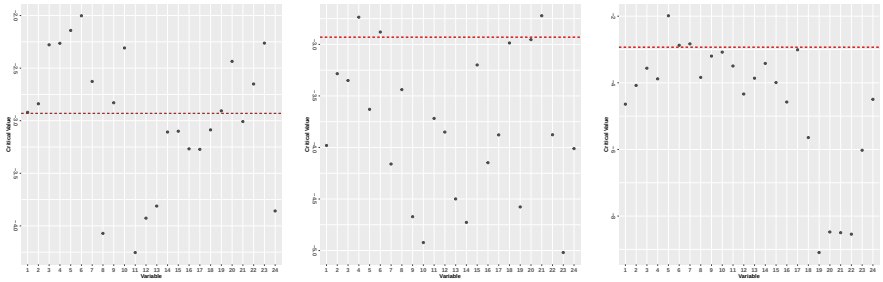

(a) Test Value for $\mathbf{P}_1^D$. **(b)** Test Value for $\mathbf{P}_2^D$. **(c)** Test Value for $\mathbf{P}_3^D$.

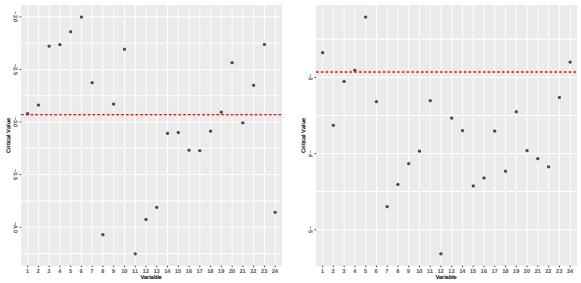

(d) Test Value for $\mathbf{P}_4^D$. **(e)** Test Value for $\mathbf{P}_5^D$.

Figura 6.2.4: Unit Root Test for $\mathbf{P}_i^D$.

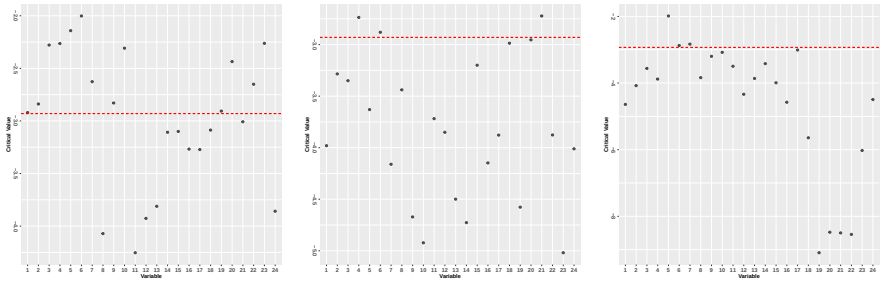

(a) Test Value for $\mathbf{Q}_1^D$. **(b)** Test Value for $\mathbf{Q}_2^D$. **(c)** Test Value for $\mathbf{Q}_3^D$.

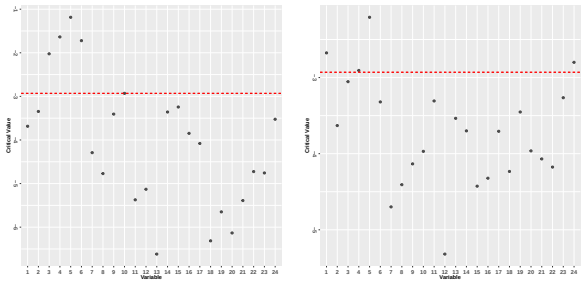

(d) Test Value for $\mathbf{Q}_4^D$. **(e)** Test Value for $\mathbf{Q}_5^D$.

Figura 6.2.5: Unit Root Test for $\mathbf{Q}_i^D$.

6.2.2.3. Statistical Models for PV Generation

At this point, it is important to note that we defined statistical models only for all the MTS whore. As seen in Figure 6.2.3, the time series are *serie.h*6 to *serie.h*18, with a total of 13 time series ($M = 13$, in this case). Thus, we reduce the data of PV generation through the TSFA technique. The TSFA model is given by:

$$\mathbf{p}_{i,d}^{pv} = \hat{\alpha} + \hat{\boldsymbol{B}}\hat{\mathbf{F}}_{i,d}^{pv} + \hat{\varepsilon}_{i,d} \tag{6.2.2}$$

where $i = 5, 8, d = 1, \ldots, N$, $\mathbf{p}_{i,d}^{pv}$ is an $M \times 1$ vector of random variables in this study, $\hat{\alpha}$ is an M-row vector of intercept parameters, $\hat{B}$ is an $M \times k$ matrix parameter of factor loadings, $\hat{\mathbf{F}}_{i,d}^{pv}$ is a $k \times 1$ vector of Bartlett predictor (or common factors) values obtained through the estimation, and $\hat{\varepsilon}_{i,d}$ is an $M \times 1$ random vector of estimated measurement errors.

The number of factors were fixed using the CFI and RMSEA criteria. The values are given in Table 6.2.1. Analyzing the results, the CFI is greater than 0.95, which verifies a good fit. Furthermore, the RMSEA shows a value between 0.05 and 0.08, which constitutes an acceptable range of fit. Based on these results, we reduced 26 variables to 10 factors.

MTS	Number of Variables (M)	CFI	RMSEA	MTS of the Factor	Number of Factors (k)
$\mathbf{p}_{5,d}^{pv}$	13	0.977	0.0764	$\hat{\mathbf{F}}_{5}^{pv}$	5
$\mathbf{p}_{8,d}^{pv}$	13	0.977	0.0764	$\hat{\mathbf{F}}_{8}^{pv}$	5
Total	26				10

Cuadro 6.2.1: Number of factors in the TSFA defined for PV Generation.

We choose the sample data from 21 April to 25 May 2016 and adjust the TSFA model for the MTS of the PV generation. Figure 6.2.6 shows the plots of the common factors resulting from the TSFA models.

Furthermore, Figure 6.2.7 displays the proportion of common variance or, stated simply, communality. In general, the random variables did not have a unique variance, with the exception of 17th and 18th hours, which share none of their variance with any other variable.

Building on the methodology of scenario generation, we proceed to verify if the time series of the common factors are stationary. This verification was done using the ADF test. Figure 6.2.8 shows the values of the ADF test for the common factors of the PV generation. In this case, the null hypothesis was accepted because all points were below the red line, resulting in the MTS of common factors being stationarity.

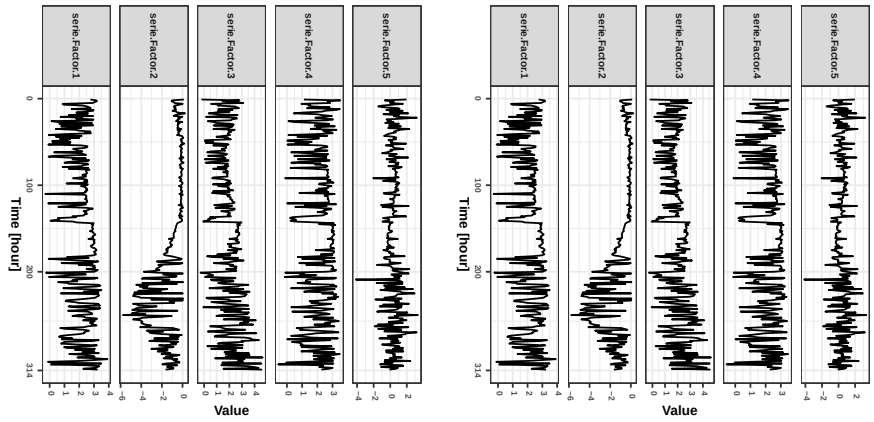

(a) Time Series of $\mathbf{p}_5^{pv}$. **(b)** Time Series of $\mathbf{p}_8^{pv}$.

Figura 6.2.6: Common Factors of $\mathbf{p}_5^{pv}$ and $\mathbf{p}_8^{pv}$.

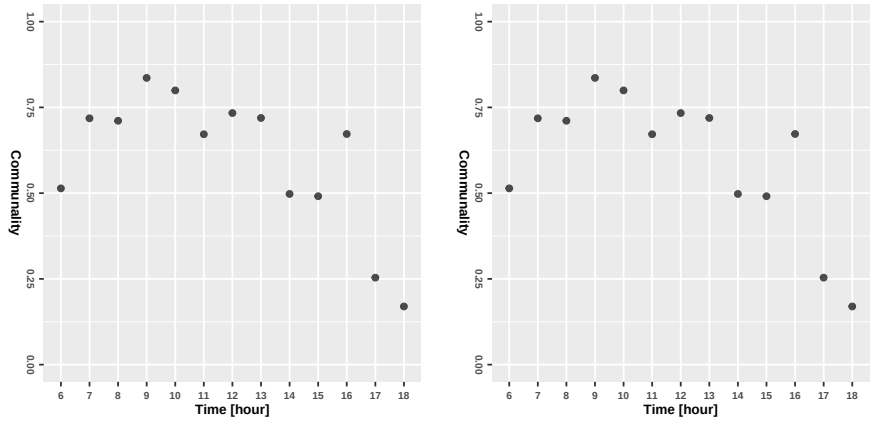

(a) Test Value for $\mathbf{p}_5^{pv}$. **(b)** Test Value for $\mathbf{p}_8^{pv}$.

Figura 6.2.7: Values of Unit Root Test for $\mathbf{p}^{pv}$.

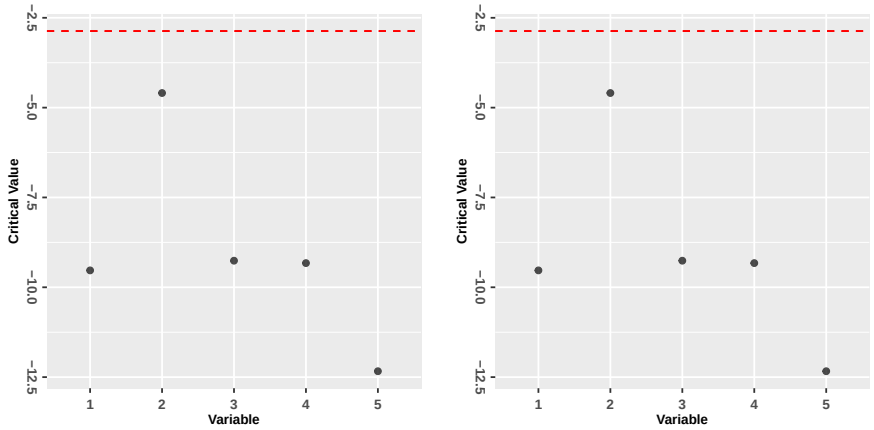

(a) Test Value for $\mathbf{p}_5^{pv}$. **(b)** Test Value for $\mathbf{p}_8^{pv}$.

Figura 6.2.8: Values of Unit Root Test for $\mathbf{p}^{pv}$.

Following the previous results, we proceed to adjust the VAR models. Furthermore, as with the random variables in the previous MTS model, the VAR model was fixed at $p = 8$. The VAR model for the common factors is given for the following equation

$$\mathbf{F}_{i,d}^{pv} = \hat{\mathbf{\Phi}}_0 + \hat{\mathbf{\Phi}}_1\mathbf{F}_{i,d-1}^{pv} + \hat{\mathbf{\Phi}}_2\mathbf{F}_{i,d-2}^{pv} + \hat{\mathbf{\Phi}}_3\mathbf{F}_{i,d-3}^{pv} + \hat{\mathbf{\Phi}}_4\mathbf{F}_{i,d-4}^{pv} + \ldots + \hat{\mathbf{\Phi}}_8\mathbf{F}_{i,d-8}^{pv} + \boldsymbol{\varepsilon}_d \quad (6.2.3)$$

where $d = 1, ..., N$ and $i = 5, 8$, $(\boldsymbol{\varepsilon}_d) \sim IID(0, \mathbf{\Sigma}_\varepsilon)$, $\mathbf{\Phi}_0, \mathbf{\Phi}_1, \mathbf{\Phi}_2, \ldots, \mathbf{\Phi}_8$ are the parameters to be estimated, and $\mathbf{F}_{i,d}^{pv}$ are the MTS of PV generation. The VAR model validations are given in Figures B.1.12 and B.1.13 of Appendix B.

6.2.3. Forecasting Models

The aim of this section is to define forecast models in order to predict future values of the random variables for the purpose of obtaining scenario trees that represent the uncertainty of the MSOODN model. The forecasting models and their results will be presented in the following sections. Section 6.2.3.1 shows the one-step-ahead forecast models for the active and reactive power load using ARIMA models, and Section 6.2.3.2 gives the one-step-ahead forecast models based on the TSFA and VAR models for the PV generation.

6.2.3.1. Forecast Models for Power Load

On the basis of future observations, the forecasts, residuals and errors obtained for the statistical models, we proceed to define the forecast models for the active and reactive power loads in order to obtain the one-day-ahead forecast. In this case, we obtained a one-day-ahead for 26 May 2016 using ARIMA models. The full model can be written as:

$$y_{N+1} = c + \phi_1 y_N + \phi_2 y_{N-1} + \ldots + \phi_p \phi_1 y_{N+1-p} + \theta_1 \varepsilon_N + \theta_2 \varepsilon_{N-1} + \ldots + \theta_p \varepsilon_{N+1-q} \quad (6.2.4)$$

where $N + 1$ indicates the one-step-ahead, y is each of the time series of $\mathbf{P}_i^D$ and $\mathbf{Q}_i^D$ $i = 1, \ldots, 5$, $c, \phi_1, \ldots, \phi_p, \theta_1, \ldots, \theta_p$, are the model parameters.

As a result of these forecast models, Figures 6.2.9 and 6.2.10 show the forecast day of the active and reactive power loads, respectively. The plots show that the forecast curve (red line) lies inside the confidence interval (dotted lines) and, in the majority of cases, the forecast curve (red line) is very close to the observed curve (blue line). These results indicate that the ARIMA models are adequate for forecasting the power load.

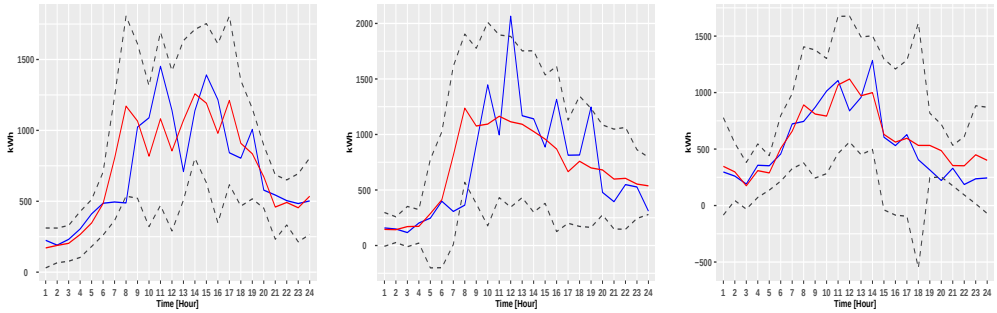

(a) $\hat{\mathbf{P}}^D_{1,N+1}$ Forecast. (b) $\hat{\mathbf{P}}^D_{2,N+1}$ Forecast. (c) $\hat{\mathbf{P}}^D_{3,N+1}$ Forecast.

(d) $\hat{\mathbf{P}}^D_{4,N+1}$ Forecast. (e) $\hat{\mathbf{P}}^D_{5,N+1}$ Forecast.

Figura 6.2.9: Forecast for $\hat{\mathbf{P}}^D_{i,N+1}$ with ARIMA Models.

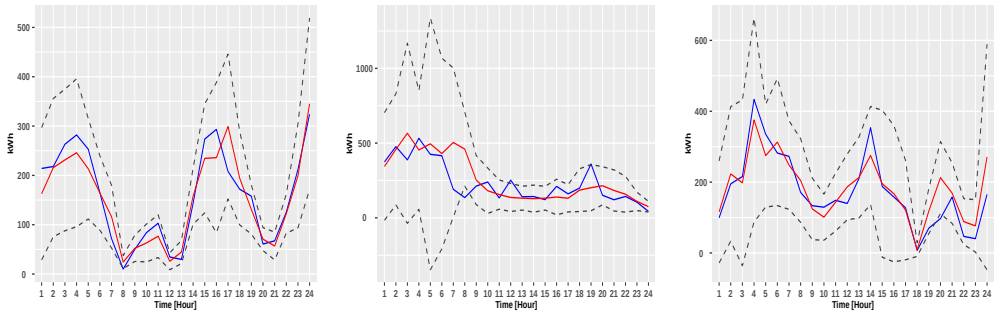

(a) $\hat{\mathbf{Q}}^D_{1,N+1}$ Forecast. (b) $\hat{\mathbf{Q}}^D_{2,N+1}$ Forecast. (c) $\hat{\mathbf{Q}}^D_{3,N+1}$ Forecast.

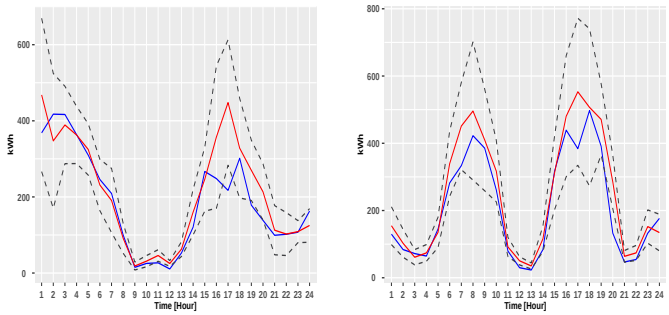

(d) $\hat{\mathbf{Q}}^D_{4,N+1}$ Forecast. (e) $\hat{\mathbf{Q}}^D_{5,N+1}$ Forecast.

Figura 6.2.10: Forecast for $\hat{\mathbf{Q}}^D_{N+1}$ with ARIMA Models.

6.2.3.2. Forecast Models for PV Generation

In accordance with the methodology developed in this thesis, we used the TSFA and VAR models to obtain forecasts for PV generation. First, we define the TSFA model for the PV generation forecast for 7 February 2018 (N+ 1). This model is defined by:

$$\mathbf{p}_{i,N+1}^{pv} = \hat{\alpha} + \hat{\boldsymbol{B}}\hat{\mathbf{F}}_{i,N+1}^{pv} \tag{6.2.5}$$

where $i = 5, 8$, $N + 1$ indicates the one-day-ahead, $\mathbf{p}_{i,d}^{pv}$ is an $M \times 1$ vector of random variables, $\hat{\alpha}, \hat{B}$ are the model parameters, and $\hat{\mathbf{F}}_{i,N+1}^{pv}$ is the forecast of the common factors.

We need to estimate the parameters $\hat{\alpha}, \hat{B}$ and obtain the forecast of the common factor $\hat{\mathbf{F}}_{i,N+1}^{pv}$. For this purpose, we use VAR models. The model is the following:

$$\mathbf{F}_{i,N+1}^{pv} = \hat{\mathbf{\Phi}}_0 + \hat{\mathbf{\Phi}}_1\mathbf{p}_{i,N}^{pv} + \hat{\mathbf{\Phi}}_2\mathbf{F}_{i,N-1}^{pv} + \hat{\mathbf{\Phi}}_3\mathbf{F}_{i,N-2}^{pv} + \hat{\mathbf{\Phi}}_4\mathbf{F}_{i,N-3}^{pv} + \ldots + \hat{\mathbf{\Phi}}_8\mathbf{F}_{i,N-7}^{pv} \tag{6.2.6}$$

where $N + 1$ is the one-day-ahead, $i = 5, 8$, $\mathbf{\Phi}_0, \mathbf{\Phi}_1, \mathbf{\Phi}_2, \ldots, \mathbf{\Phi}_8$ are the parameters to be estimated, and $\mathbf{F}_{i,d}^{pv}$ are the values of PV generation.

The results obtained using the models of Equation 6.2.6 are given in Figure 6.2.11. These are the forecasts of the common factors $\mathbf{F}_{5,d}^{pv}$ and $\mathbf{F}_{8,d}^{pv}$. Once these forecasts have been generated, we substitute them into the model of Equation (6.2.5) and obtain the forecast values for the random variables of the MSOODN model. These are shown in Figure 6.2.12. The observed values (blue line) are compared with the estimates (red line) provided by the TSFA-VAR models. These results conclude that the adjusted models obtain satisfactory forecasts for the PV generation.

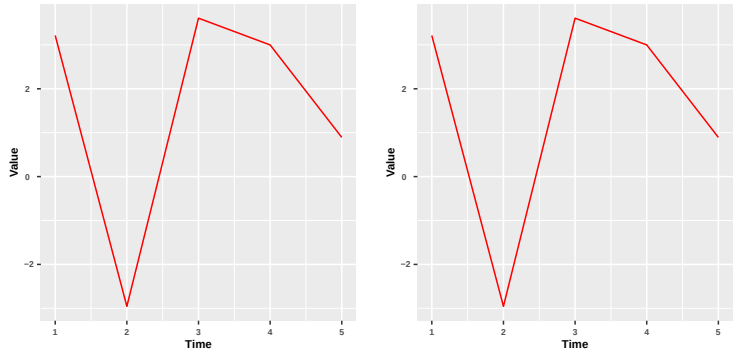

(a) $\mathbf{F}_5^{pv}$ Forecast. (b) $\mathbf{F}_8^{pv}$ Forecast.

Figura 6.2.11: Common Factors of PV Generation.

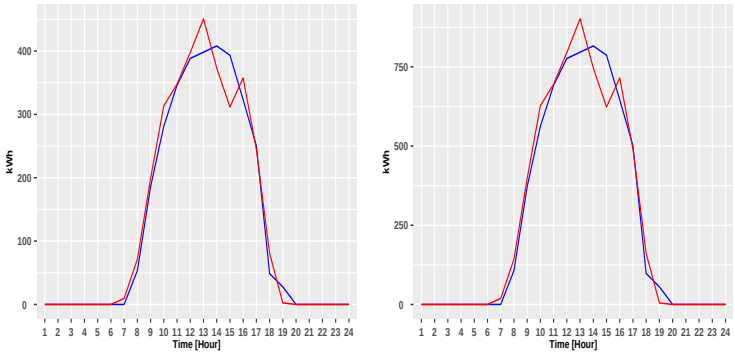

(a) $\mathbf{p}_5^{pv}$ Forecast. (b) $\mathbf{p}_8^{pv}$ Forecast.

Figura 6.2.12: Forecast of PV Generation.

6.2.4. Scenario Generation

This section presents the results obtained from the scenario generation. In this case, we generated scenario sets based on the four-step scenario generation procedure and obtained scenario sets for the same days of the forecasting tests: 26 May 2016 for the power load; and 8 February 2018 for PV generation. In addition, the size of the scenario sets was fixed in accordance with the specific needs of each scenario tree algorithm. the Forward Tree Construction Algorithm (FTCA) can work with scenario sets that are smaller than those needed by Dynamic Tree Generation with Flexible Bushiness Algorithm (DTGBA). For this test, we generated scenario sets of 300 scenarios for the FTCA, which are displayed in Figures B.4.1–B.4.5, and scenario sets of 500 scenarios for DTGBA, shown in Figures B.4.2–B.4.6, all of which are in Appendix B.

Looking at the plots, we can note that the scenario sets (black lines) cover the forecast values (red line) and observed values (blue line) of each MTS. This can be more beneficial at the time of representing the uncertainty through scenario trees, and it obtains satisfactory results for the MSOODN model. In conclusion, we can say that the procedure for generating scenarios obtained promising results at the time of obtaining scenario sets for the random variables of the MSOODN model.

6.3. Phase II: Scenario Tree Generation

Following the results obtained by the scenario procedure, we now dedicate ourselves to approximating the stochastic process through a scenario tree. To this end, Section 6.3.1 presents the initial considerations for generating scenario trees, and Sections 6.3.2 and 6.3.3 present the scenario trees resulting from the algorithms implemented in this thesis. More to the point, Section 6.3.2 shows the numerical experience of the FTCA, and Section 6.3.3 gives the results obtained through the DTGFBA.

6.3.1. Initial Considerations for the Algorithms

In accordance with the decision process of the MSOODN model, a good approximation of the stochastic process using scenarios depends, first of all, on an appropriate definition of the individual scenarios. Based on this consideration, we have defined an individual scenario for each $\omega \in \Omega_\omega$, as follows:

$$\tilde{\boldsymbol{\xi}}_\omega = (\tilde{P}^D_{1,1\omega}, \tilde{Q}^D_{1,1\omega}, \tilde{P}^D_{2,1\omega}, \tilde{Q}^D_{2,1\omega}, \tilde{P}^D_{3,1\omega}, \tilde{Q}^D_{3,1\omega}, \tilde{P}^D_{4,1\omega}, \tilde{Q}^D_{4,1\omega}, \tilde{P}^D_{5,1\omega}, \tilde{Q}^D_{5,1\omega}, \tilde{p}^{pv}_{5,1\omega}, \tilde{p}^{pv}_{8,1\omega}, \ldots, \tilde{P}^D_{1,24\omega}, \tilde{Q}^D_{1,24\omega}, \tilde{P}^D_{2,24\omega}, \tilde{Q}^D_{2,24\omega}, \tilde{P}^D_{3,24\omega}, \tilde{Q}^D_{3,24\omega}, \tilde{P}^D_{4,24\omega}, \tilde{Q}^D_{4,24\omega}, \tilde{P}^D_{5,24\omega}, \tilde{Q}^D_{5,24\omega}, \tilde{p}^{pv}_{5,24\omega}, \tilde{p}^{pv}_{8,24\omega})' \quad (6.3.1)$$

For the test, the $\tilde{\boldsymbol{\xi}}_\omega$ had a length of 288 components and 24 stages. Table D.1.4 of Appendix D shows more details about the dimensionality of $\tilde{\boldsymbol{\xi}}_\omega$. Also, we defined a realization as a vector composed of the active/reactive power loads, and PV generation (with a total length of 12 components). In mathematical terms, we defined a realization as the vector $\tilde{\xi}_{t\omega} = (\tilde{P}^D_{1,t\omega}, \tilde{Q}^D_{1,t\omega}, \tilde{P}^D_{2,t\omega}, \tilde{Q}^D_{2,t\omega}, \ldots, \tilde{P}^D_{5,t\omega}, \tilde{Q}^D_{5,t\omega}, \tilde{p}^{pv}_{5,t\omega}, \tilde{p}^{pv}_{8,t\omega})$, where $\tilde{\xi}_{t\omega}$ is a realization ω at stage t. On the other hand, the initial data of the test was represented by a scenario set that can be viewed as a fan or a matrix of an individual scenarios, depending on the algorithm used to generate the scenario tree. Moreover, equal probabilities were assigned to the elements of this initial data. Lastly, the algorithms were implemented in AMPL, and the test runs were performed on a DELL PowerEdge R630 Server with 2 x Xeon E5-2697 v4 (2,3 GHz, 18Cores/36Threads, 45 MB cache) and RAM 256 GB (8 x32 GB RDIMM, 2400 MT/s).

6.3.2. Scenario Trees Obtained by FTCA

Recall that, to reflect the structure of the information required by the MSP model, it is necessary to build scenario trees through algorithms developed for this purpose. In this case, the FTCA is used. For this test, the fan structure has a root node at $t = 0$ and is composed of the scenarios obtained in Section 6.2.4. Also, more details about the dimensionality of this fan are shown in Table 6.3.1. Figure 6.3.1a shows the structure of this initial fan.

Components	Stages	Number of Scenarios	Number of Nodes
188	24	300	7200

Cuadro 6.3.1: Dimension of Initial Fan for FTCA.

After defining the fan structure, we fixed the initial parameters values of the FTCA in order to obtain different configurations of scenario trees. These values were defined such that the obtained scenario trees were reduced to between 100 and 200 scenarios, approximately. Table 6.3.2 shows the dimension of the final scenarios obtained by the

FTCA. In this case, the numbers of reduced scenarios and nodes depend on the value of $\varepsilon_{rel,1}$.

Tree	$\varepsilon_{rel,1}$	δ_0	Number of Scenarios	Number of Nodes
1	0.87	0.00064	101	1728
2	0.83	0.00064	130	2228
3	0.69	0.00064	188	3866

Cuadro 6.3.2: Dimension of Final Scenario Trees Obtained by FTCA.

For each scenario tree obtained, the stop criteria ε_t that satisfies the condition of Equation (3.3.26) was calculated from Equations (3.3.27), (3.3.28) and (3.3.29). To this end, different values of δ_0 and ε_{rel}, are fixed. Table D.1.5 of Appendix D shows these different values. This brought about different scenario trees with different numbers of scenarios and nodes. In total, three scenario trees were calculated. The $\varepsilon_{rel,t}, \varepsilon_{max,t}$ values for each scenario tree are given in Table D.1.5. Finally, the resulting scenario trees are displayed in Figures 6.3.1b and 6.3.1d.

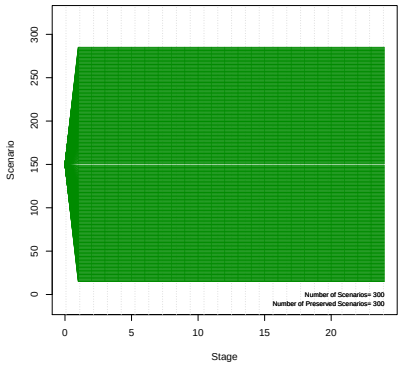

(a) Initial Fan Structure (Fan).

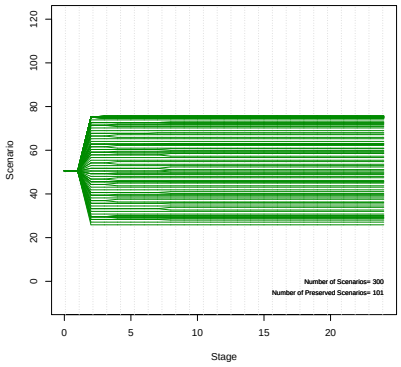

(b) Scenario Tree of 101 Scenarios (Tree 1).

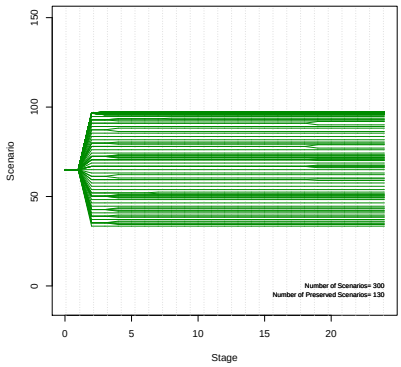

(c) Scenario Tree of 130 Scenarios (Tree 2).

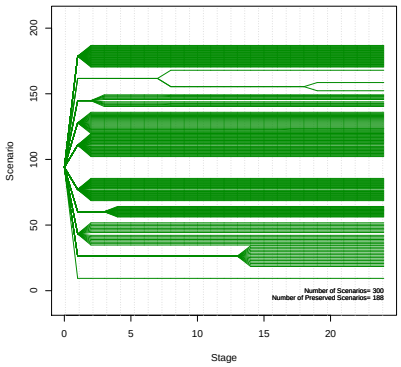

(d) Scenario Tree of 188 Scenarios (Tree 3).

Figura 6.3.1: Fan and Scenario Tree for TSFA.

The numerical results illustrate that the FTCA can obtain scenario trees for representing the uncertainty in the MSOODN model. In this case, the initial parameters that define the dimensionality of the scenario tree allow us to obtain different configurations with a specific number of scenarios and nodes for an initial fan defined. This is due to the initial parameters defining the distance between probability distributions.

6.3.3. Scenario Trees Obtained by DTGFBA

For the DTGFBA, we start with an initial matrix of scenario set composed of scenario sets obtained for each random variable in Section 6.2.4. They were ordered according to the decision process, taking the form of the set of initial scenarios defined in Equation (6.3.1). The test starts with a matrix containing a total of 500 individual scenarios and 288 components that define, for each row, equal probabilities. Table D.1.6 of Appendix D shows the input values for the DTGFBA, where ε_t was computed as follows:

$$\varepsilon_t = \delta \cdot \max_{s \in \mathcal{T}} \sum_{t' \in \mathcal{T}} \frac{d_{t,t'}}{|\mathcal{T}|} \tag{6.3.2}$$

where $d_{t,t'}$ is the Euclidean distance and δ is a branching parameter.

As in the case of the FTCA, the number of scenario trees to obtain is three. In this case, several values of δ are fixed. These values are defined taking into account the scenario number defined for the scenario trees obtained by the FTCA. The second column of Table 6.3.3 shows the value of δ for each scenario tree obtained. Furthermore, Table D.1.6 shows the ε_t values fixed for each scenario tree.

Tree	δ	Number of Scenarios	Number of Nodes
1	0.99	104	2487
2	0.98	126	2901
3	0.97	189	3153

Cuadro 6.3.3: Dimension of the Final Scenario Trees Obtained by DTGFBA.

As a final result, Table 6.3.3 shows the number of scenarios and nodes for each scenario tree obtained by the DTGFBA. Also, Figure 6.3.2 displays the resulting scenario tree plots. As in the previous algorithm, these results show that using the DTGFBA can also obtain scenario trees for the MSOODN.

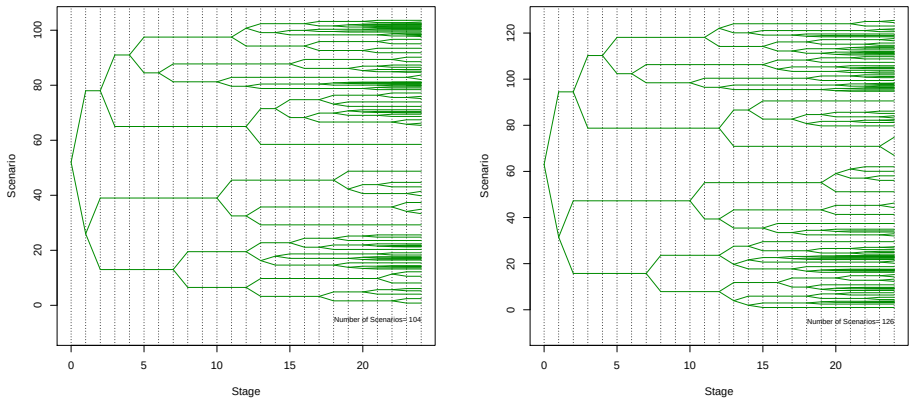

(a) Scenario Tree of 104 Scenarios (Tree 1). **(b)** Scenario Tree of 126 Scenarios (Tree 2).

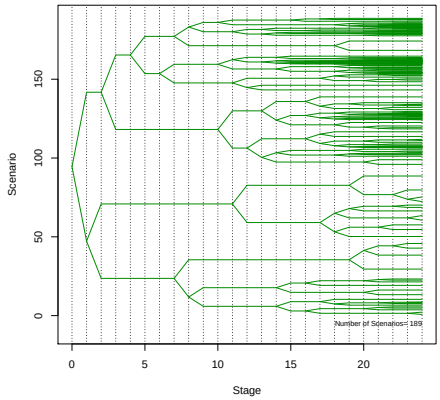

(c) Scenario Tree of 189 Scenarios (Tree 3).

Figura 6.3.2: Scenario Trees obtained by DTGFBA.

6.4. Computational Results for the MSOODN Model with Scenario Trees

The MSOODN Model was used to analyze the optimal operation of an 11-node test system proposed by Levron and Shmilovitz (2012) (see Figure 6.1.1). The proposed MSP model given in Section 4.2.3 was implemented in the mathematical programming language AMPL (Fourer et al., 1993) and solved with CPLEX (version 12.8.0.0) using a DELL PowerEdge R630 Server with 2x Xeon E5-2697 v4 (2,3 GHz, 18Cores/36Threads, 45 MB cache) and RAM 256 GB(8 x 32 GB RDIMM, 2400 MT/s). Numerical results are shown for the model for each test case given by a set of scenario trees are shown. We analyzed a slightly modified version of the microgrid proposed by Levron and Shmilovitz (2012), which is displayed in Figure 6.1.1. This test system contains 2 RS at nodes 8

and 5, respectively; 2 ESD at nodes 4 and 11; a CB at node 2; and five loads. The objective is to minimize the cost of energy purchase from node 1 (this node has the SDD). The energy cost and the load shedding at the nodes is shown for a time period of 24 hours.

The cost of energy, c_t^S, is given in Table 6.4.1. The load shedding cost was transformed into \$/kWh for a better understanding of the objective function. This transformation is given by the γ_i parameter (see Equation 4.2.4), which was defined by $\gamma_i = 5{,}98$ US\$/KWh. Furthermore, the random parameters of the models (the active and reactive power loads and the PV generation) are represented by the scenario trees built in Section 6.3.

Time period t	1-6	7	8	9	10-15	16	17-22	23	24
$c_t^{\mathcal{S}}$ [\$/kWh]	0.02838	0.04257	0.05676	0.07095	0.08514	0.07095	0.05676	0.04257	0.02838

Cuadro 6.4.1: Cost of Energy in the DSS at Node 1.

Two different case studies have been solved in order to analyze the impact of the Battery Energy Storage System (BESS) in the optimal operation of the EDN:

- Case A_1: without BESS in the system and considering a transformer with increased capacity $\overline{\mathcal{S}}_1^{dg} = 6000$ kVA.
- Case A_2: with both BESS in the system and considering the original transformer capacity: $\overline{\mathcal{S}}_1^{dg} = 6000$ kVA.

The optimal solution of the two case studies can be visualized with the help of several graphical representations:

(a) The optimal value of the state of charge and total active power extracted and injected by the BESS: $SOC_{it\omega}^*$, $P_{it\omega}^{BESS^*} = P_{it\omega}^{ch^*} - P_{it\omega}^{dis^*}$.

(b) Apparent power generation at node 1 (Distribution Substation (DSS) node) with and without the BESS in the EDN and the cost of energy purchase from node 1: $S^{S^*} = \sqrt{(P^{S^*})^2 + (Q^{S^*})^2}$.

(c) Active power losses in the lines with and without the BESS in the EDN: $P_{t\omega}^{ls^*} = \sum_{ij\in\Omega_b} R_{ij} \cdot (I_{ijt\omega}^*)^2$.

(d) Voltage profile on the load nodes with the highest and lowest voltages during the operation period: $V_{t\omega}^{min} = min_{i\in\Omega_n} V_{it\omega}^*, V_{t\omega}^{max} = max_{i\in\Omega_n} V_{it\omega}^*$.

(e) Load shedding on the load nodes: $L_{it\omega}^{shed^*}$.

(f) Frequency of charge or discharge of the BESS: $P_{it\omega}^{ch^*}, P_{it\omega}^{dis^*}$.

The complete set of plots (a)–(e) for the scenario trees shown in Tables 6.3.2 and 6.3.3 are included in Appendix D. We have analyzed the results corresponding to scenario tree 1 obtained for the FTCA and DTGFBA. The rest of the results are analyzed in a very similar form.

Plots (a)–(e) in Figures 6.4.1 and 6.4.2 show the value of the most important recourse variables corresponding to each scenario (blue thin continuous lines for the case A_1 and grey thin continuous lines for the case A_2), their mean value (red discontinuous lines) and the maximum and minimum at each time period (black discontinuous lines). Figures 6.4.1a and 6.4.2a show the optimal values of SOC and the power extracted and injected by the BESS for the test case A_2. We can observe similar results for both scenario trees (FTCA and DTGFBA). The optimal values satisfy the maximum level of the SOC (red continuous line), and the SOC varies according to the power extracted and injected by the BESS. This last observation may be due to the demand obtained with each load flow. Regarding the apparent power generation at SSD, Figures 6.4.1b and 6.4.2b show the apparent power generation of the DSS with (Case A_2) and without (Case A_1) the BESS in the system for the FTCA and DTGFBA tree, respectively. In cases A_1 and A_2, the system operation satisfies the 6000 kVA capacity of the transformer considered. Also, the largest apparent power generation coincides with the largest cost of energy purchase, which can be benefits for the DSS. Observing the results for the case A_2 for the FTCA and DTGFBA tree, the results are very similar. In addition, Figures 6.4.1c and 6.4.2c show the active power losses in the lines without (case A_1) and with (case A_2) the BESS. Analysing the results obtained using each tree, the power losses were lower in the cases with the BESS. Also, the losses increase when the BESS injects power into the system. Another interesting result, is shown in Figures 6.4.1d and 6.4.2d. This is the voltage profile on the load nodes of the case A_2 (with BESS). In these cases, the voltages satisfy their limits and the scenarios also take a similar form for both the FTCA and DTGFBA trees. Finally, Figures 6.4.1e and 6.4.2e show the active and reactive load shedding on the load nodes for the case A_2. In general, the mean is near zero only in some scenarios where the load sheddding is major. At nodes 7 and 9, active load shedding was the 50 % at and the reactive load shedding was 10 %.

On the other hand, Figures 6.4.1f and 6.4.2f show the value of the most important state variables that represent the frequency of charge and discharge of the BESS (case A_2). The results obtained for the FTCA and DTGFBA scenario trees are very similar. We observe that the discharge occurs in the first and final hours and the charge is between $t = 10$ to $t = 15$ (hours with the maximum sunshine). This effect can be due to the load demand on the EDN during these hours.

Cases A_1 and A_2 / Instance 1 FTCA / Tree 1 (101 scenarios).

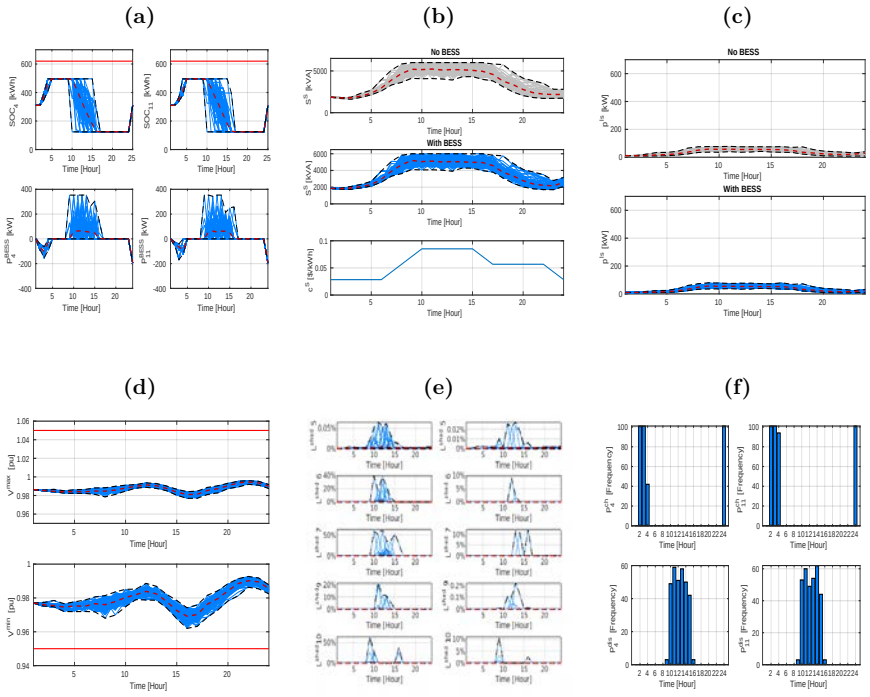

Figura 6.4.1: Results for Cases A_1 and A_2 with Scenario Tree Obtained by FTCA.

Cases A_1 and A_2 / Instance 1 DTGFBA / Tree 1 (104 scenarios).

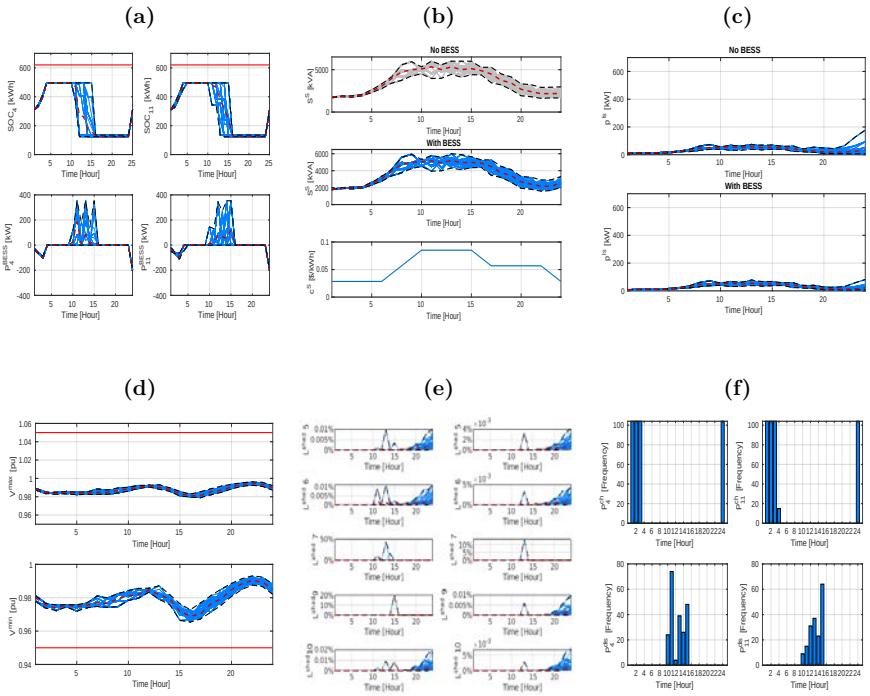

Figura 6.4.2: Results for Cases A_1 and A_2 with Scenario Tree Obtained by DTGFBA.

It was not possible to analyze the performance of the scenario trees for this study. However, we show the effect of varying the number of scenarios in a scenario tree. Table 6.4.2 gives the number of constraints, variables and nonzero coefficients for each FTCA and DTGFBA tree. We observe that the DTGFBA trees have a smaller size than the FTCA trees, resulting in less computational time to resolve the MSOODN model tests for the DTGFBA trees.

	FTCA						DTGFBA					
Tree	Scenarios	Nodes	Rows	Columns	Nonzeros	CPU-Time	Scenarios	Nodes	Rows	Columns	Nonzeros	CPU-Time
1	101	1728	139628	167438	460056	3066.91	104	2487	118208	122517	345323	1309.34
2	130	2228	179802	215676	592566	4572.54	126	2901	142346	146800	412720	1247.18
3	188	3866	274186	339586	927110	76389.1	189	3153	212724	218646	615150	1939.89

Cuadro 6.4.2: Results for the Test of Case A_2.

Table 6.4.3 shows the expected net cost RP for cases A_1 and A_2. Comparing the means of the RP for case A_1 with case A_2, we observe that the mean of the RP is 91 % (FTCA) and 97 % (DTGFBA) smaller. Also, the expected net cost in the case A_2 is 97 % smaller using the DTGFBA trees than with the FTCA trees. However, as a mentioned in Section 5.6, these results do not mean that the cost when using FTCA trees is better than the cost when using the DTGFBA trees.

	FTCA				DTGFBA			
Test Case	Tree 1	Tree 2	Tree 3	Mean	Tree 1	Tree 2	Tree 3	Mean
A_1	5320.08	5234.99	5247.67	5267.47	5328.68	5338.95	5047.76	5238.46
A_2	4952.12	4961.29	4959.12	4957.51	5086.01	5080.9	5145.76	5104.22

Cuadro 6.4.3: RP Values in \$/kWh for case A_2.

The great science [mathematics] occupies itself at least just as much with the power of imagination as with the power of logical conclusion.

— Johann Friedrich Herbart

7

Conclusions and Further Research

Contents

7.1. Conclusions

The objectives proposed for this thesis have been achieved. Throughout the chapters, a literature review has been provided on the approaches for generating scenario trees. This review was made in the context of Multistage Stochastic Programming (MSP) models in renewable energy systems. As a result, we selected two algorithms based on the principle of probability metric-based approximations. The chosen algorithms were The Forward Tree Construction Algorithm (FTCA), developed by Heitsch and Römisch (2009a), and an adapted version of Dynamic Tree Generation with Flexible Bushiness Algorithm (DTGFBA), developed by Pflug and Pichler (2014, 2015), both of which were integrated into the scenario tree generation methodology developed in this thesis. The first phase of the methodology begins with available data and sets of scenarios obtained through a procedure based on statistical models, one-step-ahead forecasting models and bootstrap techniques. In the second phase, the obtained sets of scenarios serve as the basis of an initial approximation that is defined and used as input to obtain the final scenario trees with the selected algorithms. Two MSP models in renewable energy systems we have presented and formulated. The one that models participation in the EM is called the MSWBVPP model; and the other one is the MSOODN model, which models the operation of the EDN. These models have been computationally implemented

and tested with the data input defined by scenario trees that are based on: real data of the MIBEL; and the Wind Power (WP) generation of a wind farm called Espina (for the MSWBVPP model); and data provided by FEEC-UNICAMP for the active power load; and the Photovoltaic (PV) generation on the Usina Solar Fotovoltaica Tanquinho plant (for the MSOODN model). The comparative performance of the scenario trees was analyzed for only the scenario trees obtained for the MSWBVPP model. We will present the general contributions of the whole thesis in terms of the objectives proposed in Chapter 1:

(i) Algorithms for generating scenario trees:

- The approaches for generating scenario trees have been revised (see Section 2.2). The FTCA was used more frequently in the electricity environment, and the DTGFBA was chosen as a recent development for generating scenario trees.
- A review of the most specific literature on generating scenario trees in the study areas has been addressed in this thesis, specifically for EM (Section 2.3) and EDN (Section 2.4).

(ii) A two-phase methodology for generating scenario trees:

- One of the contributions of this thesis was the design of a methodology for scenario tree generation. The methodology begins in the first phase with available data and builds sets of scenarios for each random variable. Then, these sets are used to build the individual scenarios of the stochastic process and are used as inputs to the FTCA and DTGFBA. In the second phase, the scenario trees are generated with the FTCA and DTGFBA. The main contributions of this methodology are:
  - A developed procedure similar to Muñoz et al. (2013) for generating scenarios for each random parameter of the MSP models, but with the difference being that Vector Autoregressive (VAR) models were used instead to predict the next day (Section 3.3.1).
  - A rigorous study of the algorithms that were selected for generating scenario trees (Section 3.3.2).
- Another contribution is the development of a methodology for studying the relative performance of scenario trees (Section 3.4). These parameters allow comparing scenario trees to determine which tree (or set of trees) provides the best stochastic solution of a model. This comparison is given by the best stochastic solution and the value of the deterministic solution when using the forecasted values of the random variables.

(iii) Scenario trees for the MSP models in renewable energy systems optimization:

- An analysis of the uncertainty and decision process was developed. This analysis allowed us to propose an original tree structure for each problem formulated as an MSP model (Chapter 4). These scenario trees are one of the main contributions of this thesis, and they consist of:
  - A novel MSP formulation for the participation in the EM of a Virtual Power Plant (VPP) comprising a Wind Power Plant (WPP) and Battery Energy Storage System (BESS) (Section 4.1.3). This formulation is called the MSWBVPP model. The contribution is based on considering all Intra-day Markets (IM) sessions together with the elements already considered (Day-Ahead Market (DM), Secondary Reserve Market (RM) and Imbalance Settlements (IB)).
  - A novel MSP formulation for the operation of a radial EDN composed of a Distribution Substation (DSS), Switchable Capacitor Banks (SCB), loads, non-dispatchable Renewable Sources (RS) and BESS (Section 4.2.3). This was called the MSOODN model.

(iv) Generating Scenario trees:

- First of all, we obtained scenario trees for the MSWBVPP model. The test cases take into account a VPP that contains a WP with power peaks of 18 MW and a BESS with a maximum capacity of 30 MWh, which operates in the MIBEL. The data used covers the period January 1st 2015 to December 31st 2016 for the MIBEL prices and WP generation of a wind farm called Espina. We obtained 366 scenario trees from the FTCA and the same number of the trees from the DTGFBA. The results obtained show that our methodology can successfully generate suitable scenario trees for the MSWBVPP model (Sections 5.1–5.4). Finally, an analysis based on boxplots of the elapsed time, number of scenarios and number of nodes, for the 366 trees generated by each algorithm is given. This analysis shows significant differences in the number of nodes of the trees of both algorithms.
- We were also able to apply the scenario tree generation methodology to the MSOODN model. The test case was based on an 11-node system (Levron and Shmilovitz, 2012) containing two photovoltaic RS with power peaks of 1 MW and 0.5 MW at, respectively, nodes 8 and 5; and two BESS at nodes 4 and 11 with a capacity for 0.4 MWh each. The data used was provided by FEEC-UNICAMP (active power load) and by the Usina Solar Fotovoltaica Tanquinho plant in the state of São Paulo in Brazil (PV generation). The operation was planned for one day, and a set of three scenario trees were

built by each algorithm (FTCA and DTGFBA). These trees were obtained by varying the tolerance error of the algorithms, thus obtaining scenario trees with different numbers of scenarios. The results obtained show that the scenario tree generation methodology can be applied to other MSP models (Sections 6.1–6.3).

(v) Computational results for the MSP models and comparative performance of the scenario trees:

- In the case of the MSWBVPP model, three different case studies have been solved in order to analyze the impact of the BESS and the participation in the RM. As an example, we briefly analyzed the results for the three test cases corresponding to Thursday, November 17 2016 using both the FTCA and DTGFBA scenario trees. The results lead to great differences between the test cases, specifically in terms of a huge increase in the expected net profit Recourse Problem (RP). The increase in the RP between the WDI and VDI test cases is less than 3 %, and the increase in the RP between the VDI and VDIR test cases is 65 % (FTCA) and 79 % (DTGFBA). However, these results do not mean that the actual profits for a test case are higher than the previous test case, because that net benefit depends on the tree itself and is not a fair value to compare (Section 5.6).
- To study the relative performance of the FTCA and DTGFBA scenario trees for the MSWBVPP problem, we developed a methodology based on two premises. First, we conducted a statistical analysis on the results for a complete one-year period in the three cases (WDI, VDI and VDIR) and applied two scenario trees (FTCA and DTGFBA). Second, we analyzed: the quality of the solution in terms of the usual variables RP and Expected Value of the Stochastic Solution (EVSS) (which completely depend on the scenarios themselves); and a modification of the classical Value of the Stochastic Solution (VSS), called Forecasted Value of the Stochastic Solution (FVSS) (which depends only partially on the scenario trees). To determine the significant statistical differences in the values of these variables for the different test cases and scenario trees, we compared the distribution of these variables in the 2016_MSWBVPP data. Based on the application of this methodology, we can conclude that the relative value of the stochastic solution FVSSr for the DTGFBA scenario trees is 120 %, 130 % and 40 % greater for, respectively, the test cases WDI, VDI and VDIR when compared with the corresponding values for the FTCA scenario trees (Section 5.7).

- In the case of the MSOODN model, two test cases have been solved in order to analyze the impact of the BESS in the optimal operation of the EDN. We briefly analyze the results from these two test cases for a 24-hour day using both FTCA and DTGFBA scenario trees. In both cases, the operation of the EDN satisfies the limits of the apparent power generation at the Distribution Substation (DSS) node, and the active power losses in the lines were very similar. Looking at the results of the most important recourse variables and the state variables that represent the frequency of charge and discharge of the BESS, these show that the EDN can operate correctly. However, as the tree size increases, we observed that the load shedding on the load nodes increases, which is not recommended for the real solution. On the other hand, varying the number of scenarios in a scenario tree results in less computational time; although the DTGFBA had better computational time than the FTCA, due to the scenario trees obtained by the DTGFBA having a smaller number of nodes than those by the FTCA. Finally, in terms of the net cost RP, the case A_1 had a smaller RP than case A_2. With regard to the case A_2, the expected net cost was smaller when using trees obtained by the DTGFBA than by the FTCA (Section 6.4).

7.2. Topic for Future Research

Based on the study developed in this thesis, we can define the following topics for treatment in future research:

- To generate the one-step forecast for the WP and PV generation, we used TSFA and either VARX or VAR models. A topic that needs further study is the development of statistical and forecast models that take into account the particular statistical characteristics of these random variables.
- In order to build our scenarios, we assume stage-wise independence of the data process. A topic for future research is the generation of scenario trees in which individual scenarios can be built while considering interstate dependence. For example, a multi-level clustering scheme can be to exploit all sequences in the data set.
- For the MSOODN model, a test system could not be proven that had all elements modeled (DSS, DG, RS, SCB, OLTC, RV and L). Furthermore, the data availability for proving this model was limited. As a future topic, we recommend proving the model with a bigger test system that considers all the elements. Due to the time limitations, it was not possible for this thesis to compare the performance of the

FTCA and DTGFBA scenario trees although it will be one of the next topics to be developed in the future.

- Based on the literature review developed in this thesis, we were able to define that the approach most used in renewable energy systems optimization is the approach based on probability distances and decided to use the FTCA and DTGFBA in phase II of the methodology. As a future topic, we suggest implementing other algorithms of this approach that take into account considerations about the scenario trees generation who were outside the scope of this thesis.
- As the main objective of this thesis was the scenario tree generation, and the computational time to solve the MSWBVPP model was very short, we have not been concerned about the development of algorithms to solve the MSP models. However, running time was large for the MSOODN. As a future topic, we recommend developing optimization methods that takes into account the special structure of the MSP (e.g., branch and fix coordination, Bender, dual decomposition and proximal bundle methods, specialized interior point methods).
- The methodology developed in this thesis was only applied to two optimization problems in renewable energy systems. A topic for future research is the application of the methodology in other energy problems, e.g., capacity expansion planning, energy storage management, market clearing, optimal power flow, security-constrained economic dispatch.

7.3. Scientific Production

The work in this thesis is based on and/or has resulted in the following journals publications, scientific conferences, a research stay and a BSc thesis.

Publications:

- F.-Javier Heredia, Marlyn D. Cuadrado, Cristina Corchero, "On optimal participation in the electricity markets of wind power plants with battery energy storage systems", Computers and Operations Research, vol. 96: Elsevier, pp. 316-329, 08/2018. Published.
- F.-Javier Heredia, Marlyn D. Cuadrado, J.-Anton Sánchez, a guest article in the special issue "Integration and Control of Renewable Energy and Power Electronics for Future Power Systems" about the presentation at International Symposium on Mathematical Programming, Bordeaux. Working paper to be submitted.

- Marlyn Cuadrado, F.-Javier Heredia, "Scenario trees for the multistage stochastic wind battery virtual power plant model (MSWBVPP model)". Working paper to be submitted.
- Marlyn D. Cuadrado, Luigi Viola, F.-Javier Heredia, and Marcos J. Rider, "Multistage Stochastic Optimal Operation of Radial Distribution Networks". Working paper to be submitted.

Presentations:

- F.-Javier Heredia, Cristina Corchero, Marlyn D. Cuadrado,"On the optimal participation in electricity markets of wind power plants with battery energy storage systems", 28th European Conference on Operational Research, Poznan, Poland, pp. 322, 3-6/07/2016. Contribution: A fan based on historical real data and that applies a standard scenario reduction technique to the two-stage stochastic programming model for the optimal bid of a wind producer in both spot (DM and IM1) and ancillary services electricity markets (RM and IB).
- F.-Javier Heredia, Marlyn D. Cuadrado, "A multistage stochastic programming model for the optimal management of wind-BESS virtual power plants", WindFarms 2017, Madrid, Spain, 31/05-02/06/2017. Contribution: A scenario tree based on historical real data and applies the FTCA to a new MSP model for the optimal bid of a wind producer in both spot (DM and IM1) and ancillary services electricity markets (RM and IB).
- F.-Javier Heredia, Marlyn D. Cuadrado, J.-Anton Sánchez, "A Multistage Stochastic Programming Model for the Optimal Bid of Wind-BESS Virtual Power Plants to Electricity Markets", 4th International Conference on Optimization Methods and Software 2017, La Havana, 16-21/12/2017. Contribution: A new methodology for generating scenario trees, based on forecasting models and studying of the quality of the stochastic solution of a VSS.
- F.-Javier Heredia, Marlyn D. Cuadrado, J.-Anton Sánchez, "A multistage stochastic programming model for the optimal bid of a wind producer", 23rd International Symposium on Mathematical Programming, Bordeaux, 01-06/07/2018. Contribution: A methodology for generating a set of scenario trees based on forecasting; and a three-month horizon study of the quality of the stochastic solution of an RP and VSS.

Research stays:

- 2018: a three-month stay at the Universidade Estadual de Campinas. São Paulo, Brazil.

Advised BSc Thesis:

- Serra Castilla Roger, "Generació d'arbres d'escenaris per a problemes d'oferta òptima en mercats d'electricitat", Dept. of Statistics and Operations Research. F.-Javier Heredia and Marlyn Cuadrado, advisors. Barcelona, Universitat Politècnica de Catalunya, 2019.

Appendices

My Ph.D. is in operations research. I was interested in making things work better and using mathematics to help do that. So operations research is what I studied as an undergraduate and graduate student.

— *Alvin E. Roth*

A

Basic Probability Theory

Contents

A.1. Random Variables and Stochastic Process

Definition A.1.1. A *set-valued mapping* $F : X \rightrightarrows Y$ assigns to each element x of X one or more elements of Y, or possible none. The set of elements $y \in Y$ assigned by F to x is denoted by $F(x)$.

i) The *domain* of $F : X \rightrightarrows Y$ is the set $dom\, F = \{x \in X : f(x) \neq \emptyset\}$.

ii) The *range* of F is the set $range\, F = \{y \in Y : y \in F(x) \text{ for some } x \in X\}$.

iii) The *inverse mapping* F^{-1} is the set-valued function $F^{-1} : Y \rightrightarrows X$ denoted by

$$F^{-1}(y) = \{x \in X : y \in F(x)\}$$

iv) The *image* of the set $B \subset X$ by F is the set

$$F(B) = \bigcup_{x \in B} f(x) = \{y \in Y : F^{-1}(y) \cap B \neq \emptyset\}$$

iv) The *inverse image* of the set $C \subset Y$ (or pre-image of C) by F is the set

$$F^{-1}(C) = \bigcup_{y \in C} F^{-1}(y) = \{x \in X : F(x) \cap C \neq \emptyset\}$$

We adopt a compromise that consist in calling indifferently mapping or function the relation $F : X \to Y$ that assigns to each element x of a subset $dom\, F \subset X$, one element y of a subset $range\, F$ of Y, written $y = F(x)$, and is empty-valued on $X \backslash domF$. This is because the function $F : X \to Y$ considered in the sequel are defined on the full space X anyway. The inverse mapping of F, written F^{-1} is defined on the full space Y as a set-valued mapping.

Definition A.1.2. Let $(\Omega, \mathcal{B})$ and $(\Omega, \mathcal{C})$ be measurable spaces. A mapping $F : \Omega \to \Omega^{'}$ is said to be $\mathcal{B}/\mathcal{C}-$measurable is for each $C \in \mathcal{C}$, the pre-image $F^{-1}(C)$ is $\mathcal{B}-$measurable.

when $\Omega^{'} = \mathbb{R}$ with $\mathcal{C}$ the Borel sigma-algebra $\mathcal{B}(\mathbb{R})$, then $\mathcal{B}/\mathcal{C}-$measurable mapping is a real-valued mapping corresponding to *real-valued random variable*.

Definition A.1.3. A real-valued random variable f on the probability space $(\Omega, \mathcal{B}, \mathcal{P})$ is a real-valued mapping from Ω to $\mathbb{R}$ that is $\mathcal{B}/\mathcal{C}-$measurable.

Similarly, extended-real-value random variable f on the probability space $(\Omega, \mathcal{B}, P)$ correspond to mappings $f : \Omega \to \overline{\mathbb{R}}$ that are $\mathcal{B}/\mathcal{B}(\mathbb{R})-$measurable.

Random variables with values in $\mathbb{R}^k$ are called *random vectors*.

Definition A.1.4. The *natural filtration* associated to a sequence $f_1, \ldots, f_k$ of random variables is the family $\{\mathcal{F}_i : i = 0, \ldots, k\}$ of sub-sigma-algebras of $\mathcal{B}$ generated by the growing subcollections $\{f_1, \ldots, f_i\}$ or random variables.

Definition A.1.5. Let $(\Omega, \mathcal{B})$ be measurable space. A *function* $f : \Omega \to \mathbb{R}^n$ is *measurable* if for every open set $C \subset \mathbb{R}^n$, the pre-image $f^{-1}(C)$ is in $\mathcal{B}$. If f is closed-valued (the sets $f(x)$ are closed), an equivalent measurability condition is $f^{-1}(C) \in \mathcal{B}$ for every close set C.

A random variable whose value evolves over time is known as a *multivariate stochastic process*. A multivariate stochastic process ψ is defined as a collection of dependent random vectors $\psi = \{\psi_t\}_{t=1}^{T}$ such that, for each t in the index set T, ψ_t is a random vector. A multivariate stochastic process ψ can be *continuous* or *discrete* depending on whether its components random vector $\psi_t,\ t = 1, \ldots, T$ are continuous or discrete, respectively.

Statistics is the grammar of science.

— Karl Pearson

B

Other Results of the Scenario Generation Procedure

Contents

B.1. Validation of the Adjusted VARX-VAR models

The plots we use to validate the VARX model are the following:

(a) Residual Plots: is used to study if the variance seems to be constant and if there are any outliers in the residuals (homoscedasticity assumption). This plot looks for any creasing or decreasing trend in the residuals, which would be a clear indication of correlation could mean implies that the assumption of residual independence has been violated.

(b) Normal Quantile-Quantile Plot: is used to establish if the Gaussian distribution is appropriate for the residuals (normality assumption). If the points at the extreme

positions lie far from the reference line, this could be due to the presence of outliers or excess of kurtosis (heavy tails).

(c) ACF of the Residual: is a complete autocorrelation function which gives us values of auto-correlation of any series with its lagged values.

(d) PACF of the Residual: is a partial autocorrelation function. Basically, instead of finding correlations of present with lags like ACF, it finds a correlation of the residuals with the next lag value hence partial and not complete as we remove already found variations before we find the next correlation.

The plots of the items (c) and (d), all the lags must lie between the confidence bands to establish that they are no lag different from zero. This is the condition of independence of the residuals (independence assumption). We have to take into account that the confidence bands are built by assuming confidence of % 95, so for lags far from the origin, a small number can be outside the confidence bands by randomness.

B.1.1. Validation of the Adjusted VARX Models of the MTS for the MSWBVPP Model

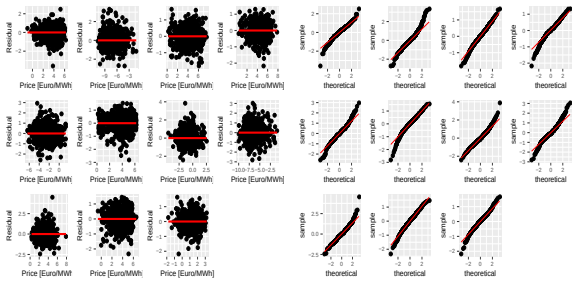

(a) Residual Plot. (b) Normal QQ-plot.

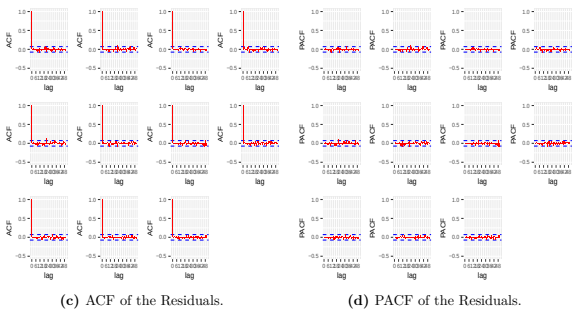

(c) ACF of the Residuals. (d) PACF of the Residuals.

Figura B.1.1: Validation of the Adjusted VARX Model for $\hat{\mathbf{F}}^D$.

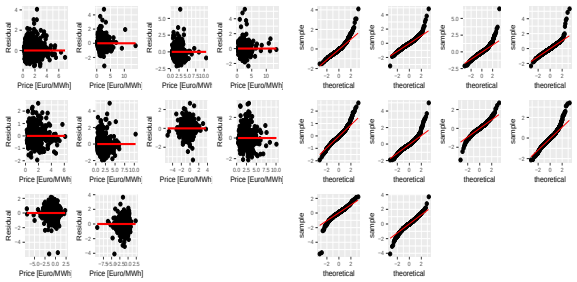

(a) Residual Plot. (b) Normal QQ-plot.

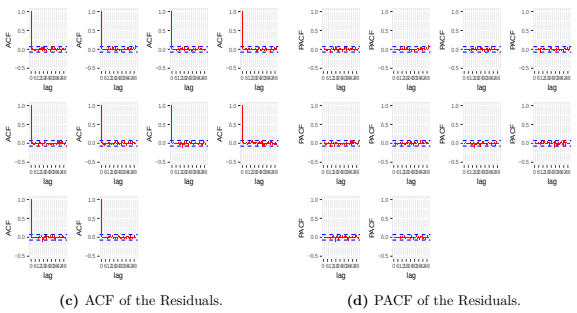

(c) ACF of the Residuals. (d) PACF of the Residuals.

Figura B.1.2: Validation of the Adjusted VARX Model for $\hat{\mathbf{F}}^R$.

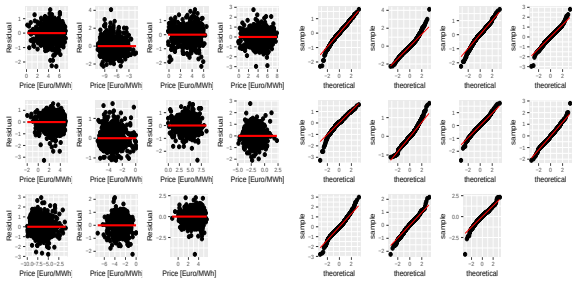

(a) Residual Plot. **(b)** Normal QQ-plot.

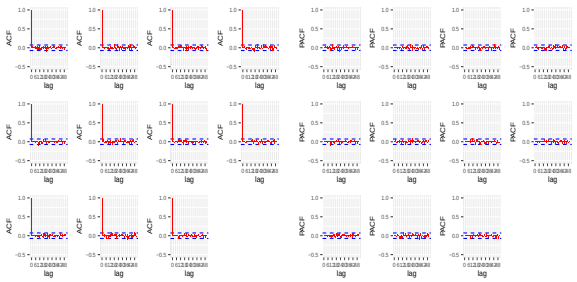

(c) ACF of the Residuals. **(d)** PACF of the Residuals.

Figura B.1.3: Validation of the Adjusted VARX Model for $\hat{\mathbf{F}}_1^I$.

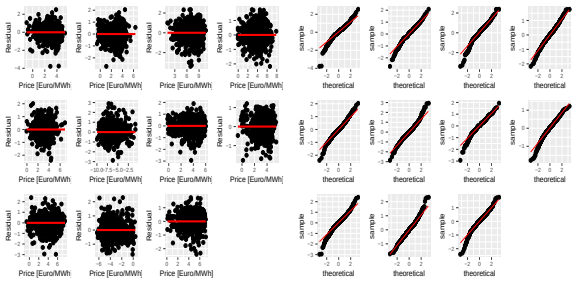

(a) Residual Plot. **(b)** Normal QQ-plot.

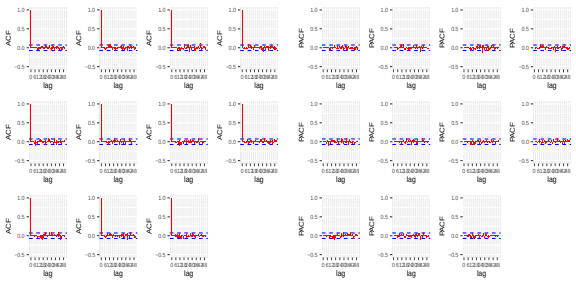

(c) ACF of the Residuals. **(d)** PACF of the Residuals.

Figura B.1.4: Validation of the Adjusted VARX Model for $\hat{\mathbf{F}}_2^I$.

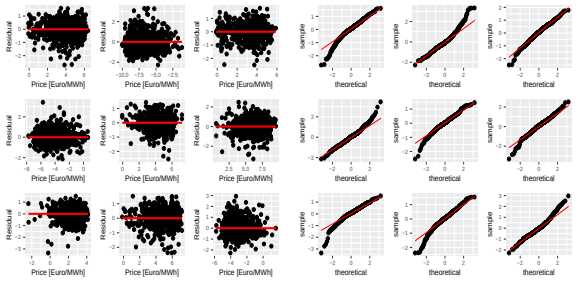

(a) Residual Plot. **(b)** Normal QQ-plot.

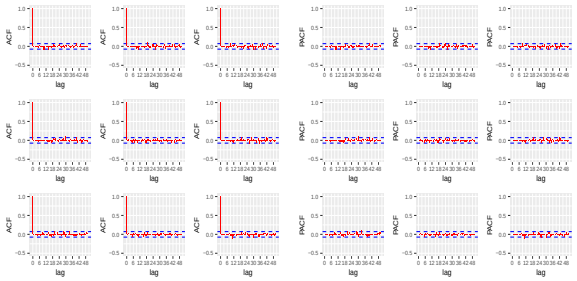

(c) ACF of the Residuals. **(d)** PACF of the Residuals.

Figura B.1.5: Validation of the Adjusted VARX Model for $\hat{\mathbf{F}}_3^I$.

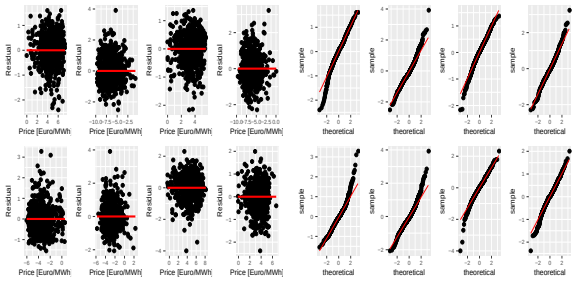

(a) Residual Plot. **(b)** Normal QQ-plot.

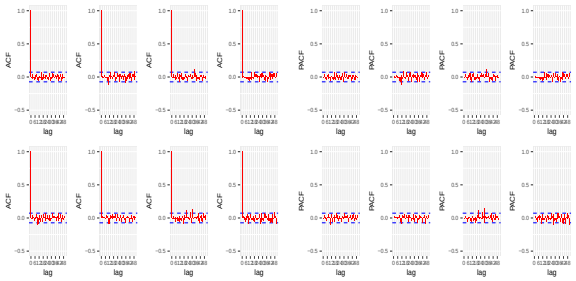

(c) ACF of the Residuals. **(d)** PACF of the Residuals.

Figura B.1.6: Validation of the Adjusted VARX Model for $\hat{\mathbf{F}}_4^I$.

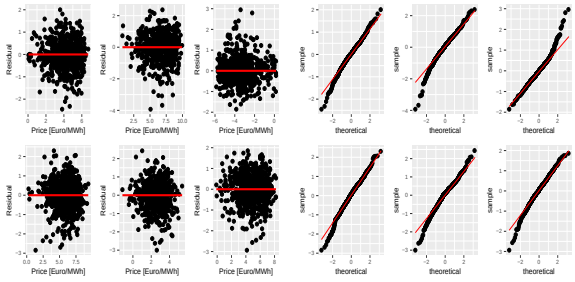

(a) Residual Plot. (b) Normal QQ-plot.

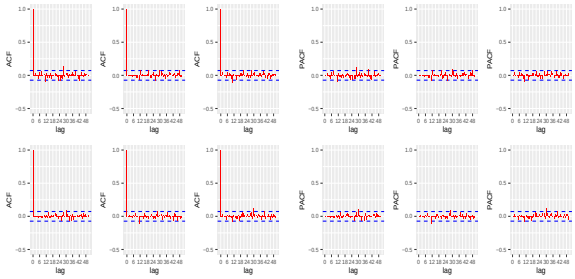

(c) ACF of the Residuals. (d) PACF of the Residuals.

Figura B.1.7: Validation of the Adjusted VARX Model for $\hat{\mathbf{F}}_5^I$.

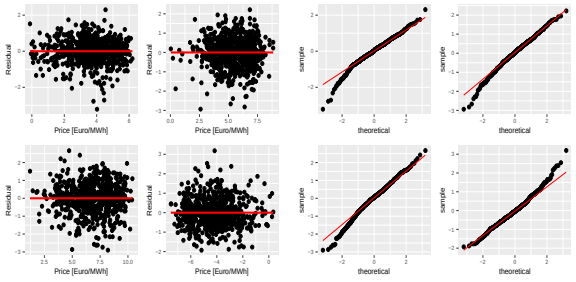

(a) Residual Plot. (b) Normal QQ-plot.

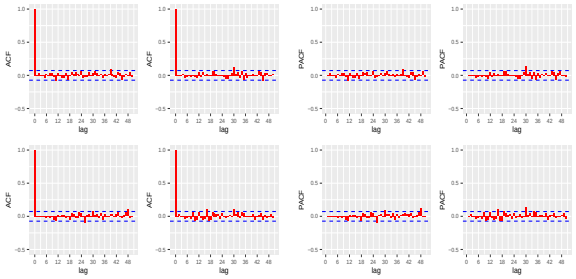

(c) ACF of the Residuals. (d) PACF of the Residuals.

Figura B.1.8: Validation of the Adjusted VARX Model for $\hat{\mathbf{F}}_6^I$.

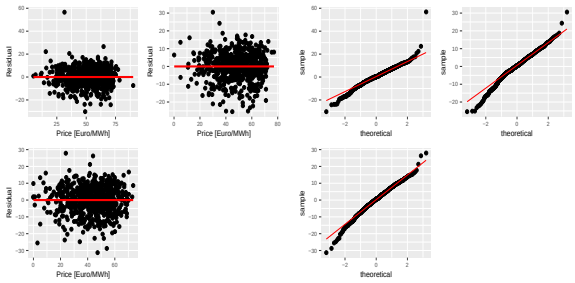

(a) Residual Plot. (b) Normal QQ-plot.

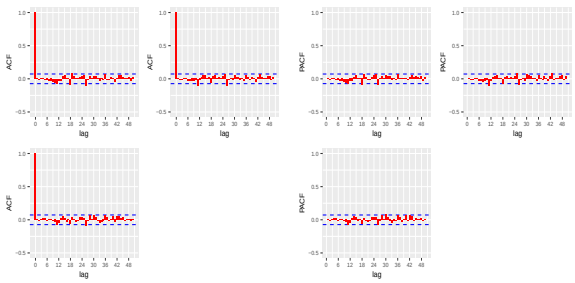

(c) ACF of the Residuals. (d) PACF of the Residuals.

Figura B.1.9: Validation of the Adjusted VARX Model for $\hat{\lambda}_7^I$.

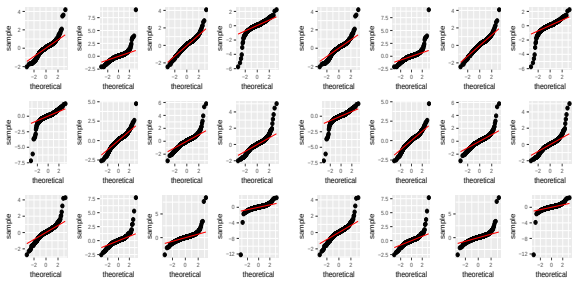

(a) Residual Plot. (b) Normal QQ-plot.

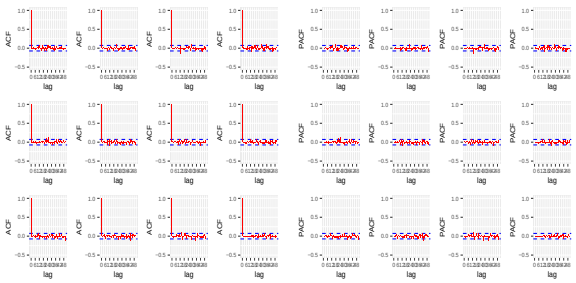

(c) ACF of the Residuals. (d) PACF of the Residuals.

Figura B.1.10: Validation of the Adjusted VARX Model for $\hat{\mathbf{F}}^{IB}$.

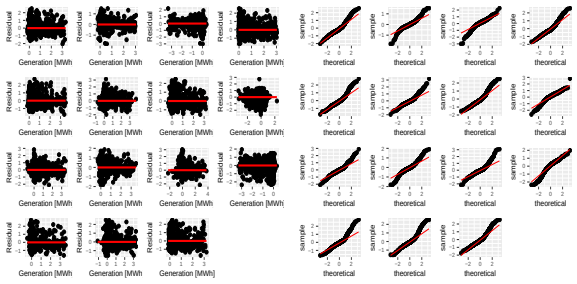

(a) Residual Plot. **(b)** Normal QQ-plot.

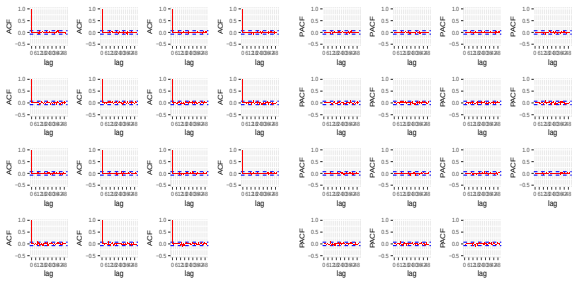

(c) ACF of the Residuals. **(d)** PACF of the Residuals.

Figura B.1.11: Validation of the Adjusted VARX Model for $\hat{\mathbf{F}}^{W}$.

B.1.2. Validation of the Adjusted VAR Models of the MTS for the MSOODN Model

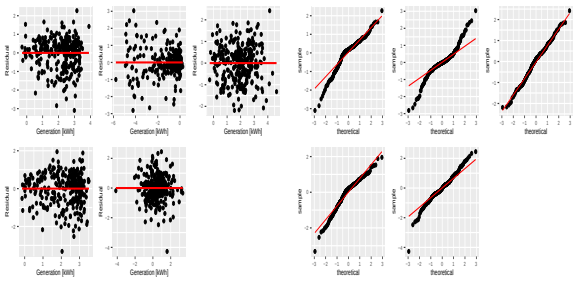

(a) Residual Plot. **(b)** Normal QQ-plot.

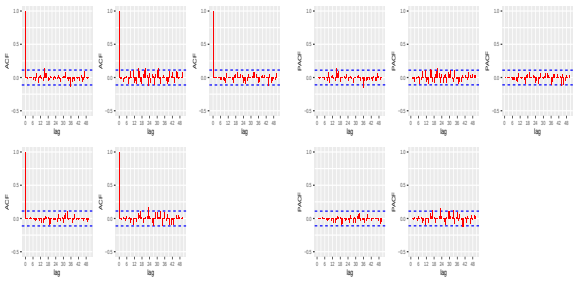

(c) ACF of the Residuals. **(d)** PACF of the Residuals.

Figura B.1.12: Validation of the Adjusted VAR Model for $\hat{\mathbf{F}}_{5}^{pv}$.

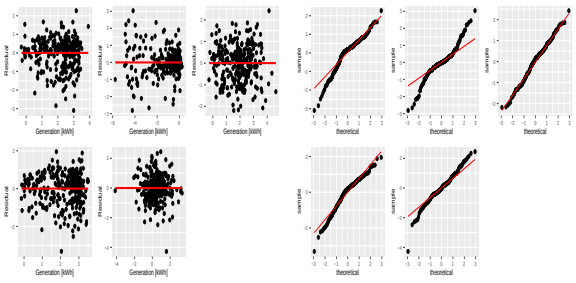

(a) Residual Plot. **(b)** Normal QQ-plot.

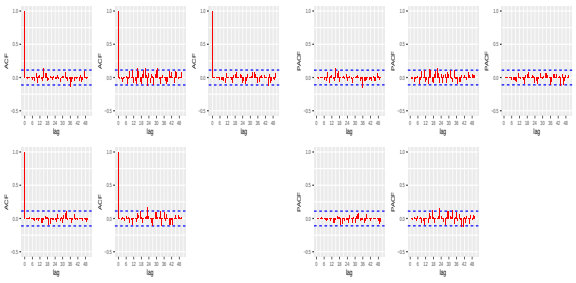

(c) ACF of the Residuals. **(d)** PACF of the Residuals.

Figura B.1.13: Validation of the Adjusted VAR Model for $\hat{\mathbf{F}}_{8}^{pv}$.

B.2. Adjusted ARIMA Models for the Active and Reactive Power Load

Serie	ARIMA Models	Models in Backshift Notation	Parameters P_1^D	Parameters for Q_1^D
$P_{1,1}^D$	ARIMA(0,1,1)	$(1-B)P_{1,1t}^D = c + (1-\theta_1 B)\varepsilon_{1,1t}$	$c = 0, \theta_1 = -0{,}3249$	$c = 0, \theta_1 = -0{,}3249$
$P_{1,2}^D$	ARIMA(0,1,0)	$(1-B)P_{1,2t}^D = c + \varepsilon_{1,2t}$	$c = 0$	$c = 0$
$P_{1,3}^D$	ARIMA(0,1,0)	$(1-B)P_{1,3t}^D = c + \varepsilon_{1,3t}$	$c = 0$	$c = 0$
$P_{1,4}^D$	ARIMA(0,1,0)	$(1-B)P_{1,4t}^D = c + \varepsilon_{1,4t}$	$c = 0$	$c = 0$
$P_{1,5}^D$	ARIMA(0,1,0)	$(1-B)P_{1,5t}^D = c + \varepsilon_{1,5t}$	$c = 0$	$c = 0$
$P_{1,6}^D$	ARIMA(0,1,0)	$(1-B)P_{1,6t}^D = c + \varepsilon_{1,6t}$	$c = 0$	$c = 0$
$P_{1,7}^D$	ARIMA(1,1,1)	$(1-\phi_1 B)(1-B)P_{1,7t}^D = c + (1+\theta_1 B)\varepsilon_{1,7t}$	$\phi_1 = 0{,}4534, c = 0, \theta_1 = -0{,}8761$	$\phi_1 = 0{,}4534, c = 0, \theta_1 = -0{,}8761$
$P_{1,8}^D$	ARIMA(1,0,0)	$(1-\phi_1 B)(1-B)P_{1,8t}^D = c + \varepsilon_{1,8t}$	$\phi_1 = 0{,}3141, c = 985{,}0170$	$\phi_1 = 0{,}3141, c = 20{,}4644$
$P_{1,9}^D$	ARIMA(0,1,2)	$(1-B)P_{1,9t}^D = c + (1+\theta_1 B+\theta_2 B^2)\varepsilon_{1,9t}$	$c = 0, \theta_1 = -0{,}9442, \theta_2 = 0{,}3208$	$c = 0, \theta_1 = -0{,}9442, \theta_2 = 0{,}3208$
$P_{1,10}^D$	ARIMA(2,0,0)	$(1-\phi_1 B-\phi_2 B^2)P_{1,10t}^D = c + \varepsilon_{1,10t}$	$\phi_1 = 0{,}3680, \phi_2 = 0{,}3109, c = 1125{,}267$	$\phi_1 = 0{,}3680, \phi_2 = 0{,}3109, c = 86{,}8250$
$P_{1,11}^D$	ARIMA(0,0,0)	$P_{1,11t}^D = c + \varepsilon_{1,11t}$	$c = 1092{,}3653$	$c = 77{,}4784$
$P_{1,12}^D$	ARIMA(0,1,1)	$(1-B)P_{1,12t}^D = c + (1+\theta_1 B)\varepsilon_{1,12t}$	$c = 0, \theta_1 = -0{,}6280$	$c = 0, \theta_1 = -0{,}6280$
$P_{1,13}^D$	ARIMA(0,0,0)	$P_{1,13t}^D = c + \varepsilon_{1,13t}$	$c = 1108{,}8210$	$c = 46{,}2996$
$P_{1,14}^D$	ARIMA(1,0,0)	$(1-\phi_1 B)P_{1,14t}^D = c + \varepsilon_{1,14t}$	$\phi_1 = 0{,}6288, c = 1184{,}7529$	$\phi_1 = 0{,}6288, c = 148{,}7075$
$P_{1,15}^D$	ARIMA(1,0,0)	$(1-\phi_1 B)P_{1,15t}^D = c + \varepsilon_{1,15t}$	$\phi_1 = 0{,}4737, c = 1218{,}9021$	$\phi_1 = 0{,}4737, c = 239{,}7831$
$P_{1,16}^D$	ARIMA(0,1,1)	$(1-B)P_{1,16t}^D = c + (1+\theta_1 B)\varepsilon_{1,16t}$	$c = 0, \theta_1 = -0{,}7338$	$c = 0, \theta_1 = -0{,}7338$
$P_{1,17}^D$	ARIMA(1,0,0)	$(1-\phi_1 B)P_{1,17t}^D = c + \varepsilon_{1,17t}$	$\phi_1 = 0{,}5162, c = 1149{,}1623$	$\phi_1 = 0{,}5162, c = 283{,}7119$
$P_{1,18}^D$	ARIMA(0,1,1)	$(1-B)P_{1,18t}^D = c + (1+\theta_1 B)\varepsilon_{1,18t}$	$c = 0, \theta_1 = -0{,}4834$	$c = 0, \theta_1 = -0{,}4834$
$P_{1,19}^D$	ARIMA(1,0,0)	$(1-\phi_1 B)P_{1,19t}^D = c + \varepsilon_{1,19t}$	$\phi_1 = 0{,}4022, c = 873{,}8628$	$\phi_1 = 0{,}4022, c = 137{,}0247$
$P_{1,20}^D$	ARIMA(0,1,1)	$(1-B)P_{1,20t}^D = c + (1+\theta_1 B)\varepsilon_{1,20t}$	$c = 0, \theta_1 = -0{,}5689$	$c = 0, \theta_1 = -0{,}5689$
$P_{1,21}^D$	ARIMA(0,1,0)	$(1-B)P_{1,21t}^D = c + \varepsilon_{1,21t}$	$c = 0$	$c = 0$
$P_{1,22}^D$	ARIMA(0,1,1)	$(1-B)P_{1,22t}^D = c + (1+\theta_1 B)\varepsilon_{1,22t}$	$c = 0, \theta_1 = -0{,}7232$	$c = 0, \theta_1 = -0{,}7232$
$P_{1,23}^D$	ARIMA(1,1,0)	$(1-\phi_1 B)(1-B)P_{1,23t}^D = c + \varepsilon_{1,23t}$	$\phi_1 = -0{,}5611, c = 0$	$\phi_1 = -0{,}5611, c = 0$
$P_{1,24}^D$	ARIMA(0,1,1)	$(1-B)P_{1,24t}^D = c + (1+\theta_1 B)\varepsilon_{1,24t}$	$c = 0, \theta_1 = -0{,}6950$	$c = 0, \theta_1 = -0{,}6950$

Cuadro B.2.1: Adjusted ARIMA Models for $\mathbf{P}_1^D$ and $\mathbf{Q}_1^D$.

Serie	ARIMA Models	Models in Backshift Notation	Parameters for P_2^D	Parameters for Q_2^D
$P_{1,1}^D$	ARIMA(0,1,2)	$(1-B)P_{1,1t}^D = c + (1-\theta_1 B-\theta_2 B^2)\varepsilon_{1,1t}$	$c = 0, \theta_1 = -1{,}0568, \theta_2 = 0{,}5870$	$c = 0, \theta_1 = -1{,}0568, \theta_2 = 0{,}5870$
$P_{1,2}^D$	ARIMA(0,1,1)	$(1-B)P_{1,2t}^D = c + (1+\theta_1 B)\varepsilon_{1,2t}$	$c = 0, \theta_1 = -0{,}4781$	$c = 0, \theta_1 = -0{,}4781$
$P_{1,3}^D$	ARIMA(0,1,1)	$(1-B)P_{1,3t}^D = c + (1+\theta_1 B)\varepsilon_{1,3t}$	$c = 0, \theta_1 = -0{,}6493$	$c = 0, \theta_1 = -0{,}6493$
$P_{1,4}^D$	ARIMA(1,1,0)	$(1-\phi_1 B)(1-B)P_{1,4t}^D = c + \varepsilon_{1,4t}$	$\phi_1 - 0{,}5533, c = 0$	$\phi_1 - 0{,}5533, c = 0$
$P_{1,5}^D$	ARIMA(0,1,1)	$(1-B)P_{1,5t}^D = c + (1+\theta_1 B)\varepsilon_{1,5t}$	$c = 0, \theta_1 = -0{,}6806$	$c = 0, \theta_1 = -0{,}6806$
$P_{1,6}^D$	ARIMA(0,1,1)	$(1-B)P_{1,6t}^D = c + (1+\theta_1 B)\varepsilon_{1,6t}$	$c = 0, \theta_1 = -0{,}6564$	$c = 0, \theta_1 = -0{,}6564$
$P_{1,7}^D$	ARIMA(0,0,0)	$P_{1,7t}^D = c + \varepsilon_{1,7t}$	$c = 772{,}1471$	$c = 479{,}9791$
$P_{1,8}^D$	ARIMA(0,0,0)	$P_{1,8t}^D = c + \varepsilon_{1,8t}$	$c = 945{,}5663$	$c = 351{,}4502$
$P_{1,9}^D$	ARIMA(0,0,0)	$P_{1,9t}^D = c + \varepsilon_{1,9t}$	$c = 1071{,}7147$	$c = 251{,}1326$
$P_{1,10}^D$	ARIMA(0,0,1)	$P_{1,10t}^D = c + (1+\theta_1 B)\varepsilon_{1,10t}$	$c = 1143{,}1315, \theta_1 = 0{,}4178$	$c = 189{,}3260, \theta_1 = 0{,}4178$
$P_{1,11}^D$	ARIMA(0,0,0)	$P_{1,11t}^D = c + \varepsilon_{1,11t}$	$c = 1159{,}2878$	$c = 154{,}9220$
$P_{1,12}^D$	ARIMA(0,1,1)	$(1-B)P_{1,12t}^D = c + (1+\theta_1 B)\varepsilon_{1,12t}$	$c = 0, \theta_1 = -0{,}8816$	$c = 0, \theta_1 = -0{,}8816$
$P_{1,13}^D$	ARIMA(0,0,0)	$P_{1,13t}^D = c + \varepsilon_{1,13t}$	$c = 1094{,}3815$	$c = 131{,}9316$
$P_{1,14}^D$	ARIMA(0,0,0)	$P_{1,14t}^D = c + \varepsilon_{1,14t}$	$c = 1029{,}9504$	$c = 128{,}6034$
$P_{1,15}^D$	ARIMA(0,0,0)	$P_{1,15t}^D = c + \varepsilon_{1,15t}$	$c = 956{,}1867$	$c = 131{,}0181$
$P_{1,16}^D$	ARIMA(0,0,0)	$P_{1,16t}^D = c + \varepsilon_{1,16t}$	$c = 881{,}8436$	$c = 141{,}1169$
$P_{1,17}^D$	ARIMA(0,1,1)	$(1-B)P_{1,17t}^D = c + (1+\theta_1 B)\varepsilon_{1,17t}$	$c = 0, \theta_1 = -0{,}8205$	$c = 0, \theta_1 = -0{,}8205$
$P_{1,18}^D$	ARIMA(0,0,0)	$P_{1,18t}^D = c + \varepsilon_{1,18t}$	$c = 760{,}2395$	$c = 185{,}4920$
$P_{1,19}^D$	ARIMA(0,0,0)	$P_{1,19t}^D = c + \varepsilon_{1,19t}$	$c = 714{,}1984$	$c = 206{,}1902$
$P_{1,20}^D$	ARIMA(0,0,2)	$P_{1,20t}^D = c + (1+\theta_1 B+\theta_2 B^2)\varepsilon_{1,20t}$	$c = 675{,}4775, \theta_1 = -0{,}0372, \theta_2 = 0{,}4806$	$c = 206{,}1902, \theta_1 = -0{,}0372, \theta_2 = 0{,}4806$
$P_{1,21}^D$	ARIMA(0,0,0)	$P_{1,21t}^D = c + \varepsilon_{1,21t}$	$c = 640{,}3886$	$c = 196{,}0186$
$P_{1,22}^D$	ARIMA(0,0,0)	$P_{1,22t}^D = c + \varepsilon_{1,22t}$	$c = 603{,}3126$	$c = 157{,}4372$
$P_{1,23}^D$	ARIMA(0,0,0)	$P_{1,23t}^D = c + \varepsilon_{1,23t}$	$c = 552{,}5695$	$c = 109{,}8067$
$P_{1,24}^D$	ARIMA(0,0,0)	$P_{1,24t}^D = c + \varepsilon_{1,24t}$	$c = 476{,}7002$	$c = 66{,}3320$

Cuadro B.2.2: Adjusted ARIMA Models for $\mathbf{P}_2^D$ and $\mathbf{Q}_2^D$.

Serie	ARIMA Models	Models in Backshift Notation	Parameters for P_3^D	Parameters for Q_3^D
$P_{1,1}^D$	ARIMA(0,0,0)	$P_{1,1t}^D = c + \varepsilon_{1,1t}$	$c = 345{,}5462$	$c = 115{,}3333$
$P_{1,2}^D$	ARIMA(0,0,0)	$P_{1,2t}^D = c + \varepsilon_{1,2t}$	$c = 297{,}0864$	$c = 222{,}2893$
$P_{1,3}^D$	ARIMA(0,1,1)	$(1-B)P_{1,3t}^D = c + (1+\theta_1 B)\varepsilon_{1,3t}$	$c = 0, \theta_1 = -0{,}7870$	$c = 0, \theta_1 = -0{,}7870$
$P_{1,4}^D$	ARIMA(0,0,0)	$P_{1,4t}^D = c + \varepsilon_{1,4t}$	$c = 310{,}1471$	$c = 377{,}0388$
$P_{1,5}^D$	ARIMA(0,1,1)	$(1-B)P_{1,5t}^D = c + (1+\theta_1 B)\varepsilon_{1,5t}$	$c = 0, \theta_1 = -0{,}3463$	$c = 0, \theta_1 = -0{,}3463$
$P_{1,6}^D$	ARIMA(0,1,1)	$(1-B)P_{1,6t}^D = c + (1+\theta_1 B)\varepsilon_{1,6t}$	$c = 0, \theta_1 = -0{,}7823$	$c = 0, \theta_1 = -0{,}7823$
$P_{1,7}^D$	ARIMA(0,1,1)	$(1-B)P_{1,7t}^D = c + (1+\theta_1 B)\varepsilon_{1,7t}$	$c = 0, \theta_1 = -0{,}6725$	$c = 0, \theta_1 = -0{,}6725$
$P_{1,8}^D$	ARIMA(0,0,0)	$P_{1,8t}^D = c + \varepsilon_{1,8t}$	$c = 887{,}0455$	$c = 203{,}3796$
$P_{1,9}^D$	ARIMA(0,1,1)	$(1-B)P_{1,9t}^D = c + (1+\theta_1 B)\varepsilon_{1,9t}$	$c = 0, \theta_1 = -0{,}8286$	$c = 0, \theta_1 = -0{,}8286$
$P_{1,10}^D$	ARIMA(0,1,1)	$(1-B)P_{1,10t}^D = c + (1+\theta_1 B)\varepsilon_{1,10t}$	$c = 0, \theta_1 = -0{,}7576$	$c = 0, \theta_1 = -0{,}7576$
$P_{1,11}^D$	ARIMA(0,0,0)	$P_{1,11t}^D = c + \varepsilon_{1,11t}$	$c = 1068{,}6999$	$c = 143{,}5188$
$P_{1,12}^D$	ARIMA(0,1,1)	$(1-B)P_{1,12t}^D = c + (1+\theta_1 B)\varepsilon_{1,12t}$	$c = 0, \theta_1 = -0{,}7125$	$c = 0, \theta_1 = -0{,}7125$
$P_{1,13}^D$	ARIMA(0,1,1)	$(1-B)P_{1,13t}^D = c + (1+\theta_1 B)\varepsilon_{1,13t}$	$c = 0, \theta_1 = -0{,}7490$	$c = 0, \theta_1 = -0{,}7490$
$P_{1,14}^D$	ARIMA(0,1,1)	$(1-B)P_{1,14t}^D = c + (1+\theta_1 B)\varepsilon_{1,14t}$	$c = 0, \theta_1 = -0{,}7259$	$c = 0, \theta_1 = -0{,}7259$
$P_{1,15}^D$	ARIMA(1,1,3)	$(1-\phi_1 B)P_{1,15t}^D = c + (1+\theta_1 B+\theta_2 B^2+\theta_3 B^3)\varepsilon_{1,15t}$	$\phi_1 = -0{,}5305, c = 0, \theta_1 = 0{,}6132, \theta_2 = -0{,}2877, \theta_3 = -0{,}8248$	$\phi_1 = -0{,}5305, c = 0, \theta_1 = 0{,}6132, \theta_2 = -0{,}2877, \theta_3 = -0{,}8248$
$P_{1,16}^D$	ARIMA(0,1,2)	$(1-B)P_{1,16t}^D = c + (1+\theta_1 B+\theta_2 B^2)\varepsilon_{1,16t}$	$c = 0, \theta_1 = -0{,}4104, \theta_2 = -0{,}3078$	$c = 0, \theta_1 = -0{,}4104, \theta_2 = -0{,}3078$
$P_{1,17}^D$	ARIMA(0,1,1)	$(1-B)P_{1,17t}^D = c + (1+\theta_1 B)\varepsilon_{1,17t}$	$c = 0, \theta_1 = -0{,}6842$	$c = 0, \theta_1 = -0{,}6842$
$P_{1,18}^D$	ARIMA(0,0,0)	$P_{1,18t}^D = c + \varepsilon_{1,18t}$	$c = 828{,}8885$	$c = 14{,}7346$
$P_{1,19}^D$	ARIMA(2,0,0)	$(1-\phi_1 B-\phi_2 B^2)P_{1,19t}^D = c + \varepsilon_{1,19t}$	$\phi_1 = -0{,}4090, \phi_2 = 0{,}5976, c = 730{,}4430$	$\phi_1 = -0{,}4090, \phi_2 = 0{,}5976, c = 161{,}9262$
$P_{1,20}^D$	ARIMA(0,0,0)	$P_{1,20t}^D = c + \varepsilon_{1,20t}$	$c = 623{,}5259$	$c = 272{,}7485$
$P_{1,21}^D$	ARIMA(0,0,1)	$P_{1,21t}^D = c + (1+\theta_1 B)\varepsilon_{1,21t}$	$c = 553{,}6742, \theta_1 = -0{,}7853$	$c = 264{,}2963, \theta_1 = -0{,}7853$
$P_{1,22}^D$	ARIMA(0,0,1)	$P_{1,22t}^D = c + (1+\theta_1 B)\varepsilon_{1,22t}$	$c = 496{,}3446, \theta_1 = -0{,}5305$	$c = 124{,}6403, \theta_1 = -0{,}5305$
$P_{1,23}^D$	ARIMA(0,0,0)	$P_{1,23t}^D = c + \varepsilon_{1,23t}$	$c = 443{,}3808$	$c = 75{,}4726$
$P_{1,24}^D$	ARIMA(0,0,0)	$P_{1,24t}^D = c + \varepsilon_{1,24t}$	$c = 396{,}1133$	$c = 268{,}2114$

Cuadro B.2.3: Adjusted ARIMA Models for $\mathbf{P}_3^D$ and $\mathbf{Q}_3^D$.

Serie	ARIMA Models	Models in Backshift Notation	Parameters for P_4^D	Parameters for Q_4^D
$P_{1,1}^D$	ARIMA(0,0,0)	$P_{1,1t}^D = c + \varepsilon_{1,1t}$	$c = 368{,}7279$	$c = 497{,}1727$
$P_{1,2}^D$	ARIMA(0,1,1)	$(1-B)P_{1,2t}^D = c + (1+\theta_1 B)\varepsilon_{1,2t}$	$c = 0, \theta_1 = -0{,}5792$	$c = 0, \theta_1 = -0{,}5792$
$P_{1,3}^D$	ARIMA(0,1,1)	$(1-B)P_{1,3t}^D = c + (1+\theta_1 B)\varepsilon_{1,3t}$	$c = 0, \theta_1 = -0{,}4212$	$c = 0, \theta_1 = -0{,}4212$
$P_{1,4}^D$	ARIMA(1,1,0)	$(1-\phi_1 B)(1-B)P_{1,4t}^D = c + \varepsilon_{1,4t}$	$\phi_1 = -0{,}3603, c = 0$	$\phi_1 = -0{,}3603, c = 0$
$P_{1,5}^D$	ARIMA(1,1,0)	$(1-\phi_1 B)(1-B)P_{1,5t}^D = c + \varepsilon_{1,5t}$	$\phi_1 = -0{,}4974, c = 0$	$\phi_1 = -0{,}4974, c = 0$
$P_{1,6}^D$	ARIMA(1,1,0)	$(1-\phi_1 B)(1-B)P_{1,6t}^D = c + \varepsilon_{1,6t}$	$\phi_1 = -0{,}5887, c = 0$	$\phi_1 = -0{,}5887, c = 0$
$P_{1,7}^D$	ARIMA(0,0,0)	$P_{1,7t}^D = c + \varepsilon_{1,7t}$	$c = 786{,}1083$	$c = 191{,}1949$
$P_{1,8}^D$	ARIMA(0,0,0)	$P_{1,8t}^D = c + \varepsilon_{1,8t}$	$c = 946{,}8231$	$c = 95{,}6265$
$P_{1,9}^D$	ARIMA(0,0,0)	$P_{1,9t}^D = c + \varepsilon_{1,9t}$	$c = 1056{,}7725$	$c = 18{,}3250$
$P_{1,10}^D$	ARIMA(0,0,0)	$P_{1,10t}^D = c + \varepsilon_{1,10t}$	$c = 1107{,}8540$	$c = 31{,}0283$
$P_{1,11}^D$	ARIMA(0,0,0)	$P_{1,11t}^D = c + \varepsilon_{1,11t}$	$c = 1118{,}4443$	$c = 45{,}9321$
$P_{1,12}^D$	ARIMA(0,0,1)	$P_{1,12t}^D = c + (1+\theta_1 B)\varepsilon_{1,12t}$	$c = 1114{,}9931, \theta_1 = -0{,}6144$	$c = 20{,}1484, \theta_1 = -0{,}6144$
$P_{1,13}^D$	ARIMA(0,0,1)	$P_{1,13t}^D = c + (1+\theta_1 B)\varepsilon_{1,13t}$	$c = 1096{,}5193, \theta_1 = -0{,}5952$	$c = 52{,}3375, \theta_1 = -0{,}5952$
$P_{1,14}^D$	ARIMA(0,0,0)	$P_{1,14t}^D = c + \varepsilon_{1,14t}$	$c = 1082{,}5050$	$c = 158{,}8550$
$P_{1,15}^D$	ARIMA(1,0,0)	$(1-\phi_1 B)P_{1,15t}^D = c + \varepsilon_{1,15t}$	$\phi_1 = 0{,}3363, c = 1051{,}5891$	$\phi_1 = 0{,}3363, c = 269{,}2443$
$P_{1,16}^D$	ARIMA(0,0,0)	$P_{1,16t}^D = c + \varepsilon_{1,16t}$	$c = 992{,}9066$	$c = 354{,}3868$
$P_{1,17}^D$	ARIMA(0,0,0)	$P_{1,17t}^D = c + \varepsilon_{1,17t}$	$c = 885{,}0801$	$c = 383{,}1718$
$P_{1,18}^D$	ARIMA(2,0,0)	$(1-\phi_1 B-\phi_2 B^2)P_{1,18t}^D = c + \varepsilon_{1,18t}$	$\phi_1 = -0{,}4612, \phi_2 = -0{,}2973, c = 740{,}5262$	$\phi_1 = -0{,}4612, \phi_2 = -0{,}2973, c = 354{,}7861$
$P_{1,19}^D$	ARIMA(0,0,0)	$P_{1,19t}^D = c + \varepsilon_{1,19t}$	$c = 577{,}8388$	$c = 287{,}8005$
$P_{1,20}^D$	ARIMA(0,0,0)	$P_{1,20t}^D = c + \varepsilon_{1,20t}$	$c = 437{,}2399$	$c = 211{,}8423$
$P_{1,21}^D$	ARIMA(2,0,2)	$(1-\phi_1 B-\phi_2 B^2)P_{1,21t}^D = c + (1+\theta_1 B+\theta_2 B^2)\varepsilon_{1,21t}$	$\phi_1 = -1{,}6529, \phi_2 = -0{,}8534, c = 344{,}4084, \theta_1 = 1{,}8762, \theta_2 = 0{,}8818$	$\phi_1 = -1{,}6529, \phi_2 = -0{,}8534, c = 149{,}5802, \theta_1 = 1{,}8762, \theta_2 = 0{,}8818$
$P_{1,22}^D$	ARIMA(0,0,0)	$P_{1,22t}^D = c + \varepsilon_{1,22t}$	$c = 304{,}1120$	$c = 114{,}1795$
$P_{1,23}^D$	ARIMA(0,0,0)	$P_{1,23t}^D = c + \varepsilon_{1,23t}$	$c = 299{,}2826$	$c = 108{,}7483$
$P_{1,24}^D$	ARIMA(1,0,0)	$(1-\phi_1 B)P_{1,24t}^D = c + \varepsilon_{1,24t}$	$\phi_1 = 0{,}3041, c = 313{,}2272$	$\phi_1 = 0{,}3041, c = 136{,}5354$

Cuadro B.2.4: Adjusted ARIMA Models for $\mathbf{P}_4^D$ and $\mathbf{Q}_4^D$.

Serie	ARIMA Models	Models in Backshift Notation	Parameters for P_5^D	Parameters for Q_5^D
$P_{1,1}^D$	ARIMA(1,0,0)	$(1-\phi_1 B)P_{1,1t}^D = c + \varepsilon_{1,1t}$	$\phi_1 = 0{,}6185, c = 333{,}1652$	$\phi_1 = 0{,}6185, c = 168{,}6776$
$P_{1,2}^D$	ARIMA(1,0,1)	$(1-\phi_1 B)P_{1,2t}^D = c + (1+\theta_1 B)\varepsilon_{1,2t}$	$\phi_1 = 0{,}8737, c = 261{,}7695, \theta_1 = -0{,}3998$	$\phi_1 = 0{,}8737, c = 109{,}6354, \theta_1 = -0{,}3998$
$P_{1,3}^D$	ARIMA(0,1,1)	$(1-B)P_{1,3t}^D = c + (1+\theta_1 B)\varepsilon_{1,3t}$	$c = 0, \theta_1 = -0{,}5571$	$c = 0, \theta_1 = -0{,}5571$
$P_{1,4}^D$	ARIMA(1,1,0)	$(1-\phi_1 B)(1-B)P_{1,4t}^D = c + \varepsilon_{1,4t}$	$\phi_1 = -0{,}4788, c = 0$	$\phi_1 = -0{,}4788, c = 0$
$P_{1,5}^D$	ARIMA(0,1,0)	$(1-B)P_{1,5t}^D = c + \varepsilon_{1,5t}$	$c = 0$	$c = 0$
$P_{1,6}^D$	ARIMA(0,1,1)	$(1-B)P_{1,6t}^D = c + (1+\theta_1 B)\varepsilon_{1,6t}$	$c = 0, \theta_1 = -0{,}5951$	$c = 0, \theta_1 = -0{,}5951$
$P_{1,7}^D$	ARIMA(0,0,0)	$P_{1,7t}^D = c + \varepsilon_{1,7t}$	$c = 667{,}6731$	$c = 418{,}5879$
$P_{1,8}^D$	ARIMA(0,0,1)	$P_{1,8t}^D = c + (1+\theta_1 B)\varepsilon_{1,8t}$	$c = 851{,}7040, \theta_1 = 0{,}358$	$c = 485{,}6111, \theta_1 = 0{,}358$
$P_{1,9}^D$	ARIMA(0,0,1)	$P_{1,9t}^D = c + (1+\theta_1 B)\varepsilon_{1,9t}$	$c = 980{,}2221, \theta_1 = 0{,}3355$	$c = 434{,}7019, \theta_1 = 0{,}3355$
$P_{1,10}^D$	ARIMA(0,0,0)	$P_{1,10t}^D = c + \varepsilon_{1,10t}$	$c = 1041{,}3964$	$c = 277{,}0536$
$P_{1,11}^D$	ARIMA(0,0,0)	$P_{1,11t}^D = c + \varepsilon_{1,11t}$	$c = 1060{,}5196$	$c = 92{,}9920$
$P_{1,12}^D$	ARIMA(4,0,0)	$(1-\phi_1 B-\phi_2 B^2-\phi_3 B^3-\phi_4 B^4)(1-B)P_{1,12t}^D = c + \varepsilon_{1,12t}$	$\phi_1 = -0{,}0425, \phi_2 = -0{,}4154, \phi_3 = -0{,}2163, \phi_4 = -0{,}5291, c = 1061{,}4256$	$\phi_1 = -0{,}0425, \phi_2 = -0{,}4154, \phi_3 = -0{,}2163, \phi_4 = -0{,}5291, c = 36{,}0064$
$P_{1,13}^D$	ARIMA(0,0,0)	$P_{1,13t}^D = c + \varepsilon_{1,13t}$	$c = 1063{,}4044$	$c = 31{,}1806$
$P_{1,14}^D$	ARIMA(0,0,1)	$P_{1,14t}^D = c + (1+\theta_1 B)\varepsilon_{1,14t}$	$c = 1072{,}5577, \theta_1 = 0{,}3421$	$c = 108{,}2635, \theta_1 = 0{,}3421$
$P_{1,15}^D$	ARIMA(0,0,0)	$P_{1,15t}^D = c + \varepsilon_{1,15t}$	$c = 1065{,}4964$	$c = 305{,}1137$
$P_{1,16}^D$	ARIMA(0,0,0)	$P_{1,16t}^D = c + \varepsilon_{1,16t}$	$c = 1024{,}3734$	$c = 1024{,}3734$
$P_{1,17}^D$	ARIMA(0,0,0)	$P_{1,17t}^D = c + \varepsilon_{1,17t}$	$c = 928{,}9658$	$c = 479{,}2664$
$P_{1,18}^D$	ARIMA(0,0,0)	$P_{1,18t}^D = c + \varepsilon_{1,18t}$	$c = 786{,}1470$	$c = 506{,}6386$
$P_{1,19}^D$	ARIMA(1,0,0)	$(1-\phi_1 B)P_{1,19t}^D = c + \varepsilon_{1,19t}$	$\phi_1 = 0{,}4875, c = 629{,}7174$	$\phi_1 = 0{,}4875, c = 380{,}7409$
$P_{1,20}^D$	ARIMA(0,0,1)	$P_{1,20t}^D = c + (1+\theta_1 B)\varepsilon_{1,20t}$	$c = 491{,}5584, \theta_1 = 0{,}3522$	$c = 215{,}8650, \theta_1 = 0{,}3522$
$P_{1,21}^D$	ARIMA(0,0,0)	$P_{1,21t}^D = c + \varepsilon_{1,21t}$	$c = 407{,}3960$	$c = 55{,}2050$
$P_{1,22}^D$	ARIMA(0,0,1)	$P_{1,22t}^D = c + (1+\theta_1 B)\varepsilon_{1,22t}$	$c = 378{,}9702, \theta_1 = 0{,}4186$	$c = 72{,}0219, \theta_1 = 0{,}4186$
$P_{1,23}^D$	ARIMA(1,0,0)	$(1-\phi_1 B)P_{1,23t}^D = c + \varepsilon_{1,23t}$	$\phi_1 = 0{,}4400, c = 383{,}6491$	$\phi_1 = 0{,}4400, c = 148{,}8331$
$P_{1,24}^D$	ARIMA(1,0,0)	$(1-\phi_1 B)P_{1,24t}^D = c + \varepsilon_{1,24t}$	$\phi_1 = 0{,}3914, c = 384{,}0515$	$\phi_1 = 0{,}3914, c = 153{,}8799$

Cuadro B.2.5: Adjusted ARIMA Models for $\mathbf{P}_5^D$ and $\mathbf{Q}_5^D$.

B.3. Sets of Scenarios for the MSWBVPP Model

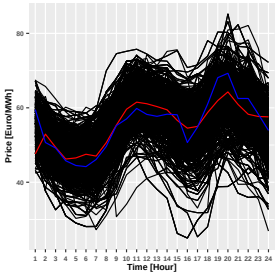

(a) Friday 15-January-2016.

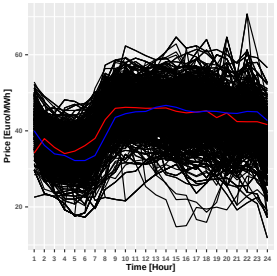

(b) Monday 06-June-2016.

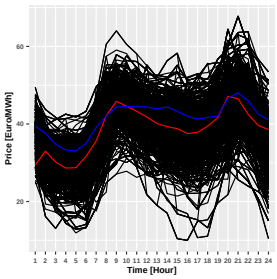

(c) Sunday 16-October-2016.

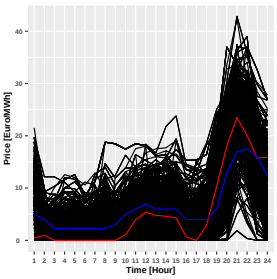

(d) Thursday 17-November-2016.

Figura B.3.1: Some scenario sets for $\boldsymbol{\lambda}^D$ with 1000 scenarios.

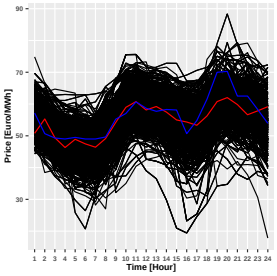

(a) Friday 15-January-2016.

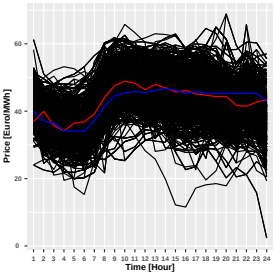

(b) Monday 06-June-2016.

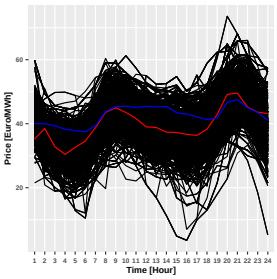

(c) Sunday 16-October-2016.

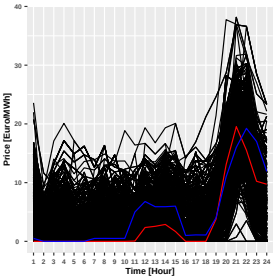

(d) Thursday 17-November-2016.

Figura B.3.2: Some scenario sets for $\boldsymbol{\lambda}_1^I$ with 1000 scenarios.

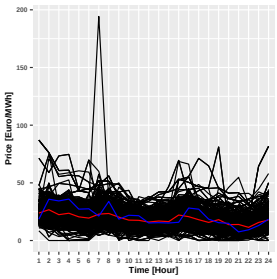

(a) Friday 15-January-2016.

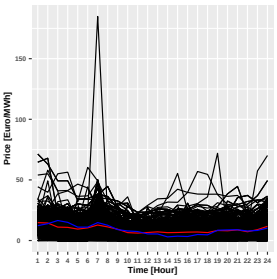

(b) Monday 06-June-2016.

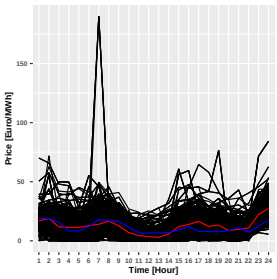

(c) Sunday 16-October-2016.

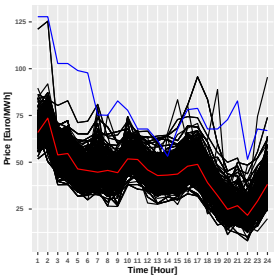

(d) Thursday 17-November-2016.

Figura B.3.3: Some scenario sets for $\boldsymbol{\lambda}^R$ with 1000 scenarios.

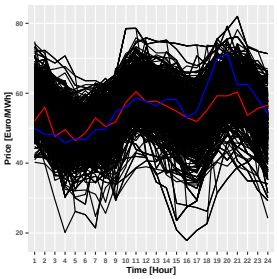

(a) Friday 15-January-2016.

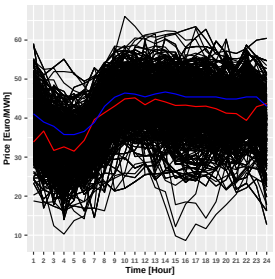

(b) Monday 06-June-2016.

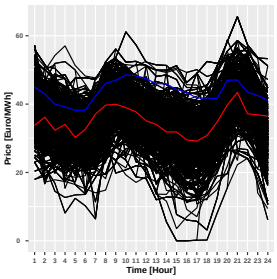

(c) Sunday 16-October-2016.

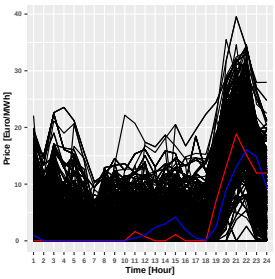

(d) Thursday 17-November-2016.

Figura B.3.4: Some scenario sets for $\boldsymbol{\lambda}_2^I$ with 1000 scenarios.

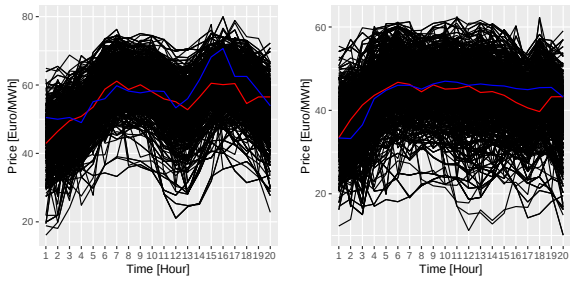

(a) Friday 15-January-2016. (b) Monday 06-June-2016.

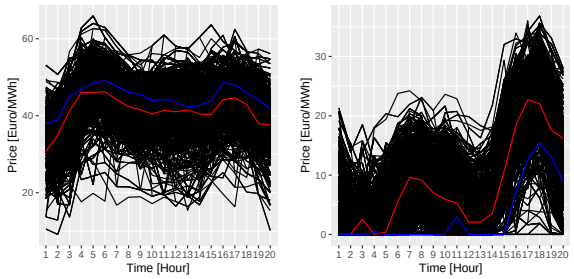

(c) Sunday 16-October-2016. (d) Thursday 17-November-2016.

Figura B.3.5: Some scenario sets for $\boldsymbol{\lambda}_3^I$ with 1000 scenarios.

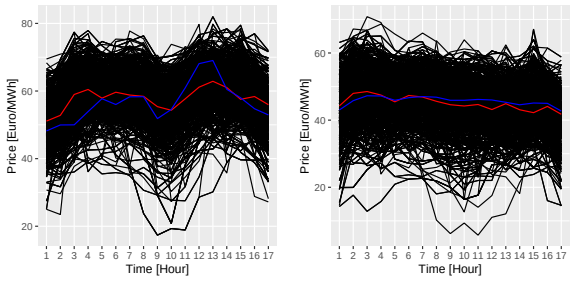

(a) Friday 15-January-2016. (b) Monday 06-June-2016.

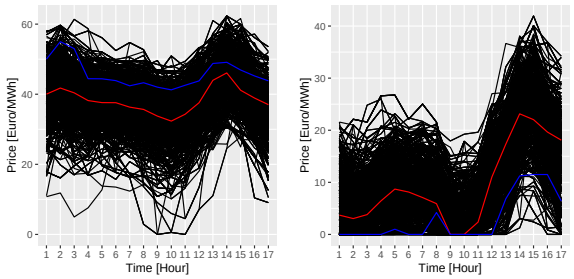

(c) Sunday 16-October-2016. (d) Thursday 17-November-2016.

Figura B.3.6: Some scenario sets for $\boldsymbol{\lambda}_4^I$ with 1000 scenarios.

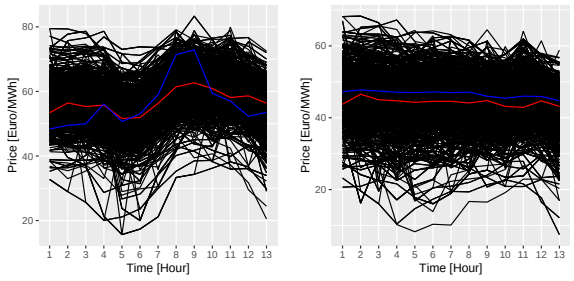

(a) Friday 15-January-2016. (b) Monday 06-June-2016.

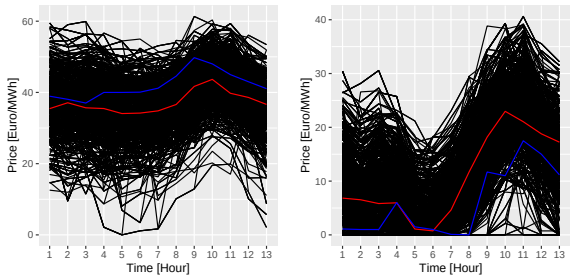

(c) Sunday 16-October-2016. (d) Thursday 17-November-2016.

Figura B.3.7: Some scenario sets for $\boldsymbol{\lambda}_5^I$ with 1000 scenarios.

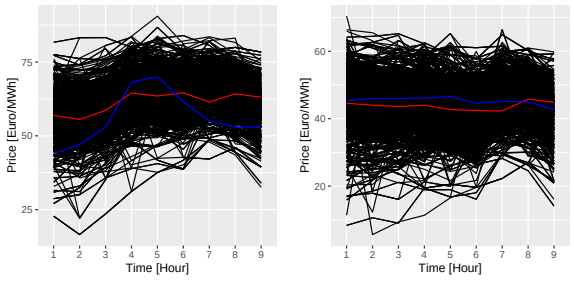

(a) Friday 15-January-2016. (b) Monday 06-June-2016.

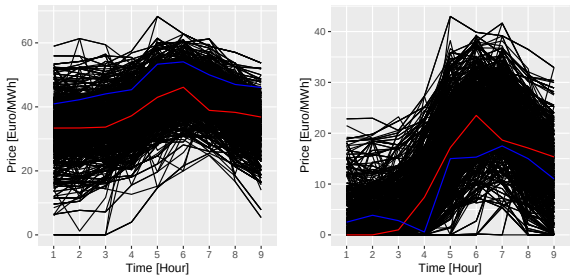

(c) Sunday 16-October-2016. (d) Thursday 17-November-2016.

Figura B.3.8: Some scenario sets for $\boldsymbol{\lambda}_6^I$ with 1000 scenarios.

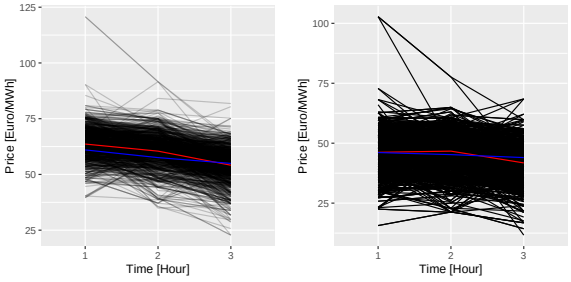

(a) Friday 15-January-2016. (b) Monday 06-June-2016.

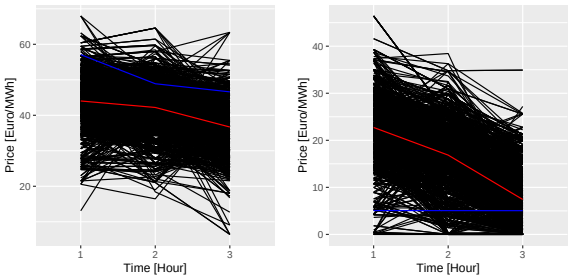

(c) Sunday 16-October-2016. (d) Thursday 17-November-2016.

Figura B.3.9: Some scenario sets for $\boldsymbol{\lambda}_7^I$ with 1000 scenarios.

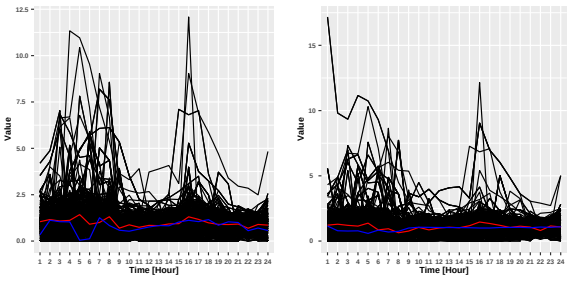

(a) Friday 15-January-2016. (b) Monday 06-June-2016.

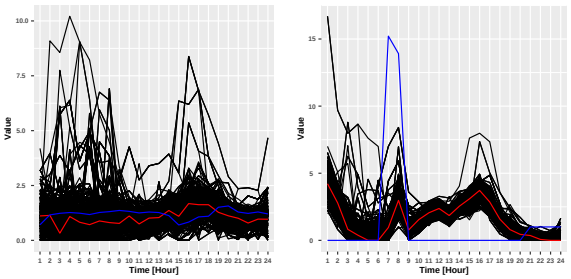

(c) Sunday 16-October-2016. (d) Thursday 17-November-2016.

Figura B.3.10: Some scenario sets for $\boldsymbol{\lambda}^{IB}$ with 1000 scenarios.

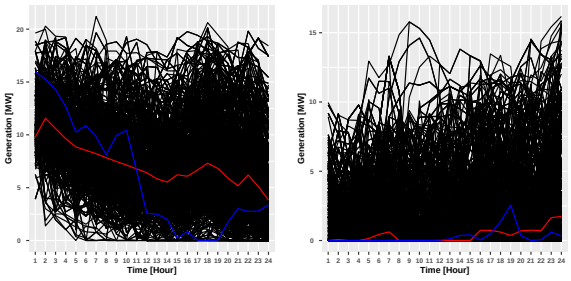

(a) Friday 15-January-2016. (b) Monday 06-June-2016.

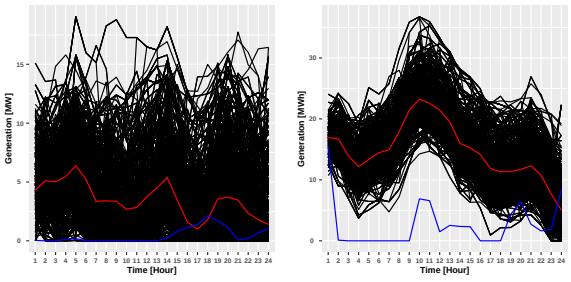

(c) Sunday 16-October-2016. (d) Thursday 17-November-2016.

Figura B.3.11: Some scenario sets for $\mathbf{P}^W$ with 1000 scenarios.

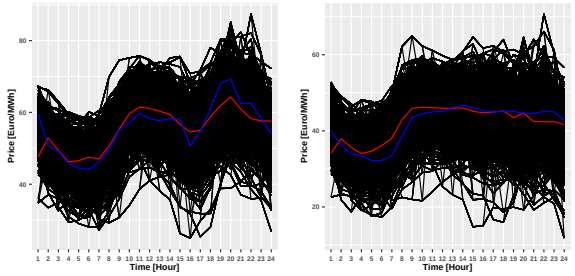

(a) Friday 15-January-2016. **(b)** Monday 06-June-2016.

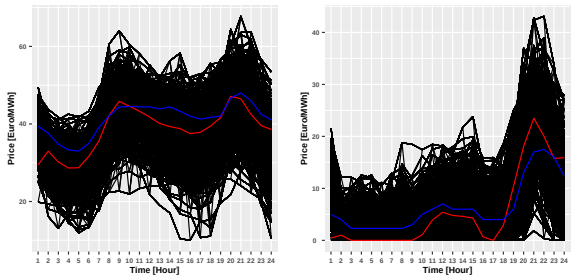

(c) Sunday 16-October-2016. **(d)** Thursday 17-November-2016.

Figura B.3.12: Some scenario sets for $\boldsymbol{\lambda}^D$ with 10000 scenarios.

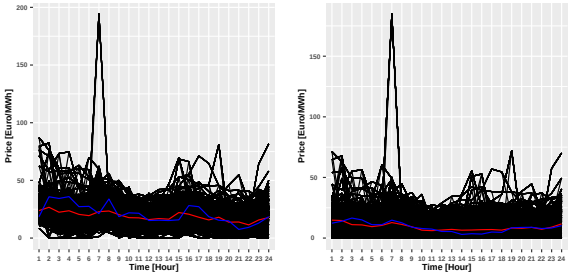

(a) Friday 15-January-2016. **(b)** Monday 06-June-2016.

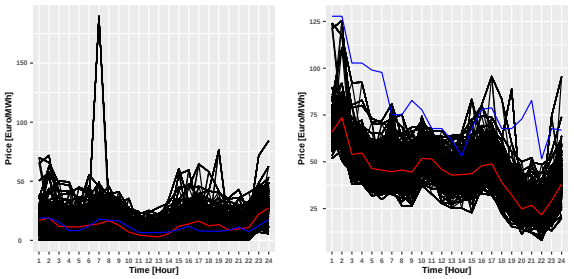

(c) Sunday 16-October-2016. **(d)** Thursday 17-November-2016.

Figura B.3.13: Some scenario sets for $\boldsymbol{\lambda}^R$ with 10000 scenarios.

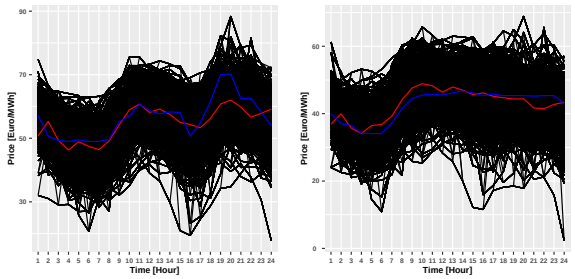

(a) Friday 15-January-2016. **(b)** Monday 06-June-2016.

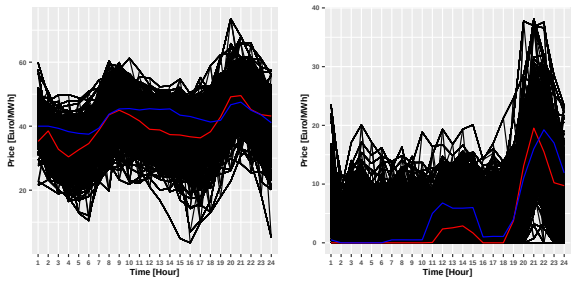

(c) Sunday 16-October-2016. **(d)** Thursday 17-November-2016.

Figura B.3.14: Some scenario sets for $\boldsymbol{\lambda}_1^I$ with 10000 scenarios.

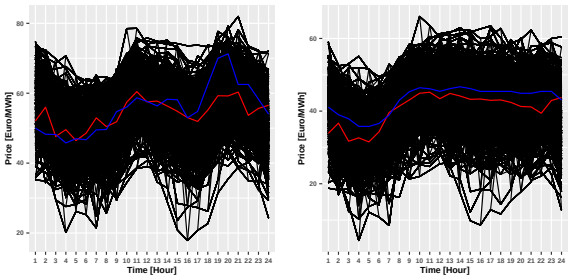

(a) Friday 15-January-2016. **(b)** Monday 06-June-2016.

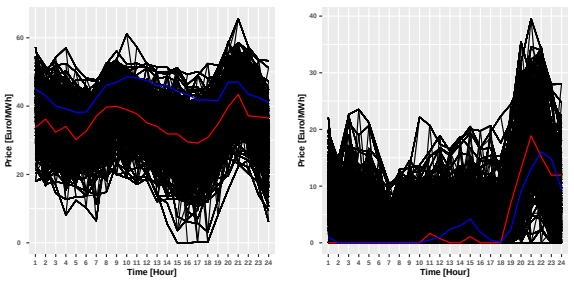

(c) Sunday 16-October-2016. **(d)** Thursday 17-November-2016.

Figura B.3.15: Some scenario sets for $\boldsymbol{\lambda}_2^I$ with 10000 scenarios.

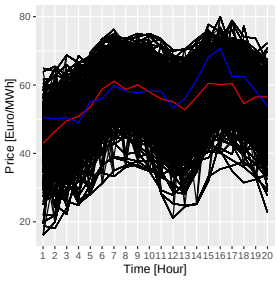

(a) Friday 15-January-2016.

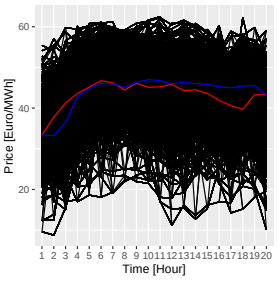

(b) Monday 06-June-2016.

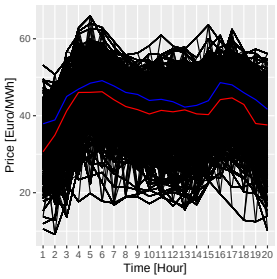

(c) Sunday 16-October-2016.

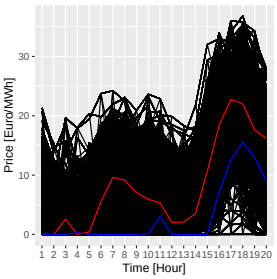

(d) Thursday 17-November-2016.

Figura B.3.16: Some scenario sets for $\boldsymbol{\lambda}_3^I$ with 10000 scenarios.

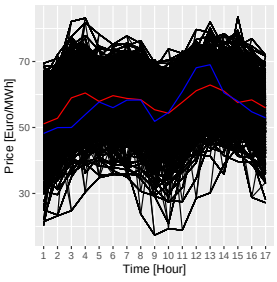

(a) Friday 15-January-2016.

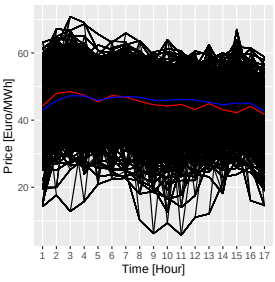

(b) Monday 06-June-2016.

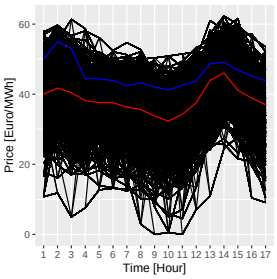

(c) Sunday 16-October-2016.

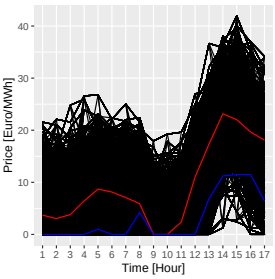

(d) Thursday 17-November-2016.

Figura B.3.17: Some scenario sets for $\boldsymbol{\lambda}_4^I$ with 10000 scenarios.

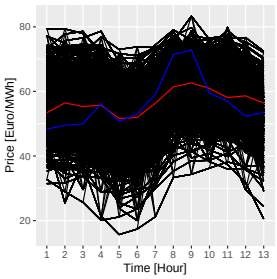

(a) Friday 15-January-2016.

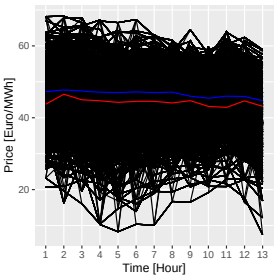

(b) Monday 06-June-2016.

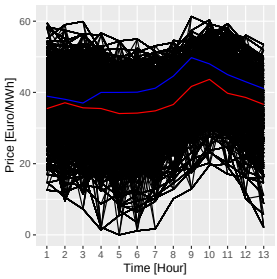

(c) Sunday 16-October-2016.

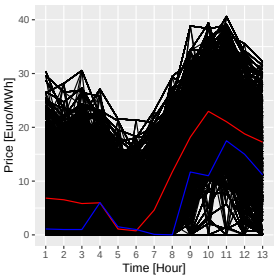

(d) Thursday 17-November-2016.

Figura B.3.18: Some scenario sets for $\boldsymbol{\lambda}_5^I$ with 10000 scenarios.

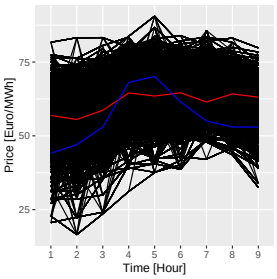

(a) Friday 15-January-2016.

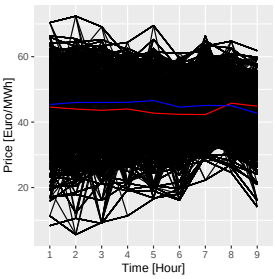

(b) Monday 06-June-2016.

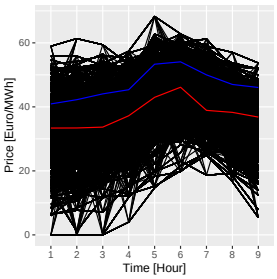

(c) Sunday 16-October-2016.

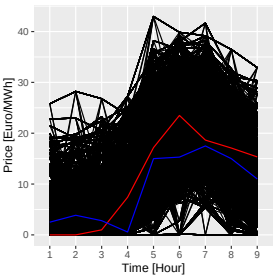

(d) Thursday 17-November-2016.

Figura B.3.19: Some scenario sets for $\boldsymbol{\lambda}_6^I$ with 10000 scenarios.

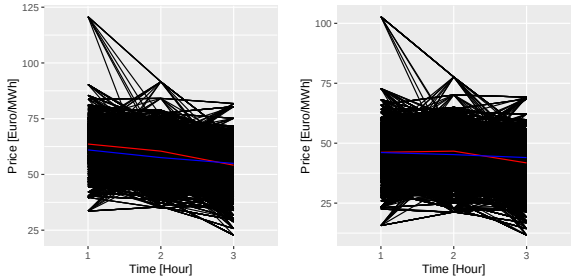

(a) Friday 15-January-2016. (b) Monday 06-June-2016.

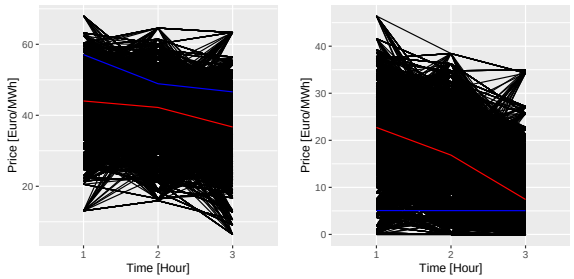

(c) Sunday 16-October-2016. (d) Thursday 17-November-2016.

Figura B.3.20: Some scenario sets for $\boldsymbol{\lambda}_7^I$ with 10000 scenarios.

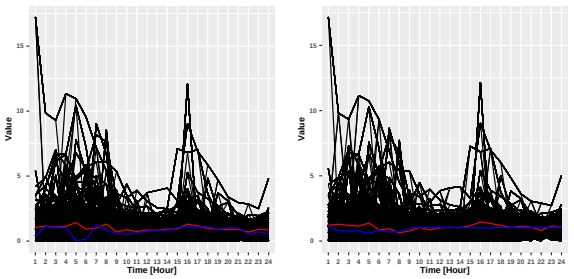

(a) Friday 15-January-2016. (b) Monday 06-June-2016.

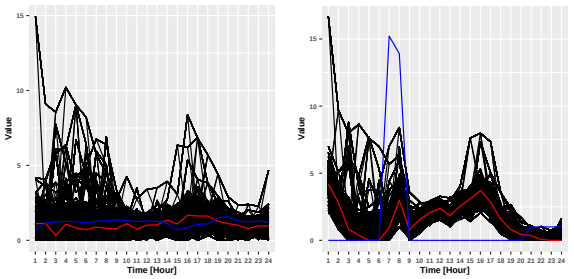

(c) Sunday 16-October-2016. (d) Thursday 17-November-2016.

Figura B.3.21: Some scenario sets for $\boldsymbol{\lambda}^{IB}$ with 10000 scenarios.

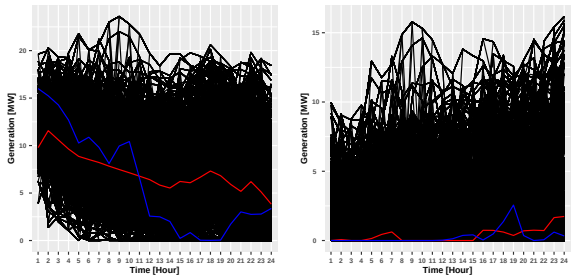

(a) Friday 15-January-2016. (b) Monday 06-June-2016.

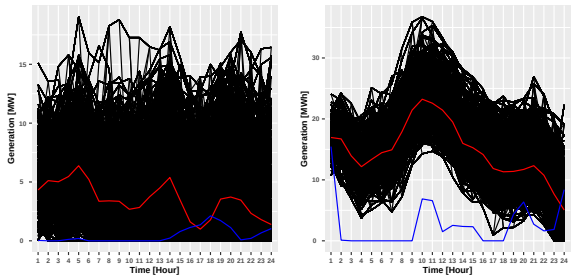

(c) Sunday 16-October-2016. (d) Thursday 17-November-2016.

Figura B.3.22: Some scenario sets for $\mathbf{P}^W$ with 10000 scenarios.

B.4. Sets of Scenarios for the MSOODN Model

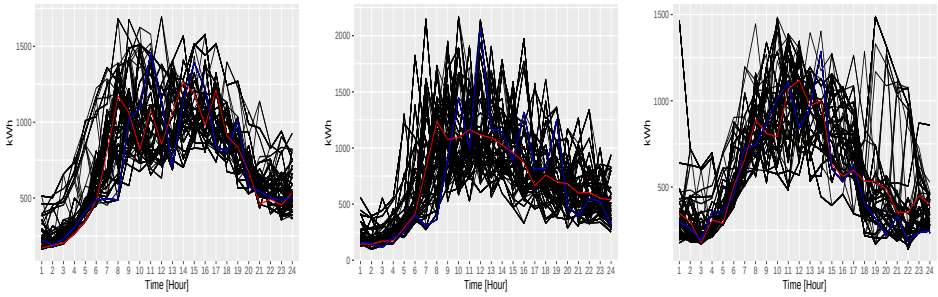

(a) Scenarios for $\hat{\mathbf{P}}^{D}_{1,N+1}$. **(b)** Scenarios for $\hat{\mathbf{P}}^{D}_{2,N+1}$. **(c)** Scenarios for $\hat{\mathbf{P}}^{D}_{3,N+1}$.

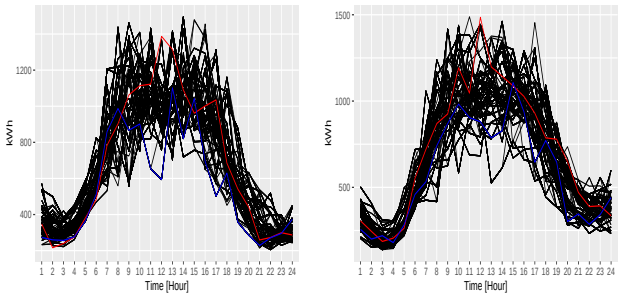

(d) Scenarios for $\hat{\mathbf{P}}^{D}_{4,N+1}$. **(e)** Scenarios for $\hat{\mathbf{P}}^{D}_{5,N+1}$.

Figura B.4.1: Scenario sets for $\hat{\mathbf{P}}^{D}_{i,N+1}$ with 300 Scenarios.

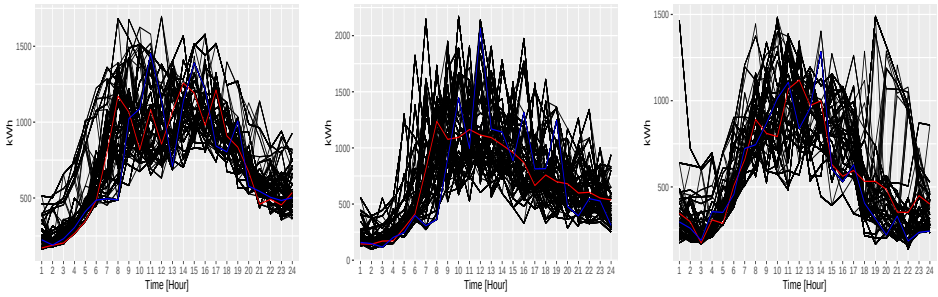

(a) Scenarios for $\hat{\mathbf{P}}^{D}_{1,N+1}$. **(b)** Scenarios for $\hat{\mathbf{P}}^{D}_{2,N+1}$. **(c)** Scenarios for $\hat{\mathbf{P}}^{D}_{3,N+1}$.

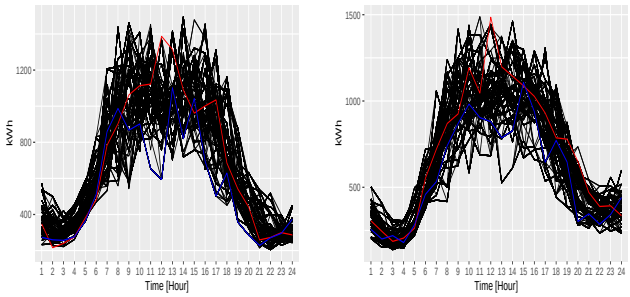

(d) Scenarios for $\hat{\mathbf{P}}^{D}_{4,N+1}$. **(e)** Scenarios for $\hat{\mathbf{P}}^{D}_{5,N+1}$.

Figura B.4.2: Scenario Sets for $\hat{\mathbf{P}}^{D}_{i,N+1}$ with 500 Scenarios.

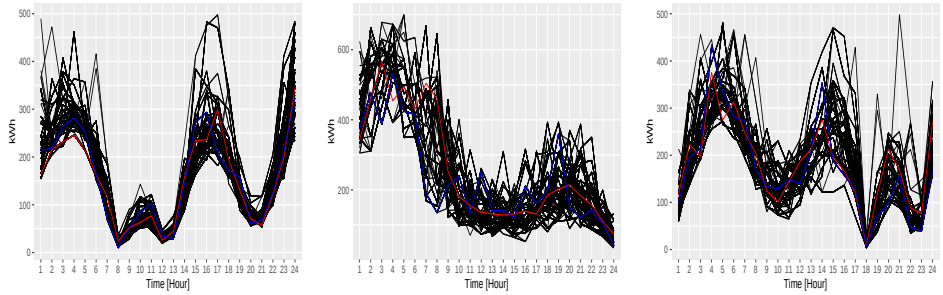

(a) Scenarios for $\hat{\mathbf{Q}}^D_{1,N+1}$. **(b)** Scenarios for $\hat{\mathbf{Q}}^D_{2,N+1}$. **(c)** Scenarios for $\hat{\mathbf{Q}}^D_{3,N+1}$.

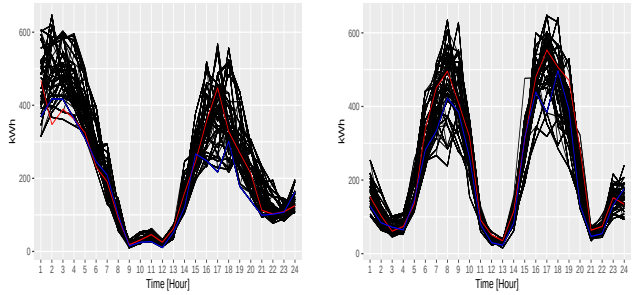

(d) Scenarios for $\hat{\mathbf{Q}}^D_{4,N+1}$. **(e)** Scenarios for $\hat{\mathbf{Q}}^D_{5,N+1}$.

Figura B.4.3: Scenario Sets for $\hat{\mathbf{Q}}^D_{i,N+1}$ with 300 Scenarios.

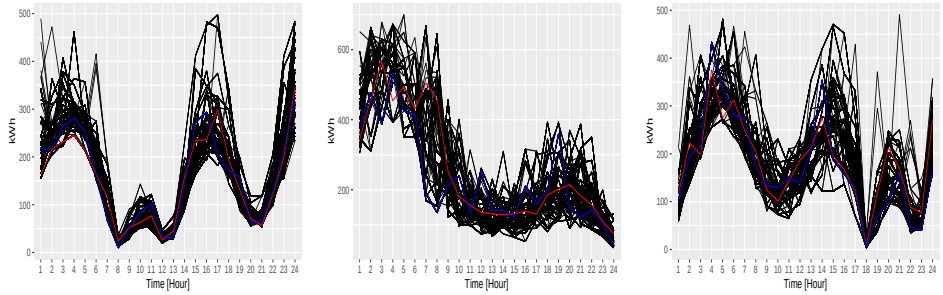

(a) Scenarios for $\hat{\mathbf{Q}}^D_{1,N+1}$. **(b)** Scenarios for $\hat{\mathbf{Q}}^D_{2,N+1}$. **(c)** Scenarios for $\hat{\mathbf{Q}}^D_{3,N+1}$t.

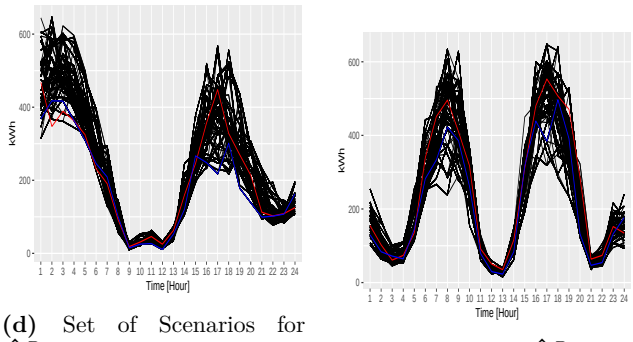

(d) Set of Scenarios for $\hat{\mathbf{Q}}^D_{4,N+1}$. **(e)** Scenarios for $\hat{\mathbf{Q}}^D_{5,N+1}$.

Figura B.4.4: Scenario Sets for $\hat{\mathbf{Q}}^D_{N+1}$ with 500 Scenarios.

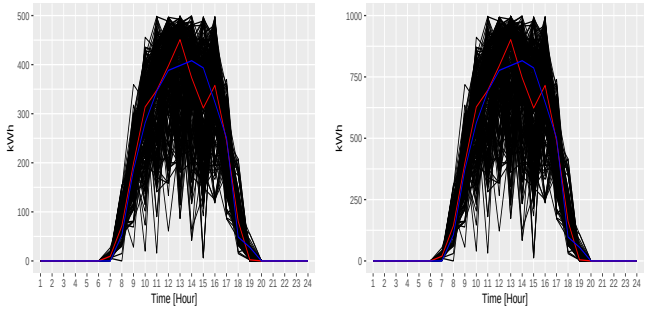

(a) Scenarios for $\mathbf{p}^{pv}_{5,N+1}$. **(b)** Scenarios for $\mathbf{p}^{pv}_{8,N+1}$.

Figura B.4.5: Scenario Sets for $\hat{\mathbf{p}}^{pv}_{i,N+1}$ with 300 Scenarios.

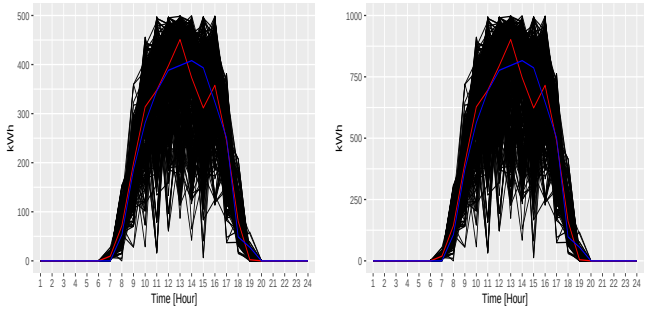

(a) Scenarios for $\mathbf{p}^{pv}_{5}$. **(b)** Scenarios for $\mathbf{p}^{pv}_{8}$.

Figura B.4.6: Scenario Sets for $\hat{\mathbf{p}}^{pv}_{i}$ with 500 Scenarios.

An evolving system increases its complexity
unless work is done to reduce it.

— Meir M. Lehman

C

Implementation of the TSFA

```
reset;

param pas integer;        # step wise

#Headboard of forward construction#
param nT integer;         # number of stages
param nV integer;         # number of time periods
set T=0..nT by pas;       # index set of stages
set TT=1..nT by pas within T; # index subset of stages
param epst{TT}>=0;        # epsilon tolerance for time period t
param eps>=0;             # sum of epsilon tolerance

#Headboard of forward selection#
param nS integer;         # scenarios numbers
param i;                  # auxiliary param for algorithm calculations
set S=0..nS by pas;       # index set of scenarios
set SS=1..nS by pas within S; # index subset of scenarios
set J{S,T} ordered;       # index set of scenarios deleted
set u{S,T} ordered default {}; # index set of scenarios preserved
set uu{2..4} ordered default {};# auxiliary index set for scenarios
   preserved
param E {SS,1..nV};       # scenario values of stocastic process
param Scen0{SS,1..nV};    # actualization of scenario values for
   stocastic process
param Scen0_re {SS,1..nV}; # actualization of scenario values
   redistribution
param Prob0{SS};          # probabilities of scenarios
param U {SS};           # minimal argument of Lr-distance
param UU {SS,SS};         # Lr distance
set argmin_U ordered; # index set of scenarios deleted for each step i
```

```
param F {SS,SS};      # distance between scenarios deleted to
   scenarios preserved
set argmin_F{SS} ordered;# scenario preserved nearest to scenario
   deleted
set index_F{SS,SS} ordered; # index for reordering scenario values
param snorm{SS};          # sum of norms
param norm{0..1,TT};      # norm
set c{T,SS} ordered default {}; # set of nodes preserved
set npres{T};             # number of scenarios
set aa ordered;           # auxiliary set for algorithm calculations
param pp{SS};             # auxiliary set for algorithm calculations
set bb;                   # auxiliary parameter for algorithm
   calculations
set mm{S} default {};     # auxiliary set for algorithm calculations
param d{T};               # time periods for stage t
param ddmin{T};           # first component of a time period of stage t
param ddmax{T};           # last component of a time period of stage t
param r;                  # distance type
param nesce;              # number of final scenarios
param norm1{SS,SS};       # initial norm
set JJ{S,T} ordered;      # index set of scenarios deleted
param eemax{SS};          # the initial best possible distance
set argmin_eemax;         # minimal argument of the best possible
   distance
param nSG;                # final number of scenarios
param nRVSG{TT};          # final time periods for stage t

param nnodes{T} default 1; # number of nodes for stage t
param matt_clust{SS,T} default 0;# parameter for scenario tree plots
param pred{SS,T} default 0; # index of nodes preserved
param fila integer;       # parameter for scenario tree plots
param cont{T} integer default 1;# parameter for scenario tree plots
param aux;                # auxiliary parameter
#########################################################
#INICIAL PARAMETERS FORWARD CONSTRUCTION
param emaxt{TT};          # the best distance
param emax;               # sum of the emaxt
param erel;               # relative tolerance
param erelt{TT};          # relative tolerance for stage t
param norm11{SS,SS,TT};   # initial norm for stage t
param ssize integer > 0; # number of scenario preserved for stage t
param item symbolic;      # dummy parameter to hold each selection
param sample {1..ssize} symbolic;# sample number for select scenario
   preserved
#param VP{SS,1..nV};      #
param Scen0{1..nV};       # matrix of observed values
```

```
param ScenF{1..nV};       # matrix of forecasted values
param snnodes;

set CASES = 322 .. 322;

for {jj in CASES}
{
   display jj;
   reset data;
   data ("/home/ucct2/projectes/TSFA_7intradays_VE/FAN
   /FAN_1000_Febrary-2020/20200219_1000_" & jj &".txt");
#########################################################
#INICIAL PARAMETERS
   let pas:=1;
   let r:=2;
   let nS:=1000;
   let nT:=34;
   let nV:=sum{it in TT} d[it];
   let{s in SS} Prob0[s]:=1/nS;
#########################################################
   #let{s in SS, l in 1..nV} E[s,l]:=VP[s,l];
#########################################################
   let ddmin[0]:=1;
   let ddmax[0]:=0;
   let{it in TT}ddmin[it]:=ddmin[it-1]+d[it-1];
   let{it in TT}ddmax[it]:=ddmax[it-1]+d[it];
#########################
# FORWARD CONSTRUCTION #
#########################
### STEP 1 ###
   let uu[3] := {floor(card(S)/2)};
   let uu[4] := {floor(card(S)/2)};
   let c[0,floor(card(S)/2)] := {floor(card(S)/2)} union ({SS} diff
      {floor(card(S)/2)});
   let npres[0]:={floor(card(S)/2)};
   let{it in TT} JJ[0,it]:={};
#########################################################
   let nnodes[0] := card(npres[0]);
   let{ii in SS} pred[ii,0]:= floor(card(S)/2);
   let{it in TT} cont[it]:=1;
#########################################################
### STEP t ###
#####################
# FORWARD SELECTION #
#####################
#########################################################
```

```
#The best possible distance between the probability distribution of
    the initial scenario set
# and the distribution of one of its scenarios endowed with unit mass
   let{k in SS, s in SS:s<=k} norm1[k,s]:=sum{it in TT, j in
      ddmin[it]..ddmax[it]}abs(E[s,j]-E[k,j]);
   let{k in SS, s in SS:s>k} norm1[k,s] :=norm1[s,k];
   let{k in SS} eemax[k]:=(sum{s in
      SS:s<>k}Prob0[s]*norm1[k,s]^r)^(1/r);

#The minimum argument of the best previos distance possible.
   let argmin_eemax:= {k in SS: eemax[k] = min {j in SS} eemax[j]};

#The best possible distance between the probability distribution of
    the initial scenario set
# and the distribution of one of its scenarios endowed with unit mass
    for each stage it
   let{it in TT, k in SS, s in SS:s<=k} norm11[k,s,it]:=sum{j in
      ddmin[it]..ddmax[it]}abs(E[s,j]-E[k,j]);
   let{it in TT, k in SS, s in SS:s>k} norm11[k,s,it] :=norm11[s,k,it];
   let{k in argmin_eemax, it in TT} emaxt[it]:=(sum{s in
      SS}Prob0[s]*norm11[k,s,it]^r)^(1/r);
#############################################################
   let erel:=0.85;
   let aux:=0;

   for{t in TT}
   {
   let erelt[t]:=(erel-aux);
   let aux:=aux+0.005;
   }

   let{t in TT} epst[t]:=erelt[t]*emaxt[t];
   let eps:= sum{t in TT} epst[t];
   let emax:=sum{t in TT} emaxt[t];
   display erel,erelt,emaxt,epst,emax,eps;

#############################################################
### step 0 ###
   for{it in TT}
   {
      let{l in SS, j in SS:l<=j} UU[l,j] := sum{m in
         ddmin[it]..ddmax[it]}abs(E[l,m] - E[j,m]);
      let{l in SS, j in SS: l>j} UU[l,j] :=UU[j,l];
      let uu[2]:={};
      let uu[4]:={};
   ##################################################################
```

```
      let ssize := card(npres[it-1]);  # omit if sampling with
         replacement
      for {ii in 1..ssize}
      {
         let item := member(ceil(Uniform(1, card(uu[3]))), uu[3]);
         let sample[ii] := item;
         let uu[3] := uu[3] diff {item}; # omit if sampling with
            replacement
         let uu[4] := uu[4] union {item};
      };#end ramdomness
   ######################################################################
      for {k in uu[4]}
      {
         let norm[0,it]:=120000000;
### step i ###
         let u[0,it] := {};
         let J[0,it] := c[it-1,k];
         let i:=0;
         repeat while norm[0,it]>epst[it] and i<nS
         {
            let i:=i+1;
            let{w in J[i-1,it]} U[w] := sum {l in J[i-1,it] diff
               {w}}Prob0[l]*min {j in {w}} UU[l,j]^r;

            if i=1 then
            {
               let argmin_U:= {l in J[i-1,it]: U[l] = min {j in
                  J[i-1,it]} U[j]};
               let argmin_U:={first(argmin_U)};
               let J[i,it] := J[i-1,it] diff argmin_U;
               let u[i,it] := u[i-1,it] union argmin_U;
               let{m in u[i,it],l in J[i,it]} pp[l]:= UU[m,l];
               let aa:={l in J[i,it]: pp[l]=0};
               let bb := J[i,it];
               let mm[i]:=mm[i-1] union aa;
               let bb:=bb diff mm[i];
            }
            else
            {
               let argmin_U:= {l in bb: U[l]= min {j in bb} U[j]};
               let argmin_U:={first(argmin_U)};
               let J[i,it] := J[i-1,it] diff argmin_U;
               let u[i,it] := u[i-1,it] union argmin_U;
               let{m in u[i,it],l in J[i,it]} pp[l]:= UU[m,l];
               let aa:={l in J[i,it]: pp[l]=0};
               let bb := J[i,it];
```

```
            let mm[i]:=mm[i-1] union aa;
            let bb:=bb diff mm[i];
         };#end if
      for {j in J[0,it]}
      {
         let argmin_F[j]:= {l in u[i,it] : UU[j,l]^r = min {w in
            u[i,it]} UU[j,w]^r};
         let argmin_F[j]:={first(argmin_F[j])};
      }; #end argmin_F

      for{j in J[i,it],l in argmin_F[j],z in u[i,it]}
      {
         if z==l then
         {
            let index_F[j,z]:={j};
            let{w in index_F[j,z], m in ddmin[it]..ddmax[it]}
               Scen0_re[w,m]:=E[z,m];
         };
      }; #end index F
      let JJ[0,it] := JJ[0,it] union J[0,it];
      let{s in u[i,it],l in ddmin[it]..ddmax[it]} Scen0[s,l]:=E[s,l];
      let{s in J[0,it] diff u[i,it],l in ddmin[it]..ddmax[it]}
         Scen0[s,l] := Scen0_re[s,l];
      let{s in SS diff JJ[0,it],l in ddmin[it]..ddmax[it]}
         Scen0[s,l] := E[s,l];
      let{s in SS} snorm[s]:=sum{l in
         ddmin[it]..ddmax[it]}abs(Scen0[s,l]-E[s,l]);
      let norm[1,it]:=(sum{s in SS}Prob0[s]*snorm[s]^r)^(1/r);
      let norm[0,it]:=norm[1,it];
      ##################################################

      }; #end repeat
   let uu[2] := uu[2] union u[i,it];
   let {w in u[i,it]} c[it,w]:= {w};
   let {j in J[i,it], l in argmin_F[j]} c[it,l]:=c[it,l] union {j};

   let{w in u[i,it]} pred[w,it]:=first(c[it,w]);
   let{j in J[i,it], l in argmin_F[j]} pred[j,it]:=first(c[it,l]);
### step n+1: Optimal redistribution ###
   }; #end k
  let uu[3]:=uu[2];
  let npres[it]:=uu[3];
  let nesce:=card(npres[it]);
  let nnodes[it] :=card(npres[it]);
##############################################
  let nSG:=nT;
```

```
   let{t in TT} nRVSG[t]:=d[t];
   }; #end it

   let snnodes:=sum{it in TT}nnodes[it];
   display snnodes;

   let{it in {nT},l in uu[3]} Prob0[l] :=sum{k in c[it,l]} Prob0[k];
   let{j in SS diff uu[3]} Prob0[j] := 0;
################################Results#############################
#scenario tree#
####################################################################
   if (jj<10) then
   {
      printf "#erel:= %.3f;\n",erel> ("20200219_1000-00"& jj &".dat");
      printf "#emax:= %.3f;\n",emax> ("20200219_1000-00"& jj &".dat");
      printf "#nesce:= %5i;\n",nesce> ("20200219_1000-00"& jj
         &".dat");
      printf "param nS:= %5i;\n", nS> ("20200219_1000-00" & jj
         &".dat");
      printf "param nSG:= %5i;\n", nSG> ("20200219_1000-00" & jj
         &".dat");

      printf "param "> ("20200219_1000-00" & jj &".dat");
      display nRVSG > ("20200219_1000-00" & jj &".dat");

      #ScenF
      printf"param " > ("20200219_1000-00" & jj &".dat");
      display ScenF> ("20200219_1000-00"& jj &".dat");


      #Scen0
      printf"param " > ("20200219_1000-00" & jj &".dat");
      display Scen0> ("20200219_1000-00"& jj &".dat");

      #Scen0
      printf"param Scen0 (tr)\n " > ("20200219_1000-00" & jj &".dat");
      printf":" > ("20200219_1000-00" & jj &".dat");
      printf{l in 1..nV} "%5i\t",l > ("20200219_1000-00" & jj &".dat");
      printf":=\n" > ("20200219_1000-00" & jj &".dat");
      for{s in SS}
      {
         printf "%5i\t",s > ("20200219_1000-00" & jj &".dat");
         for{l in 1..nV}
         {
            printf"%.6f\t",Scen0[s,l] > ("20200219_1000-00" & jj
               &".dat");
```

```
      };
      printf "\n" > ("20200219_1000-00" & jj &".dat");
   };
   printf";" > ("20200219_1000-00" & jj &".dat");
   printf"\n" > ("20200219_1000-00" & jj &".dat");

   #Prob0
   printf"param Prob0 :=\n" > ("20200219_1000-00" & jj &".dat");
   for{s in SS}
   {
      printf "%5i\t",s > ("20200219_1000-00" & jj &".dat");
      printf"%.3f\n",Prob0[s] > ("20200219_1000-00" & jj &".dat");
   }
   printf";\n" > ("20200219_1000-00" & jj &".dat");
   display c> ("20200219_1000-00"& jj &".dat");
}
else
{
if (jj>=10 and jj<=99) then
   {
   printf "#erel:= %5i;\n",erel> ("20200219_1000-0"& jj &".dat");
   printf "#emaxt:= %.3f;\n",emax> ("20200219_1000-0"& jj &".dat");
   printf "#nesce:= %5i;\n",nesce> ("20200219_1000-0"& jj &".dat");
   printf "param nS:= %5i;\n", nS> ("20200219_1000-0" & jj &".dat");
   printf "param nSG:= %5i;\n", nSG> ("20200219_1000-0" & jj
      &".dat");

   printf "param "> ("20200219_1000-0" & jj &".dat");
   display nRVSG > ("20200219_1000-0" & jj &".dat");

   #ScenF
   printf"param " > ("20200219_1000-0" & jj &".dat");
   display ScenF> ("20200219_1000-0"& jj &".dat");


   #Scen0
   printf"param " > ("20200219_1000-0" & jj &".dat");
   display Scen0> ("20200219_1000-0"& jj &".dat");

   #Scen0
   printf"param Scen0 (tr)\n " > ("20200219_1000-0" & jj &".dat");
   printf":" > ("20200219_1000-0" & jj &".dat");
   printf{l in 1..nV} "%5i\t",l > ("20200219_1000-0" & jj &".dat");
   printf":=\n" > ("20200219_1000-0" & jj &".dat");
   for{s in SS}
   {
```

```
      printf "%5i\t",s > ("20200219_1000-0" & jj &".dat");
      for{l in 1..nV}
      {
         printf"%.6f\t",Scen0[s,l] > ("20200219_1000-0" & jj
            &".dat");
      }
      printf "\n" > ("20200219_1000-0" & jj &".dat");
   }
   printf";" > ("20200219_1000-0" & jj &".dat");
   printf"\n" > ("20200219_1000-0" & jj &".dat");

   #Prob0
   printf"param Prob0 :=\n" > ("20200219_1000-0" & jj &".dat");
   for{s in SS}
   {
      printf "%5i\t",s > ("20200219_1000-0" & jj &".dat");
      printf"%.3f\n",Prob0[s] > ("20200219_1000-0" & jj &".dat");
   }
   printf";\n" > ("20200219_1000-0" & jj &".dat");
   display c> ("20200219_1000-0"& jj &".dat");
}
else
{
printf "#erel:= %5i;\n",erel> ("20200219_1000-"& jj &".dat");
   printf "#emaxt:= %.3f;\n",emax> ("20200219_1000-"& jj &".dat");
   printf "#q:= %.3f;\n",q> ("20200219_1000-"& jj &".dat");
   printf "#nesce:= %5i;\n",nesce> ("20200219_1000-"& jj &".dat");
   printf "param nS:= %5i;\n", nS> ("20200219_1000-" & jj &".dat");
   printf "param nSG:= %5i;\n", nSG> ("20200219_1000-" & jj
      &".dat");

   printf "param "> ("20200219_1000-" & jj &".dat");
   display nRVSG > ("20200219_1000-" & jj &".dat");

   #ScenF
   printf"param " > ("20200219_1000-" & jj &".dat");
   display ScenF> ("20200219_1000-"& jj &".dat");


   #Scen0
   printf"param " > ("20200219_1000-" & jj &".dat");
   display Scen0> ("20200219_1000-"& jj &".dat");

   #Scen0
   printf"param Scen0 (tr)\n " > ("20200219_1000-" & jj &".dat");
   printf":" > ("20200219_1000-" & jj &".dat");
```

```
      printf{l in 1..nV} "%5i\t",l > ("20200219_1000-" & jj &".dat");
      printf":=\n" > ("20200219_1000-" & jj &".dat");
      for{s in SS}
      {
         printf "%5i\t",s > ("20200219_1000-" & jj &".dat");
         for{l in 1..nV}
         {
            printf"%.6f\t",Scen0[s,l] > ("20200219_1000-" & jj &".dat");
         }
         printf "\n" > ("20200219_1000-" & jj &".dat");
      }
      printf";" > ("20200219_1000-" & jj &".dat");
      printf"\n" > ("20200219_1000-" & jj &".dat");

      #Prob0
      printf"param Prob0 :=\n" > ("20200219_1000-" & jj &".dat");
      for{s in SS}
      {
         printf "%5i\t",s > ("20200219_1000-" & jj &".dat");
         printf"%.3f\n",Prob0[s] > ("20200219_1000-" & jj &".dat");
      }
      printf";\n" > ("20200219_1000-" & jj &".dat");
      display c> ("20200219_1000-"& jj &".dat");
   }#end if
}
#####################################################################
#scenario tree plot#
#####################################################################
   for{t in T}
   {
      for{l in npres[t]}
      {
         if l==first(c[t,l]) then
         {
            let matt_clust[l,t]:=cont[t];
            let{ss in c[t,l]} matt_clust[ss,t]:=cont[t];
         }
         let cont[t]:=cont[t]+1;
      }

      for{s in SS}
      {
         if Prob0[s]==0 then let matt_clust[s,t]:=0;
         else let matt_clust[s,t]:=matt_clust[s,t];
      }
   }
```

```
   printf "param T:= %5i;\n", nT> ("grafics_" & jj &".dat");
   printf "param nS:= %5i;\n", nS> ("grafics_" & jj &".dat");
   printf "param fila:= %5i;\n",nesce> ("grafics_" & jj &".dat");

   printf"param matt_clust[*,*] (tr) \n " > ("grafics_" & jj &".dat");
   printf":" > ("grafics_" & jj &".dat");
   printf{k in SS} "%5i\t",k > ("grafics_" & jj &".dat");
   printf":=\n" > ("grafics_" & jj &".dat");
   for{j in T}
      {
         printf "%5i\t",j > ("grafics_" & jj &".dat");
            for{k in SS}
            {
               printf"%5i\t",matt_clust[k,j] > ("grafics_" & jj
                  &".dat");
            }
         printf "\n" > ("grafics_" & jj &".dat");
      }
   printf";" > ("grafics_" & jj &".dat");
   printf"\n" > ("grafics_" & jj &".dat");
   printf"param nnodes :=\n" > ("grafics_" & jj &".dat");
   for{it in T}
   {
      printf "%5i\t",it > ("grafics_" & jj &".dat");
      printf "%5i\t",nnodes[it] > ("grafics_" & jj &".dat");
   }
   printf";\n" > ("grafics_" & jj &".dat");
########################################################################
};#end cases
```

The probability of success is difficult to estimate; but if we never search the chance of success is zero.

— Philip Morrison

D

Other Results of the Scenario Tree Generation

Contents

D.1. Initial Parameter Values for the Scenario Tree Algorithms

Cuadro D.1.1: Dimensionality of the Individual Scenario $\tilde{\boldsymbol{\xi}}_\omega$ for the MSWBVPP model.

$\tilde{\boldsymbol{\xi}}_\omega$	$\tilde{\lambda}^D_\omega$	$\tilde{\lambda}^R_\omega$	$\tilde{\lambda}^I_{1\omega}$	$\tilde{\lambda}^I_{2\omega}$	$\tilde{P}^W_{1\omega}, \tilde{P}^W_{2\omega}$	$\tilde{\lambda}^I_{3\omega}$	$\tilde{P}^W_{3\omega}, \ldots, \tilde{P}^W_{7\omega}$	$\tilde{\lambda}^I_{4\omega}$	$\tilde{P}^W_{6\omega}, \ldots, \tilde{P}^W_{9\omega}$	$\tilde{\lambda}^I_{5\omega}$	$\tilde{P}^W_{10\omega}, \ldots, \tilde{P}^W_{13\omega}$	$\tilde{\lambda}^I_{6\omega}$	$\tilde{P}^W_{14\omega}, \ldots, \tilde{P}^W_{19\omega}$	$\tilde{\lambda}^I_7$	$\tilde{P}^W_{20\omega}, \ldots, \tilde{P}^W_{24\omega}$	$\tilde{\lambda}^{IB}_\omega$
Stage s	1	2	3	4	5	6	7	8	9	10	11	12	13	14	15	16
Time Period t	$1,\ldots,24$	$1,\ldots,24$	$1,\ldots,24$	$1,\ldots,24$	$5,6$	$5,\ldots,24$	$3,\ldots,5$	$8,\ldots,24$	$6,\ldots,9$	$12,\ldots,24$	$8,\ldots,10$	11	$12,\ldots,15$	16	$17,\ldots,20$	21	$22,\ldots,27$	28	$29,\ldots,33$	34
$\lvert\mathcal{T}\rvert$ or $\lvert\mathcal{T}_t\rvert$	24	24	24	24	2	20	3	17	4	13	4	9	6	3	5	24
$\tilde{\boldsymbol{\xi}}_\omega$ length	$1,\ldots,24$	$25,\ldots,48$	$49,\ldots,72$	$73,\ldots,96$	$97,98$	$99,\ldots,118$	$119,\ldots,121$	$122,\ldots,138$	$139,\ldots,142$	$143,\ldots,155$	$156,\ldots,159$	$160,\ldots,168$	$169,\ldots,174$	$175,\ldots,177$	$178,\ldots,182$	$183,\ldots,206$

Cuadro D.1.2: Initial Parameter Values of the FTCA for the MSWBVPP model

Stage s	1	2	3	4	5	6	7	8	9	10	11	12	13	14	15	16	17	18	19	20	21	22	23	24	25	26	27	28	29	30	31	32	33	34
ε_{vcla}	0.85	0.845	0.84	0.835	0.83	0.825	0.82	0.815	0.81	0.805	0.8	0.795	0.79	0.785	0.78	0.775	0.77	0.765	0.76	0.755	0.75	0.745	0.74	0.735	0.73	0.725	0.72	0.715	0.71	0.705	0.7	0.695	0.69	0.685
$\varepsilon_{max,s}$	104.637	123.342	109.782	118.927	1.71591	1.71591	107.579	2.28871	2.54159	2.70711	102.127	2.60187	2.99455	3.07027	2.94827	83.9313	2.78705	2.98838	2.73986	3.00397	60.2964	2.95967	3.02469	3.19563	3.20425	3.20455	3.35494	19.8508	3.46439	3.38619	3.54311	3.4632	3.34525	7.46886
ε_s	88.9418	104.224	92.2169	99.3041	1.4242	1.41562	88.2144	1.849	2.05868	2.25167	81.7013	2.06849	2.36569	2.41016	2.29065	65.0468	2.14603	2.27081	2.12334	2.26799	15.2223	2.20495	2.23827	2.34879	2.3301	2.3223	2.41356	14.1933	2.19971	2.38727	2.48018	2.40693	2.30822	5.1148

Cuadro D.1.3: Initial Parameter Values of the DTGFBA for the MSWBVPP model.

Stage s	1	2	3	4	5	6	7	8	9	10	11	12	13	14	15	16	17	18	19	20	21	22	23	24	25	26	27	28	29	30	31	32	33	34
h_s	2	2	2	1	1	1	1	1	1	1	1	1	1	1	1	1	1	1	1	1	1	1	1	1	1	1	1	1	1	1	1	1	1	1
ε_s	30.2165	32.2572	41.0031	26.5677	1.98576	2.53883	62.8845	1.04759	3.427	2.03339	31.211	2.90171	3.65257	2.83823	1.44138	40.2943	2.06162	2.88603	3.20381	3.29803	28.5625	5.04821	6.05895	3.89044	3.47483	1.50935	4.7525	16.0059	6.4849	4.01202	2.0903	1.53109	5.3495 19	2.08564
n_s	6	6	6	5	5	5	5	5	5	5	5	5	5	5	5	5	5	5	5	5	5	5	5	5	5	5	5	5	5	5	5	5	5	5

$\tilde{\xi}_\omega$	$\tilde{\xi}_{1\omega}$	$\tilde{\xi}_{2\omega}$	$\tilde{\xi}_{3\omega}$	$\tilde{\xi}_{4\omega}$	$\tilde{\xi}_{5\omega}$	$\tilde{\xi}_{6\omega}$	$\tilde{\xi}_{7\omega}$	$\tilde{\xi}_{8\omega}$	$\tilde{\xi}_{9\omega}$	$\tilde{\xi}_{10\omega}$	$\tilde{\xi}_{11\omega}$	$\tilde{\xi}_{12\omega}$	$\tilde{\xi}_{13\omega}$	$\tilde{\xi}_{14\omega}$	$\tilde{\xi}_{15\omega}$	$\tilde{\xi}_{16\omega}$	$\tilde{\xi}_{17\omega}$	$\tilde{\xi}_{18\omega}$	$\tilde{\xi}_{19\omega}$	$\tilde{\xi}_{20\omega}$	$\tilde{\xi}_{21\omega}$	$\tilde{\xi}_{22\omega}$	$\tilde{\xi}_{23\omega}$	$\tilde{\xi}_{24\omega}$
Stage (Time period)	1	2	3	4	6	5	7	8	9	10	11	12	13	14	15	16	17	18	19	20	21	22	23	24
$\lvert\mathcal{T}\rvert$ or $\lvert\mathcal{T}_t\rvert$	12	12	12	12	12	12	12	12	12	12	12	12	12	12	12	12	12	12	12	12	12	12	12	12
$\tilde{\xi}_\omega$ length	$1,\ldots,12$	$13,\ldots,24$	$25,\ldots,36$	$37,\ldots,48$	$49,\ldots,60$	$61,\ldots,72$	$73,\ldots,84$	$85,\ldots,96$	$97,\ldots,108$	$109,\ldots,120$	$121,\ldots,132$	$133,\ldots,144$	$145,\ldots,156$	$157,\ldots,168$	$169,\ldots,180$	$181,\ldots,192$	$193,\ldots,204$	$205,\ldots,216$	$217,\ldots,228$	$229,\ldots,240$	$241,\ldots,252$	$253,\ldots,264$	$265,\ldots,276$	$277,\ldots,288$

Cuadro D.1.4: Dimensionality of the Individual Scenario $\tilde{\boldsymbol{\xi}}_\omega$ for the MSOODN model

Tree	Stage t	1	2	3	4	5	6	7	8	9	10	11	12	13	14	15	16	17	18	19	20	21	22	23	24
1	$\varepsilon_{rel,t}$	0.87	0.86936	0.86782	0.86808	0.86744	0.8668	0.86616	0.86552	0.86488	0.86424	0.8636	0.86296	0.86232	0.86168	0.86104	0.8604	0.85976	0.85912	0.85848	0.85784	0.8572	0.85656	0.85592	0.85528
	$\varepsilon_{max,t}$	803.05	607.233	591.718	540.426	678.063	937.783	1362.52	1520.07	1733.44	1687.48	1907.88	1938.44	1870.17	1290.65	1563.01	1694.01	1369.36	1274.84	1038.58	1075.37	885.102	846.718	710.122	739.813
	ε_t	698.654	527.904	514.037	469.133	588.179	812.87	1180.16	1315.65	1499.22	1458.39	1647.65	1672.8	1612.68	1112.12	1345.82	1457.53	1177.32	1095.24	891.603	922.496	758.709	725.265	607.808	632.747
2	$\varepsilon_{rel,t}$	0.83	0.82936	0.82872	0.82808	0.82744	0.8268	0.82616	0.82552	0.82488	0.82424	0.8236	0.82296	0.82232	0.82168	0.82104	0.8204	0.81976	0.81912	0.81848	0.81784	0.8172	0.81656	0.81592	0.81528
	$\varepsilon_{max,t}$	803.05	607.233	591.718	540.426	678.063	937.783	1362.52	1520.07	1733.44	1687.48	1907.88	1938.44	1870.17	1290.65	1563.01	1694.01	1369.36	1274.84	1038.58	1075.37	885.102	846.718	710.122	739.813
	ε_t	666.532	503.614	490.368	447.516	561.056	775.359	1125.66	1254.85	1429.88	1390.89	1571.33	1595.26	1537.88	1060.5	1283.3	1389.77	1122.54	1044.24	850.059	879.481	723.305	691.396	579.403	603.155
3	$\varepsilon_{rel,t}$	0.69	0.68936	0.68872	0.68808	0.68744	0.6868	0.68616	0.68552	0.68488	0.68424	0.6836	0.68296	0.68232	0.68168	0.68168	0.6804	0.67976	0.67912	0.67848	0.67784	0.6772	0.67656	0.67592	0.67528
	$\varepsilon_{max,t}$	803.05	607.233	591.718	540.426	678.063	937.783	1362.52	1520.07	1733.44	1687.48	1907.88	1938.44	1870.17	1290.65	1563.01	1694.01	1369.36	1274.84	1038.58	1075.37	885.102	846.718	710.122	739.813
	ε_t	554.105	418.602	407.528	371.856	466.128	644.069	934.908	1042.04	1187.2	1154.64	1304.23	1323.88	1276.05	879.807	1064.47	1152.61	930.833	865.767	704.658	728.929	599.391	572.855	479.986	499.581

Cuadro D.1.5: Initial Parameter Values of the FTCA for the MSOODN model.

Tree	Stage t	1	2	3	4	5	6	7	8	9	10	11	12	13	14	15	16	17	18	19	20	21	22	23	24
1-3	b_t	2	2	2	1	1	1	1	1	1	1	1	1	1	1	1	1	1	1	1	1	1	1	1	1
1-3	n_s	6	6	6	5	5	5	5	5	5	5	5	5	5	5	5	5	5	5	5	5	5	5	5	5
1	ε_t	285.532	241.946	317.953	264.5	417.933	1134.51	804.082	762.713	780.078	1110.1	981.877	525.488	768.787	769.631	612.143	972.133	431.811	761.86	620.417	744.818	722.032	536.648	329.234	292.677
2	ε_t	282.648	239.503	314.741	261.828	413.711	1123.05	795.96	755.009	695.915	899.619	666.117	971.927	831.77	527.013	715.067	1183	704.478	667.817	557.722	837.062	760.829	516.2	342.873	510.409
3	ε_t	279.764	237.059	311.53	259.157	409.489	1111.59	787.838	739.195	567.669	1165.38	731.711	511.71	692.271	573.657	691.87	765.976	588.78	619.252	461.735	857.176	284.83	275.576	479.585	228.356

Cuadro D.1.6: Initial Parameters Values of the DTGFBA for the MSOODN model.

D.2. Other Plots of the Numerical Results for the MSWBVPP Model

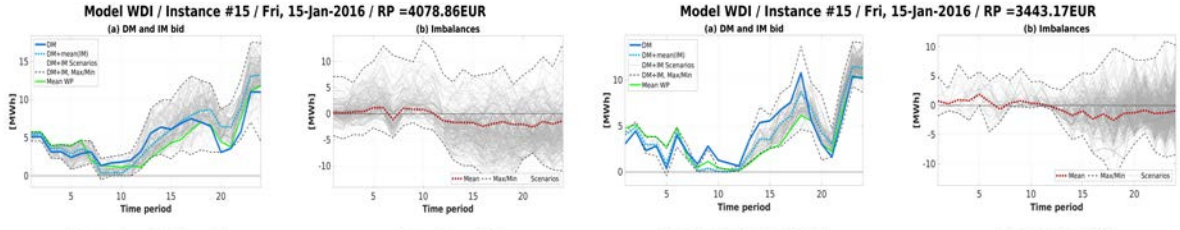

Figura D.2.1: Results for case WDI of Instance #15.

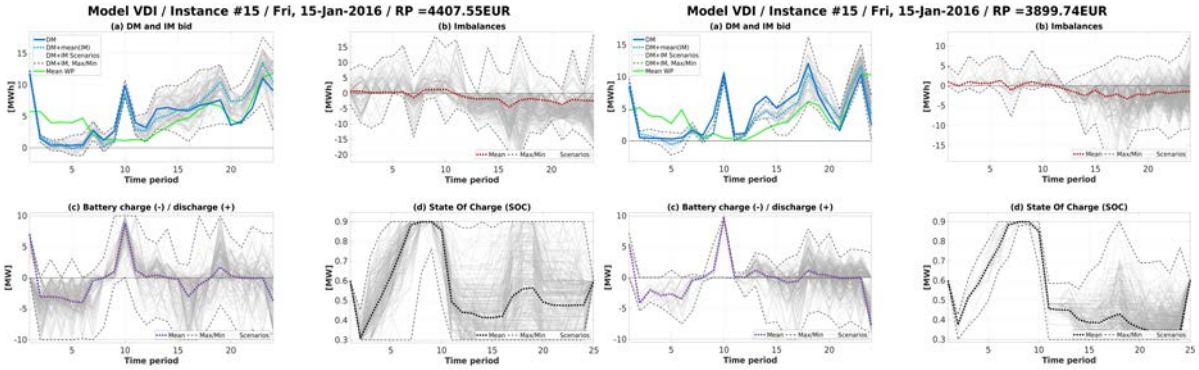

Figura D.2.2: Results for case VDI of Instance #15.

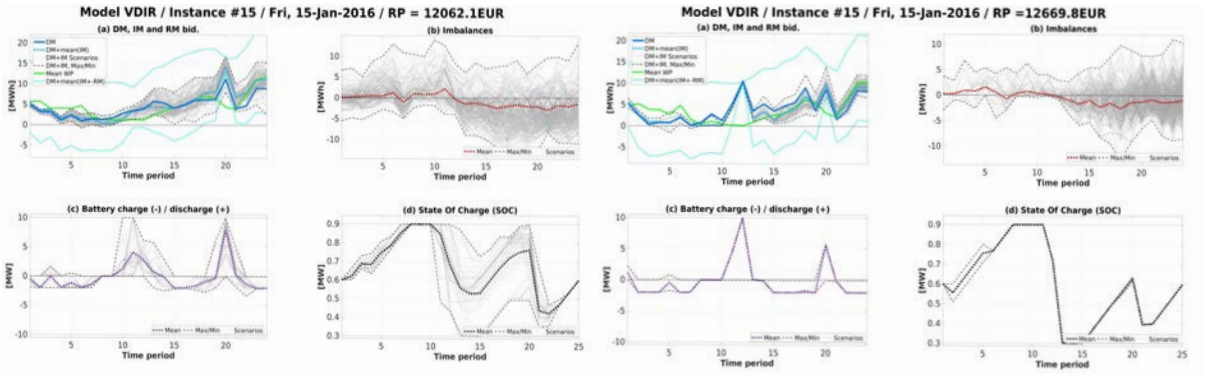

Figura D.2.3: Results for Case VDIR of Instance #15.

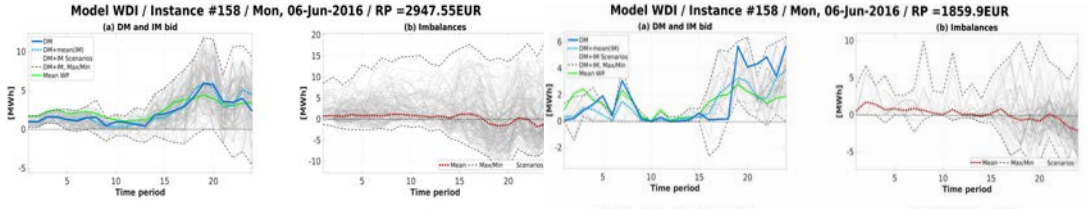

Figura D.2.4: Results for case WDI of Instance #158.

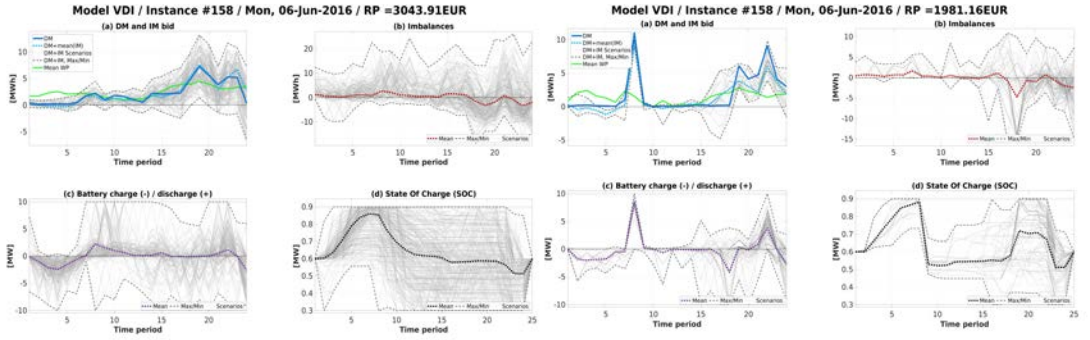

Figura D.2.5: Results for case VDI of Instance #158.

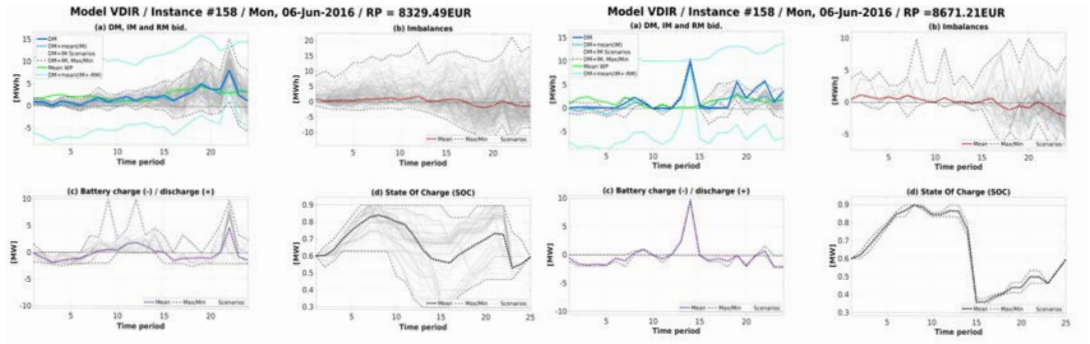

Figura D.2.6: Results for Case VDIR of Instance #158.

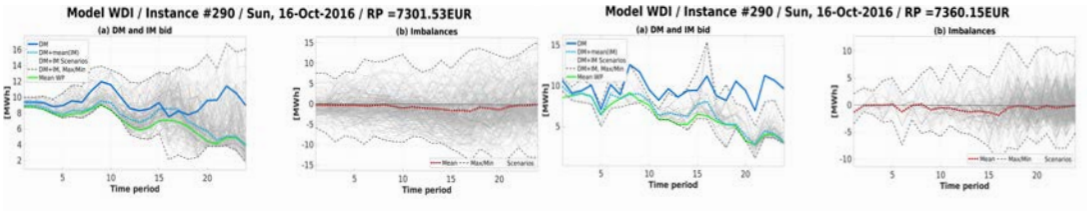

Figura D.2.7: Results for Case WDI of Instance #290.

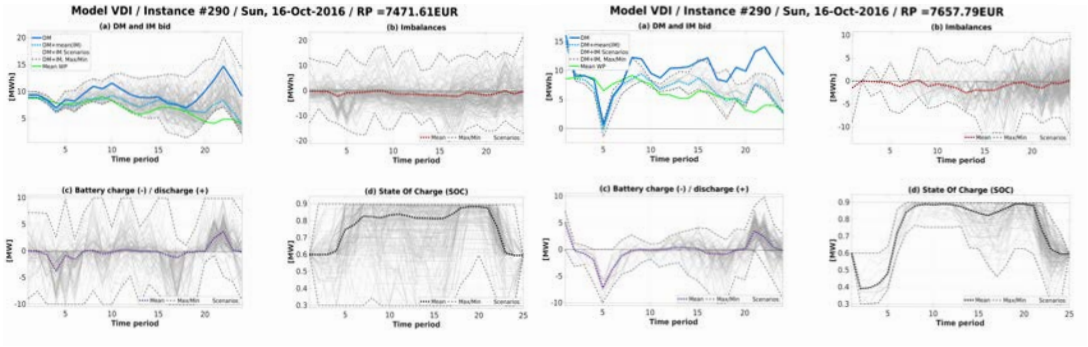

Figura D.2.8: Results for Case VDI of Instance #290.

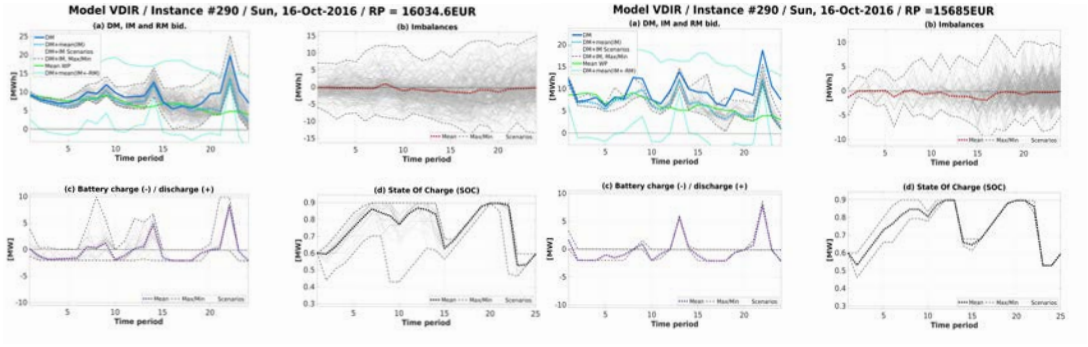

Figura D.2.9: Results for Case VDIR of Instance #290.

D.3. Other Plots of the Numerical Results for the MSOODN Model

Cases A_1 and A_2 / Instance 2 FTCA / Tree 1 (130 scenarios).

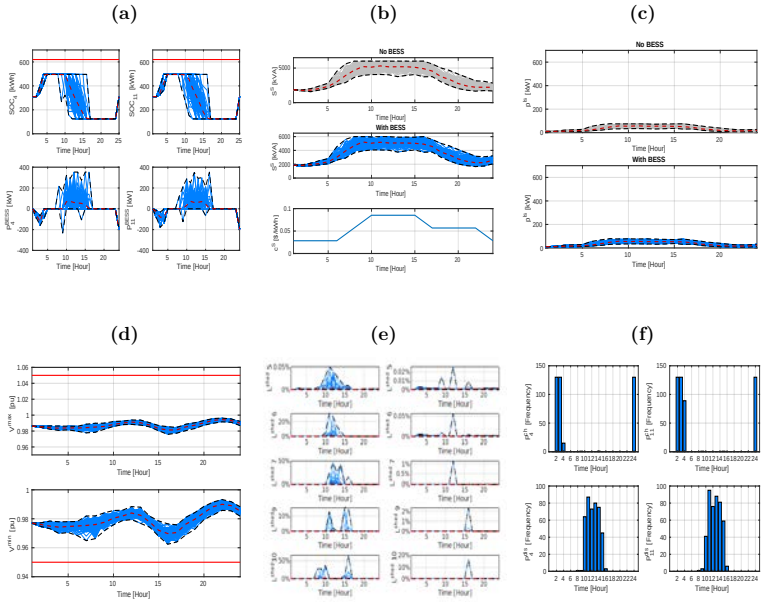

Figura D.3.1: Results for Cases A_1 and A_2 with Scenario Tree of 130 Scenarios Obtained by FTCA.

Cases A_1 and A_2 / Instance 2 DTGFBA / Tree 1 (126 scenarios).

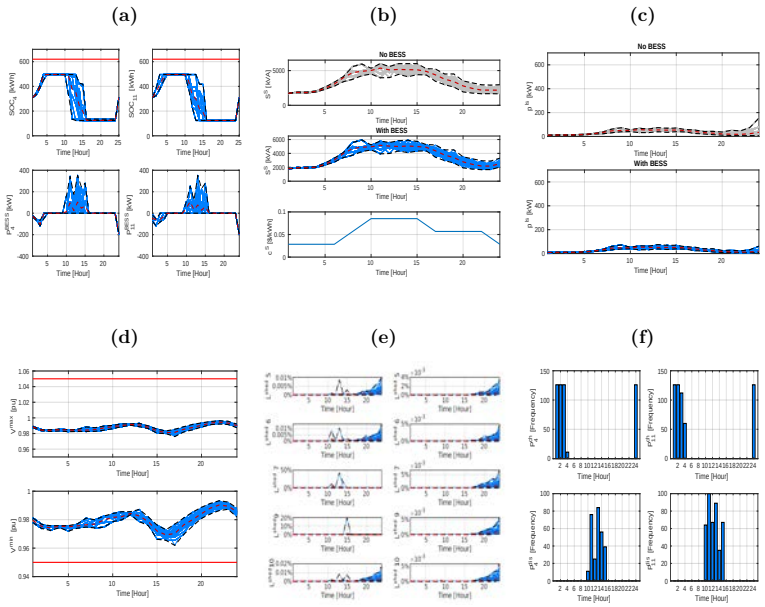

Figura D.3.2: Results for Cases A_1 and A_2 with Scenario Tree of 126 Scenarios Obtained by DTGFBA.

Cases A_1 and A_2 / Instance 3 FTCA / Tree 1 (188 scenarios).

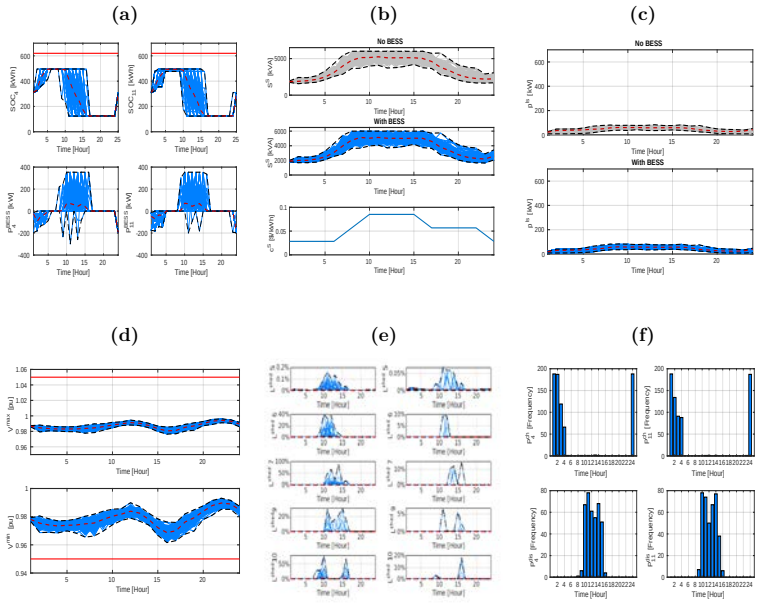

Figura D.3.3: Results for Cases A_1 and A_2 with Scenario Tree of 188 Scenarios Obtained by FTCA.

Cases A_1 and A_2 / Instance 3 DTGFBA / Tree 1 (189 scenarios).

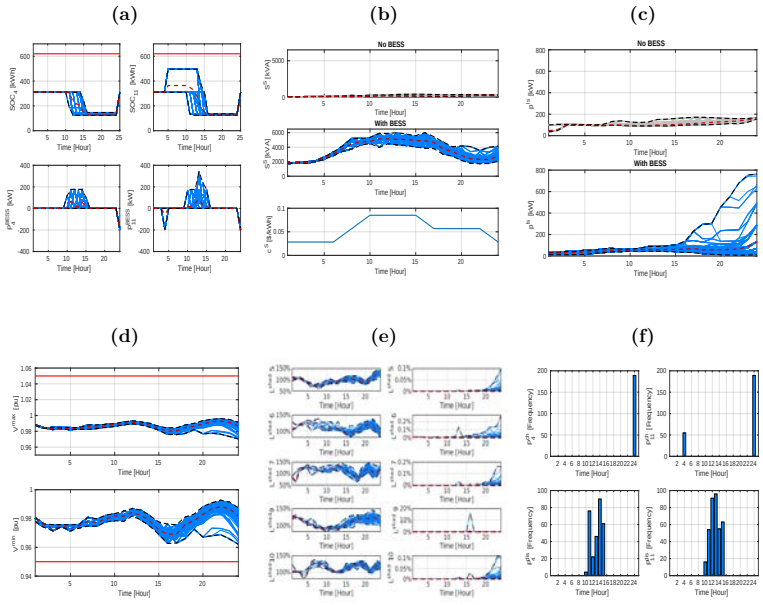

Figura D.3.4: Results for Cases A_1 and A_2 with Scenario Tree of 189 Scenarios Obtained by DTGFBA.

Equipped with his five senses, man explores the universe around him and calls the adventure Science.…

— Edwin Powell Hubble

Bibliografía

Akhavan-Hejazi, H. and Mohsenian-Rad, H. (2013). Optimal operation of independent storage systems in energy and reserve markets with high wind penetration. *IEEE Transactions on Smart Grid*, 5(2):1088–1097.

Ali, A. S. (2013). *Smart grids: opportunities, developments, and trends*. Springer.

Bacher, P., Madsen, H., and Nielsen, H. A. (2009). Online short-term solar power forecasting. *Solar Energy*, 83(10):1772–1783.

Banshwar, A., Sharma, N. K., Sood, Y. R., and Shrivastava, R. (2019). Market-based participation of energy storage scheme to support renewable energy sources for the procurement of energy and spinning reserve. *Renewable energy*, 135:326–344.

Bentler, P. M. (1990). Comparative fit indexes in structural models. *Psychological bulletin*, 107(2):238.

Bhattacharya, A., Kharoufeh, J. P., and Zeng, B. (2018). Managing energy storage in microgrids: A multistage stochastic programming approach. *IEEE Transactions on Smart Grid*, 9(1):483–496.

Boomsma, T. K., Juul, N., and Fleten, S.-E. (2014). Bidding in sequential electricity markets: The nordic case. *European Journal of Operational Research*, 238(3):797–809.

Breeze, P. (2016). *Wind power generation*. Academic Press.

Chambers, J. M., Cleveland, W. S., Kleiner, B., and Tukey, P. A. (1983). Comparing data distributions. *graphical methods for data analysis*, 62.

Conejo, A. J., Contreras, J., Espinola, R., and Plazas, M. A. (2005). Forecasting electricity prices for a day-ahead pool-based electric energy market. *International journal of forecasting*, 21(3):435–462.

Cplex, I. I. (2009). V12. 1: User's manual for cplex. *International Business Machines Corporation*, 46(53):157.

Defourny, B., Ernst, D., and Wehenkel, L. (2013). Scenario trees and policy selection for multistage stochastic programming using machine learning. *INFORMS Journal on Computing*, 25(3):488–501.

Del Granado, P. C., Wallace, S. W., and Pang, Z. (2016). The impact of wind uncertainty on the strategic valuation of distributed electricity storage. *Computational Management Science*, 13(1):5–27.

Dempster, M. A. H. (2006). Sequential importance sampling algorithms for dynamic stochastic programming. *Journal of Mathematical Sciences*, 133(4):1422–1444.

Díaz-González, F., Sumper, A., Gomis-Bellmunt, O., and Villafáfila-Robles, R. (2012). A review of energy storage technologies for wind power applications. *Renewable and sustainable energy reviews*, 16(4):2154–2171.

Ding, H., Pinson, P., Hu, Z., and Song, Y. (2016). Optimal offering and operating strategies for wind-storage systems with linear decision rules. *IEEE Transactions on Power Systems*, 31(6):4755–4764.

Dudek, G. (2016). Pattern-based local linear regression models for short-term load forecasting. *Electric Power Systems Research*, 130:139 – 147.

Dupačová, J., Consigli, G., and Wallace, S. W. (2000). Scenarios for multistage stochastic programs. *Annals of operations research*, 100(1-4):25–53.

Dupačová, J., Gröwe-Kuska, N., and Römisch, W. (2003). Scenario reduction in stochastic programming. *Mathematical programming*, 95(3):493–511.

Efron, B. and Tibshirani, R. J. (1994). *An introduction to the bootstrap*. CRC press.

Escudero, L. F., Garín, A., Merino, M., and Pérez, G. (2007). The value of the stochastic solution in multistage problems. *Top*, 15(1):48–64.

Escudero, L. F., Kamesam, P. V., King, A. J., and Wets, R. J. (1993). Production planning via scenario modelling. *Annals of Operations research*, 43(6):309–335.

Fan, S., Liao, J. R., Yokoyama, R., Chen, L., and Lee, W. (2009). Forecasting the wind generation using a two-stage network based on meteorological information. *IEEE Transactions on Energy Conversion*, 24(2):474–482.

Fatouros, P., Konstantelos, I., Papadaskalopoulos, D., and Strbac, G. (2017). A stochastic dual dynamic programming approach for optimal operation of der aggregators. In *2017 IEEE Manchester PowerTech*, pages 1–6. IEEE.

Field, A. (2013). *Discovering statistics using IBM SPSS statistics*. sage.

Fourer, R., Gay, D. M., and Kernighan, B. W. (1993). Ampl. a modeling language for mathematical programming.

Frangioni, A. and Gentile, C. (2006). Perspective cuts for a class of convex 0–1 mixed integer programs. *Mathematical Programming*, 106(2):225–236.

Frauendorfer, K. (1996). Barycentric scenario trees in convex multistage stochastic programming. *Mathematical Programming*, 75(2):277–293.

García-Martos, C., Rodríguez, J., and Sánchez, M. J. (2011). Forecasting electricity prices and their volatilities using unobserved components. *Energy Economics*, 33(6):1227–1239.

Gasch, R. and Twele, J. (2011). *Wind power plants: fundamentals, design, construction and operation*. Springer Science & Business Media.

Gibbons, J. D. and Chakraborti, S. (2014). *Nonparametric Statistical Inference: Revised and Expanded*. CRC press.

Giebel, G., Brownsword, R., Kariniotakis, G., Denhard, M., and Draxl, C. (2011). The state-of-the-art in short-term prediction of wind power: A literature overview. *ANEMOS. plus*.

Gilbert, P. D., Meijer, E., et al. (2005). *Time series factor analysis with an application to measuring money*. Rijksuniversiteit Groningen.

Gilbert, P. D., Meijer, E., et al. (2006). *Money and Credit Factors*. Bank of Canada.

González-Garrido, A., Villarreal, I., Gaztañaga, H., Saez-de Ibarra, A., and Eguia, P. (2019). Optimized energy management strategy for wind plants with storage in energy and reserve markets. In *Journal of Physics: Conference Series*, volume 1222, page 012039. IOP Publishing.

Growe-Kuska, N., Heitsch, H., and Romisch, W. (2003). Scenario reduction and scenario tree construction for power management problems. In *2003 IEEE Bologna Power Tech Conference Proceedings,*, volume 3, pages 7–pp. IEEE.

Gröwe-Kuska, N., Kiwiel, K. C., Nowak, M. P., Römisch, W., and Wegner, I. (2002). Power management in a hydro-thermal system under uncertainty by lagrangian relaxation. In *Decision making under uncertainty*, pages 39–70. Springer.

Gülpınar, N., Rustem, B., and Settergren, R. (2004). Simulation and optimization approaches to scenario tree generation. *Journal of economic dynamics and control*, 28(7):1291–1315.

Hafiz, F., de Queiroz, A. R., Fajri, P., and Husain, I. (2019). Energy management and optimal storage sizing for a shared community: A multi-stage stochastic programming approach. *Applied Energy*, 236:42–54.

Hahn, H., Meyer-Nieberg, S., and Pickl, S. (2009). Electric load forecasting methods: Tools for decision making. *European Journal of Operational Research*, 199(3):902 – 907.

Heitsch, H. and Römisch, W. (2003). Scenario reduction algorithms in stochastic programming. *Computational optimization and applications*, 24(2-3):187–206.

Heitsch, H. and Romisch, W. (2005). Generation of multivariate scenario trees to model stochasticity in power management. In *2005 IEEE Russia Power Tech*, pages 1–7. IEEE.

Heitsch, H. and Römisch, W. (2009a). Scenario tree modeling for multistage stochastic programs. *Mathematical Programming*, 118(2):371–406.

Heitsch, H. and Römisch, W. (2009b). Scenario tree reduction for multistage stochastic programs. *Computational Management Science*, 6(2):117–133.

Heitsch, H. and Römisch, W. (2010). Stability and scenario trees for multistage stochastic programs. In *Stochastic programming*, pages 139–164. Springer.

Heitsch, H. and Römisch, W. (2011). Scenario tree generation for multi-stage stochastic programs. In *Stochastic optimization methods in finance and energy*, pages 313–341. Springer.

Heitsch, H., Römisch, W., and Strugarek, C. (2006). Stability of multistage stochastic programs. *SIAM Journal on Optimization*, 17(2):511–525.

Heredia, F.-J., Cuadrado, M. D., and Corchero, C. (2018). On optimal participation in the electricity markets of wind power plants with battery energy storage systems. *Computers & Operations Research*, 96:316–329.

Heredia, F.-J., Riera, J., Mata, M., Escuer, J., and Romeu, J. (2015). Economic analysis of battery electric storage systems operating in electricity markets. In *2015 12th International Conference on the European Energy Market (EEM)*, pages 1–5. IEEE.

Høyland, K. and Wallace, S. W. (2001). Generating scenario trees for multistage decision problems. *Management science*, 47(2):295–307.

Huisman, R., Huurman, C., and Mahieu, R. (2007). Hourly electricity prices in day-ahead markets. *Energy Economics*, 29(2):240–248.

Infanger, G. and Morton, D. P. (1996). Cut sharing for multistage stochastic linear programs with interstage dependency. *Mathematical Programming*, 75(2):241–256.

Kall, P., Mayer, J., et al. (1976). *Stochastic linear programming*, volume 7. Springer.

Kaut, M. (2003). Scenario tree generation for stochastic programming: Cases from finance.

Koopman, S. J., Ooms, M., and Carnero, M. A. (2007). Periodic seasonal reg-arfima–garch models for daily electricity spot prices. *Journal of the American Statistical Association*, 102(477):16–27.

Kouwenberg, R. (2001). Scenario generation and stochastic programming models for asset liability management. *European Journal of Operational Research*, 134(2):279–292.

Kuhn, D. (2006). *Generalized bounds for convex multistage stochastic programs*, volume 548. Springer Science & Business Media.

Kumbartzky, N., Schacht, M., Schulz, K., and Werners, B. (2017). Optimal operation of a chp plant participating in the german electricity balancing and day-ahead spot market. *European Journal of Operational Research*, 261(1):390–404.

Lamperti, J. (1977). Stochastic processes: a survey of the mathematical theory.

Latorre, J. M., Cerisola, S., and Ramos, A. (2007). Clustering algorithms for scenario tree generation: Application to natural hydro inflows. *European Journal of Operational Research*, 181(3):1339–1353.

Laur, A., Nieto-Martin, J., Bunn, D. W., and Vicente-Pastor, A. (2018). Optimal procurement of flexibility services within electricity distribution networks. *European Journal of Operational Research*.

Levron, Y. and Shmilovitz, D. (2012). Power systems' optimal peak-shaving applying secondary storage. *Electric Power Systems Research*, 89:80–84.

Liebl, D. et al. (2013). Modeling and forecasting electricity spot prices: A functional data perspective. *The Annals of Applied Statistics*, 7(3):1562–1592.

Liu, D., Niu, D., Wang, H., and Fan, L. (2014). Short-term wind speed forecasting using wavelet transform and support vector machines optimized by genetic algorithm. *Renewable Energy*, 62:592–597.

Lombardi, P., Powalko, M., and Rudion, K. (2009). Optimal operation of a virtual power plant. In *2009 IEEE Power & Energy Society General Meeting*, pages 1–6. IEEE.

Lorca, Á. and Prina, J. (2014). Power portfolio optimization considering locational electricity prices and risk management. *Electric Power Systems Research*, 109:80–89.

Macedo, L. H., Franco, J. F., Rider, M. J., and Romero, R. (2015). Optimal operation of distribution networks considering energy storage devices. *IEEE Transactions on smart grid*, 6(6):2825–2836.

Morales, J. M., Conejo, A. J., and Pérez-Ruiz, J. (2010). Short-term trading for a wind power producer. *IEEE Transactions on Power Systems*, 25(1):554–564.

Muñoz, A., Sánchez-Úbeda, E. F., Cruz, A., and Marín, J. (2010). Short-term forecasting in power systems: a guided tour. In *Handbook of power systems II*, pages 129–160. Springer.

Muñoz, M. P., Corchero, C., and Heredia, F.-J. (2013). Improving electricity market price forecasting with factor models for the optimal generation bid. *International Statistical Review*, 81(2):289–306.

Musmanno, R., Scordino, N., Triki, C., and Violi, A. (2009). A multistage formulation for generation companies in a multi-auction electricity market. *IMA Journal of Management Mathematics*, 21(2):165–181.

Nowicka-Zagrajek, J. and Weron, R. (2002). Modeling electricity loads in california: Arma models with hyperbolic noise. *Signal Processing*, 82(12):1903 – 1915.

Pallottino, S., Sechi, G. M., and Zuddas, P. (2005). A dss for water resources management under uncertainty by scenario analysis. *Environmental Modelling & Software*, 20(8):1031–1042.

Panagiotelis, A. and Smith, M. (2008). Bayesian density forecasting of intraday electricity prices using multivariate skew t distributions. *International Journal of Forecasting*, 24(4):710–727.

Peña, D. (2005). *Análisis de series temporales*. Alianza.

Pennanen, T. (2009). Epi-convergent discretizations of multistage stochastic programs via integration quadratures. *Mathematical Programming*, 116(1-2):461–479.

Pflug, G. C. (2001). Scenario tree generation for multiperiod financial optimization by optimal discretization. *Mathematical programming*, 89(2):251–271.

Pflug, G. C. and Pichler, A. (2014). *Multistage stochastic optimization*. Springer.

Pflug, G. C. and Pichler, A. (2015). Dynamic generation of scenario trees. *Computational Optimization and Applications*, 62(3):641–668.

Pflug, G. C. and Pichler, A. (2016). From empirical observations to tree models for stochastic optimization: convergence properties. *SIAM Journal on Optimization*, 26(3):1715–1740.

Phinikarides, A., Makrides, G., Zinsser, B., Schubert, M., and Georghiou, G. E. (2015). Analysis of photovoltaic system performance time series: Seasonality and performance loss. *Renewable Energy*, 77:51–63.

Plazas, M. A., Conejo, A. J., and Prieto, F. J. (2005). Multimarket optimal bidding for a power producer. *IEEE Transactions on Power Systems*, 20(4):2041–2050.

Ren, G., Liu, J., Wan, J., Guo, Y., and Yu, D. (2017). Overview of wind power intermittency: Impacts, measurements, and mitigation solutions. *Applied Energy*, 204:47 – 65.

Serra Castilla, R. et al. (2019). Generació d'arbres d'escenaris per a problemes d'oferta òptima en mercats d'electricitat. B.S. thesis, Universitat Politècnica de Catalunya.

Shang, Y., Wu, W., Liao, J., Jianbo, G., Su, J., Liu, W., and Huang, Y. (2020). Stochastic maintenance schedules of active distribution networks based on monte-carlo tree search. *IEEE Transactions on Power Systems*.

Shapiro, A. (2003). Inference of statistical bounds for multistage stochastic programming problems. *Mathematical Methods of Operations Research*, 58(1):57–68.

Shapiro, A., Dentcheva, D., and Ruszczyński, A. (2009). *Lectures on stochastic programming: modeling and theory*. SIAM.

Shcherbakov, M. V., Brebels, A., Shcherbakova, N. L., Tyukov, A. P., Janovsky, T. A., and Kamaev, V. A. (2013). A survey of forecast error measures. *World Applied Sciences Journal*, 24(24):171–176.

Sims, C. A. (1980). Macroeconomics and reality. *Econometrica: journal of the Econometric Society*, pages 1–48.

Singh, K. J. and Mason, A. (2004). Column-generation for capacity-expansion planning of electricity distribution networks. In *Proceedings of the 39th Annual OR Society of New Zealand Conference*, pages 76–85. Citeseer.

Steiger, J. H. (1980). Statistically based tests for the number of common factors. In *the annual meeting of the Psychometric Society. Iowa City, IA. 1980*.

Team, R. et al. (2015). Rstudio: integrated development for r. *RStudio, Inc., Boston, MA URL http://www. rstudio. com*, 42:14.

Triki, C., Beraldi, P., and Gross, G. (2005). Optimal capacity allocation in multi-auction electricity markets under uncertainty. *Computers & operations research*, 32(2):201–217.

Trück, S. (2011). The dynamics of hourly electricity prices. In *Institutions, Efficiency and Evolving Energy Technologies, 34th IAEE International Conference, June 19-23, 2011*. International Association for Energy Economics.

Tsay, R. S. (2013). *Multivariate time series analysis: with R and financial applications*. John Wiley & Sons.

Wang, Y., Zhao, H., and Li, P. (2019). Optimal offering and operating strategies for wind-storage system participating in spot electricity markets with progressive stochastic-robust hybrid optimization model series. *Mathematical Problems in Engineering*, 2019.

Wansbeek, T. J. and Meijer, E. (2000). *Measurement error and latent variables in econometrics*, volume 37. North-Holland.

we energize the world 2019 (2019). Intensium max for efficient trackside energy storage. https://www.saftbatteries.com/products-solutions/products/intensium®-max-efficient-trackside-energy-storage?page=1. Online; accessed 26 May 2020.

Wozabal, D. and Rameseder, G. (2020). Optimal bidding of a virtual power plant on the spanish day-ahead and intraday market for electricity. *European Journal of Operational Research*, 280(2):639–655.

Wu, X., Liu, W., Wang, N., and Ma, Y. (2013). Short-term wind power prediction based on time series analysis model. In *Proceedings of the 2nd International Conference on Computer Science and Electronics Engineering*. Atlantis Press.

Xu, B., Zhong, P.-A., Zambon, R. C., Zhao, Y., and Yeh, W. W.-G. (2015). Scenario tree reduction in stochastic programming with recourse for hydropower operations. *Water Resources Research*, 51(8):6359–6380.

Zhu, H., Lian, W., Lu, L., Dai, S., and Hu, Y. (2017). An improved forecasting method for photovoltaic power based on adaptive bp neural network with a scrolling time window. *Energies*, 10(10):1542.

Ziel, F. and Weron, R. (2018). Day-ahead electricity price forecasting with high-dimensional structures: Univariate vs. multivariate modeling frameworks. *Energy Economics*, 70:396–420.